

Charles University

Faculty of Science

Department of Physical and Macromolecular Chemistry

Study programme: Macromolecular Chemistry



DOCTORAL THESIS

**HIGHT-RATE SUPERCAPACITORS BASED ON CONDUCTING
POLY(3,4-ETHYLENEDIOXYTHIOPHENE)**

Iryna Ivanko, MSc.

Supervisor: Ing. Elena Tomšík, PhD.



Institute of Macromolecular Chemistry,
Academy of Sciences of the Czech Republic

Prague 2021

Univerzita Karlova

Přírodovědecká fakulta

Katedra fyzikální a makromolekulární chemie

Studijní program: Makromolekulární chemie



DISERTAČNÍ PRÁCE

**VYSOKORYCHLOSTNÍ SUPERKONDENZÁTORY NA BÁZI
VODIVÉHO POLY(3,4-ETHYLENDIOXYTHIOFENU)**

Mgr. Iryna Ivanko

Školitel: Ing. Elena Tomšík, PhD.



Ústav makromolekulární chemie,
Akademie věd České republiky, v.v.i.

Praha 2021

Tímto prohlašuji, že jsem tuto disertační práci zpracovala samostatně pod vedením Ing. Eleny Tomšík, PhD. a že jsem uvedla všechny použité informační zdroje a literaturu.

Tato práce ani její podstatná část nebyla předložena k získání jiného nebo stejného akademického titulu.

Hereby I declare that this Thesis describes my original work that has been done by myself under the supervision of Dr. Elena Tomšík. To the best of my knowledge, I have cited all used information sources and relevant literature.

This work has not been submitted to obtain any other degree, diploma or qualification.

Mgr. Iryna Ivanko

Acknowledgment

First of all, I would like to thank my supervisor Dr. Elena Tomšík for her support during my study, patience, guidance, valuable advices, and great motivation that push this work toward great publications. Also, I am very grateful to Prof. Tom Lindfors and the laboratory of analytical chemistry Åbo Akademi University for their warm welcome and the opportunity to be a part of a leading sensor-focused group.

Many thanks also belong to colleagues who helped me with measurements and provided valuable discussion, namely Jan Svoboda for XPS measurements, Ivanna Šeděnkova for Raman spectra, Andrii Mahun for NMR characterization and others.

I would also like to thank all my friends and mates who surrounded me during this time, for their ability to cheer me up me and their favor to me any time. A special thanks to my lovely family in Ukraine for their great support and belief. Finally, special thanks to my lovely husband for his uncounted love and big hopes.

Table of Contents

List of abbreviations	2
Abstract	4
Abstrakt	5
1. State of the art	6
1.1 Different method of PEDOT preparation	6
1.2 Effect of structure-making and structure-breaking ions on polymer' properties	10
1.3 Effect of an intermolecular interactions in organic semiconductors on optical properties and charge-carrier transport	12
1.4 Effect of structure feature on the transport properties of conducting polymers	13
1.5 Perspectives of application of conducting polymers as energy storage systems	15
1.6 Solid-state ion-selective electrodes based on conducting polymers as ion-to-electron transducers	17
1.7 Electrochemical characterization of PEDOT and PEDOT based supercapacitor	18
2. Aims of the Thesis	20
3. Results and discussion	21
3.1 Synthesis of hydrated PEDOT chains using chemical oxidation polymerization and its effect on the physicochemical properties	21
3.2 Impact of the nature of supporting electrolyte during electrochemical synthesis of PEDOT on enhancement the density of charge carriers	25
3.3 Acid-assisted preparation of electroactive PEDOT	30
3.4 Interaction of PEDOT with light.....	35
3.4.1 Absorption spectra	35
3.4.2 Photoluminescence spectra.....	37
3.5 Application.....	39
3.1.1 Effect of H-bonding on the value of an open circuit potential of PEDOT	39
3.5.2 Solid state electrodes based on the derivative of PEDOT for selective detection of K ⁺	43
4. Conclusions	47
5. References	49
6. List of papers and contributions presented at conferences	57
7. Appendices – attached publications	59

List of abbreviations

BQ - benzoquinone

CV - cyclic voltammetry

DBEDOT- 2,5-dibromo-3,4-ethylenedioxythiophene

DSC - differential scanning calorimetry

EDOT - 3,4-ethylenedioxythiophene

EIS - electrochemical impedance spectroscopy

EPR - electron paramagnetic resonance

FTO - fluorine tin oxide

GCD - galvanostatic charge–discharge

HQ - hydroquinone

HS - Hofmeister series

iR drop – ohmic drop

ISE - ion-selective electrode

ISM - ion-selective membrane

ITO - indium tin oxide

KTFAB - potassium tetrakis(pentafluorophenyl)borate

LED - light-emitting diode

MALDI-ToF – matrix-assisted laser desorption/ionization time-of-flight

MD - molecular dynamic

MeCN- acetonitrile

NMR - nuclear magnetic resonance

OCP – open-circuit potential

PANI - polyaniline

PEDOT - poly(3,4-ethylenedioxythiophene)

PIC - pseudoisocyanine chloride

PL - photoluminescence

PMNT - poly(3-alkoxy-4-methylthiophene)

SC - solid contact

SCISE – solid-contact ion-selective electrode

SD - standard deviation

TD-DFT - time-dependent density-functional theory

TGA - thermogravimetric analysis

UV-vis - ultraviolet-visible spectroscopy

XPS - X-ray photoelectron spectroscopy

XRD - X-ray diffraction

Abstract

An understanding of the effect of molecular structure on physicochemical properties of organic semiconducting polymers requires a proper method of preparation during which it is possible to obtain a polymer with a well-defined chemical structure. Therefore, in this work three methods of preparation of poly(3,4-ethylenedioxythiophene) (PEDOT), such as chemical oxidation, electrochemical polymerization, and a new method, namely acid-assisted polymerization, were utilized. Using chemical oxidation polymerization, it was investigated the effect of ions from Hofmeister series, specifically formate ion, on PEDOT physicochemical properties. In particular, it was shown the formation of hydrated oligomer chains which assemble into semicrystalline structure. Moreover, it was demonstrated that hydrated oligomers undergo rearrangement of its chains during the electrochemical treatment with the formation of anisotropic structure, and unique photoluminescence properties. Next method for PEDOT preparation, which was for the first time introduced by us, is acid-assisted polymerization. It was shown that it is possible to prepare, by using polar Brønsted acid, the PEDOT solution without applying oxidant at room temperature. Moreover, we have shown a way to control the optical properties of PEDOT, by the mean of a correlation between the process of self-assembly of PEDOT chains. The fundamental understanding the nature of the formation of charge carriers in energy storage devices sheds a light on the proper and precise way of their design. It was shown, during the electrochemical polymerization of PEDOT, the effect of the nature of supporting electrolyte, namely formic acid, on the formation of cation radicals in PEDOT structure. It was demonstrated the ability of formic acid to H-bonding formation with PEDOT monomer units with further formation of localized cation radicals. This knowledge, in turn, was applied for the construction of symmetrical PEDOT based supercapacitors and showed the major role of H-bonding formation on charge storage ability. Particularly, it was shown the device, made up from a dried and wet, prior to soaking in formic acid, electrodes show stable in time 900 mV open-circuit potential. The wide demand for semiconducting polymers, as ion-to-electron transducers, for analytes detection requires a material with reasonable properties. For that purpose, PEDOT with covalently bonded hydroquinone group was used. Thanks to the high redox capacitance of solid contact, based on PEDOT-HQ, it was constructed as the solid contact ion selective electrode with high potential reproducibility in relevant range of analyte concentrations.

Keywords: PEDOT, formic acid, hydrated chains, H-bonding, acid-assisted polymerization, supercapacitor, open-circuit potential, PEDOT-HQ.

Abstrakt

Pochopení vlivu molekulární struktury na fyzikálně-chemické vlastnosti organických vodivých polymerů vyžaduje správný způsob přípravy, během kterého je možné získat polymer s dobře definovanou chemickou strukturou. Proto byly v této práci využity tři metody přípravy poly(3,4-ethylendioxythiofenu) (PEDOT) jako jsou chemická oxidace, elektrochemická polymerace a nová metoda, a to kyselě katalyzovaná polymerace. Pomocí chemické oxidační polymerace byl zkoumán vliv iontů Hofmeisterovy řady, konkrétně formiátového iontu, na fyzikálně-chemické vlastnosti PEDOTu. Zejména byla ukázána tvorba hydratovaných oligomerních řetězců, které se skládají do semikrystalické struktury. Navíc bylo prokázáno, že hydratované oligomery podléhají přeskupení svých řetězců během elektrochemického měření za vzniku anizotropní struktury a jedinečných fotoluminiscenčních vlastností. Další metodou přípravy PEDOTu, která byla u nás poprvé představena, je kyselě katalyzovaná polymerace. Bylo ukázáno, že je možné připravit pomocí polární Bronstedovy kyseliny roztok PEDOT bez použití oxidantu při pokojové teplotě. Navíc jsme ukázali způsob, jak řídit optické vlastnosti PEDOTu, pomocí korelace mezi procesem samouspořádání řetězců PEDOTu. Základní pochopení podstaty vzniku nosičů náboje v zařízeních pro ukládání energie vrhá světlo na správný a přesný způsob jejich návrhu. Při elektrochemické polymeraci PEDOTu byl prokázán vliv povahy nosného elektrolytu, konkrétně kyseliny mravenčí, na tvorbu kation-radikálů ve struktuře PEDOTa. Dále byla prokázána schopnost kyseliny mravenčí tvořit H-můstky s monomerními jednotkami PEDOTa s další tvorbou lokalizovaných kation-radikálů. Tyto poznatky byly následně aplikovány pro konstrukci symetrických superkondenzátorů na bázi PEDOTu a ukázaly hlavní roli tvorby H-můstek na schopnost akumulace náboje. Konkrétně bylo ukázáno, že kondenzátor, vyrobený z suchého a vlhkého elektrodového materiálu vykazuje stabilní potenciál otevřeného obvodu 900 mV. Široká poptávka po vodivých polymerech jako ion-elektronových převodnicích pro detekci analytů vyžaduje materiál s definovanými vlastnostmi. Pro tento účel byl použit PEDOT s kovalentně vázaným hydrochinonovým substituentem. Díky vysoké redoxní kapacitě pevného kontaktu na bázi PEDOT-hydrochinonu byla zkonstruována pevná kontaktní iontově selektivní elektroda s vysokou reprodukovatelností potenciálu v relevantním rozsahu koncentrací analytu.

Klíčová slova: PEDOT, kyselina mravenčí, hydratované řetězce, H-můstky, kyselě katalyzovaná polymerace, superkondenzátor, potenciál otevřeného obvodu, PEDOT-HQ.

1. State of the art

1.1 Different methods of PEDOT preparation

Organic electronics is a field of materials science that deals with design, synthesis, characterization and application of organic molecules including organic polymers for construction of electronic devices. Unlike conventional inorganic-based conductors, organic electronic devices possess noticeable benefits such as low cost, high electrical conductivity and mechanical flexibility. The π -conjugated polymers, called also conducting polymers, concerned great interest from both scientific and practical industrial viewpoints for developing organic electronics. Subsequently, various novel applications of conducting polymers have been proposed, which also stimulated fundamental studies of conducting polymers and the development of new conducting polymers. Polyacetylene was the first conducting polymer reported with conductivity above 10^5 S cm^{-1} , and transport properties close to the metals.¹ However, this material is air-sensitive and not processable, hence not suitable for engineering applications.² The reason of it is the lack of stability of the π -electrons system in the conducting (doped) state. Other alternatives of polyacetylene are polyaniline, polypyrrole, and polythiophene.³ These polymers, in fact, are also in general unstable in conducting state, infusible and most of them are insoluble, except some stable derivatives of polythiophenes.^{4,5} Consequently, these drawbacks led to necessity for investigation of alternative conjugated backbone which provides a stable, processable, highly conducting polymer. More than quarter of century ago a great effort was made by Bayer Central Research Department in order to obtain a stable and efficient polymer, poly(3,4-ethylenedioxythiophene) (PEDOT), that is relevant for industrial application. The first attempt of 3,4-ethylenedioxythiophene (EDOT) polymerization was chemical oxidation using iron (III) chloride, as an oxidative reagent. The obtained PEDOT appeared as a breakthrough in the field of conducting polymers, since it was found to be stable in its doped state and had conductivity up to 200 S cm^{-1} .^{3,6} Following the oxidative polymerization of EDOT, researchers from Bayer as well discovered another method to obtain polymer using electrochemical technique.⁷

Among other conducting polymers PEDOT ensures its unique place due to the high and stable intrinsic conductivity in the wide range of potentials.⁸ In order to get the full insight into the mechanism of processes going on within organic electronic devices, the correlation between structure and physicochemical properties of material is required to be known. There is no doubt that the preparation process is of vital importance for morphology, electrical, and mechanical properties of final polymer, and, consequently, for its application. Generally, the polymerization of EDOT starts with the formation of cation radicals generated from EDOT monomer, proceeds

via further radical–radical coupling reactions growing progressively, and ends with the insoluble PEDOT chain reaching a sufficient length during which negatively charged counter-ions in different sizes join to maintain polymers as electrically neutral. The overall polymerization can be separated into two steps: (1) oxidative polymerization of EDOT by formation of neutral polymer, and (2) oxidative doping of the neutral polymer to the conductive form (polycation). The first step of EDOT oxidation, where free radicals are formed, is the rate-determining step with reaction rate constant ($k_1 = 0.16 \text{ L}^3 \text{ mol}^{-3} \text{ h}^{-1}$). This step is followed by dimerization of the free radicals ($k_2 = 10^9 \text{ L mol}^{-1} \text{ h}^{-1}$). Oxidation of the end group of dimers, which is considered to be faster than the monomer oxidation ($k_5 = 3000 \text{ L mol}^{-1} \text{ h}^{-1}$), followed by the recombination of two cation radicals with the formation of higher oligomers. Finally, oligomers and/or polymers by further oxidation undergo doping.⁹ Numerous methods are available for the synthesis of PEDOT-based materials such as chemical polymerization,^{10,11} interfacial polymerization,¹² vapor phase polymerization,¹³ metal-mediated cross-coupling reactions, solid-state polymerization,¹⁴ and electrochemical polymerization.^{15,16} Among widely used methods of polymer preparation, the chemical polymerization in the presence of powerful oxidants is the most studied. Simply, PEDOT might be prepared from the monomer EDOT, which is commercially available. The oxidative polymerization of EDOT to electroactive polymer is performed by applying oxidant such as sodium or ammonium peroxydisulfate,¹⁷ iron(III) salts such as iron (III)tosylate⁷ or iron(III) chloride,⁶ and some other oxidants.¹⁸ Iron(III) complexes, for example, proved to be efficient oxidants, the standard redox potential of the cation being high, 0.77 V.¹⁹ The significant benefit of using chemical polymerization is primarily based on facility using for the large-scale production of polymer with adjustment of morphology. It is possible to prepare one dimensional PEDOT nanomaterials with controlled morphology ranging from ellipsoidal nanoparticles and nanorods to nanotubes, by carefully adjusting the additive amount of FeCl_3 in the sodium sodium *bis*(2-ethylhexyl)sulfosuccinate reverse cylindrical micelle phase.¹⁰ The next alternative way of EDOT polymerization is based on cross-coupling reactions. The key point of these reactions is coupling of two fragments with the aid of a metal catalyst. The main mechanism of cross-coupling reaction is polycondensation character where the main group of an organometallic compound of the type R-Me (R = organic fragment, Me = main group center) reacts with an organic halide of the type R'-X of monomer with the formation of a new carbon–carbon bond in the product R-R'. Using this method, it is conceivable to get a complete neutral polymer which might be easily characterized by nuclear magnetic resonance (NMR) and electron paramagnetic resonance (EPR) spectroscopies.²⁰ Another method, how EDOT can be polymerized, is electrochemical polymerization, which takes place in a three-electrode cell containing an electrolyte solution. The

formation of electroactive material occurs on the anode conducting surface, such as indium tin oxide (ITO), carbon paper or Au plate.²¹ Electropolymerization may be carried out through different electrochemical techniques for instance by chronoamperometry,²² chronopotentiometry,²³ and cyclic voltammetry.¹⁵ The presence of different solvents and supporting electrolytes during electrochemical polymerization can influence the properties of the synthesized polymer film as well. For example, PEDOT film with a smooth and homogeneous morphology can be prepared from aqueous sodium dodecylsulfate micellar solution with lithium perchlorate (LiClO_4) as the supporting electrolyte. In contrast, polymer synthesized from acetonitrile solution with same supporting electrolyte leads to formation of rough cauliflower-like structure.²⁴ In addition to morphology, the conductivity also strongly depends on the conditions in which polymerization takes place. For example, PEDOT films synthesized potentiostatically in acetonitrile solution containing 0.01 M EDOT and different nature of supporting electrolytes possesses different magnitude of conductivity, namely in Bu_4NClO_4 , Et_4NBF_4 , $\text{Et}_4\text{NCF}_3\text{SO}_3$, Bu_4NPF_6 - 400, 280, 200 and 120 S cm^{-1} , respectively.²⁵ Regardless the simplified way of preparation, above-mentioned methods, namely chemical oxidation and electropolymerization, might suffer from drawbacks such as, poor processability, size of the working electrode, solvent utility, etc.²⁶ Additionally, the electropolymerization is limited to the synthesis of films on conducting substrates.²⁷ Similar to chemical oxidation, the coupling reactions likewise involve chemical reagents and/or transition metal which should be removed from the ultimate polymer. The purification of polymer from by-products always requires monotonous work-up procedures. Recently, Wudl and co-workers reported a simple route towards PEDOT polymerization. It has been demonstrated that 2,5-dibromo-3,4-ethylenedioxythiophene (DBEDOT)^{28,29} undergoes spontaneous polymerization in its crystalline form or even as a film deposited on different surfaces.¹⁴ The colorless crystalline DBEDOT, with time, transformed into a black material without apparent change of morphology and with conductivity around 80 S cm^{-1} . This reaction is not affected by air, vacuum, or light. Based on these studies, authors proposed an oxidative polymerization mechanism for DBEDOT, like oxidation of EDOT by FeCl_3 (the standard reduction potential of Br_2 is 1.07 V that is 0.3 V higher than that of FeCl_3 , 0.77 V, in solution). The reaction is autocatalytic, catalyzed by the released bromine.²⁹ Lately, a pioneering method has been introduced by Officer and Swager groups where no oxidation reagent was used, and reaction has been autocatalyzed (in neat form) or catalyzed by the acid. Officer and co-workers reported the polymerizations of several bromothiophenes catalyzed by HBr and proposed a cationic mechanism to obtain a conjugated polymer. The polymerization occurs when conditions are following: the presence of labile proton in monomer structure, and/or availability of external

proton source in the polymerization mixture. The reaction does not undergo polymer growing in protons-free medium, even when polymerization mixture is heated up to the solvent boiling point. The first step in this mechanism (initiation) relies on protonation of the oxygen of the alkoxy group. Secondly, thiophene then act as a nucleophile and attacks the position 5 of the protonated moiety (propagation). Finally, rearomatization and elimination of hydrogen bromide, results in the formation of a dimer. Reaction of the dimer with protonated monomer or protonation of the dimer and reaction with monomer would generate longer oligomers. However, in order to satisfy the autopolymerization reaction the structure of monomer and arrangement of its substitutes plays an important role.³⁰ Namely, the reaction proceeds with those monomers where an alkoxy and a halide group are in *ortho* position to each other. Additionally, the presence of unsubstituted α -hydrogen in the alkoxybromothiophenes by interaction with other molecule would lead to elimination of molecular hydrogen halide with further formation of dimer. Despite the eagerness to autopolymerize polythiophenes and their derivatives, the utilized the 2-bromothiophene derivatives caused to be unstable,^{31,32} and the uncontrolled nature of reaction did not provide useful polymers. In order to evade drawbacks of autopolymerization reaction proposed by Officer, Swager in turn, made efforts by changing conditions of the reaction.³³ Firstly, by replacing the alkoxybromothiophenes to alkoxychlorothiophenes as monomers for the polymerization reaction. The reason for this is the fact of the lower acidity of the eliminated HCl, which is desirable to prevent degradation of the polymer and/or side reactions. Secondly, the Lewis acid has been introduced as a catalytic reagent. The role of Lewis acid might be elucidated as a strong reagent to create, with eliminated HCl, a strong Brønsted acid. Under these conditions, the growing polymer is protonated, reducing the degree of ionization of the chains, and HCl complexation of the Lewis acid lowers its effectiveness as a catalyst.^{34,35} The transformation of alkoxychlorothiophenes to poly alkoxychlorothiophenes begins with the reaction with Lewis acid (such as SnCl₂) with formation of zwitterion. After further adding of monomer and elimination of SnCl₅⁻ the formation of dimer occurs. Using 2-chloroethylenedioxythiophene as monomer and SnCl₄ as catalytical reagent allows to obtain PEDOT as a dark-blue solid in 91% yield in doped state with conductivity 50 S cm⁻¹. Considering the chain-growth and living character of this polymerization, it is applicable for the synthesis of block copolymers.³⁶

1.2 Effect of structure-making and structure-breaking ions on polymer properties

Throughout science and technology, electrolytes are used to control the ionic strength, but beyond this the specific nature of the electrolytes is of fundamental importance. It is well known that the addition of different ions into the polymerization mixture plays outstanding role for the structure feather of polymer/polymer solution, such as adjustment of solubility, change of molecule structure conformation, and tuning of lower and upper critical solution temperature.³⁷ Once electrolytes dissolve in water, they dissociate into hydrated ions. Water molecules rearrange themselves in the hydration shells of the smaller ions due to the electric field around the small ions.^{38,39} The first studies of the effect of ions on the behavior of proteins were done by the Hofmeister at the end of the 19th century. Hofmeister observed that different electrolytes have different effects on the stability of egg-white protein solutions in water: some electrolytes destabilize them that cause to proteins precipitation (salting-out effect). On the other hand, some group of ions enhance the stability of proteins in solution (salting-in effect). Moreover, the influence of positive ions on precipitating proteins is smaller than negative charged ions.⁴⁰ At present, this effect is classified as the Hofmeister series (HS) or lyotropic sequences, **Fig. 1**. Generally, the native structure of every protein molecule is associated with water, due to fact that the hydration of the protein influences its folding process. Based on that ions in HS are divided into two different groups: strongly hydrated ions and weakly hydrated ions. Anions on the left of Cl^- are well hydrated, classified as kosmotrope ions (water structure maker), and tend to stabilize the native fold structure of proteins, leading to salting-out behavior.⁴¹ Hence, anions on the right of Cl^- are poorly hydrated, called chaotropic ions (water structure breaker), and tend to facilitate protein denaturation, showing salting-in behavior (**Fig. 1**).

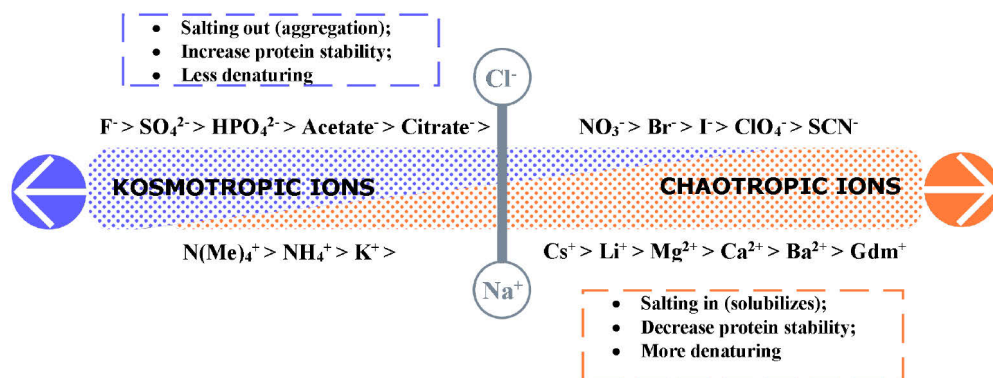


Fig. 1 Hofmeister arrangement of ions in sequence based on their hydration ability.

With growing of interests to the effect of ions on the structure of proteins, scientists made an effort to define a thermochemical function, such as entropy (ΔS) and heat capacity (ΔC_p) for water structure in the presence of structure-making and structure-breaking ions. Markus summarized the value of water structural entropy and judged that, in the presence of structure-maker ions, the value of ΔS is $< 60 \text{ J K}^{-1}\text{mol}^{-1}$, while for water-breaking ions the value of ΔS is $> 60 \text{ J K}^{-1}\text{mol}^{-1}$.⁴² For Cl^- the ΔS is equal $60 \text{ J K}^{-1}\text{mol}^{-1}$) and therefore Cl^- anion is represented as the border line between kosmotropic and chaotropic sequence. The introduction of different anions and cations may lead to appreciable variation in the water solubility of neutral species.⁴³ For instance, in the presence of kosmotropic anions, such as SO_4^{2-} , the solubility of polymer is reducing whereas in the presence of chaotropic one the solubility is rising by making polymer more hydrophilic.⁴⁴ Hydration of neural species it is possible to gain through the perturbation of water structure using chaotropic ions from HS. In turn, this ability of perturbation is connected to ions solvation specificity. Recently, Gospodinova et al. synthesized polyaniline (PANI) film with 80% crystallinity and strong anisotropy in the growth of the nano-sized crystals. This was achieved in the presence of structure breaking anion, such as formate (HCOO^-), with the formation of fibrillar PANI chains. As a result, authors showed that intercalation of free water molecules between the PANI chains caused their ordering throughout the synthesis of polymer. Consequently, highly crystalline film of pure PANI with strong π - π stacking alignment parallel to the film surface containing micrometer-length fibrils perpendicular to the film surface was formed.^{45,46} Later on, authors published a communication, where they showed an effect of water containing well hydrated ions on a value of an open circuit voltage of ITO/PANI/Al cell.⁴⁷ As result, authors showed firstly, substantial increase of V_{oc} (open-circuit voltage) from 0.2 to 0.6 V, and, secondly, the high stability of this parameter in time. The author suggests that an increasing of V_{oc} is related to raising of the lifetime of the excitons as well as their dissociation in the interpenetrating network of PANI and water.⁴⁷ In addition, the Xia group has studied the effect of HS on the conformational features of poly(3-alkoxy-4-methylthiophene) (PMNT) and its optical properties.⁴⁸ Using ultraviolet-visible spectroscopy (UV-vis) they found the polymers surrounded by chaotropic anions as Γ^- or SCN^- produce the bathochromic shift. Whereas in the presence of kosmotropic anions, for example, SO_4^{2-} or F^- , no variation in UV-vis spectra was observed. Authors claim that the presence of chaotropic anions, namely Γ^- , leads to conformation changes of PMNT through the formation of more extended and ordered polymer chains with the bathochromic shift. Using molecular dynamic (MD) simulation technique, it showed the direct interaction of hydrated anions Γ^- with PMNT backbone where *anti*-conformation is dominated. Consequently, the backbone torsion in that conformation results in reduction of optical band gap. On the other hand, during the interaction of

PMNT with kosmotropic ion (F^-), the folded arrangement of backbone is observed with *syn*-conformation and higher energy. Despite the phenomena of HS has been widely studied, the explanation of the underlying mechanism behind the effect is still under discussion.^{49,50}

1.3 Effect of an intermolecular interaction in organic semiconductors on optical properties and charge-carrier transport

The ability to control optical and electronic properties of conjugated oligomers and/or polymers is a long-held goal, which is currently an important issue in the design of new organic-based materials. The capability of solid-state organic semiconductors to ensure efficient charge carriers and/or exciton transfer is a mandatory requirement for their application in electronic and photo-electronic devices. One of the ways it might be achieved is the presence of intermolecular forces between sequences of polymer chains. Intermolecular interaction determines the mutual orientation and distances between molecules in the solid state. Generally, these intermolecular interactions are weaker in organic solids compared to inorganic ones and are defined as weak interactions. Among intermolecular interactions, H-bonding and Coulomb interactions are the most important. However, the Coulombic interaction for unperturbed state in organic solids is almost absent and it is electrically neutral.⁵¹ Therefore, the attractive interactions for organic neutral solids are described in the terms of the polarization and dispersive energies, depending on the overlapping charge densities.⁵² A large contribution of the polarization energy, required for the formation of the highly directional intermolecular interactions, is recognized to be critical for electronic and optoelectronic devices. The main idea proposed by Hunter and Sanders in early 1990s is that polarization in the π -systems of aromatic or hetero-rings plays a crucial role on their mutual orientation.⁵³ Authors demonstrated that most aromatic rings, being entities with a partial negative charge above both aromatic faces and a partial positive charge around the periphery, could be assembled together in pairs only by perpendicular (edge-to-face) or off-centered parallel stacking. Face-to-face or π - π stacking of aromatic rings was presumed to be favorable when one member of the pair possesses strong electron-withdrawing groups. Another possible way to produce π - π stacking is attributed to pairs of aromatic rings with different polarization which are referred to as aromatic donor-acceptor interactions. For conducting polymers, the interactions between the weakly polarized π -systems of the aromatic or heterocyclic moieties (π - π stacking) guiding assembly in the direction perpendicular to the molecular planes are dominated by hydrogen bonds between the polarized peripheries and directing assembly in the axis parallel to

the planes of π -conjugated moieties. The benefit of this intermolecular interaction is fast charge carrier and exciton transport along the polymer chain. However, that might be achieved whether the highly directional intermolecular forces, such as H-bonding, are present.⁵⁴ Hydrogen bonds, traditionally thought to be restricted to the intermolecular attraction between F–H, O–H and N–H groups (proton donors) and O and N (proton acceptors),⁵⁵ have now been expanded to include intermolecular interactions that have a preferential direction. The direction of the intermolecular interactions as well as contact distance are strongly dependent on the electron-donating ability of the electron donor. Specifically, it was found that short contact distance and alignment along the same direction are appropriate for strong electron donor, hence large distance and isotropic orientation for weaker donors. Furthermore, it has been found that the presence of H-bonding in modified oligothiophenes displays strong bathochromic shift and field-effect holes and electron mobilities of $6.7 \times 10^{-3} \text{ cm}^2/\text{V s}$ and $5.6 \times 10^{-3} \text{ cm}^2/\text{V s}$, respectively.⁵⁶ However, the blocking of the hydrogen-bonded sites leads to the decrease in the charge mobility by more than three orders of magnitude and by insufficient exciton coupling, which leads to the absence of red-shifted long-wavelength absorption. Effect of intermolecular interactions on optical properties of material was discovered for J-aggregates by Jelley and Sheppard.^{57–60} Authors explored an effect of intermolecular interactions in diluted pseudoisocyanine chloride (PIC) in water on strong and narrow long-wavelength absorption. Also, the influence of intermolecular forces was studied for molecules in the excited state. For example, during the studying of photoluminescence (PL) of J-aggregates of PIC Scheibe discovered the less quencher required with increasing of concentration of dye. This is because of the rapid propagation of excitons throughout the aggregates composed of 1000 molecules. It was shown a strong interaction between the transition dipole moments of adjacent molecules leads to the splitting of the individual molecular levels with formation of new levels with lower energies (Davydov splitting).

1.4 Effect of structure feature on the transport properties of conducting polymers

Optimization of the electrical properties such as electrical conductivity is highly desirable, and it is a challenge to find tools for controlling it. The conductivity is inherently linked to the transport properties which are in correlation with packing polymer chains in structure.⁶¹ Conducting polymers are in general disordered materials due to their high molecular weight they tend to entanglement of polymer chains with the formation of an amorphous structure. The conjugation, where carbon orbitals are in sp^2 configuration in which the orbitals of successive

carbon atom along the backbone overlap, leads to electrons delocalization along the backbone of polymer. This electronic delocalization provides the highway for charge mobility along the backbone of the polymer chain. The conductivity results from the existence of charge carriers (through doping) and from the ability of those charge carriers to move along the π -bonded highway. In the first case by introducing carriers (by chemical or electrochemical doping) into the electronic structure the electrochemical potential (Fermi level) is moved into the region of energy where there is a high density of electronic states (high density of charge carriers). The attraction of an electron in one repeat unit to the nuclei in the neighboring units leads to the carrier delocalization along the polymer chain and to charge mobility. It is commonly admitted that high carrier mobility is linked to the degree of order and the relative stacking between the chains. The π - π interactions between chains, by delocalization of electrons along the chains, can give rise to weak van der Waals forces so that polymer chains are well stacked. Materials which are constituted by polymer chains with various lengths and different non-uniformly distributed within the chain possesses diverse mechanism of transport of electrons. For example, in disordered materials, the charge transport is fast along the chains, moderate between the chains and slow between the lamellar planes.⁶²⁻⁶⁴ Anderson predicts, highly disordered materials, induce localization charges' function, and there is absence the transport of charge along chains or between the lamellar planes, but by jumping from one localized site to another.⁶⁵ However, based on Mott variable-range hopping theory, for strongly disordered semiconductors, the transport of charges is a function of the distance between two localized sites and the difference between the associated energies.⁶⁶ Thus, in conducting polymers, hopping between two localized states occurs when the thermal vibration of the chain changes the energy of these states. The mobile charge (soliton, polaron or bipolaron) hops from a site to another. This hopping is possible if there is no charge in the terminal site, and if there is a fixed charge nearby (the counter-ion) as there is a strong coupling between the mobile and fixed charges. The conductivity is given by **Equation 1**:

$$\sigma_{VRH} = \sigma_0 \exp \left[- \left(\frac{T_0}{T} \right)^{\frac{1}{n+1}} \right] \quad (1)$$

where, σ_0 corresponds to overall conductivity, T_0 relates to activation energy and n is the dimension of conduction. For example, for PEDOT with $n = 3$ the 3 D hopping between the localized sites (polarons and/or bipolarons) occurs. On the other hand, when $n = 2$, the hopping take place in some favorable directions meaning moderate order and anisotropy.⁶⁷ In such anisotropic systems the transport properties are exacerbated along the chains direction so that the transport is considered quasi one-dimensional. Although, hopping model is beneficial for highly

disordered models, but contradicted relatively high conductivity of conducting polymer, highly doped PANI or PEDOT.^{68,69} Therefore, Sheng states the transport of mobile charge happens between large conducting segments by tunneling rather than by hopping.⁷⁰ Additionally, Zuppiroli based on calculations claimed that transport of mobile charge is taken place between polaronic clusters dispersed in the polymer matrix by hopping between two strongly doped polaronic clusters separated by less doped domains.⁷¹ With the progress in conducting polymers more and more efforts were made in order to obtain well-ordered polymer system with metallic features. For that case, neither hoping nor tunneling described transport of charge is applied. In this case, the transport occurs without the coupling of charge carriers and counter-ions. Whereas, due to the nearing alignment and strong π - π interactions, counter-ions are spatially removed that in fact leads to avoidance of localization of charges.⁷² Conducting polymers, such as polyacetylene, PANI and PEDOT were reported to be depicted as semi-crystalline polymers that have anisotropy. For example, polyacetylene is described as an anisotropic metal in which the charge density is high enough to create the overlapping of their wavefunctions on long distances and the coupling between charge and counter-ions is weak.⁷³ In such anisotropic systems, the transport properties are determined along the chain direction so that the transport is considered as quasi one-dimensional. Although progress in the field of conducting polymers is getting interesting to large number of researchers over the time, there is still a challenge to obtain highly crystalline polymer with fast charge transport mobilities.

1.5 Perspectives of application of conducting polymers as energy-storage systems

Urgent requirements of innovative and sustainable types of energy sources stimulate a lot of interests in using naturally renewable source of energy, such as solar, wind-accumulative, hydropower, geothermal, etc. However, environmentally acquired sources of electricity are considered to be costly with non-constant power generation, and the complexity of the distribution of energy toward energy consumers. Therefore, the conventional well-known system has great demand to be promoted and developed. These systems include batteries, fuel cells, and electrochemical capacitors (supercapacitors). Batteries and fuel cells are generally used for energy storage in industrial and consumer electronic devices because of their high energy density. Batteries can hold large amounts of power, but it takes hours to charge up. In turn, fuel cells have low energy density.⁷⁴ Although the energy storage and conversion mechanisms are different, there are “electrochemical similarities” between these three systems. Common features are that the

energy-providing processes take place at the phase boundary of the electrode/electrolyte interface and that electron and ion-transport are separated.⁷⁵ On the other hand, capacitors charge instantaneously but store only small amounts of power. According to demand, it is necessary to store and release large amounts of electricity very quickly. Owing to this, energy-storage devices, such as electrochemical capacitors (supercapacitors), which are having high capacitance density, high power density, long cycle-life, cost-effective and small size are useful.⁷⁶ According to the definition, supercapacitors are electrochemical devices that can store and release charge at high power densities over short periods of time. Pursuant to a mechanism of the charge storage they can be divided into double-layer supercapacitor and pseudocapacitor. The double-layer supercapacitors store charge by the electrostatic process. On the other hand, pseudocapacitors store charge by redox process occurring at electrode–electrolyte interface. Pseudocapacitors have become potential energy storage units due to their much higher energy density compared to convention capacitors and elevated power density compared to batteries.⁷⁷ Electrical energy can be store in two ways; indirectly, when Faradaic process (oxidation and reduction) that takes place on the electrically active material release charges that can perform electrical work when they flow between two electrodes having different electrical potential, and directly, in electrostatic way, as negative and positive charges on the plates of capacitors, well known as non-Faradaic electrical energy storage. Supercapacitors based on non-Faradaic (double-layer capacitance) reactions have much lower charge-storage ability compared to pseudocapacitors where a Faradaic redox reaction takes place on the surface. Materials for pseudocapacitors can be divided into two groups: transition metal oxides and semiconducting polymers. Due to the fast-redox conversion on surface, semiconducting conjugated polymers are of considerable interest for the application.⁷⁸ One of the most promising fields where conducting polymers have pioneering perspectives is devices for electrochemical energy storage and conversion. The PEDOT is an important conducting polymer that forms some of the most environmentally and thermally stable materials that can be used as electrical conductors, non-linear optical devices, polymer LEDs,⁷⁹ smart windows,⁸⁰ sensors,⁸¹ batteries, electromagnetic shielding materials, memory devices, transistors, artificial muscles, etc. The high conductivity with the combination of great optical transparency in the visible-light region, easy way of preparation by variety deposition techniques and relatively good environmental stability in oxidized state make PEDOT valuable, low-cost material for application in various domains.

1.6 Solid-state ion-selective electrodes based on conducting polymers as ion-to-electron transducers

Chemical sensing is the part of the information obtained about processes going on and chemical composition of the system in real-time.⁸² Generally, the sensing of analyte consists of two steps: selective recognition (which is provided by the chemical interaction with ionophores) and quantitative distribution of detected species (provided by the transducer of signal). Among different kinds of detection ways, potentiometric sensors are known to be an easily-operated device with trustworthy detection. Potentiometric sensors are attractive for practical application, due to their portability, low cost, and almost no energy consumption compared with other analytical detectors.⁸³ Potentiometric sensing is the method of detection of ions by measuring electrical potential. All potentiometric measurements are done under the condition when no current passes through the system and the interface of the system remains non-polarized during the operation. Generally, potentiometric sensors are made up of three parts: current collector, ion-to-electron transducer, and ion-selective membrane (ISM). A couple of years ago, the design of ion-selective electrode (ISE) was different where the current collector was covered by ISM directly, a so-called coated-wire electrode.⁸⁴ However, due to the blocked interface between the current collector and ISM the deviation of electrode potential was relatively high. To overcome this drawback the liquid-state ion-to-electron transducers were introduced. The construction of this ion-to-electron transducer of ISEs is alike an inner part of convenient reference electrode (Ag/AgCl) where the internal electrolyte was replaced by a hydrogel-based electrolyte.^{85,86} However, the liquid-state ISEs have not found a practical application due to some limitations such as the deviation of the concentration of salt in the hydrogel electrolyte with time and accumulation of water layer at the interface. As result, that crucially affects the potential stability and reproducibility of ISEs. Therefore, a new type of ISE where stability of potential was improved by the introducing solid-state layer with appropriate redox and ion-exchange properties. This model is called solid-contact ion-selective electrodes (SCISEs) where SC acts as an intermediate layer between current collector and ISM. The role of this layer is to convert ions to electrons. In principle, ion-to-electron transducer process proceeds like in the internal part of conventional reference electrode and as shown in the **Equation 2**.⁸⁷



M^+ is oxidized conducting polymer unit (e.g., Ag^+), e is electron, M is neutral conducting polymer unit (Ag), A^- is an anion.

For reliable operation of SCISEs, an intermediate layer, namely solid contact of ISE, in turn ought to form an ohmic contact (with the linear current–voltage dependence) between current collector and SC with high work function. Among various metals and carbon-based materials, conducting polymers are a good choice because of representation of a linear dependence of the current on the applied potential. Thanks to the fact, that conducting polymer has combination of electronic and ionic conductivity, last may easy transduce ionic signal to electronic one. In order to satisfy a reliable conversion, namely to prevent polarizing of intermediate layer, SC based on conducting polymers should possess a high redox efficiency.⁸⁸ That might be done either by simple chemical or electrochemical doping of conjugated polymer or by tailoring of conjugated backbone via functionalization by groups that enhance redox capacitance of solid-contact ion-to-electron transducer.⁸⁹ In order to gain an ion selectivity of SCISEs the introducing of ISM (with ionophores) on the top of SC might be done. Due to the presence of highly selective ISM, which contains neutral or charges species (ionophores), it is possible to use membrane-based sensor for daily routine usage, clinical testing, with high detection limit (picomolar concentration range).^{90,91} The second way to achieve selectivity of SCISEs is direct incorporation of ion-recognitive ion into the polymer matrix of SC.⁹² By the doping of conducting polymer, and/or by covalent binding of ionophores to the matrix of polymer it is possible to get SCISEs selective toward a specific ion.

1.7 Electrochemical characterization of PEDOT and PEDOT-based supercapacitor

All electrochemical measurements (characterization of materials) were performed using three-electrode set-up at ambient temperature using an AUTOLAB PGSTAT302N potentiostat with a FRA32M Module and Nova 2.1 software in different electrolytes (6 M H_3PO_4 , 1 M H_2SO_4 or 1 M KCl). Pt electrode with an area of 1.2 cm^2 was used as counter electrode and $Ag/AgCl$ (3 M KCl) was utilized as a reference electrode. Cyclic voltammetry was carried out within the potential window from -0.1 to 0.8 V vs. $Ag/AgCl$ at scan rates 30, 50, and 100 $mV s^{-1}$. Electrochemical impedance spectroscopy (EIS) was determined in the frequency range from 10 kHz to 100 mHz with a 10-mV amplitude, at an open-circuit potential. The Kronig–Kramers test was applied to fit obtained EIS data, and to find out the main characteristic values, such as electrolyte resistance, material (charge transfer) resistance, capacitance (non-Faradaic and Faradaic), Warburg element, and constant element of electrochemical cell.

Electrochemical characterization of the PEDOT symmetrical supercapacitor, constructed in the 3.5.1, was performed in a two-electrode cell configuration. The wet electrode (anode) was the working electrode and the dried electrode (cathode) was as a counter and a reference electrode, respectively.

The areal capacitance C (for one electrode) was calculated by using **Equation 3**:

$$C = 2It/(\Delta V \times A) \quad (3)$$

where I is the applied discharge current (A), t is the discharge time (s), ΔV is the potential window without iR drop (V), and A is the area of the PEDOT/CC electrode (cm^2).

The areal energy density E was calculated by using **Equation 4**:

$$E = (C \times \Delta V^2) / 3600 \quad (4)$$

where C is the areal capacitance (mF cm^2).

The areal power density P was calculated using **Equation 5**:

$$P = (I \times \Delta V) / A \quad (5)$$

2 Aims of the Thesis

The aim of this Thesis is to find a correlation between the method of preparation of organic semiconducting polymer, PEDOT, and physicochemical properties of the final material. For that, PEDOT was polymerized using three main methods: chemical oxidation polymerization, electrochemical polymerization, and acid-assisted polymerization. The main goal of this Thesis was to answer following questions:

During the chemical polymerization of EDOT:

1. An effect of Hofmeister ion, namely formate ion, during the chemical polymerization of EDOT, on the water solvation ability of polymer chains.
2. Influence of hydration of polymer chains on the self-assembly ability, and impact of electrochemical treatment on the rearrangement of polymer hydrate chains, and PL properties of PEDOT.

While electrochemical polymerization of EDOT:

1. Effect of the nature of supporting electrolyte, namely ability to H-bonding formation on electronic (cation radicals formation), optical, and redox properties of PEDOT.

During acid-assisted polymerization of EDOT:

1. Effect of H-bonding interaction on the ionization energy of EDOT.
2. Impact of polar Brønsted acid on the formation of oligomer/polymer chains and their ability to assemble into nanoobjects.
3. Correlation between length of the PEDOT (individual chains/aggregates) and position of its absorption/excitation energies.

As a result, the obtained knowledge about the main features of structure and its joint with the process of the preparation of PEDOT, was applied for the construction of symmetrical supercapacitor, and solid contact electrode ion-selective electrode based on electroactive semiconducting, PEDOT.

3 Results and discussion

3.1 Synthesis of hydrated PEDOT chains using chemical oxidation polymerization and its effect on the physicochemical properties

For the preparation of the electroactive PEDOT, the oxidation polymerization of EDOT in the presence of FeCl_3 as oxidant reagent was carried out. The conditions of the polymerization, namely the presence of suitable ions, plays a crucial role on further physicochemical properties of polymer. For that reason, the polymerization of PEDOT was performed in the presence of ions from Hofmeister series. Our choice was to use ions, such as formates, which have chaotropic behavior in lipophilic series. It is known, the oxygen-containing anions, such as formate, involve more water in its hydration shell compared to single-atom ones.⁹³ Moreover, the well-hydrated oxygen-containing ions possess reduced capability to Coulombic interaction with the oxidized heteroatoms, compared, for example, to frequently used non-hydrated Cl^- anion. Using formate ions, we suppose that the breaking of cluster-like structure of water occurs which mainly depends on its solvation capability. The idea is that the structure-breaking nature of ions leads to perturbation of water structure by the weakening of intermolecular interaction between its molecules. Due to the good solvation ability of formate ions, we assume efficient hydration of S atom in thiophene ring is provided. As a result, such hydrated polymer chains might assemble into nanosheet-like structure as confirmed by transmission electron microscope (TEM) (**Fig. 3(b)**) Using matrix-assisted laser desorption/ionization time-of-flight (MALDI-ToF) technique the molecular weight of obtained hydrated polymer chains was determined. The mass-charge ratio showed the distribution of chains with molecular weight corresponding to tri-, tetra-, pentamers, and match to oligomeric nature of PEDOT suspension. In order to prove we are dealing with hydrated oligomeric chains, the presence of water content was confirmed by thermogravimetric analysis (TGA) and differential scanning calorimetry (DSC) techniques. The weight loss of around 2 wt. % in TGA **Fig. 2(a)** curves at 100°C proves the presence of water in oligomeric chains. Additionally, the heat flux peak at 100°C in DSC shown in the **Fig. 2(b)** provides the information about water content. According to the literature,⁹⁴ the presence of bonded water is determined by the presence of a broad exothermic peak at DSC curve, on the other hand the free water possesses the narrow one. Based on the obtained data we conclude the oligomeric chains are H-bonded with water. Moreover, using **Equation 6**, the energy of bonded water with oligomeric chains was calculated:

$$E_{\text{water}} = \Delta Q M_{\text{water}} / \Delta P \quad (6)$$

where ΔP is the weight loss, ΔQ is the amount of heat evolved during the dehydration, and M_{water} is the molecular weight of water.

The computed value of bonded water E_{water} was equal to 4 kcal mol⁻¹ that corresponds to the water joined by hydrogen-bonding (around 5 kcal mol⁻¹).^{95,96} Supported by DSC data, the thermal stability of PEDOT powder is demonstrated as well. As can be seen by heating of PEDOT powder in the air to 600°C, the loss is just 27 wt.%. This loss consists from formic acid evaporation and partially PEDOT degradation. Despite that fact, the material consisted from hydrated chains that possess much better thermal stability compared to those reported in the literature, where the 55 wt. % are lost by heating to 550°C.⁹⁷

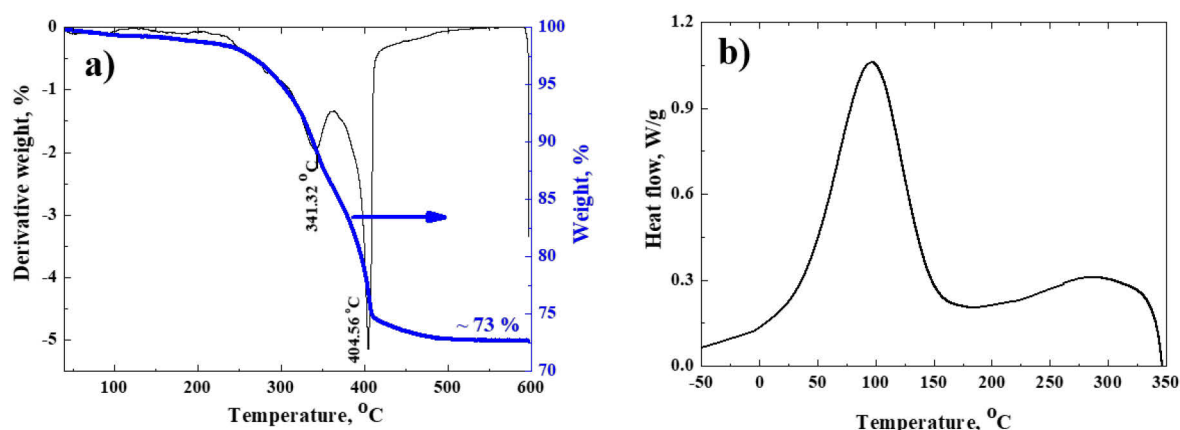


Fig. 2 (a) TGA and (b) DSC of PEDOT powder prepared in the presence of ions(formate) of Hofmeister series.

For the structure characterization of hydrated oligomers chains the Raman spectra were recorded (**Fig. 3(a)**). The 785 nm was found to be an appropriate excitation laser energy for characterization due to the resonance effect of laser wavelength and molecular structure of studied polymer. The main peak related to $C_{\alpha}=C_{\beta}$ stretching vibration in thiophene ring corresponds to the symmetric stretching mode and it is assigned to the reduced state of polymer. The narrowest appearance and intensity of the mentioned peak indicated the presence of high conjugation in the material. Similarly, to dyes^{60,98} the high degree of conjugation is mainly depending on the intermolecular interactions between chains. Particular interaction in our case is provided by the presence of water-hydrated polymer chains and its interaction by H-bonding. On the other hand, the existence of the shoulder located at 1540 cm⁻¹ is associated with the asymmetric stretching vibration of $C_{\alpha}=C_{\beta}$. According to the literature, this stretching vibration is observed for PEDOT in

oxidized state.⁹⁹ Besides, the X-ray photoelectron spectroscopy (XPS) was recorded to prove the structure the synthesized polymer and shown the PEDOT possesses all peaks reported previously.^{100,101} Furthermore, using XPS spectra the atomic composition of formate per polymer unit was estimated. (cf. Appendix 1). By the ratio of S atom to formate ions, it is possible to claim that eight polymer units hold one molecule of formate.

In summary, the hydrated PEDOT chains consist from reduced and oxidized sequences and possess a high level of conjugation due to the presence of intermolecular interactions.

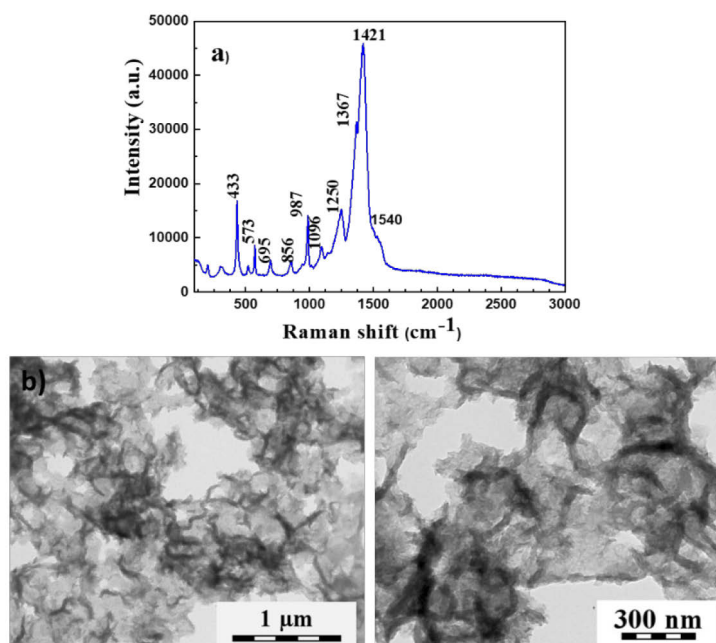


Fig. 3 (a) Raman spectra and (b) TEM images of PEDOT suspension in aqueous solution of formic acid.

In order to characterize the electroactivity of polymer, the electrochemical measurements were done as well. The electrochemical properties were characterized using cyclic voltammetry (CV) and electrochemical impedance spectroscopy (EIS). For that, electroactive material, namely PEDOT, was drop-casted on the conducting support, fluorine-tin-oxide (FTO) glass and recorded in 3-cell configuration set-up. The CV curves scanned in different sweep rate show the rectangular shape of voltammogram (**Fig. 4(a)**). This indicates the anodic and cathodic current density during the oxidation and reduction respectively are similar and these processes are fully reversible. EIS supplies an extra information, such as charge transfer resistance, diffusion-controlled process, capacitance of material (**Fig. 4(b)**). The spectra of PEDOT were recorded at open-circuit potential, when no current passed through the system, in the range of frequency from 0.1 Hz–10 kHz, and results are shown in Nyquist plot. As can be seen, the absence of semi-circuit arc at high frequency

region indicates that the facile charge-transfer process takes place in electroactive material PEDOT. On the other hand, the almost vertical straight line at low frequency indicates the capacitive behavior and no diffusion-controlled process taken place during measurements **Fig. 4(b)**.

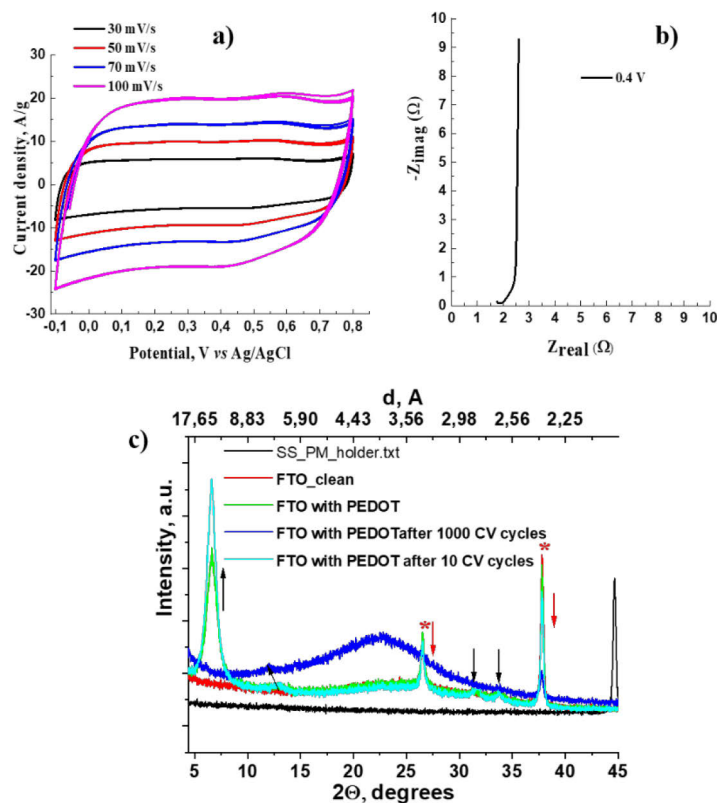


Fig. 4 (a) Cyclic voltammetry, (b) EIS of PEDOT deposited onto FTO glass, and (c) progress of the crystallinity of the PEDOT film during the electrochemical treatment.

The organization of hydrated PEDOT chains before and after electrochemical treatment were studied as well using X-ray diffraction (XRD) technique. As can be seen on the **Fig. 4(c)** the X-ray diffractogram for PEDOT drop-casted onto FTO glass possesses three peaks at $2\theta = 6.5^\circ$, 31° , and 33.7° , respectively. The presence of these peaks indicates the assemblage of hydrated polymer chains, namely interchain packing of two polymer chains ($2\theta = 6.5^\circ$).^{102,103} The nature of two other peaks is still unknown to us, however, we supposed they correspond to the water structure located between polymer chains. On the other hand, it was observed using optical microscope, the non-uniformly covered FTO glass by PEDOT prior cycling converted to uniformly coated one after electrochemical measurement. Based on XRD data, it has been shown the structure of PEDOT after the CV cycling is changing to amorphous one, where the main peaks (at $2\theta = 6.5^\circ$, 31° , 33.7°) disappeared. However, that contradicts Lang's study where the structure

of PEDOT changed from amorphous to partially crystalline after a repeated number of overoxidation cycles.¹⁰⁴

Conclusion:

In the current work we have shown an effect of ion from Hofmeister series during preparation of PEDOT and final physicochemical properties of material. It has been shown the presence of structure-breaking ions leads to perturbation of water clusters with formation of hydrated polymer chains. Using the Raman and XPS spectroscopies the structure of obtained polymer was proved. Via XRD, the packing of polymer chains into structure was shown, and it corresponds to semi-crystalline structure where water plays a crucial role in assembling of chains. Additionally, the capability of hydrated polymer chains to rearrangement during the electrochemical treatment, and formation of anisotropy has been shown.

3.2 Impact of the nature of supporting electrolyte during electrochemical synthesis of PEDOT on enhancement the density of charge carriers.

The chemical composition of conducting polymers and further physicochemical properties depend on several characteristics, such as method of preparation, conditions of synthesis (for instance, reaction temperature, nature of supporting electrolyte, presence of additives, etc.), and post-treatment (doping/dedoping). An effect of condition where polymerization takes place namely the supporting electrolyte plays a crucial role. For example, the deviation of polymerized chains from planarity causes to hypsochromic shift in optical absorption and poor charge transfer and, consequently, low conductivity. However, introducing of electrolytes that might enforce the planarization of chains structure by the formation of intermolecular interactions might be a promising solution for further application.

In the current work, the effect of supporting electrolyte, namely formic acid, was investigated. The preparation of semiconducting PEDOT was carried out in the presence of acid which can form H-bonding between polymer chains as well as own molecules. For that purpose, the simplest carboxylic acid, formic acid, was used as a supporting electrolyte. Our assumption is that formic acid is small in size and might penetrate between polymer chains and form intermolecular electrostatic interactions between lone pair of sulfur and its molecules, namely H-bonding and/or Coulombic type. Using galvanostatic deposition, by the applying constant current density for constant time, EDOT in the presence of 5M formic acid as supporting electrolyte was polymerized. In order to prove the key role of formic acid, the polymerization in the presence of

neutral salt (NaCl) and inorganic acid (H_3PO_4) were done as well. So that to investigate the structure of polymer the Raman spectra at excitation wavelengths 514 (for fully reduced),⁹⁹ 785, 1064 nm, were recorded for EDOT electropolymerized in the presence of different electrolytes. As can be seen from **Fig. 5(a)**, the chemical structure of PEDOT films synthesized in the presence of different electrolytes recorded at 785 nm is similar and corresponds to the Raman spectra published in the literature so far.¹⁰⁵ The only difference for PEDOT in the presence of formic acid among other is the presence the peak corresponding to symmetrical $\text{C}_\alpha=\text{C}_\beta$ stretching vibration at 1432 cm^{-1} which is splitting into two peaks 1436 and 1427 cm^{-1} respectively **Fig. 5(a)** (upper). However, treating the polymer with the base (NaOH) with further removing of the formic acid caused the disappearance of splitting of the peak at 1432 cm^{-1} . Furthermore, the narrowest of the peaks after processing of polymer film with the solution of NaOH indicate that we are dealing with reduced state of PEDOT. That means, during the electrochemical deposition of PEDOT, the withdrawal of electrons from monomer units led to formation of reduced PEDOT. We suggest the nature of the splitting of the main peak at 1432 cm^{-1} is caused by electrostatic interactions, such as H-bonding and/or Columbic. That might be proved by the presence of peak at 205 cm^{-1} assigned to the spectral region where the H-bonding mode are in resonance with excitation energy ($80\text{--}300\text{ cm}^{-1}$).

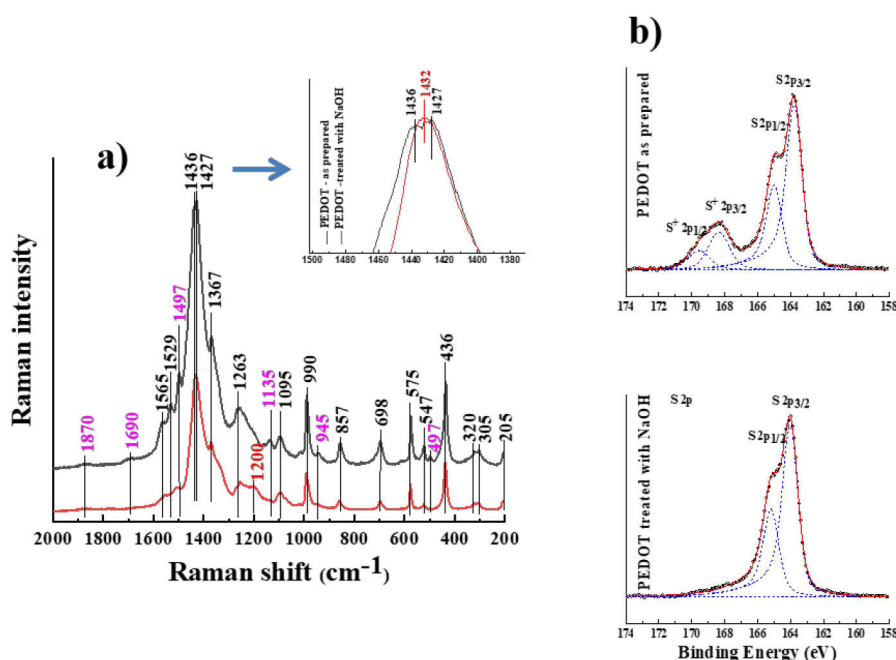


Fig. 5 (a) Raman spectra of PEDOT prepared in the presence of HCOOH (black curve) and after the washing with the NaOH (red curve) recorded at laser wavelength 785 nm, and (b) high-resolution core-level of S2p XPS spectra of PEDOT in HCOOH and PEDOT treated with base.

For further examination, the structure of PEDOT in the presence of different electrolytes the XPS was used. The high-resolution core-level of C 1s spectra of $-C-S-$, $C-O-$, and $-CH_2-CH_2-$ located at 284.2, 285.1, and 286 eV, respectively, observed for PEDOT prepared in the presence of different electrolytes (Appendix 2). On the other hand, the high-resolution core-level of S 2p XPS for PEDOT in the presence of salt and inorganic acid are differ than in formic acid. The main difference is the appearance of the peak located at 168 eV binding energy for EDOT polymerized in the presence of formic acid. The nature of that peak corresponds to the loss of electron density on the S atom due to the intermolecular electrostatic interactions (Columbic or H-bonding). According to the literature published so far, the nature of that peak corresponds to the presence of partly oxidized S, for example, to one in sulfate or polystyrenesulfonate.¹⁰⁶ However, this is not our case, no chemicals except formic acid was used as doping agent. Also, based on literature date, the presence of peak at 168 eV indicates that PEDOT is in oxidized state with the loss of its conjugation.¹⁰⁷ In order to prove the fact, that appearance of doublet peak at 168 eV was caused rather by the presence of intermolecular electrostatic interactions (Columbic or H-bonding) than oxidation of PEDOT, the treatment by NaOH was done. Using this procedure, it was supposed to remove the residual of formic acid and observe whether the partial “oxidation” of S is still existing. As it is seen on the **Fig. 5(b)** after removing formic acid the peak located at 168 eV binding energy has disappeared. Based on the fact that formic acid does not present reductant properties it was proved that the last acts as an agent which forms intermolecular electrostatic interactions (Columbic or H-bonding).

For further investigation of an effect of formic acid during electrochemical preparation of PEDOT, the EPR was used as well. The formation of cation radicals might be either by overoxidation of polymer chains or with help of electrostatic interactions (H-bonding). In the first case, by the applying an overpotential, the formation of non-paired cation radicals stabilized by formate counter-ions occurs. On the other hand, the cation radicals also might be generated by the formation of H-bonding. We suggest the formation intermolecular electrostatic interaction, namely H-bonding between formic acid and monomer units which leads to partial displacement of electron density over constitutional monomer unit toward acid with the formation of localized cation radicals. As can be seen in the **Fig. 6(a)** (black curve) PEDOT prepared in the presence of formic acid possesses sharp narrow peak at 3410 G, proving the presence of cation radicals. However, after removing the forming acid by NaOH, the intensity of EPR peak is reduced **Fig. 6(a)** (blue curve). It is surprising that after the washing acid still small amount of formate anions are present, that shows minor quantity of strongly bonded acid it is a challenge to eliminate.

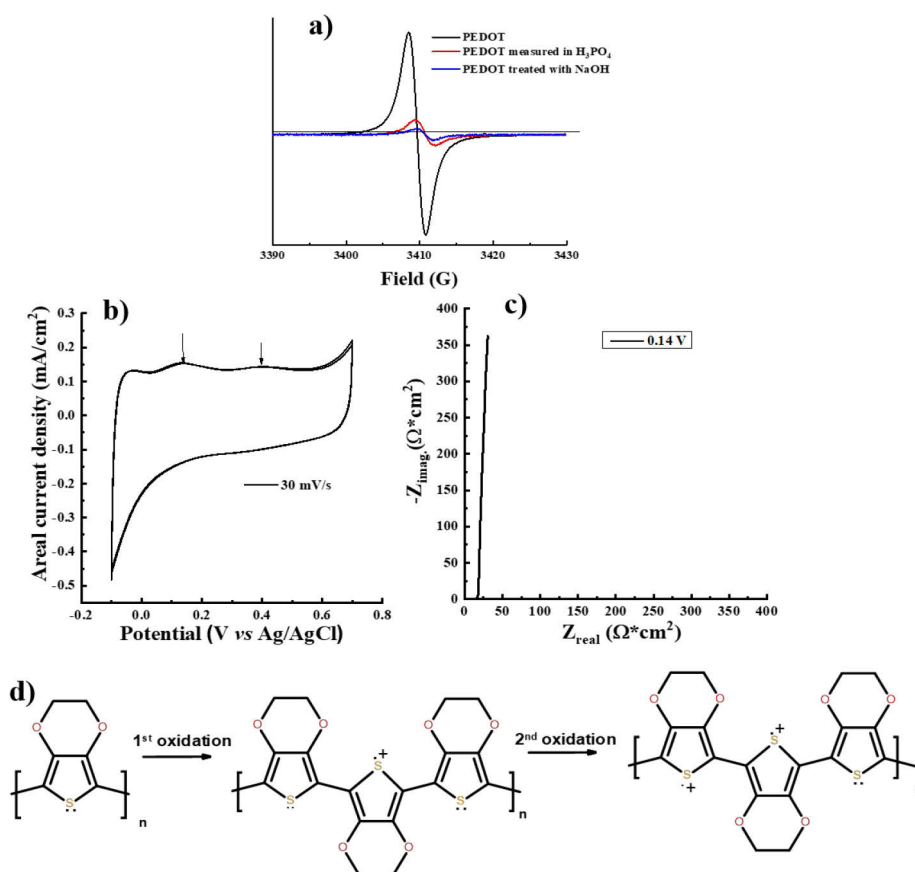


Fig. 6 (a) Electron spin resonance spectra of the PEDOT prepared in HCOOH (black curve), PEDOT treated with base (blue curve), and PEDOT after electrochemical annealing in H₃PO₄, (b) cyclic voltammogram scanned at 30 mV s⁻¹ sweep rate, (c) electrochemical impedance spectroscopy at OCP, (d) the scheme of oxidation processes taken place during cycling from -0.1 to 0.7 V.

Among different methods to improve polymer conductivity, the annealing by proper solvent is one of the promising. For example, authors by the treating of aqueous solution of poly(3,4-ethylenedioxythiophene) polystyrene sulfonate (PEDOT:PSS) with assistance solvent such as dimethyl sulfoxide enhanced the conductivity to 3000 S cm⁻¹.¹⁰⁸ Moreover, they claim it is possible to tune the potential working window (potential range within which the polymer is conducting) by simple annealing with solvent. According to published sources the CV curve of PEDOT during the cycling has rectangular shape without any peaks representing Faraday processes.^{109,110} As can be seen in the **Fig. 6(b)** in PEDOT polymerized in the presence of formic acid with further electrochemical treatment in the H₃PO₄ possesses two peaks at $E_a = 180$ mV and $E_a = 400$ mV, respectively. It interested to notice that the existence of these peaks is possible just in the presence of acidic medium. Whereas, in the presence of neutral medium (NaCl) the

voltammogram curve has rectangular shape. Based on that, we might conclude, the appearance of these oxidation peaks is induced by the formic acid present during the preparation of electroactive PEDOT. The detailed mechanism of processes taken place during oxidation is illustrated in **Fig. 6(d)**. As it is shown, during the first oxidation at 180 mV, the formation of polarons occurs. Whereas, after the second oxidation at 400 mV the bipolarons are formed which are stabilized by phosphate counter-ions.

To prove our assumption, the EPR spectra after electrochemical measurements in the presence of phosphoric acid were obtained. As it is represented in the **Fig. 6(a)**, the intensity of EPR signal recorded for PEDOT prepared in the presence formic acid (black curve) decreased (red curve) after electrochemical oxidation of PEDOT in the presence of phosphoric acid, with formation of dication radicals.

The improvement of conductivity and processes taken place during the electrochemical operating of PEDOT can be studied using EIS. The impedance was recorded for PEDOT in the presence of H_3PO_4 at 0.14 V vs Ag/AgCl (at open-circuit potential) in the frequency range 0.1 Hz–10 kHz. Obtained results were plotted in the form of Nyquist plot and presented in the **Fig. 6(c)**. The straight line of the complex impedance and the absence of semicircle arc indicate the diffusional non-controlled processes, and facile charge transport processes taken place in electroactive material during electrochemical operating, respectively. The detailed fitting of equivalent circuit which match to obtained measured data provide the information of the individual sequence of circuit, such as solution resistance (R_s), double layer capacitance (C_1), charge-transfer resistance of PEDOT film (R_{ct}), Warburg impedance (W), and Faradaic capacitance (C_2) (more in Appendix 2, **Fig. 6**). To shed the light for the conductivity measured in the 3-cell configuration is the value of R_{ct} corresponding to a conductivity of 960 S cm^{-1} .

In addition, the bulk conductivity of PEDOT film was measured in dried form using four-point probe method. The obtained value of conductivity was in range 47.6 S cm^{-1} . On the other hand, the measurements of PEDOT soaked prior in H_3PO_4 shows the conductivity 670 S cm^{-1} . As the electrode was dried under the boiling temperature of H_3PO_4 , the acid penetrates in the bulk of soft polymers into the channels between polymer chains. As a result, the modulation of the redox states of PEDOT (by the doping level) led to the formation of charge carriers with further enchantment of conductivity.

In the next step of this research the effect of incorporation of phosphate ions into the structure of PEDOT during the electrochemical cycling were studied. Using XRD the crystallinity of polymer as prepared (in formic acid) and after electrochemical cycling were estimated (more appendix 2 **Fig. 8**). It was shown by incorporating of phosphate ions into the structure of PEDOT

the degree of crystallinity is increased after electrochemical cycling. Moreover, after the electrochemical measurements the orientation of polymer chains possesses orientation along the surface, namely stacking to each other.

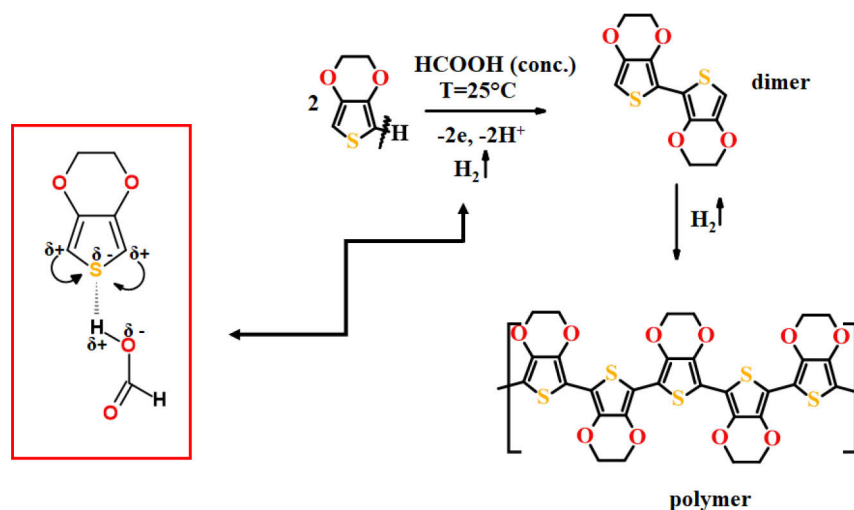
Conclusion:

In the current work the electrochemical galvanostatic deposition of electroactive PEDOT in the presence of formic acid was provided. Using different techniques, it was shown that the intermolecular electrostatic interaction (Coulombic and H-bonding) between acid and polymer chains occurs. Moreover, these interactions induced charge carriers and enhance the electroactive properties of PEDOT.

3.3 Acid-assisted preparation of electroactive PEDOT

Among diverse methods of preparation of conducting polymers mentioned in the part 1.1, it is still a challenge to find out an easy single-step procedure without tedious elimination of byproducts. In the current work, a new way of preparation of PEDOT was proposed where the electroactive polymer was polymerized just by applying Brønsted acids. Moreover, using the proposed method it is possible to gain completely soluble polymer solutions at room temperature. An effect of solvent, namely, its polarity has been in a deep study by Menshutkin. Autor claims the course and rate of any reaction directly depends on the polarity of the medium where the reaction takes place.¹¹¹ In turn, the polarity of medium features by its solvation ability of analyte, which strongly depends on the existence of intermolecular interactions (hydrogen-bonding, Coulomb, dispersion, inductive, and charge-transfer forces). Hydrogen-bonding is an interaction that involves the H atom and atom with a high affinity for electrons. Formic acid is a good candidate for forming aggregates of its molecules via formation of H-bonding intermolecular interactions.¹¹² In the current work we propose a single-step method of preparation of PEDOT, called acid-assisted polymerization. The main idea of that reaction is based on the fact that protic acid, namely formic acid, might initiate the formation of PEDOT oligomers due to the forming of H-bonding between formic acid and lone pair electrons of S of thiophene in monomer molecule. As it is shown in **Scheme 1**, H-bonding formation between the acid and monomer causes the shiftiness of electrons density over C_α in the thiophene ring toward acid, with further weakening of the C_α - C_β bond. That, in turn, leads to the formation of the dimer with the elimination of H_2 gas. Using the Quantitative Gas Analysis method, it was showed the concentration of H_2 before mixing and after 24 h of polymerization proceeding increased by 2.2 times (more Appendix 3) indicating

the elimination of H₂ during the formation of PEDOT oligomers. To prove the reaction proceeds in the presence of other Brønsted acids, the polymerizations of PEDOT were done in the acetic and *ortho*-phosphoric acids as well. As a result, it was observed the formation of PEDOT oligomer in the presence of all protic acids, but with different kinetics. (more Appendix 4)



Scheme 1. Scheme of acid-assisted polymerization of EDOT in the presence of 98% formic acid.

Generally, chemical and electrochemical polymerization of conducting polymers occurs after the withdrawing of two electrons from monomer molecules, and with forming of stable cation radicals. The formation of dimer happens throughout the coupling of two cation radicals and the removal of two protons. In order to prove we are dealing with the mechanism through the formation of cation radicals, the EPR spectra were recorded in 1 h of polymerization (a) in 2 weeks (b), and for PEDOT ultimate powder. As can be seen in **Fig. 7(a)**, at the beginning of acid-assisted polymerization of EDOT, the EPR signal is not visible that corresponds to an absence of cation radicals. Even after two weeks of polymerization proceeding, the PEDOT solution possesses a fairly low signal of EPR. However, for the ultimate powder of PEDOT, the EPR signal is presented as a narrow line, indicating the presence of localized cation radicals.²⁹ The presence of the EPR signal for the powder might be explained by the formation of localized cation radicals induced by the H-bonding interaction between oligomer chains and formic acid (more Appendix 4). Based on EPR characterization, it was concluded the formation of dimer and/or oligomers proceeds without formation of cation radicals. The Raman and XPS spectra were recorded as well to prove the structure of an obtained polymer. The recorded spectra of both spectroscopy methods verify the polymerized EDOT using acid-assisted polymerization corresponds to the structure of PEDOT published in the literature (more Appendix 4)

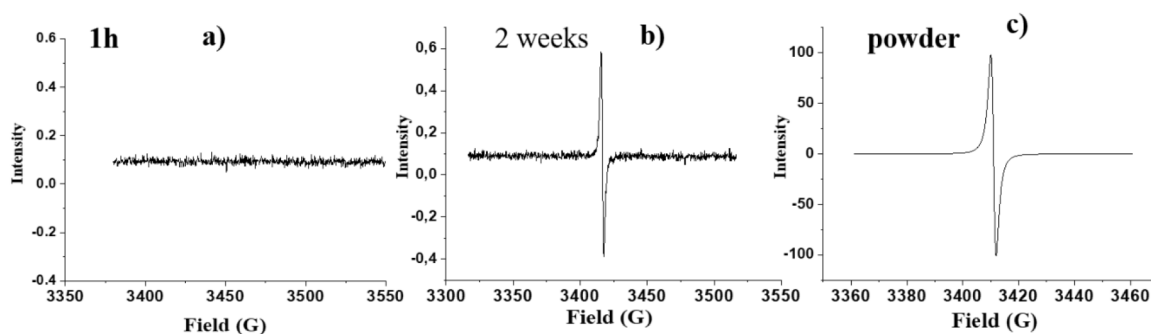


Fig. 7 (a) EPR signal of EDOT mixed with $\text{HCOOH}_{\text{conc}}$ after 1h, (b) after 2 weeks, and (c) PEDOT powder prepared by acid-assisted polymerization.

In order to investigate the kinetics of acid-assisted polymerization and structure of obtained polymer the ^1H hR-NMR, liquid, and solid ^{13}C -NMR was applied. The in situ ^1H hR-NMR spectra in the range from 1 min to 144 h were recorded to find the conversion of the acid-assisted polymerization. As can be seen in the **Fig. 8(b)** the conversion EDOT to PEDOT is around 80 % after 144 h of polymerization. This indicates the acid-assisted polymerization is a time-consuming process to achieve full conversion of monomer to polymer. It was shown by the increasing the concentration of the monomer in 20 times, the polymerization starts immediately. The characteristic ^1H -NMR spectra of obtained PEDOT corresponds to signals reported for PEDOT in literature¹¹³ (Appendix 3). The liquid ^{13}C -NMR was used to confirm the formation of PEDOT oligomers as well. As can be seen in the **Fig. 8(a)**, group of signals assigned to PEDOT (marked as 4 and 5) appeared indicating the formation of PEDOT oligomers. Solid-state ^{13}C -NMR of final PEDOT powder (obtained by heating at 100°C) was measured. The appearance of signals assigned to PEDOT is in great agreement with the literature published so far.²⁹ Evaluation of integral intensity from EDOT and signal from the formic acid shows the one molecule of formic acid is present per three monomer units. (app.3) After removing formic acid (by heating under 150°C) based on NMR spectra it was showed the structure of PEDOT has not changed but an integral intensity of peak assigned to formic acid is reduced. That means the residual amount of acid is strongly bonded with PEDOT chains.

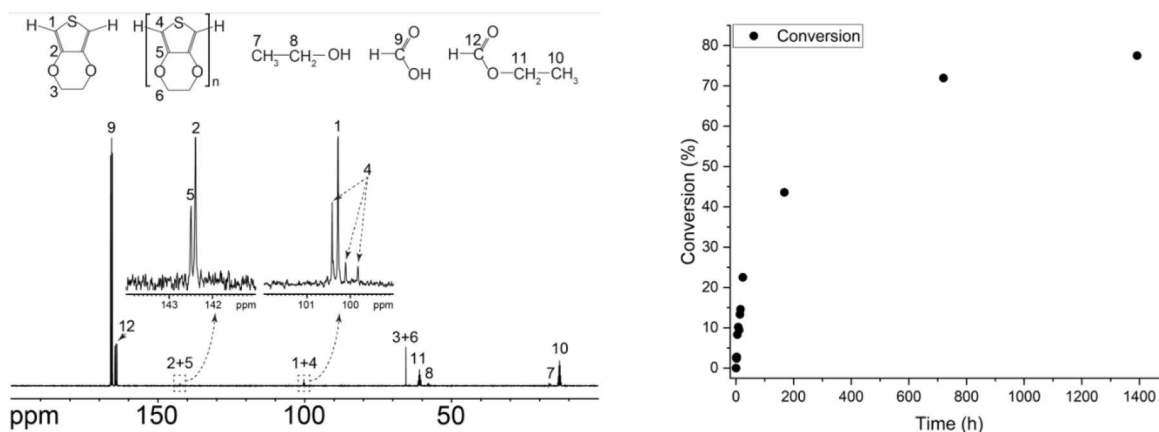


Fig. 8 (a) ^{13}C NMR spectra for EDOT dissolved in a mixture of d_6 -ethanol and d_2 -formic acid (3:7 vol.), (b) and conversion of EDOT to PEDOT with time determined using ^1H NMR.

The evolution of the molecular weight of PEDOT prepared by acid-assisted polymerization was measured in situ using the MALDI-ToF technique. The growth of molecular weight during the reaction was observed by the changing of the color of the polymer mixture, from colorless (immediately after mixing) to dark blue color (ultimate state). Based on measured data (more Appendix 3) molecular weight of obtained oligomers after mixing corresponds to dimer, and trimer. However, after 48 h (intermediate state) of reaction, the molecular weight is rising and corresponds to pentamers. We suggest the reason for it is assembling of short trimers, tetramers into the chains with higher molecular weight. Based on the results we got from the MALDI-ToF, TEM and Cryo-TEM were also used to prove the formation of nanoobjects (more Appendix). It was shown for intermediate PEDOT solution (means the concentration of oligomer chains is relatively low) the formation of black dots related to the creation of nano-objects. Moreover, it must be underlined, the clear contrast of black dots was observed that is associated with the high electron density of assembled chains. On the other hand, with the increasing of concentration of oligomer chains with time (ultimate state), it was shown on TEM image the formation of low-density globular aggregate with the size around 150 nm. The size and density of PEDOT aggregates were proved by dynamic light scattering as well and correspond to hydrodynamic radius R_h 144 nm and density 0.068 g cm^{-3} , respectively (more Appendix 3).

To investigate the redox properties of PEDOT prepared in formic acid the electrochemical techniques, such as CV and EIS, were used. For that, PEDOT ultimate solution was drop-cast on the conducting glass and measured in H_3PO_4 medium. The interesting fact is that PEDOT prepared

by acid-assisted polymerization can be used in a state of powder, by simply dissolving in formic acid or other solvents.

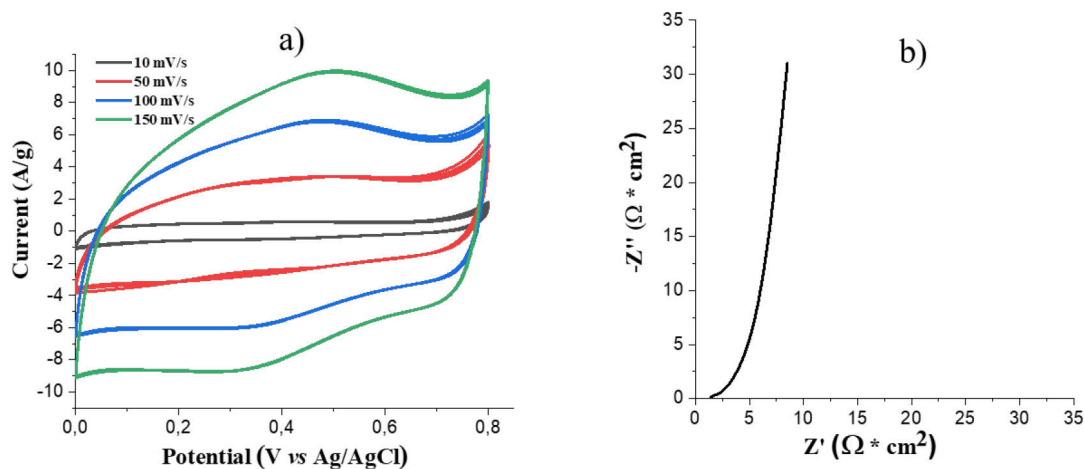


Fig. 9 (a) Cyclic voltammogram of PEDOT, and (b) electrochemical impedance spectroscopy of PEDOT prepared using acid-assisted polymerization.

The CVs at different scan rates were recorded for PEDOT and are presented on the **Fig. 9(a)**. As can be seen, the CV curves possess the single oxidation peak which is located at 0.5 V vs Ag/AgCl reference electrode, and one reduction peak at 0.3 V vs Ag/AgCl. The rectangular shape of the CV curve indicates the reversible processes taken place during the oxidation and reduction (ox/red). Using EIS it was shown **Fig. 9(b)** that facile charge transport took place by the absence of semicircle arc at high frequency. After the fitting of data obtained from EIS, the resistance of PEDOT film was found (3.95Ω) and corresponds to the conductivity of 120 S cm^{-1} .

Conclusion:

In the current work it was shown that by using of Brønsted acid it is possible to polymerize EDOT to semiconducting polymer at room temperature, and without adding any oxidant or other additives. Using MALDI-ToF it was concluded the only short oligomer chains are produced which form spherical nanogels by intermolecular interaction (H-bonding). Also, it is noteworthy, that obtained PEDOT is soluble in different solvents (organic, and for example formic acid) that make it interesting in terms of characterization and application.

3.4 Interaction of PEDOT with light

3.4.1 Absorption spectra

Investigation of the effect of intermolecular hydrogen bonding on electronic absorption spectra is of great importance for the further explanation of the nature of the absorption bands of complex molecules. It was found that the presence of intermolecular interaction, such as H-bonding between polymer chains leads to the strong red-shift in the solid-state absorption spectra compared to the polymer solution. For example, the absorption of the film of oligothiophenes functionalized by phthalohydrazide displays a bathochromic shift due to the presence of H-bonding.¹¹⁴ In order to investigate the effect of ions from HS, during the preparation of PEDOT on the excitation energy (required to excite electrons from lower bonding to higher anti-bonding molecular orbitals) solid-state UV-vis spectroscopy was used. Since ions that have chaotropic character, they might perturb water cluster that causes the hydration of polymer chains. That in fact leads to the assembly of hydrated polymer chains into nanostructure via H-bonding interaction with the rising of the level of conjugation. As can be seen in **Fig. 10(a)** the absorption of PEDOT chemically prepared in the presence of formic acid possesses a broad peak starting from 500 nm to 1000 nm. Using deconvolution of obtained spectra in **Fig. 10(d)** it was shown that PEDOT has two chromophores located at 540 nm and 800 nm, respectively. Using time-dependent density-functional theory (TD-DFT) calculations, Zozoulenko showed the absorption spectrum of a neutral chain exhibits an absorption peak with a wavelength of $\lambda_{\text{abs}} = 481 \text{ nm}$.¹¹⁵ Therefore, we suggest the nature of the peak located at 540 corresponds to the neutral (reduced) or to the state with low oxidation level of PEDOT chains. On the other hand, the peak situated at 800 nm relates to the formation of delocalized electrons caused by a high level of conjugation due to the presence of intermolecular interactions between hydrated polymer chains.

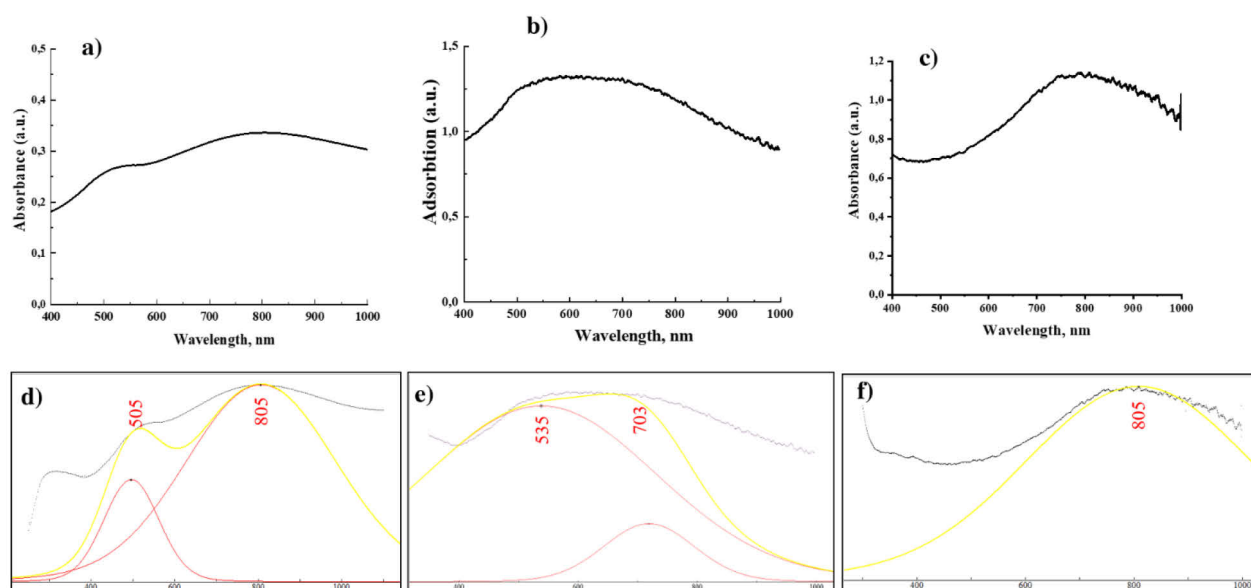


Fig. 10 (a) UV-vis spectra of PEDOT drop-cast onto the glass prepared chemically, (b) electrochemically, and (c) by acid-assisted polymerization, and deconvoluted spectra of them (d), (e), and (f) respectively.

Generally, the electronic and optical properties of conducting polymers are related to the conjugated nature of their backbones and to the formation charged quasiparticles (polarons and bipolarons) that are localized along the polymer chains due to a strong electron–phonon coupling.¹¹⁵ The solid-state UV-vis absorption spectra for the PEDOT electrochemically polymerized in the presence of formic acid as a supporting electrolyte are shown in **Fig. 10(b)**. As can be seen, the spectrum has a very broad peak starting from 400 to 1000 nm, representing overlapping of different transition states. By the deconvolution of the obtained spectra, it was shown in **Fig.10(e)** the presence of two chromophores which are in the resonance with applied energy. The corresponding spectra located at 535 nm and 703 nm correspond to 3.21 and 1.76 eV respectively. We assume the chromophore which absorbs at 535 nm refers to the reduced PEDOT (neutral state), whereas the peak at 703 nm corresponds to the polaron absorption, which is predominant in the spectrum when the number of charge carriers (oxidation state) is relatively low. We speculate that the characteristic peak at 703 nm depicts the formation of localized polarons (proved in 3.2 part) caused by the formation of intermolecular interactions between formic acid and PEDOT chains. Using the TD-DFT approach it was found the absorption peak located at 800 nm is assigned to low oxidation level of PEDOT, and attribute to polaronic and bipolaronic states, where transitions occur from the occupied HOMO levels to the empty polaronic and bipolaronic levels.¹¹⁵ Moreover, it was shown after removing the formic acid by treating with base (NaOH) that the peak located at 703 nm is vanishing, where the absorption of reduced PEDOT at 520 nm remains, with the low intensive shoulder appearing at 620 nm corresponding strongly bonded acid (more Appendix 2). The nature of this peak corresponds to the reduced state, with the absorption peak at 600 nm, which is attributed to the HOMO-LUMO transition in neutral chains.¹¹⁵ As can be seen in **Fig. 10(c)**, the solid-state UV-vis spectra for the PEDOT polymerized using acid-assisted polymerization possesses one broad peak in the range of 600 to 1000 nm. Unlike, polymers obtained using chemical, and electrochemical polymerization, PEDOT prepared in the presence of acid possesses just one absorption peak located at 800 nm (**Fig. 10(f)**). That, in turn, indicates there is no reduced state but just oxidized one. We suggest the peak located at 800 nm corresponds to transitions from the HOMO level to the levels in the conducting band, and either for polaronic or bipolaronic states. These results are in good agreement with the calculated optical transitions by Zozoulenko for polaronic state with 799 nm and bipolaronic state with 791 nm,

respectively. Also, the author estimated the percentages of oxidized sequence in the PEDOT (N=12), when polarons or bipolarons are present that correspond to 8% and 17%, respectively.

3.4.2 Photoluminescence spectra

In general, all electronic polymers exhibit photoluminescence only in their fully reduced state.¹¹⁶ It was shown, for example, the benzenoid sequence of PANI shows PL spectra, whereas the quinonoid one does not. The reason for it is intrachain migration of energy of the neighbored quinonoid group which acts as an excitation trap and quench the PL of the polymer at all.¹¹⁷ Generally, the oxidation level of a pristine PEDOT (as it is polymerized) is about $C_{ox} \approx 33\%$, where there is one positive charge per three monomer units.¹¹⁸ It was shown, using Raman and UV-vis spectra, the PEDOT chemically polymerized in the presence of formic acid, possesses a reduced and oxidized sequence, that contradict PL state-of-the-art. However, we believe the incorporated water (proved by TGA and DSC) between the PEDOT oligomers might extend the benzoic sequences by linking with other PEDOT chains. Analogous studies were done by MacDiarmid and Shimano, where authors showed the effect of water on the PL properties of PANI.¹¹⁹ In order to investigate the effect of water on the chains assembling into nanostructure during chemical polymerization of PEDOT and their interaction with light, the PL were measured as well. The PL spectra with the excitation wavelength 442 nm were recorded for PEDOT film prepared using chemical polymerization in the presence of formic acid. As can be seen in **Fig.11(c)**, the spectrum shows the maximum emission peak at 715 nm with the shoulder at 547 nm and corresponds to the higher Stokes shifts (273 nm and 108 nm respectively) stated in the literature.^{120–122}

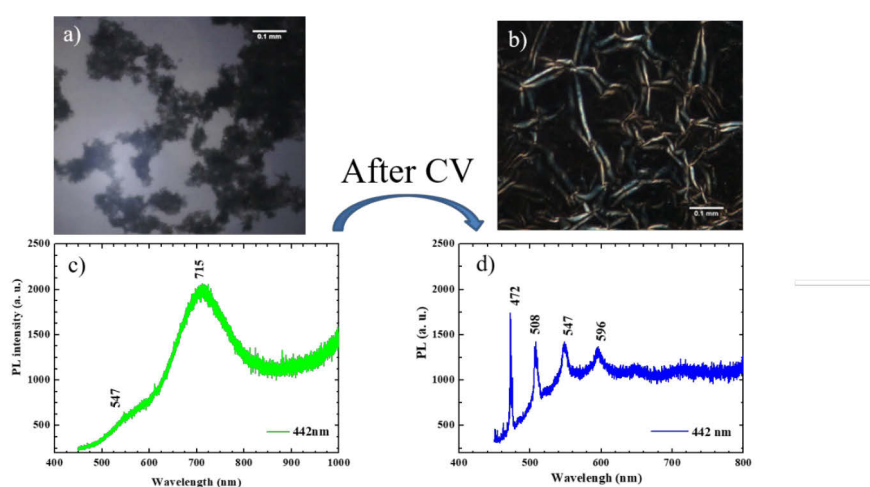


Fig.11 (a) Polarized optical microscopy of PEDOT film before and (b) after electrochemical treatment; (c) the PL spectra of the PEDOT film as prepared, (d) and after electrochemical measurements.

The time-life of the excited state was determined using the time-resolved fluorescence intensity (more Appendix 1). It was showed the lifetime of the excited state is in the range of nanoseconds and prove the PL originates from a singlet excited state. Furthermore, the PL spectra of the PEDOT film after electrochemical cycling (1000 cycles) are differ compared to spectra for PEDOT before measurements. As can be seen on the **Fig.11(d)**, the emission spectra are shifted to a shorter wavelength with appearance of three narrow emission peaks at 472 nm, 508 nm, 596 nm compared to the PEDOT before electrochemical measurements. The appearance of narrow PL peaks at higher energies after electrochemical measurements are linked with the formation of more localized states at the amorphous structure of PEDOT proved by XRD (more Appendix 1). Due to the fact the benzoic sequence, in the amorphous state, could rotate (compared to semi-crystalline structure) the absorbed energy might dissipate caused by the rotational mode. Moreover, using a polarized microscope it was shown the formation of anisotropy, one direction organization, after electrochemical treatment **Fig.11(b)** compared to PEDOT before the electrochemical measurements **Fig.11(a)**.

In order to investigate an effect of light on the aggregation of PEDOT chains, the synchronous PL spectra were recorded for the PEDOT prepared by acid-assisted polymerization. For that, the synchronous PL was measured for different states of the polymerization time: an intermediate state where small nanoobjects are formed (**Fig.12(a)**) and the ultimate state with larger globular aggregates (**Fig.12(b)**). As can be seen the PL for the intermediate state, where the concentration of oligomer chains is relatively low, the PL spectra possess three peaks located at 445 nm, 630, 730 nm, compared to one peak at 650 nm for the ultimate state of PEDOT suspension.

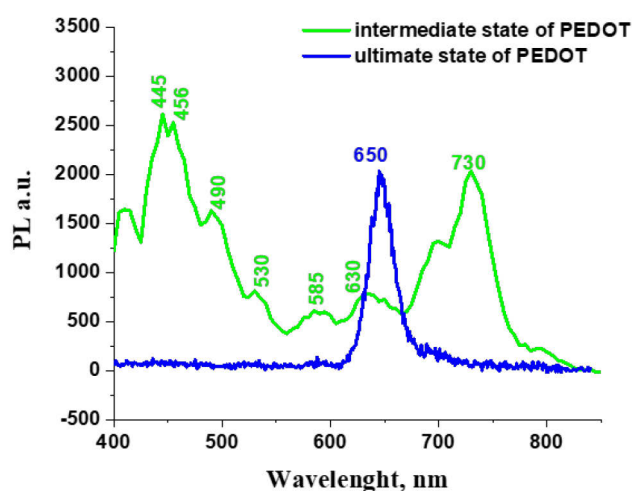


Fig.12 Synchronous photoluminescence spectra for intermediate state (green line), and ultimate state (blue line).

We suppose the nature of PL peaks located at 445/456 nm (green line) corresponds to the PL of individual chains, peaks situated at 630/650 nm (green and blue line) to the small nonobjects (size 5 nm), and peak at 730 nm related to the PL of large aggregates. As can be seen, the ultimate suspension of PEDOT has one peak located at 650 nm, and no peak at 730 nm. We assume it is related to the quenching effect of PL for larger aggregates occurred at the ultimate state of polymerization (where the concentration of PEDOT chains is relatively high). The reason of it might be either planarization of aromatic structures organic chromophores, which promote the π - π stacking of the chromophores and/or other physical interactions (e.g., energy transfer, inter-, or intramolecular charge transfer).¹²³⁻¹²⁵ A similar effect was shown for J-aggregates of PIC, where it was shown that with the increasing of concentration of dye the less quencher required, caused by rapid propagation of exciton through the structure of aggregates.¹²⁶ The author proposed the energy might transfer across the aggregate over thousands of dye molecules.

Conclusion:

In the current work it was shown an effect of hydration of polymer chains as well as effect of H-bonding formation on the optical and PL properties. Moreover, during electrochemical measurements the hydrated polymer chains undergo the rearrangement of its chains with the formation of short-range order and unique PL properties. Also, it was shown the correlation between chain length/aggregation and excitation energy of the system.

3.5 Application

3.5.1 Effect of H-bonding on the open circuit potential of PEDOT

According to the definition, the electrical potential is the work, which is spent to move the charge from one point to infinity (means out of electrical circuit). The higher the electrical potential of the system, the less work should be done. In order to set up of supercapacitor for real application, the output voltage of last should be high enough. To minimize the number of cells and prevent the leakage of electric current during the construction of the device, the working voltage of each cell must be as high as possible.

In this work the symmetrical supercapacitor based on PEDOT was assembled and fundamental parameter were measured. For that, PEDOT was polymerized using galvanostatic deposition in the presence of formic acid as supporting electrolyte. Our choice was made based on the previous studies (more Appendix 2) where unique properties of formic acid are shown, and as well as the

effect of H-bonding formation between PEDOT chains and its molecules on the generation of charge carriers. As a substrate, C-cloth was applied which is made from long fibers networking together providing high surface area. As shown in the **Fig. 13 (left)**, the assembled supercapacitor consists from one wet electrode which was prior soaked in 6M H₃PO₄ and dried one, used as prepared in formic acid. To provide runs of electrons through the external circuit from one side, and to prevent from penetrating the electrolyte from wet to dry electrode, the water non-permeable dielectric membrane from poly(phenylene oxide) was used. As shown on the **Fig. 13 (right)**, the assembled supercapacitor possesses the value of open circuit potential (OCP) when no current passes, 900 mV. Moreover, the obtained value of OCP for PEDOT-based supercapacitor is stable in time. Generally, for obtaining such high value of OCP, the pre-polarization of electrodes is required. That is, the polymer at the anode is pre-polarized to fully reduced (undoped) form, and polymer at the cathode becomes fully oxidized (doped) using over potential. However, in the current work the OCP of the device was gained by the simple using of protic acids, which might form H-bonding intermolecular interactions.

Our assumption was based on the fact, that high value of OCP device is gained due to the formation of delocalized cation radicals, for the cathode (wet electrode) by the formation of H-bonding. Based on our previous studies, the effect of acid during the polymerization plays a crucial role. As it was shown, formic acid is good candidate in making H-bonding, with further generation of cation radicals. Due to the fact, formic acid is small in size, last might penetrate into the bulk of polymer and produce relatively high density of charge carriers. Using the EPR technique, the presence of polarons was proved by the occurrence of narrow high-intensity peak at 3410 G. However, by the replacing of formic with *ortho*-phosphoric acid during post-treatment, the peak completely disappeared. That means during replacement of formic acid into the *ortho*-phosphoric, the delocalized cation radicals are formed. Moreover, the highly reactive localized cation radicals, which possess low lifetime are replaced into delocalized ones.^{128,129} The stability of the delocalized carriers might be obtained either by the counter-ion, phosphate, or mesomeric effect of unsaturated π -bond in a position toward vacant p-orbital of cation radical center.

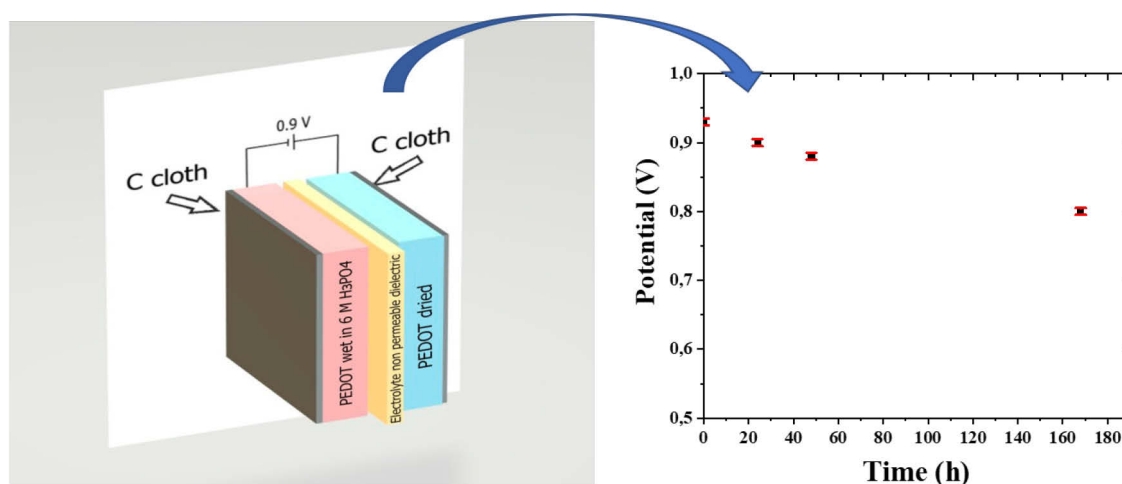


Fig. 13 Schematic illustration of symmetrical PEDOT-based supercapacitor (left), and the stability of OCP in time (right).

In order to prove an effect of H-bonding on the value of OCP, the electrochemical cell was assembled in different configuration. As can be seen in the **Table 1**, the cell made up from two dried and two wet electrodes holds the difference of potential 20 and 100 mV, respectively. It is different from the expected value (predictable value is 0 V), and our assumption is that this might refer to the difference of loaded mass onto the substrates. On the other hand, when anode was prior soaked in the neutral salt, which does not provide H-bonding, but just takes place in Coulombic interactions, the OCP is equal 160 mV. Finally, the set up where one electrode is dry and/or soaked in neutral salt solution and the second in soaked in *ortho*-phosphoric acid produces 920 and 900 mV, respectively. The reason of this is the ability of protic acid to form H-bonding with polymer chains and induce the delocalized charge carriers. It must be mentioned that the OCP of cell, where two electrodes are wet, is not stable in time.

Table 1 Value of OCP of PEDOT-based supercapacitor for different assembling configuration.

Anode	Cathode	OCP/mV
PEDOT dried	PEDOT dried	20
PEDOT wet in 6 M H ₃ PO ₄	PEDOT dried	900
PEDOT wet in 6 M H ₃ PO ₄	PEDOT wet in 6 M H ₃ PO ₄	100
PEDOT wet in 1 M NaCl	PEDOT dried	160
PEDOT wet in 6 M H ₃ PO ₄	PEDOT wet in 1 M NaCl	920

For detailed characterization of pseudocapacitance performance of PEDOT-based device, the following methods have been used: CV, galvanostatic charge-discharge (GCD), and EIS. Using recorded data from above methods, main characteristics, such as capacitance, energy and power density were calculated by the Eq. 2-4. In order to investigate the electrochemical process taking place during redox reactions, the CV has been performed at 30 and 100 mV sweep rates, respectively. The reversible redox process was observed for both sweep rates. The shape of CV curve for two-electrode cell configuration does not alike mirror-like, as was measured in three-electrode cell configuration. Based on the fact, the interface between two electrodes is separated by electrolyte non-permeable membrane, it is possible to claim the Faradaic content of capacitance is preferable rather than double-layer capacitance. Additionally, GCD measurements for PEDOT symmetrical supercapacitor were recorded for different areal current density. As can be seen in the Fig. 14(b) the value of iR drop represented by complex resistance is relatively small and indicates a low interface resistance between PEDOT and carbon cloth and/or other interfaces in the assembled supercapacitor. Furthermore, by the analyzing the charge and discharge time for the different current density it is possible to estimate the Coulombic efficiency. The charging time is longer than discharging one, and that tendency is increasing with the decreasing of current density as well as Coulombic efficiency. Using Eq. 3, the areal capacitance for the electrochemical cell was calculated and the obtained value 56.7 mF cm^{-2} for 0.5 mV cm^{-2} is higher compared to published one.¹²⁹

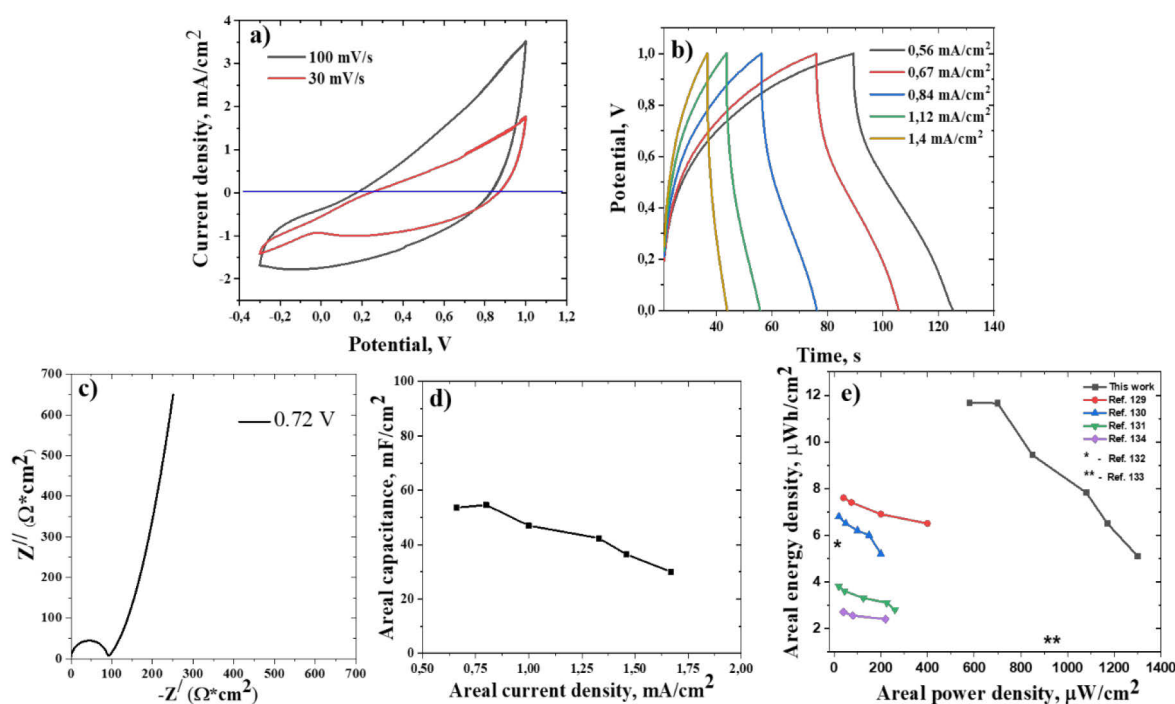


Fig. 14 (a) Cyclic voltammogram, (b) galvanostatic charge-discharge curves, (c) electrochemical impedance spectroscopy, (d) dependence of areal capacitance vs areal current density, (e) dependence of areal energy density vs areal power density and comparison of it with literature data of PEDOT-based supercapacitor measured in 2-electrode cell configuration.

Using EIS, the results in the form of Nyquist plot measured at OCP are presented in the **Fig. 14(c)**. It was showed that a small semi-circle is present at high frequency corresponding low interface resistance, and this result agrees with the low value of iR drop measured using GCD (**Fig. 14(b)**). An almost vertical line is observed at low frequency, indicating capacitive behavior of the assembled symmetrical PEDOT-based supercapacitor. Ragone plot **Fig. 14(e)** was plotted which represents energy and power which are considered to be significant parameters for practical applications of the devices. The obtained values of areal energy density and areal power density (**Fig. 14(e)**) were calculated using **Eq. 4 and 5** and compared with previously published ones and, as might be seen the electrochemical cell prepared by us, possess much higher values.^{129–134}

Conclusion:

It demonstrated the possibility to minimize the number of electrochemical cells for the energy-storage device by the increasing V_{oc} of it. That has been provided without pre-polarization of electrodes but by the pre- and post-treatment of electrodes with the acids, which can form H-bonding interactions. As a result, the electrochemical cell based on PEDOT shows the V_{oc} of 900 mV and possesses much higher areal energy and power compared to literature data.

3.5.2 Solid state electrodes based on the derivate of PEDOT for selective detection of K^+

Electroactive conducting polymers are currently the most popular materials for the preparation of SCISEs. The reason of it that last fulfilled the next requirements: high capacitance (double-layer/redox), good conductivity, and relatively low interfacial resistance (current collector/SC, SC/ISM). Redox couple of conducting polymer is one of the simplest ways to adjust the standard potential of SCISEs. However, it is still a challenge to get reliable initial reproducibility of series of electrodes over time that caused concerns during the certainty of detection. One of reason of that might be hidden in the leaching out of non-covalently bonded redox molecules from ISE during operating. In addition to an undesirable deviation of potential the value of capacitance of SC constructed from conducting polymer reduce as well. A reasonable solution of it might be introduction of pedant groups to the electroactive polymer, which is

covalently bonded to prevent from leaching out and at the same time the charge storage is rising in over than 30 times, compared to unsubstituted one.

In the current work, the PEDOT substituted with hydroquinone (HQ) group was polymerized and studied for K^+ -SCISEs application. The electropolymerization of PEDOT-HQ was carried out using cyclic voltammetry in acetonitrile (MeCN) in the presence of highly hydrophobic ion, potassium tetrakis(pentafluorophenyl)borate (KTFAB), as the supporting electrolyte. The role and nature of counter-ion were well-studied by Lindor et al.,¹³⁵ where authors claim the presence of highly hydrophobic ions avoids accumulation of water, which is diffused through ion-selective membrane (ISM) to the top of SC. Consequently, the existence of unwanted water prevents from deviating and instability of standard potential. Therefore, in the current work, the electropolymerization of PEDOT-HQ was done in the presence of highly hydrophobic KTFAB supporting electrolytes. Using SEM, it was proved PEDOT-HQ polymerized in the presence of TFAB-ion possesses a smooth surface without pores where water molecules might be accumulated (Appendix 6).

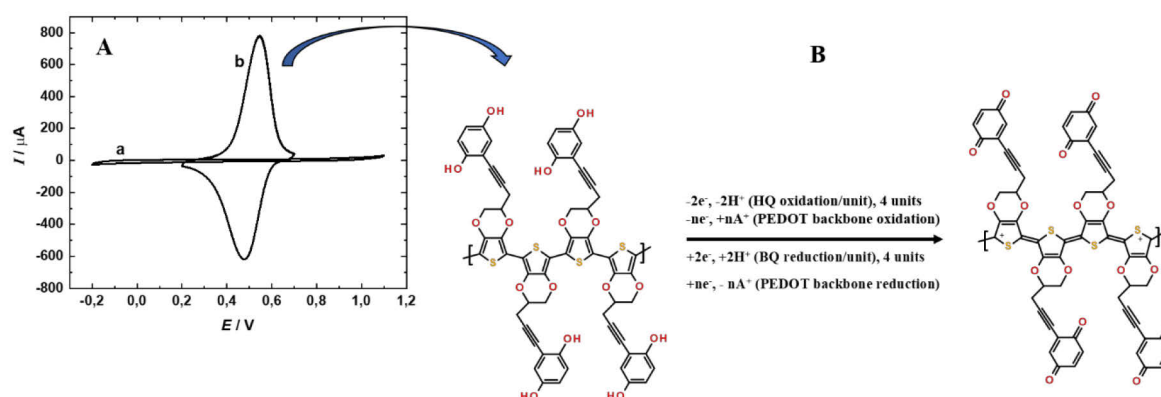


Fig. 15 A (a) Cyclic voltammograms of the unsubstituted PEDOT film without HQ pendant groups, and (b) the PEDOT-HQ film measured in aqueous buffer solution at pH 0 with $V = 50 \text{ mV s}^{-1}$. RE: Ag/AgCl/3M KCl(left), and B schematic representation of oxidation and reduction of PEDOT/HQ polymer (right).

The method of preparation and structure characterization of EDOT/HQ was fully studied and shown by authors, as well as electrochemical polymerization of PEDOT/HQ.¹³⁶ Detailed electrochemical characterization of SC based on PEDOT/HQ was studied using CV and EIS technics in aqueous buffer solution at pH 0. As can be seen in the **Fig. 15A(b)** the recorded voltammogram possesses one broad ox/red peak corresponding to oxidation of HQ.¹³⁷ Generally, the oxidation of HQ to benzoquinone (BQ) consists firstly of the partial oxidation of HQ with the

formation of HQ^+ or semiquinone (SQ^-) and finally full oxidation to benzoquinone. In the **Fig. 15B** is represents the schematic redox reaction of the PEDOT/HQ group. Usually, the oxidation of the PEDOT backbone occurs at lower oxidation potential and results in the formation of charge carriers approximately 0.4 – 0.6 electrons per EDOT unit on the polymer backbone.¹³⁸ On the other hand, the oxidation of the HQ group happens at higher potential and two electrons per every repeating unit take place in storing charge. In order to fulfill the electroneutrality, the highly hydrophobic counter-ion $TFAB^-$ is inserted from polymer mixture. An effect of the pendant group on the value of gained current might be clearly seen on the **Fig. 15A(a)** where the difference of redox current of unsubstituted PEDOT (a) and PEDOT/HQ (b) is shown. To estimate the value of the redox capacitance of PEDOT/HQ the EIS was recorded at 0.3, 0.55, and 0.7 V, respectively. The chosen values of potential for EIS corresponds to the potentials before the HQ/BQ redox peak, at the peak, and after the peak. The calculated capacitance is taken from the low-frequency part of the impedance curve and corresponds to 43 (0.3 V), 489 (0.55 V), and 18 (0.7 V) $mF\ cm^{-2}$. Based on the computed capacitance, the higher value is recorded at the peak (0.55 V) of red/ox of the HQ group and reflects the higher density of charge storage. On the other, it is not possible to gain such a value at lower (0.3 V) and higher (0.7 V) potentials, because these values of applied potentials are not enough to oxidize the HQ to BQ, and is too low to reduce BQ to HQ back, respectively. In order to improve the potential reproducibility of the series of SCs, the pre-polarization of electrodes might be a good solution of it.^{139,140} Therefore, in this work, 5 electrodes were pre-polarized in organic solvent (MeCN), and in the presence of highly hydrophobic $KTFA^-$ counter ions, to prevent from accumulating water. However, it was noticed during the oxidation of PEDOT/HQ in the aprotic medium the only one oxidation peak is occurring, and no reduction peak is observed. The reason for it might be the fact during the oxidation of HQ to BQ the protons are diffuse into the bulk of electrolyte content, and no protons remain close to the interface to take part in the reduction of BQ to HQ. Therefore, by adding a proton source, namely 0.2 M $HClO_4$, it was supposed to overcome this drawback.

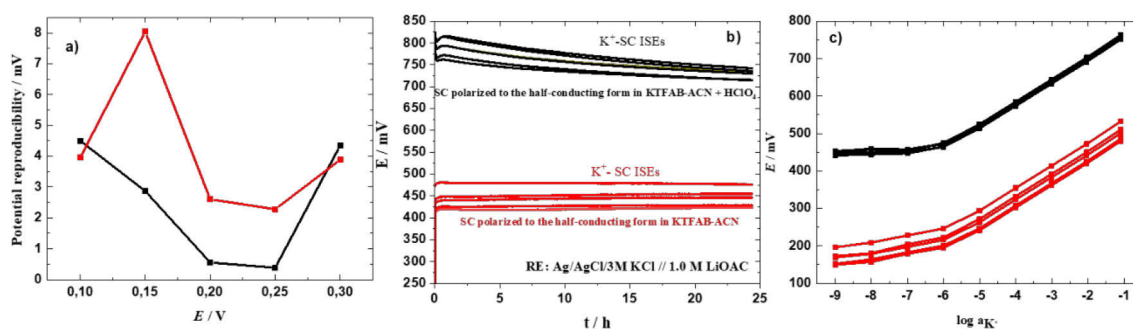


Fig. 16 (a) Potential reproducibility of SC based on PEDOT-HQ initially pre-polarized at the different potential at KTFAB-MeCN (red curve), and KTFAB-MeCN + HClO₄ (black curve), (b) initial potential stability and reproducibility of K-SCISEs_{org} (red curve), and K-SCISEs_{mix} (black curve), (c) potentiometric response of K-SCISEs_{org} (red curve), and K-SCISEs_{mix} (black curve) measured in range 10⁻⁹–10⁻¹ M KCl.

In order to find out the suitable potential for the pre-polarization of SC, the potential reproducibility of SCs in KTFAB-MeCN **Fig. 16(a)** (red curve) and KTFAB-MeCN contained HClO₄ (black curve) at different potential were plotted. As it is shown in the **Fig.16(a)**, the SC pre-polarized in HClO₄ containing KTFAB-MeCN possess the lowest standard deviation (SD) of 0.6 mV and 0.4 mV at 0.2 V and 0.25 V, respectively. On the other hand, SCs pre-polarized in the proton-free solution of KTFAB-MeCN show SD of 2.3 and 2.6 mV at 0.25 and 0.2 V, respectively. We assume, higher irreproducibility of SCs after pre-polarization in proton-free solution is joined with difficulties in adjusting the redox state of HQ in the absence of protons in an aprotic solvent. In the next stage of this study, the initial potential stability of K-SCISEs with SC based on PEDOT/HQ was measured in 0.01 M KCl. As shown in the **Fig. 16(b)**, the initial potential stability of the PEDOT/HQ pre-polarized at 0.25 V (chosen based on previous studies) in the proton containing KTFAB-MeCN(K-SCISEs_{mix}) (**Fig. 16(b)** black curve) is drifting much more than for PEDOT/HQ pre-polarized in aprotic acid (K-SCISEs_{org}) (**Fig. 16(b)** red curve). Also, as shown in the **Fig. 16(b)** the potential reproducibility of K-SCISEs_{mix} and K-SCISEs_{org} deviate in time from ±16 mV to ±9 mV, and ±21.2 mV to ±19 mV during the initial potential stability test. The obtained high values of potential irreproducibility K-SCISEs compared to the SC (±0.4 and ±2.3 mV) are caused by the effect of ISM deposition on the top of SC.¹⁴¹

The calibration curves for the K-SCISEs measured in the concentration range 10⁻⁹-10⁻¹ M KCl for K-SCISEs_{mix} (black curve) and K-SCISEs_{org} (red curve) are shown in the **Fig. 16(c)**. As can be seen in the **Fig. 16(c)** both K-SCISEs have Nernstian response slope (60.8 and 60.9 +0.1 mV pK⁻¹) and detection limit ca 2×10⁻⁷ M KCl. The selectivity of ISM of K-SCISEs was studied as well and, and shown the ISM possesses good selectivity ability towards other ions (more Appendix 6). Additionally, it was showed the prepared K-SCISEs are non-sensitive towards atmosphere-contained gases (such as N₂, O₂, CO₂), and light as well (more in Appendix 6)

Further characterization of K-SCISEs using EIS demonstrate a capacitance of K-SCISE_{mix} and K-SCISE_{org} sufficiently decrease to the 1.1 and 1.5 mF cm⁻² for compared with the measured values 489 mF cm⁻² of SC based on PEDOT/HQ. The reason for it is beneath in the effect of ISM on the top of SC and detection just a minor fraction of capacitance. The existence of the PVC-

based ISM causes insufficient ion transfer in the SC/ISM interface and at the same time prevention from efficient redox reaction of PEDOT/HQ. However, it has been found an obtained value of capacitance 1.1 and 1.5 mF cm⁻² to be enough to avoid changes of $a_{\text{ox}}/a_{\text{red}}$ of PEDOT/HQ -based SC, and consequently drift of potentials (Appendix 6, S.7)

Conclusions:

It was used for the first time, PEDOT with covalently bonded HQ group as solid contact (ion-to-electron transducer) in K-SCISEs. The introduction of covalently joined pedant HQ group increases the redox capacitance of SC in five times (compared to non-substituted PEDOT) and prevent from leaching out of non-covalently bonded redox groups from intermediate layer between current collector and ISM. As a result, the obtained SCISEs based on PEDOT-HQ are insensitive to gases, light with electrodes potential reproducibility ± 2.8 mV (n=5).

4. Conclusions

Within this Thesis, three methods of synthesis of semiconducting organic polymer, PEDOT, were applied. Particularly, during chemical oxidation polymerization, it was shown an effect of Hofmeister ions on polymer structure and its physicochemical properties. Specifically, it has been shown by insertion of ions, which have structure-breaking nature, such as formate, that it is possible to perturb the water cluster-like structure with further hydration of polymer chains. Thanks to the hydration shell over the polymer chains, last might assemble, by H-bonding interactions, into a semi-crystalline structure with bathochromic absorption shift and unique PL properties. Moreover, it was shown, utilizing electrochemical treatment hydrated polymer chains undergo rearrangement of its chains, with the following anisotropy structure formation.

During the electrochemical polymerization of EDOT, the effect of the nature of supporting electrolytes on the structure and physicochemical properties of the obtained polymer was shown. Utilizing different techniques, it was confirmed the intermolecular electrostatic interaction (Coulombic or/and H-bonding) between acid and polymer chains occurs. Furthermore, it was shown that these interactions induced the concentration of localized cation radicals and enhanced the electroactive properties of PEDOT. The obtained results motivated us to construct a symmetrical supercapacitor based on the PEDOT where one electrode was taken as prepared and the second was pre-treated with acid which is good at forming H-bonding. As a result, the electrochemical cell shows the V_{oc} of 900 mV with much better device performance (specific capacity, specific energy and specific power) compared to the published data. Consequently, we

were able to minimize the number of electrochemical cells by increasing of V_{oc} of the cell with help of post-treatment of an electrode by acid.

During acid-assisted polymerization it was demonstrated, for the first time, *via* utilizing Brønsted acid, which is good at making H-bonding, it is possible to prepare stable and soluble semiconducting polymers at room temperature without adding oxidant. The obtained chains have oligomeric nature, which by H-bonding interactions between each other and/or acid form spherical nanostructures. Moreover, by acid-assisted polymerization it is possible to obtain individual polymer chains and study physical-chemical properties of such chains.

During an internship in Finland, it was for the first time used derivate PEDOT, namely to PEDOT-HQ, as solid contact (ion-to-electron transducer) in ISE for the detection of K^+ ions. It was showed the covalently bonded pedant HQ group rise the redox capacitance of solid contact in five times compared to neat PEDOT. As a result, the prepared SCISEs based on PEDOT-HQ possess electrodes potential reproducibility $\pm 2,8$ mV ($n=5$) and are operable in the relevant concentrations of K^+ ions.

5. References

1. H. Naarmann, N. Theophilou New process for the production of metal-like, stable polyacetylene. *Synth. Met.*, **1987**, 22, 1-8.
2. H. Münstedt Aging of electrically conducting organic materials. *Polymer* **1988**, 29, 296-302.
3. F. Jonas, L. Schrader Conductive modifications of polymers with polypyrroles and polythiophenes. *Synth. Met.*, **1991**, 41, 831-836.
4. L. Groenendaal, F. Jonas, D. Freitag, H. Pielartzik, J. R. Reynolds Poly (3,4-ethylenedioxythiophene) and its derivatives: past, present, and future. *Adv. Mater.*, **2000**, 12, 481-494.
5. B. A. Bolto, D. E. Weiss Electronic conduction in polymers. II. The electrochemical reduction of polypyrrole at controlled potential. *Aust. J. Chem.*, **1963**, 16, 1076-1089.
6. G. Heywang, F. Jonas Poly(alkylenedioxythiophene)s – new, very stable conducting polymers. *Adv. Mater.*, **1992**, 116-118.
7. F. Jonas, G. Heywang, W. Schmidtberg, J. Heinze, M. Dietrich Neue Polythiophene, Verfahren zu ihrer Herstellung und ihre Verwendung. **1988**, Eur. Pat. EP 339 340.
8. M.N. Gueye, A. Carella, J. Faure-Vincent, R. Demadrille, J. P. Simonato Progress in understanding structure and transport properties of PEDOT-based materials: A critical review. *Prog. Mater. Sci.*, **2020**, 108, 100616.
9. K. Reuter, S. Kirchmeyer, A. Elschner, PEDOT–properties and technical relevance. *Handbook of Thiophene-Based Materials*. **2009**.
10. H. Yoon, M. Chang, J. Jang Formation of 1D poly (3,4-ethylenedioxythiophene) nanomaterials in reverse microemulsions and their application to chemical sensors. *Adv. Funct. Mater.*, **2007**, 17, 431-436.
11. F. Jiang, R. Yue, Y. Du, J. Xu, P. Yang A one-pot ‘green’ synthesis of Pd-decorated PEDOT nanospheres for nonenzymatic hydrogen peroxide sensing. *Biosens. Bioelectron.*, **2013**, 44, 127-131.
12. Y. Zuo, J. Xu, X. Zhu, X. Duan, L. Lu, Y. Gao, Y. Yu Poly(3,4-ethylenedioxythiophene) nanorods/graphene oxide nanocomposite as a new electrode material for the selective electrochemical detection of mercury (II). *Synth. Met.*, **2016**, 220, 14-19.
13. E. Spain, T. E. Keyes, R. J. Forster DNA sensor based on vapor polymerized PEDOT films functionalized with gold nanoparticles *Biosens. Bioelectron.*, **2013**, 41, 65-70.
14. H. Meng, D. F. Perepichka, F. Wudl, Facile solid-state synthesis of highly conducting poly(3,4-ethylenedioxythiophene). *Angew. Chem.-Int. Edit.*, **2003**, 42, 658-661.
15. A. Özcan, S. İlkbaş Preparation of poly(3,4-ethylenedioxythiophene) nanofibers modified pencil graphite electrode and investigation of over-oxidation conditions for the selective and sensitive determination of uric acid in body fluids. *Anal. Chim. Acta*, **2015**, 891, 312-320.
16. N. Kaur, H. Thakur, R. Kumar, N. Prabhakar An electrochemical sensor modified with poly(3,4-ethylenedioxythiophene)-wrapped multi-walled carbon nanotubes for enzyme inhibition-based determination of organophosphates. *Microchim. Acta*, **2016**, 183, 2307-2315.
17. F. Jonas, W. Krafft EP 440 957 (Bayer AG). Prior: December, **1990**, 20.

18. R. Corradi, S. P. Armes, Chemical synthesis of poly (3,4-ethylenedioxythiophene). *Synth. Met.*, **1997**, 84, 453-454.
19. R. Brooke, P. Cottis, P. Talemi, M. Fabretto, P. Murphy, D. Evans Recent advances in the synthesis of conducting polymers from the vapour phase. *Prog. Mater. Sci.*, **2017**, 86, 127-146.
20. T. Yamamoto, M. Abla Synthesis of non-doped PEDOT and its spectroscopic data. *Synth. Met.* **1999**, 100, 237-239.
21. Q. Pei, G. Zuccarello, M. Ahlskog, O. Inganäs Electrochromic and highly stable poly(3,4-ethylenedioxythiophene) switches between opaque blue-black and transparent sky blue. *Polymer*, **1994**, 35, 1347-1351.
22. O. Zhang, Y. Wen, J. Xu, L. Lu, X. Duan, H. Yu One-step synthesis of poly(3,4-ethylenedioxythiophene)-Au composites and their application for the detection of nitrite. *Synth. Met.*, **2013**, 164, 47-51.
23. J. Bobacka Potential stability of all-solid-state ion-selective electrodes using conducting polymers as ion-to-electron transducers. *Anal. Chem.*, **1999**, 71, 4932-4937.
24. N. Sakmeche, J. J. Aaron, M. Fall, S. Aeiyaeh, M. Jouini, J. C. Lacroix, P. C. Lacaze Anionic micelles: a new aqueous medium for electropolymerization of poly(3,4-ethylenedioxythiophene) films on Pt electrodes. *Chem. Commun.*, **1996**, 24, 2723-2724.
25. K. Cysewska, J. Karczewski, P. Jasiński Influence of electropolymerization conditions on the morphological and electrical properties of PEDOT film. *Electrochim. Acta*, **2015**, 176, 156-161.
26. T. Y. Kim, J. E. Kim, K. S. Suh Effects of alcoholic solvents on the conductivity of tosylate-doped poly(3,4-ethylenedioxythiophene) (PEDOT-OTs). *Polym. Int.*, **2006**, 55, 80-86.
27. E. Poverenov, M. Li, A. Bitler, M. Bendikov Major effect of electropolymerization solvent on morphology and electrochromic properties of PEDOT films. *Chem. Mater.*, **2010**, 22, 4019-4025.
28. N. J. Guernion, W. Hayes 3-and 3,4-substituted pyrroles and thiophenes and their corresponding polymers - A review. *Curr. Org. Chem.*, **2004**, 8, 637-651.
29. H. Meng, D. F. Perepichka, M. Bendikov, F. Wudl, G. Z. Pan, W. Yu, S. Brown solid-state synthesis of a conducting polythiophene via an unprecedented heterocyclic coupling reaction. *J. Am. Chem. Soc.*, **2003**, 125, 15151-15162.
30. P. Wagner, K. W. Jolley, D. L. Officer Why do some alkoxybromothiophenes spontaneously polymerize? *Aust. J. Chem.*, **2011**, 64, 335.
31. D. K. Grant, K. W. Jolley, D. L. Officer, K. C. Gordon, T. M. Clarke Towards functionalized poly(terthiophenes): regioselective synthesis of oligoether-substituted bis (styryl) sexithiophenes. *Org. Biomol. Chem.*, **2005**, 3, 2008-2015.
32. P. Wagner, A. M. Ballantyne, K. W. Jolley, D. L. Officer Synthesis and characterization of novel styryl-substituted oligothiophenylenevinylenes. *Tetrahedron*, **2006**, 62, 2190-2199.
33. B. Bonillo, T. M. Swager Chain-growth polymerization of 2-chlorothiophenes promoted by Lewis acids. *J. Am. Chem. Soc.*, **2012**, 134, 18916.
34. F. Genoud, I. Kulszewicz-Bajer, B. Dufour, P. Rannou, A. Pron Lewis acid doping of poly(aniline)-processing, spectroscopic and structural consequences. *Synth. Met.*, **2001**, 119, 415-416.

35. K. Bienkowski, I. Kulszewicz-Bajer, F. Genoud, J. L. Oddou, A. Pron Conjugated polymers doped with Lewis acids. *Synth. Met.*, **2003**, 135, 159-160.
36. F. S. Bates, G. H. Fredrickson, Block copolymers-designer soft materials. *Phys. Today*, 2000, 52.
37. R. Umapathi, P. M. Reddy, A. Rani, P. Venkatesu Influence of additives on thermoresponsive polymers in aqueous media: a case study of poly (*N*-isopropylacrylamide). *Phys. Chem. Chem. Phys.*, **2018**, 20, 9717-9744.
38. Y. Marcus, Effect of ions on the structure of water: structure making and breaking. *Chem. Rev.*, **2009**, 109, 1346-1370.
39. E. Lee, J. H. Choi, M. Cho The effect of Hofmeister anions on water structure at protein surfaces. *Phys. Chem. Chem. Phys.*, **2017**, 19, 20008-20015.
40. K. Aoki, K. Shiraki, T. Hattori Salt effects on the picosecond dynamics of lysozyme hydration water investigated by terahertz time-domain spectroscopy and an insight into the Hofmeister series for protein stability and solubility *Phys. Chem. Chem. Phys.*, **2016**, 18, 15060-15069.
41. T. Janc, M. Lukšič, V. Vlachy, B. Rigaud, A. L. Rollet, J. P. Korb, N. Malikova Ion-specificity and surface water dynamics in protein solutions. *Phys. Chem. Chem. Phys.*, **2018**, 20, 30340-30350.
42. Y. Marcus Viscosity B-coefficients, structural entropies and heat capacities, and the effects of ions on the structure of water. *J. Sol. Chem.*, **1994**, 23, 831-848.
43. J. Chik, S. Mizrahi, S. Chi, V. A. Parsegian, D. C. Rau Hydration forces underlie the exclusion of salts and of neutral polar solutes from hydroxypropylcellulose. *J. Phys. Chem. B*, **2005**, 109, 9111-9118.
44. B. Kang, H. Tang, Z. Zhao, S. Song Hofmeister series: Insights of ion specificity from amphiphilic assembly and interface property. *ACS Omega*, **2020**, 5, 6229-6239.
45. N. Gospodinova, S. Dorey, D. Anokhin, D. Ivanov, Y. Romanova, H. Kolev Method of preparation polyaniline films and highly self-oriented films obtained **2008**; FR Pat 2, 928, 646.
46. N. Gospodinova, D. Ivanov, D. Anokhin, I. Mihai, L. Vidal, S. Brun, J. Romanova, A. Tadjer Unprecedented route to ordered polyaniline: direct synthesis of highly crystalline fibrillar films with strong π - π stacking alignment. *Macromol. Rapid Commun.* **2009**, 30, 29-33.
47. N. Gospodinova, E. Tomsik, J. Romanova Thin mesoporous polyaniline films manifesting a water-promoted photovoltaic effect. *Chem. Pap.*, **2013**, 67, 972-978.
48. M. Qiu, S. Long, B. Li, L. Yan, W. Xie, Y. Niu, A. Xia Toward an understanding of how the optical property of water-soluble cationic polythiophene derivative is altered by the addition of salts: The Hofmeister effect. *J. Phys. Chem. C*, **2013**, 117, 21870-21878.
49. W. J. Xie, Y. Q. Gao, A simple theory for the Hofmeister series. *J. Phys. Chem. Lett.*, **2013**, 4, 4247-4252.
50. T. Oncsik, A. Desert, G. Trefalt, M. Borkovec, I. Szilagyi Charging and aggregation of latex particles in aqueous solutions of ionic liquids: towards an extended Hofmeister series. *Phys. Chem. Chem. Phys.*, **2016**, 18, 7511-7520.
51. N. Gospodinova, E. Tomšik Hydrogen-bonding versus π - π stacking in the design of organic semiconductors: From dyes to oligomers. *Prog. Polym. Sci.*, **2015**, 43, 33-47.

52. J. D. Dunitz, A. Gavezzotti How molecules stick together in organic crystals: weak intermolecular interactions. *Chem. Soc. Rev.*, **2009**, 38, 2622-2633.
53. C. A. Hunter, J. K. Sanders The nature of π - π interactions. *J. Am. Chem. Soc.*, **1990**, 112, 5525-5534.
54. J. D. Dunitz, Weak intermolecular interactions in solids and liquids. *Mol. Cryst. Liq. Cryst. Sci. Technol. A: Mol. Cryst. Liq. Cryst.*, **1996**, 279, 209-218.
55. K. S. Pitzer, The nature of the chemical bond and the structure of molecules and crystals: an introduction to modern structural chemistry. *J. Am. Chem. Soc.*, **1960**, 82, 4121-4121.
56. Y. Suna, J. I. Nishida, Y. Fujisaki, Y. Yamashita Ambipolar behavior of hydrogen-bonded diketopyrrolopyrrole–thiophene co-oligomers formed from their soluble precursors. *Org. Lett.*, **2012**, 14, 3356-3359.
57. E. E. Jelley Spectral absorption and fluorescence of dyes in the molecular state. *Nature*, **1936**, 138, 1009-1010.
58. E. E. Jelley Molecular, nematic and crystal states of I: I-diethyl-cyanine chloride. *Nature*, **1937**, 139, 631-631.
59. S. E. Sheppard The optical and sensitising properties of the iso cyanine dyes. *J. Chem. Soc. Trans.*, **1909**, 95, 15-19.
60. S. E. Sheppard, The effects of environment and aggregation on the absorption spectra of dyes. *Rev. Mod. Phys.*, **1942**, 14, 303.
61. J. Zhou, B. Liao, G. Chen First-principles calculations of thermal, electrical, and thermoelectric transport properties of semiconductors. *Semicond. Sci. Technol.*, **2016**, 31, 043001.
62. Y. Yao, H. Dong, W. Hu Charge transport in organic and polymeric semiconductors for flexible and stretchable devices. *Adv. Mater.*, **2016**, 28, 4513-4523.
63. Q. Wei, M. Mukaida, K. Kirihara, T. Ishida, Experimental studies on the anisotropic thermoelectric properties of conducting polymer films. *ACS Macro Lett.*, **2014**, 3, 948-952.
64. S. N. Patel, M. L. Chabinye Anisotropies and the thermoelectric properties of semiconducting polymers. *J. Appl. Polym. Sci.*, **2017**, 134, 44403.
65. P. W. Anderson Absence of diffusion in certain random lattices. *Phys. Rev.*, **1958**, 109, 1492.
66. N. F. Mott Conduction in non-crystalline materials: III. Localized states in a pseudogap and near extremities of conduction and valence bands. *Phil. Mag.*, **1969**, 19, 835-852.
67. S. Ihnatsenka, X. Crispin, I. Zozoulenko Understanding hopping transport and thermoelectric properties of conducting polymers. *Phys. Rev. B*, **2015**, 92, 035201.
68. R. Menon, C. O. Yoon, D. Moses, A. J. Heeger, Y. Cao, Transport in polyaniline near the critical regime of the metal-insulator transition. *Phys. Rev. B*, **1993**, 48, 17685.
69. D. Farka, H. Coskun, J. Gasiorowski, C. Cobet, K. Hingerl, L. M. Uiberlacker, P. Stadler Anderson-localization and the Mott–Ioffe–Regel limit in glassy-metallic PEDOT. *Adv. Electron. Mater.*, **2017**, 3, 1700050.
70. P. Sheng Fluctuation-induced tunneling conduction in disordered materials. *Phys. Rev. B* **1980**, 21, 2180.
71. L. Zuppiroli, M. N. Bussac, S. Paschen, O. Chauvet, L. Forro Hopping in disordered conducting polymers. *Phys. Rev. B*, **1994**, 50, 196–203.
72. S. Kivelson, G. T. Zimanyi High temperature superconductors, RVB, and conducting polymers. *Mol. Cryst. Liq. Cryst.*, **1988**, 160, 457-481.

73. S. Kivelson, A. Heeger Intrinsic conductivity of conducting polymers. *Synth. Met.* **1988**, 22, 371–84.
74. M. Winter, R. J. Brodd What are batteries, fuel cells, and supercapacitors? *Chem. Rev.*, **2004**, 104, 4245-4270.
75. P. S. Joshi, D. S. Sutrave Supercapacitor: Basics and overview. *J. Inf. Comput. Sci.*, **2019**, 9, 609–625.
76. P. Simon, Y. Gogotsi Materials for electrochemical capacitors. *Nanoscience and technology: a collection of reviews from Nature journals*, **2010**, 320-329.
77. M. Zhi, C. Xiang, J. Li, M. Li, N. Wu Nanostructured carbon–metal oxide composite electrodes for supercapacitors: a review. *Nanoscale*, **2013**, 5, 72-88.
78. W. H. Kim, A. J. Mäkinen, N. Nikolov, R. Shashidhar, H. Kim, Z. H. Kafafi Molecular organic light-emitting diodes using highly conducting polymers as anodes. *Appl. Phys. Lett.*, **2002**, 80, 3844-3846.
79. M. Fabretto, J. P. Autere, D. Hoglinger, S. Field, P. Murphy Vacuum vapour phase polymerised poly(3,4-ethylenedioxythiophene) thin films for use in large-scale electrochromic devices. *Thin Solid Films*, **2011**, 519, 2544-2549.
80. A. Kros, van S. W. Hövell, N. A. Sommerdijk, R. J. Nolte Poly(3,4-ethylenedioxythiophene) -based glucose biosensors. *Adv. Mater.*, **2001**, 13, 1555-1557.
81. J. Reynolds, T. A. Skotheim, R. L. Elsenbaumer Handbook of Conducting Polymers. Transition in Doped Conducting Polymers. Texas Univ. at Arlington, **1995**.
82. J. Janata, Principles of chemical sensors. Springer Science and Business Media, **2010**.
83. E. Bakker, M. Telting-Diaz Electrochemical sensors. *Anal. Chem.*, **2004**, 76, 3285.
84. R. W. Cattrall, H. Freiser, Coated wire ion-selective electrodes. *Anal. Chem.*, **1971**, 43, 1905.
85. E. Lindner, V. V. Cosofret, S. Ufer, T. A. Johnson, R. B. Ash, H. T. Nagle, M. R. Neuman, R. P. Buck, J. Fresenius In vivo and in vitro testing of microelectronically fabricated planar sensors designed for applications in cardiology. *Anal. Chem.*, **1993**, 346, 584.
86. V. V. Cosofret, M. Erdçsy, T. A. Johnson, R. P. Buck, R. B. Ash, M. R. Neuman, Microfabricated sensor arrays sensitive to pH and K⁺ for ionic distribution measurements in the beating heart. *Anal. Chem.*, **1995**, 67, 1647.
87. J. Bobacka Conducting polymer-based solid-state ion-selective electrodes. *Electroanalysis*, **2006**, 18, 7-18.
88. J. Bobacka Potential stability of all-solid-state ion-selective electrodes using conducting polymers as ion-to-electron transducers. *Anal. Chem.*, **1999**, 71, 4932
89. J. Bobacka, A. Ivaska, A. Lewenstam Potentiometric ion sensors. *Chem. Rev.*, **2008**, 108, 329-351.
90. E. Bakker, D. Diamond, A. Lewenstam, E. Pretsch, Ion sensors: current limits and new trends. *Anal. Chim. Acta* **1999**, 393, 11.
91. T. Sokalski, A. Ceresa, T. Zwickl, E. Pretsch, Large improvement of the lower detection limit of ion-selective polymer membrane electrodes *J. Am. Chem. Soc.*, **1997**, 119, 11347.
92. F. Garnier, Functionalized conducting polymers—Towards intelligent materials. *Angew. Chem.*, **1989**, 101, 529-533.
93. F. F. Jian, E. Liu, J. Ma Effects of different oxygen-containing anions on the structure of water clusters. *Supramol. Chem.*, **2019**, 31, 283-287.

94. E. S. Matveeva, R. D. Calleja, V. P. Parkhutik Thermogravimetric and calorimetric studies of water absorbed in polyaniline. *Synth. Met.*, **1995**, 72, 105-110.
95. H. Yoshida, T. Hatakeyama, H. Hatakeyama, *Polym. Prepr.*, **1992**, 41, 1287.
96. Y. Jin, Q. Chen, P. Lessner, Thermal stability investigation of PEDOT films from chemical oxidation and prepolymerized dispersion. *Electrochem.*, **2013**, 81, 801-803.
97. W. E. B. Shepherd, R. Grollman, A. Robertson, K. Paudel, R. Hallani, M. A. Loth, J. E. Anthony, O. Ostroverkhova Single-molecule imaging of organic semiconductors: Toward nanoscale insights into photophysics and molecular packing. *Chem. Phys. Lett.*, **2015**, 629, 29-39.
98. S. Garreau, G. Louarn, J. P. Buisson, G. Froyer, S. Lefrant In situ spectroelectrochemical Raman studies of poly(3,4-ethylenedioxythiophene) (PEDOT). *Macromolecules*, **1999**, 32, 6807-6812.
99. S. A. Spanninga, D. C. Martin, Z. Chen X-ray photoelectron spectroscopy study of counterion incorporation in poly(3,4-ethylenedioxythiophene). *J. Phys. Chem. C*, **2009**, 113, 5585.
100. M. Bowker, R. J. Madix XPS, UPS and thermal desorption studies of the reactions of formaldehyde and formic acid with the Cu (110) surface. *Surf. Sci.*, **1981**, 102, 542-565.
101. K. E. Aasmundtveit, E. J. Samuelsen, L. A. A. Pettersson, O. Inganas, T. Johansson, R. Feidenhans'l Structural aspects of electrochemical doping and dedoping of poly(3,4-ethylenedioxythiophene). *Synth. Met.*, **1999**, 101, 561.
102. L. Niu, C. Kvarnstrom, K. Froberg, A. Ivaska Electrochemically controlled surface morphology and crystallinity in poly(3,4-ethylenedioxythiophene) films. *Synth. Met.*, **2001**, 122, 425
103. T. L. Malkin, B. J. Murray, A. V. Brukhno, J. Anwar, C. G. Salzmann Structure of ice crystallized from supercooled water. *Proc. Natl. Acad. Sci. U. S. A.*, **2012**, 109, 1041.
104. M. Ujvári, J. Gubicza, V. Kondratiev, K. J. Szekeres, G. G. Láng Morphological changes in electrochemically deposited poly(3,4-ethylenedioxythiophene) films during overoxidation. *J. Solid State Electrochem.*, **2015**, 19, 1247-1252.
105. W. W. Chiu, J. Travas-Sejdić, R. P. Cooney, G. A. Bowmaker Studies of dopant effects in poly(3,4-ethylenedioxythiophene) using Raman spectroscopy. *J. Raman Spectrosc.*, **2006**, 37, 1354-1361.
106. X. Crispin, S. Marciniak, W. Osikowicz, G. Zotti, A. W. D. van der Gon, F. Louwet, M. Fahlman, L. Groenendaal, F. De Schryver, W. R. Salaneck Conductivity, morphology, interfacial chemistry, and stability of poly(3,4-ethylenedioxythiophene)-poly(styrene sulfonate): A photoelectron spectroscopy study. *J. Polym. Sci., Part B: Polym. Phys.* **2003**, 41, 2561-2583.
107. C. V. Amanchukwu, M. Gauthier, T. P. Batcho, C. Symister, Y. Shao-Horn, J. M. D'Arcy, P. T. Hammond Evaluation and stability of PEDOT polymer electrodes for Li-O₂ batteries. *J. Phys. Chem. Lett.* **2016**, 7, 3770-3775.
108. N. Kim, B. H. Lee, D. Choi, G. Kim, H. Kim, J.-R. Kim, J. Lee, Y. Kang, K. Lee Role of interchain coupling in the metallic state of conducting polymers. *Phys. Rev. Lett.* **2012**, 109, 106405
109. H. C. Tian, J. Q. Liu, X. Y. Kang, D. X. Wei, C. Zhang, J. C. Du, C. S. Yang Biotic and abiotic molecule dopants determining the electrochemical performance, stability and

- fibroblast behavior of conducting polymer for tissue interface. *RSC Adv.*, **2014**, 4, 47461-47471.
110. N. K. Sidhu, A. C. Rastogi Electrochemical performance of supercapacitors based on carbon nanofoam composite and microporous poly (3,4-ethylenedioxythiophene) thin film asymmetric electrodes. *Mater. Chem. Phys.*, **2016**, 176, 75-86.
 111. N. Z. Menshutkin *Physik. Chem.* **1890**, 5, 589–600.
 112. R. J. Bartholomew, D. E. Irish, Raman spectral study of ‘neat’ formic acid and aqueous and organic solutions of formic acid. *J. Raman Spectrosc.* **1999**, 30, 325-334.
 113. D. Han, J. Li, Q. Zhang, Z. He, Z. Wu, J. Chu, Y. Lu Synthesis of π -conjugated polymers containing benzotriazole units via palladium-catalyzed direct C–H cross-coupling polycondensation for OLEDs applications. *Polymers*, **2021**, 13, 254.
 114. B. M. Schulze, N. T. Shewmon, J. Zhang, D. L. Watkins, J. P. Mudrick, W. Cao, R. B. Zerdan, A. J. Quartarao, I. Ghiviriga, J. Xue, R. K. Castellano Consequences of hydrogen bonding on molecular organization and charge transport in molecular organic photovoltaic materials. *J. Mater. Chem. A*, **2014**, 2, 1541-1549.
 115. I. Zozoulenko, A. Singh, S. K. Singh, V. Gueskine, X. Crispin, M. Berggren Polarons, bipolarons, and absorption spectroscopy of PEDOT. *ACS Appl. Polym. Mater.*, **2018**, 1, 83-94.
 116. M. Kumar Ram, G. Mascetti, S. Paddeu, E. Maccioni, C. Nicolini Optical, structural and fluorescence microscopic studies on reduced form of polyaniline: the leucoemeraldine base. *Synth. Met.*, **1997**, 89, 63-69.
 117. R. G. Thorne, J. G. Master, S. A. Williams, A. G. MacDiarmid, R. M. Hochstrasser Polyaniline, a dynamic block copolymer: key to attaining its intrinsic conductivity? *Synth. Met.*, **1992**, 49, 423-428
 118. A. Elschner, S. Kirchmeyer, W. Lovenich, U. Merker, K. Reuter PEDOT: principles and applications of an intrinsically conductive polymer. CRC Press, **2010**.
 119. J. Y. Shimano, A. G. MacDiarmid Polyaniline, a dynamic block copolymer: key to attaining its intrinsic conductivity? *Synth. Met.*, **2001**, 123, 251-262.
 120. H. Sun, B. Lu, X. Duan, J. Xu, L. Dong, X. Zhu, K. Zhang, D. Hu, S. Ming Electrosynthesis and characterization of a new conducting copolymer from 2'-aminomethyl-3,4-ethylenedioxythiophene and 3,4-ethylenedioxythiophene. *Int. J. Electrochem. Sci.*, **2015**, 10, 3236-3249.
 121. K. P. Prasad, Y. Chen, M. A. Sk, A. Than, Y. Wang, H. Sun, K. H. Lim, X. Dong, P. Chen Fluorescent quantum dots derived from PEDOT and their applications in optical imaging and sensing. *Mater. Horizons*, **2014**, 1, 529-534.
 122. I. Cruz-Cruz, M. Reyes-Reyes, I. A. Rosales-Gallegos, A. Y. Gorbachev, J. M. Flores-Camacho, R. Lopez-Sandoval Visible luminescence of dedoped DBU-treated PEDOT: PSS films. *J. Phys. Chem. C*, **2015**, 119, 19305-19311.
 123. M. Fakis, D. Anastopoulos, V. Giannetas, P. Persephonis Influence of aggregates and solvent aromaticity on the emission of conjugated polymers. *J. Phys. Chem. B*, **2006**, 110, 24897-24902.
 124. A. Y. Sosorev, O. D. Parashchuk, S. A. Zapunidi, G. S. Kashtanov, I. V. Golovnin, S. Kommanaboyina, D. Y. Paraschuk Threshold-like complexation of conjugated polymers

- with small molecule acceptors in solution within the neighbor-effect model. *Phys. Chem. Chem. Phys.*, **2016**, 18, 4684-4696.
125. S. R. Amrutha, M. Jayakannan Probing the π -stacking induced molecular aggregation in π -conjugated polymers, oligomers, and their blends of p-phenylenevinylenes. *J. Phys. Chem. B*, **2008**, 112, 1119-1129.
 126. G. Scheibe, A. Schontag, F. Katheder Fluorescence and energy transmission in reversible polymerized pigments, *Sci. Nat.* **1939**, 27, 499-501.
 127. B. P. Sogo, M. Nakazaki, M. Calvin Free radical from perinaphthene. *J. Chem. Phys.*, **1957**, 26, 1343-1345.
 128. D. H. Reid Stable π -electron systems and new aromatic structures. *Tetrahedron*, **1958**, 3, 339-352.
 129. Z. Wang, J. Cheng, Q. Guan, H. Huang, Y. Li, J. Zhou, W. Ni, B. Wang, S. He, H. Peng All-in-one fiber for stretchable fiber-shaped tandem supercapacitors. *Nano Energy*, **2018**, 45, 210-219.
 130. D. Yuan, B. Li, J. Cheng, Q. Guan, Z. Wang, W. Ni, C. Li, H. Liu, B. Wang Twisted yarns for fiber-shaped supercapacitors based on wet-spun PEDOT: PSS fibers from aqueous coagulation. *J. Mater. Chem. A*, **2016**, 4, 11616-11624.
 131. G. Qu, J. Cheng, X. Li, D. Yuan, P. Chen, X. Chen, B. Wang, H. Peng A fiber supercapacitor with high energy density based on hollow graphene/conducting polymer fiber electrode. *Adv. Mater.* **2016**, 28, 3646-3652.
 132. L. Kou, T. Huang, B. Zheng, Y. Han, X. Zhao, K. Gopalsamy, H. Sun, C. Gao Coaxial wet-spun yarn supercapacitors for high-energy density and safe wearable electronics. *Nat. Commun.*, **2014**, 5, 1-10.
 133. Y. Fu, X. Cai, H. Wu, Z. Lv, S. Hou, M. Peng, X. Yu, D. Zou Fiber supercapacitors utilizing pen ink for flexible/wearable energy storage. *Adv. Mater.*, **2012**, 24, 5713-5718.
 134. Y. Jin, Z. Li, L. Qin, X. Liu, L. Mao, Y. Wang, F. Qin, Y. Liu, Y. Zhou, F. Zhang Laminated free standing PEDOT:PSS electrode for solution processed integrated photocapacitors via hydrogen-bond interaction. *Adv. Mater. Interfaces*, **2017**, 1700704.
 135. T. Lindfors, F. Sundfors, L. Höfler, R. E. Gyurcsányi FTIR-ATR study of water uptake and diffusion through ion-selective membranes based on plasticized poly (vinyl chloride). *Electroanalysis*, **2009**, 21, 1914-1922.
 136. M. Sterby, R. Emanuelsson, X. Huang, A. Gogoll, M. Strømme, M. Sjödin Characterization of PEDOT-quinone conducting redox polymers for water based secondary batteries. *Electrochim. Acta*, **2017**, 235, 356-364.
 137. M. Sterby, R. Emanuelsson, F. Mamedov, M. Stromme, M. Sjodin Investigating electron transport in a PEDOT/quinone conducting redox polymer with in situ methods. *Electrochim. Acta*, **2019**, 308, 277-284.
 138. L. Groenendaal, G. Zotti, P. H. Aubert, S.M. Waybright, J. R. Reynolds, Electrochemistry of poly(3,4-alkylenedioxythiophene) derivatives, *Adv Mater.*, **2003**, 15, 855-879.
 139. T. Lindfors Light sensitivity and potential stability of electrically conducting polymers commonly used in solid contact ion-selective electrodes, *J. Solid State Electrochem.*, **2009**, 13, 77-89.
 140. N. He, R. E. Gyurcsanyi, T. Lindfors Electropolymerized hydrophobic polyazulene as solid-contacts in potassium-selective electrodes. *Analyst*, **2016**, 141, 2990-2997.

141. S. Papp, M. Bojtar, R. E. Gyurcsanyi, T. Lindfors Potential reproducibility of potassium-selective electrodes having perfluorinated alkanooate side chain functionalized poly(3,4-ethylenedioxythiophene) as a hydrophobic solid contact. *Anal. Chem.*, **2019**, 91, 9111–9118.

6. List of publications and contributions at conferences

Publications included into this Thesis

1. Ivanko, I.; Pánek, J.; Svoboda, J.; Zhigunov, A.; Tomšík, E. Tuning the photoluminescence and anisotropic structure of PEDOT, *J. Mater. Chem. C*, **7**, 7013-7019 (2019). IF = 7,393.
Doi [10.1039/c9tc00955h](https://doi.org/10.1039/c9tc00955h)
2. Ivanko, I.; Svoboda, J.; Lukešová, M.; Šeděnková, I.; Tomšík, E. Hydrogen Bonding as a Tool to Control Chain Structure of PEDOT: Electrochemical Synthesis in the Presence of Different Electrolytes, *Macromolecules*, **53**, 2464-2473 (2020). IF = 5,985.
Doi [10.1021/acs.macromol.9b02627](https://doi.org/10.1021/acs.macromol.9b02627)
3. Tomšík, E.; Ivanko, I.; Svoboda, J.; Zhigunov, A.; Hromádková, J.; Pánek, J.; Lukešová, M.; Velychkivska, N.; Janisová, L. Method of Preparation of Soluble PEDOT: Self-Polymerization of EDOT without Oxidant at Room Temperature, *Macromol. Chem. Phys.* **221**, 2000219 (2020). IF = 2,527.
Doi [10.1002/macp.202000219](https://doi.org/10.1002/macp.202000219)
4. Ivanko, I.; Mahun, A.; Kobera, L.; Černochová, Z.; Pavlova, E.; Toman, P.; Pientka, Z.; Štěpánek, P.; Tomšík, E. Synergy between assembly of individual PEDOT chains and their interaction with light, *Macromolecules*, **54**, 10321-10330 (2021). IF = 5,985.
Doi doi.org/10.1021/acs.macromol.1c01975
5. Ivanko, I.; Tomšík, E. Effect of hydrogen bonding on a value of an open circuit potential of poly-(3,4-ethylenedioxythiophene) as a beneficial mode for energy storage devices, *Adv. Funct. Mater.* **31**, 2103001(2021). IF = 18,808.
Doi [10.1002/adfm.202103001](https://doi.org/10.1002/adfm.202103001)
6. Ivanko, I.; Lindfors, T.; Emanuelsson, R.; Sjodin, M. Conjugated redox polymer with poly(3,4-ethylenedioxythiophene) backbone and hydroquinone pendant groups as the solid contact in potassium-selective electrodes, *Sens. Actuators B Chem.* **329**, 129231(2021). IF = 7,460.
Doi [10.1016/j.snb.2020.129231](https://doi.org/10.1016/j.snb.2020.129231)

Publications not included into this Thesis

1. Tomšík, E.; Ivanko, I.; Kohut, O.; Hromádková, J. High-Rate Polyaniline/Carbon-Cloth Electrodes: Effect of Mass Loading on the Pseudocapacitive Performance, *ChemElectroChem*, **4**, 2884-2890(2017). IF = 4.590.
Doi 10.1002/celec.201700793
2. Tomšík, E.; Konefal, M.; Kohut, O.; Ivanko, I.; Hromádková, J.; Zhigunov, A.; Steinhart, M. Phase Transitions of Polyaniline Induced by Electrochemical Treatment, *Macromol. Chem. Phys.* **219**, 1700627(2017). IF = 2,527.
Doi 10.1002/macp.201700627
3. Tomšík, E.; Kohut, O.; Ivanko, I.; Pekarek, M.; Biellošapka, I.; Dallas, P. Assembly and Interaction of Polyaniline Chains: Impact on Electro- and Physical-Chemical Behavior, *J. Phys. Chem. C*, **122**, 8022–8030(2018). IF = 4,126.
Doi 10.1021/acs.jpcc.8b01948
4. Urbánek, T.; Ivanko, I.; Svoboda, J.; Tomšík, E.; Hrubý, M. Selective potentiometric detection of reactive oxygen species (ROS) in biologically relevant concentrations by modified metalized polyporphyrine sensing layer coated with nonbiofouling poly(2-alkyl-2oxazoline)s, *Sens. Actuators B Chem.* **under review**.

Contributions at international conferences

Oral presentation

1. Ivanko I., Tomšík, E., Effect of hydrogen bonding on a value of an open circuit potential of poly-(3,4-ethylenedioxythiophene) as a beneficial mode for energy storage devices, 72. sjezd chemiků, Praha, ČR, 2020.

Poster presentations

1. Ivanko, I., Kredatusová, J., Tomšík, E., Physical-chemical properties of hydrated and self-assembled poly (3,4- ethylenedioxythiophene) chains, Workshop "Career in Polymers X". Prague, CR, 2018.
2. Ivanko, I., Svoboda, J., Šeděnková, I., Lukešová, M., Tomšík E., Elucidating the role of hydrogen-bond interactions on physicochemical properties of PEDOT, Workshop "Career in Polymers X". Prague, CR, 2019.
3. Ivanko I., Tomšík, E., Correlation between H-bonding formation and value of an open circuit potential of symmetrical supercapacitor based on poly(3,4-ethylenedioxythiophene), Young Polymer Scientists Conference and Short Course /72/, Lodz, Poland, 2021.

7. Appendices – attached publications

List of appendices – publications included into this Thesis

Appendix 1

Ivanko, I.; Pánek, J.; Svoboda, J.; Zhigunov, A.; Tomšík, E. Tuning the photoluminescence and anisotropic structure of PEDOT, *J. Mater. Chem. C*, **7**, 7013-7019 (2019). IF = 7,393.

Appendix 2

Ivanko, I.; Svoboda, J.; Lukešová, M.; Šeděnková, I.; Tomšík, E. Hydrogen Bonding as a Tool to Control Chain Structure of PEDOT: Electrochemical Synthesis in the Presence of Different Electrolytes, *Macromolecules*, **53**, 2464-2473 (2020). IF = 5,985.

Appendix 3

Ivanko, I.; Mahun, A.; Kobera, L.; Černochová, Z.; Pavlova, E.; Toman, P.; Pientka, Z.; Štěpánek, P.; Tomšík, E. Synergy between assembly of individual PEDOT chains and their interaction with light, *Macromolecules*, **54**, 10321-10330 (2021). IF = 5,985.

Appendix 4

Tomšík, E.; Ivanko, I.; Svoboda, J.; Zhigunov, A.; Hromádková, J.; Pánek, J.; Lukešová, M.; Velychkivska, N.; Janisová, L. Method of Preparation of Soluble PEDOT: Self-Polymerization of EDOT without Oxidant at Room Temperature, *Macromol. Chem. Phys.* **221**, 2000219 (2020). IF = 2,527.

Appendix 5

Ivanko, I.; Tomšík, E. Effect of hydrogen bonding on a value of an open circuit potential of poly-(3,4-ethylenedioxythiophene) as a beneficial mode for energy storage devices, *Adv. Funct. Mater.* **31**, 2103001(2021). IF = 18,808.

Appendix 6




Ivanko, I.; Lindfors, T.; Emanuelsson, R.; Sjödin, M. Conjugated redox polymer with poly(3,4-ethylenedioxythiophene) backbone and hydroquinone pendant groups as the solid contact in potassium-selective electrodes, *Sens. Actuators B Chem.* **329**, 129231(2021). IF = 7,460.

Appendix 1

Ivanko, I.; Pánek, J.; Svoboda, J.; Zhigunov, A.; Tomšík, E. Tuning the photoluminescence and anisotropic structure of PEDOT, *J. Mater. Chem. C*, **7**, 7013-7019 (2019). IF = 7,393.

Cite this: *J. Mater. Chem. C*, 2019,
7, 7013

Tuning the photoluminescence and anisotropic structure of PEDOT†

Iryna Ivanko,  ‡ Jiří Pánek, Jan Svoboda,  Alexander Zhigunov and Elena Tomšik  *

In the current work, we study the photoluminescence and anisotropic structure of PEDOT which is obtained in the presence of ions that perturb the water structure (ions in Hofmeister series). The water content in PEDOT has been confirmed by TGA and DSC measurements. The weight loss and heat flux together provided refined information about water content in the synthesized PEDOT, and based on the characteristic energy value, we conclude that the water molecules are bonded to the PEDOT chains by hydrogen bonds. The physicochemical properties of the such prepared PEDOT have been studied, e.g. the presence of photoluminescence is observed for PEDOT in the solid-state (thin film) with the longest Stokes shift (273 nm). Similarly, photoluminescence has been detected for the aqueous PEDOT suspension with the lifetime of the excited state in the range of nanoseconds. Moreover, the PEDOT chains can undergo rearrangements under electrochemical performance with the formation of an anisotropic structure, which is confirmed by polarized microscopy and XRD measurements. The photoluminescence spectrum of the anisotropic PEDOT film contains sharp, well-resolved peaks.

Received 18th February 2019,
Accepted 10th May 2019

DOI: 10.1039/c9tc00955h

rsc.li/materials-c

Introduction

Conducting polymers, such as polyaniline, polypyrrole, polythiophene, and poly(3,4-ethylenedioxythiophene) (PEDOT), and their derivatives, are the most promising materials for polymer-based pseudocapacitors.^{1,2} A pseudocapacitor stores energy through fast and reversible redox (faradaic) processes at characteristic potentials.³ Interest in conducting polymers is primarily related to their unique physical and physicochemical properties: high electrical conductivity, paramagnetism, and redox transformation.⁴

PEDOT is a conjugated polymer with high electrical conductivity in the doped state and fast electrochemical switching. Moreover, among conducting polymers, PEDOT exhibits also an unusual stability in the oxidized state, being considered as the most stable conducting polymer currently available.⁵

The electrochemical properties of conducting polymers depend not only on the chemical composition but also on the structure, morphology, and thickness of the polymer film.^{4–6} Elucidation of the effect of the polymer chain packing on the precise mechanism of the electrode processes (electro-physical and electro-chemical) would open a pathway for the preparation

of conducting polymer films with reproducible physicochemical properties.

PEDOT has been intensively studied during the last few decades by many authors.^{7–9} The most investigated composite is PEDOT:PSS.^{10–13} However, it is still a challenge to make a series of thin films with exactly reproducible properties, especially if large-area devices are desired. As many physical processes rely on the nanoscale morphology and local nano-environment, studies of physics on the molecular level by various techniques represent a powerful tool for understanding the physics behind intermolecular interactions in organic devices.¹⁴

In this work, we present the physicochemical properties of hydrated PEDOT chains synthesized in the presence of ions that perturb the water structure (ions in Hofmeister series). The role of the Hofmeister series has not been elucidated yet, however, the interaction of water molecules with ions and macromolecules is observed.¹⁵ The hydration of the polymer chains has been done during synthesis (formate and chloride ions were added) and the advantages of such PEDOT chains are based on several facts: first of all, photoluminescence is detected for the aqueous PEDOT suspension as well as for the solid state (PEDOT film); secondly, the PEDOT polymer chains are able to rearrange during electrochemical performance with the formation of an anisotropic structure, which was confirmed by polarized microscopy and XRD measurements.

Recently, it has been shown that the hydration of polyaniline chains (another conducting polymer) has a crucial impact on its electrochemical performance.¹⁶ Based on such knowledge, it

Institute of Macromolecular Chemistry AS CR, Heyrovsky Sq. 2, 162 06 Prague 6, Czech Republic. E-mail: tomsik@imc.cas.cz

† Electronic supplementary information (ESI) available: TEM, MALDI ToF, position of the binding energy, composition of PEDOT, survey XPS, UV-vis, and SEM. See DOI: 10.1039/c9tc00955h

‡ Faculty of Science, Charles University, Prague 2, Czech Republic.

has been decided to perform the synthesis of PEDOT in the presence of ions, which are able to perturb the water structure. Water molecules will interact with the polymer chains by hydrogen bonding. The crucial role of the water-mediated hydrogen bonds for self-assembling of dyes has been shown by Jelley and Sheppard.^{17–19} According to Sheppard, the appearance of a long-wavelength absorption results from the self-assembly of dyes by the interactions with water molecules between hydrophilic substituents, allowing the maintenance of the union of the conjugated molecules.^{16–19} The influence of the water-mediated hydrogen bonding on the self-assembly and optical properties of the porphyrin-based dyes has been studied by McHale²⁰ and Villari.²¹ The role of water-mediated hydrogen bonding in polyaniline has been studied by the authors.^{22–24}

To elucidate the role of water in the synthesized PEDOT, the measurements of some fundamental properties have been done by following physical, physicochemical and electrochemical methods, such as transmission electron microscopy (TEM), X-ray diffraction (XRD), Raman spectroscopy, X-ray photoelectron spectroscopy (XPS), thermogravimetric analysis (TGA) and differential scanning calorimetry (DSC), cyclic voltammetry and electrochemical impedance spectroscopy (EIS). The obtained knowledge has shed light on the nature of processes taking place in the synthesized PEDOT chains.

Results and discussion

As shown in the ESI† (Fig. S1), the PEDOT suspension under TEM revealed the assembly of polymer chains into nanosheets. To determine the number of monomer units in the PEDOT chains, MALDI ToF analysis was performed (Fig. S2, ESI†). The mass-to-charge ratio has a broad distribution, which corresponds to the number of monomer units in the range from 3 to 5. This means that the PEDOT chains synthesized by us have oligomeric nature.

The presence of water in the PEDOT chains was confirmed by the following methods: TGA and DSC measurements, and the results are present in Fig. 1a and b, respectively.

The weight loss in TGA (around 2 wt%) and heat flux peak in DSC at 100 °C together provide refined information about the water content. The characteristic energy for the escape of water was calculated using the following expression: $E_{\text{water}} = (\Delta Q \times M_{\text{water}}) / \Delta P$, where ΔP is the weight loss, ΔQ is the amount of heat evolved during the dehydration, and M_{water} is the molecular weight of water.²⁵ The value of E_{water} was calculated to be 4 kcal mol⁻¹, and appears to correspond to a single hydrogen bond (about 5 kcal mol⁻¹).²⁵ Moreover, the bond in water has a broad exothermic peak (Fig. 1b) compared to the free water that has a sharp exothermic peak.²⁵ Two more peaks have been observed in the TGA data at ≈ 341 °C and 404 °C, which are probably connected with the loss of acid and partial degradation of the PEDOT chains. We have to point out that the total loss in PEDOT powder in the air is around 27 wt% up to 600 °C. The best thermal stability for the intensively studied PEDOT/PSS suspension was reported in the literature, and it is approximately 55 wt% loss up to 550 °C.²⁶

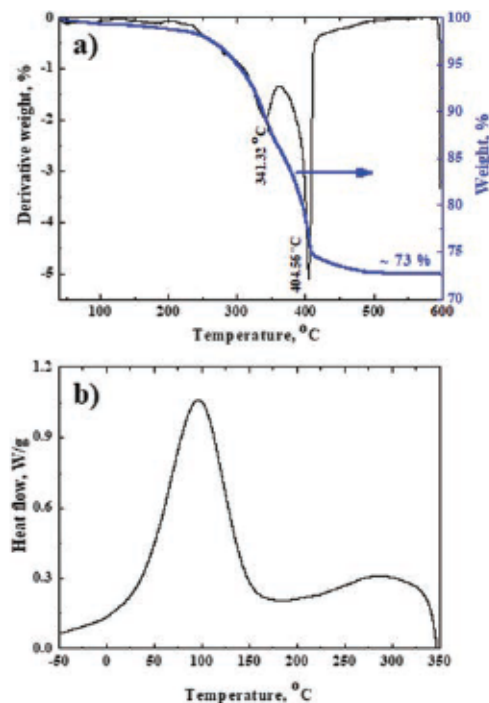


Fig. 1 (a) TGA and (b) DSC of PEDOT powder.

The synthesized PEDOT chains were studied by XPS and the spectra possess all XPS peaks previously reported in the literature.^{27,28} In high resolution core-level S 2p spectra (Fig. 2a), only one chemical state of sulphur was found with a doublet at 163.2 eV (S 2p_{3/2}) and 164.5 eV (S 2p_{1/2}). In high-resolution core-level C 1s spectra (Fig. 2b) three different peaks located at 284.2, 285.1 and 286.0 eV and corresponding to =CH-S-, =C-O- and -CH₂-O- were observed. Moreover, both S 2p and C 1s spectra show a high energy tail. The binding energy recorded in the literature for PEDOT and binding energy measured by us are summarized in Table S1, ESI†.^{27,28} Additionally, the presence of formic acid in PEDOT was confirmed by XPS analysis (formate ions are present in the polymerization mixture); the binding energy peak of -O-C=O is located at 288.4 eV (Fig. 2b).²⁸

The atomic percent composition of the PEDOT film determined by XPS is presented in Table S2 (ESI†), and the survey XPS spectrum of the PEDOT film can be seen in Fig. S3, ESI†. The ratio of sulphur to formate ions is 8, which means that eight monomer units have one formate ion. It has to be noted that the XPS spectra of the PEDOT film after electrochemical measurements are identical to the ones before treatment (Fig. S4, ESI†). The above-described data clearly demonstrate, on one hand, that we obtained PEDOT, which is similar to that reported in the literature so far (chemical composition), but on the other hand, the polymer chains synthesized by us are hydrated (which is confirmed by the DSC and TGA measurements).

The Raman spectrum of the hydrated PEDOT chains is presented in Fig. 3a. The intensities of the bands of the PEDOT structure are enhanced due to the resonance effect. This means that the excitation wavelength (785 nm) corresponds to an electronic transition occurring in the studied PEDOT.^{29–31}

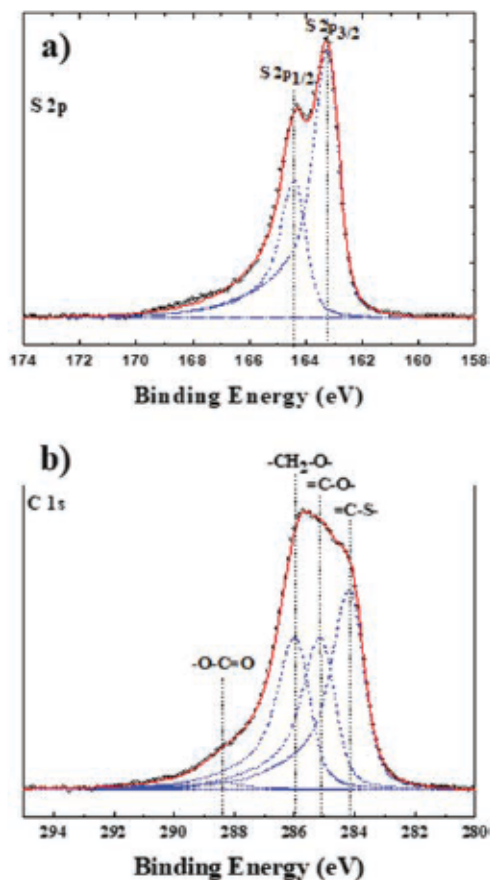


Fig. 2 (a) High-resolution core-level S 2p and (b) C 1s XPS spectra of the PEDOT film. The spectra are presented with black circles, while their corresponding fitted envelopes are in red. The individual contributions are represented with blue lines.

The shoulder band at 1540 cm^{-1} is associated with the $C_{\alpha}=C_{\beta}$ antisymmetric stretching vibration. According to Garreau *et al.* the above-mentioned peak is observed for PEDOT in the oxidized state.³² On the other hand the most intense and narrow band at 1421 cm^{-1} is assigned to the symmetric stretching mode of the aromatic $C_{\alpha}=C_{\beta}$ bond.²⁹ Such characteristic has been observed by Ouyang *et al.* and explained by the resonance structure of the PEDOT chains changing from a benzoid to a quinoid (the quinoid structure may be the favourite for a linear structure).³⁰

Moreover, the intense and narrow band is indicative of a high level of conjugation in the PEDOT structure.^{31,33} The high level of conjugation is provided by the water molecules, similar to dyes.^{17–19} The bands at 987 and 573 cm^{-1} are attributed to the oxyethylene ring deformation, and the peak at 695 cm^{-1} is associated with the symmetric C–S–C deformation.^{31,33} We must emphasize that the band at 526 cm^{-1} is very weak; this band is usually associated with the defects in the polymer chains.³⁰ Based on this result we can conclude that the synthesized PEDOT chains are highly regular, possess a high level of conjugation and have oxidized and reduced species. We suggest that the water-mediated hydrogen bonding, similar to in dyes and polyaniline, plays an important role in the regularity and conjugation of the PEDOT chains.

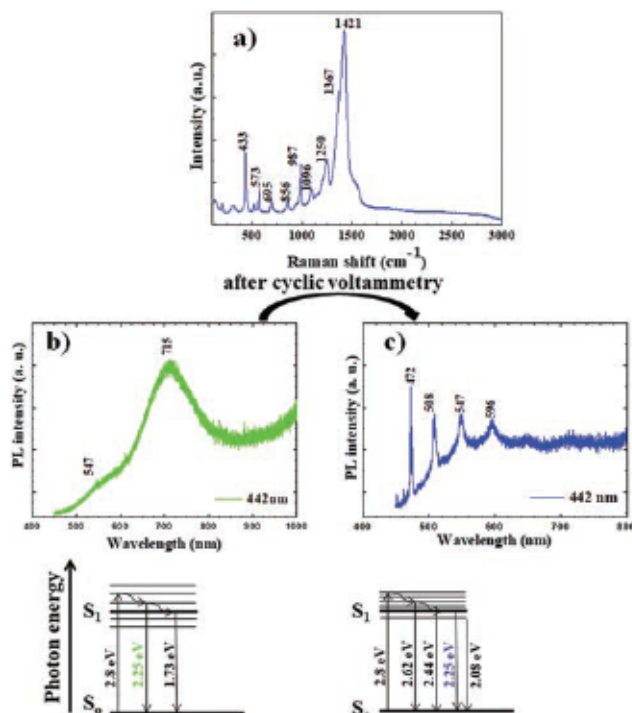


Fig. 3 Raman spectroscopy of PEDOT (a). The photoluminescence spectra of the PEDOT as synthesized (b); PL of the PEDOT film after electrochemical measurements (c). Jablonski diagrams are shown below for corresponding PL excitation and relaxation processes.

To further study the physical properties of the hydrated PEDOT chains, the photoluminescence (PL) spectra, time-resolved PL, and confocal microscopy measurements were performed. In Fig. 3b the PL spectra are presented for the PEDOT film with the excitation wavelength at $\lambda_{\text{exc}} = 442\text{ nm}$. The spectrum shows that the maximum emission peak in the visible region at $\sim\lambda_{\text{em}} = 715\text{ nm}$ (sharp) corresponds to the energy band gap of 1.73 eV , with a shoulder at $\lambda_{\text{em}} = 547\text{ nm}$ (2.25 eV), which relates to 273 nm and 108 nm Stokes shifts, respectively. This is the longest Stokes shift reported in the literature for any semiconducting polymer up to now. According to the literature, the maximum emission peak at $\lambda_{\text{em}} = 602\text{ nm}$ was reported for PEDOT dissolved in DMSO.³⁴ Also, the quantum dots obtained from the non-photoluminescent PEDOT possess an emission peak at 450 nm (excited at 360 nm) in water.³⁵ Recently, the visible luminescence of the de-doped PEDOT:PSS films have been reported.³⁶ It must be emphasized that we observed PL for PEDOT in its doped state, confirmed by the UV-visible measurement (Fig. S5, ESI†). Such observation contradicts the state-of-the-art. However, MacDiarmid and Shimano observed the effect of water on the PL spectra of the polyaniline cast film. They proposed that the water molecules incorporated between the amino groups have extended benzenoid sequences (responsible for the PL) arising from the linking between different polymer chains.³⁷ We can conclude that the synthesized PEDOT chains also possess an extended benzoid sequence (confirmed by Raman spectroscopy), which is accompanied by incorporation of water molecules between the polymer chains (confirmed by TGA and DSC).

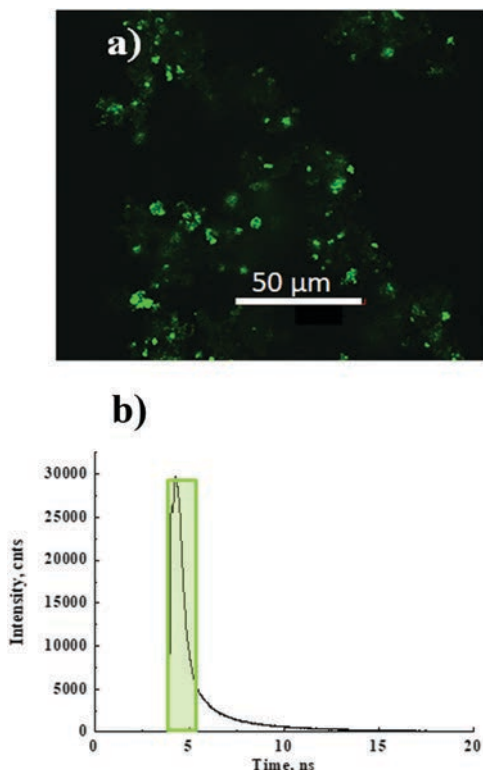


Fig. 4 (a) The confocal microscopy image of the PEDOT suspension and (b) the time-resolved fluorescence intensity.

The confocal microscopy image of the PEDOT suspension in an aqueous medium is presented, in order to visualize the PL intensity of PEDOT. The excitation was done at $\lambda_{\text{ex}} = 485$ nm pulsed laser (Fig. 4a). No bleaching was observed after long-term imaging. To study the lifetime of the excited state, time-resolved fluorescence intensity measurements have been done (Fig. 4b). The PL decay signal was fitted by a triple exponential function with decay time values: $\tau_1 \approx 5.9$ ns, $\tau_2 \approx 1.9$ ns, and $\tau_3 \approx 0.3$ ns. The χ^2 value of 0.986 indicated a good fit of the curve. The lifetime of the excited state is in the range of nano-seconds, which confirms that the PL originates from the singlet excited state (visualised by Jablonski diagram, Fig. 3).

The UV-visible measurement of the PEDOT suspension is presented in Fig. S6, ESI.† In order to investigate the anisotropy (chain organization) of PEDOT, its suspension has been deposited on the top of fluorine-doped tin oxide (FTO), as can be seen in Fig. 5a. It is clear that under such conditions the PEDOT film is not uniform; a part of the FTO electrode was not covered. It must be emphasized that under polarized light such deposited PEDOT film does not reveal any anisotropic structure (Fig. 5b).

On the other hand, the organization was observed by XRD measurements. The X-ray diffraction data of the PEDOT film is presented in Fig. 6 (before, during, and after electrochemical measurements). It is apparent by the presence of the three peaks at $2\theta = 6.5^\circ$, 31° and 33.7° that the PEDOT chains are able to assemble; their positions indicate interchain packing and the clearly defined scattering indicates the crystallinity of the film. The diffraction peak at $2\theta = 6.5^\circ$ (distance 13.38 Å) is

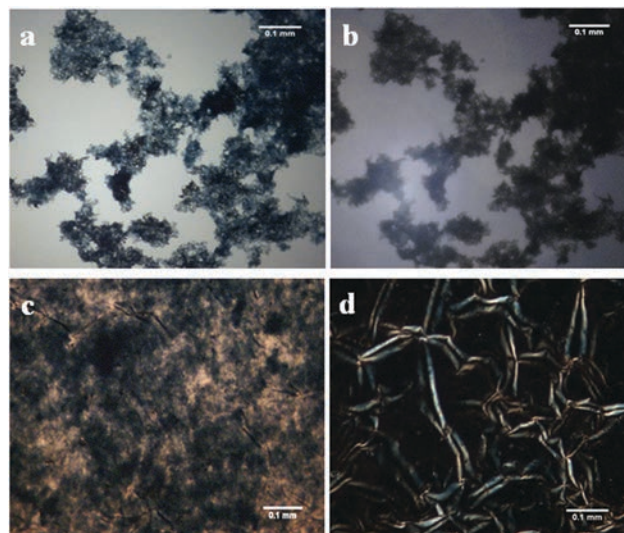


Fig. 5 (a) Optical microscopy of the PEDOT film before and (c) after electrochemical measurements; (b) polarized optical microscopy of the PEDOT film before and (d) after electrochemical measurements.

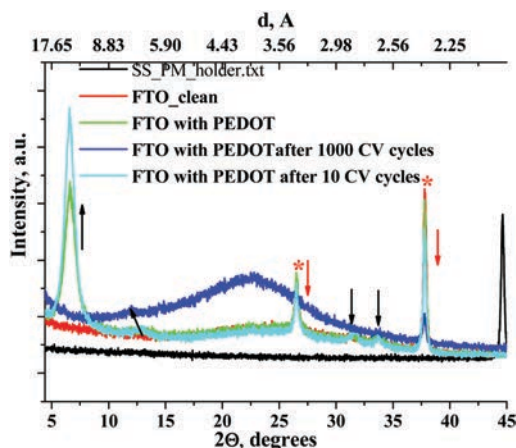


Fig. 6 Evolution of the crystal structure of the PEDOT film during electrochemical measurements.

narrow and corresponds to the distance between two polymer chains.^{38–40} The indexation of the two other reflections is unclear. However, we proposed an explanation that these peaks could correspond to the water structure located close to the polymer chains.⁴¹ The structure of the PEDOT film during repeating numbers of cyclic voltammetry has changed to an amorphous one, which is shown by the blue curve in Fig. 6. The peaks at $2\theta = 6.5^\circ$, 31° and 33.7° disappeared, with the simultaneous occurrence of two peaks at $2\theta = 12^\circ$, and 22.5° . Moreover, the peaks correlated to FTO (marked by red asterisk and arrows) were depleted, which means that all the FTO surface was covered by the PEDOT film after cyclic voltammetry.

To our knowledge, there is no information in the literature concerning such organization and/or reorganization of the PEDOT chains prepared by chemical polymerization. Furthermore, we decided to analyse the PEDOT film by optical and polarized microscopy after cyclic voltammetry measurements (Fig. 5c and d).

It was observed by optical microscopy that the PEDOT film became uniform and smooth, compared to the PEDOT film deposited on FTO before electrochemical measurements (Fig. 5a). The whole area of the FTO electrode was covered by the PEDOT film. Moreover, it was demonstrated by applying polarized light that such film became anisotropic (Fig. 5d) (the appearance of long fibrils), in contrast to PEDOT before the electrochemical treatment. The scanning electron microscopy image of the PEDOT film after cyclic voltammetry measurement is shown in Fig. S7, ESI.†

Moreover, the PL measured for the PEDOT film after the cyclic voltammetry measurements (1000 cycles by cyclic voltammetry at a scan rate of 50 mV s^{-1}) is different compared to the one obtained for PEDOT as synthesized (Fig. 3b and c). Such change in the PL is connected with the formation of the amorphous structure on one hand, and simultaneously the presence of anisotropy on the other, organized in one direction (confirmed by optical microscopy and XRD). It is obvious from Fig. 3c that the emission peaks are narrow and shifted to shorter wavelength: the most intensive emission peak is located at $\lambda_{\text{em}} = 472 \text{ nm}$ (2.62 eV) and followed by three emission peaks at $\lambda_{\text{em}} = 508$ (2.44 eV), $\lambda_{\text{em}} = 547$ (2.25 eV) and $\lambda_{\text{em}} = 596$ (2.08 eV). It must be emphasized that in the PL spectra for the PEDOT film before and after cyclic voltammetry measurements the same emission peak is observed at $\lambda_{\text{em}} = 547$ (2.25 eV) visualized by Jablonski diagrams (Fig. 3). From this data, we conclude that the same emitting centres are present in both the PEDOT films. The other emission peaks shown in Fig. 3c could be explained by the presence of a localized state in the amorphous structure of the film, which was confirmed by XRD (Fig. 6). Similar behaviour has been observed and reported for crystalline and amorphous silicon.⁴² We proposed that the benzoid sequences are present and could rotate (because of the amorphous structure); as a consequence, the absorbed energy is partly dissipated due to the rotational mode. The rotation is not possible in the semi-crystalline PEDOT film before cyclic voltammetry measurements, that is why the PL spectra have only one main emission peak $\lambda_{\text{em}} = 715 \text{ nm}$ (Fig. 3b). It is still not clear why the emission peaks for the PEDOT film after cyclic voltammetry measurements are narrow (FWHM $\sim 50 \text{ nm}$). The narrow emitting peaks have been detected only at low temperatures, for example at 3 K for the Mn^{4+} where thermal broadening could be avoided.⁴³

Electrochemical performance of the anisotropic PEDOT film was characterized by cyclic voltammetry and EIS, and the results are presented in Fig. 7. The profile of the cyclic voltammograms of the positive charging current is almost the mirror image of the negative discharging current (Fig. 7 top), with the value of specific current of 20 A g^{-1} for the 100 mV s^{-1} scan rate. Moreover, switching the direction of sweep during the potential scan produces almost immediate reverse of the direction of the current. This behaviour is also characteristic of a reversible, capacitive charge and discharge process.^{1,2}

EIS provides complementary information to that obtained from cyclic voltammetry. The impedance was measured at a constant potential of 0.4 V vs. the Ag/AgCl reference electrode.

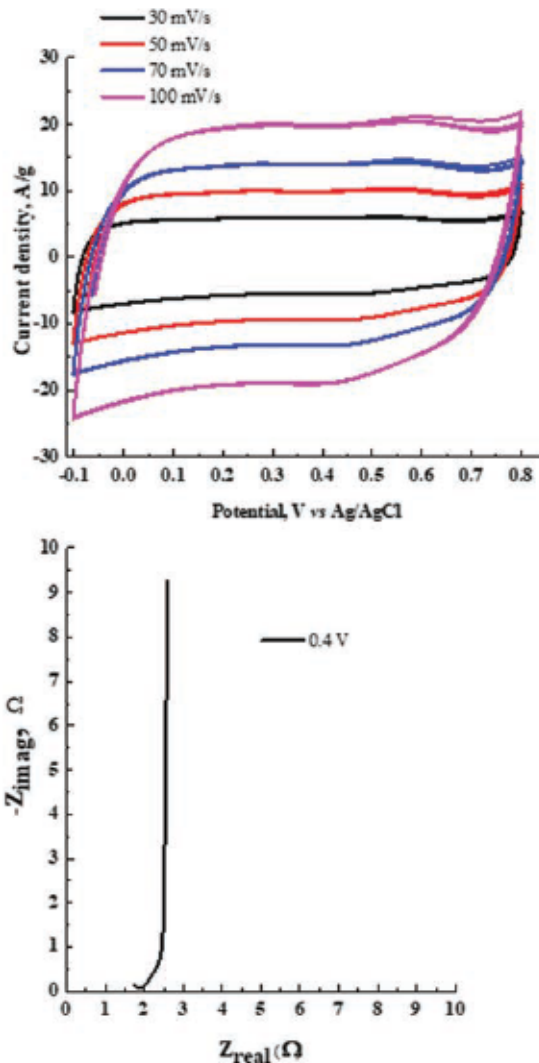


Fig. 7 Cyclic voltammetry of PEDOT deposited on FTO (top) and EIS of PEDOT deposited on FTO, measured at 0.4 V applied potential (bottom).

The result in the form of a complex plane plot is presented in Fig. 7 bottom and it exhibits a straight line without the presence of a semi-circle arc at high frequency, which can be explained by the facile processes of charge transfer and charge transport in the electrochemically active PEDOT.⁴⁴ Such behaviour proves that the hydrated PEDOT chains are a suitable material for pseudocapacitor applications.

Experimental

Synthetic procedures

The synthesis of PEDOT was carried out by dissolving 1.7 mol L^{-1} of NaCl in water and then 5 mol L^{-1} of formic acid was added. $\text{FeCl}_3 \cdot 6\text{H}_2\text{O}$ ($10 \times 10^{-4} \text{ mol L}^{-1}$) was used as an oxidant. Polymerization was performed at $25 \text{ }^\circ\text{C}$ for 24 h. Monomer, 3,4-ethylenedioxythiophene (EDOT), $5 \times 10^{-4} \text{ mol L}^{-1}$ was solubilized by 2 mL of ethanol and then added to the polymerization mixture. The mole ratio of monomer:oxidant was 1:2. After the reaction was completed, the PEDOT suspension was

filtered and washed with an aqueous solution of formic acid (5 mol L⁻¹). Furthermore, PEDOT was redistributed in an aqueous solution of formic acid. Such PEDOT suspension was deposited (drop casting) onto current-collector supports (FTO) and dried in an oven over a few days to a constant weight. The yield of the polymerization is 68%.

Materials and methods

Cyclic voltammetry and electrochemical impedance spectroscopy (EIS) were performed using an AUTOLAB PGSTAT302N potentiostat with FRA32M Module and Nova software 2.1. All measurements were performed using the three-electrode set up at an ambient temperature in 6 M H₃PO₄. A Pt counter electrode with an area of 1.2 cm² was used and Ag/AgCl (3 M KCl) was utilized as a reference electrode. Complex impedance measurements were performed in the frequency range from 10 kHz to 0.1 Hz with 10 mV amplitude at 0.4 V constant potential (vs. Ag/AgCl). The Kramers-Kronig test was applied to verify the obtained EIS data. Cyclic voltammetry was measured within the potential window from -0.1 to 0.8 V vs. Ag/AgCl at scan rates 30, 50, 70 and 100 mV s⁻¹.

Thermogravimetric analysis (TGA) was carried out on a PerkinElmer TGA 7 Thermogravimetric Analyzer (Norwalk, CT, USA) in the air at a heating rate of 10 °C min⁻¹.

The differential scanning calorimetry (DSC) analysis was carried out using a PerkinElmer 8500 DSC apparatus. The sample of 5–6 mg was heated from -50 °C to 350 °C at the heating rate of 10 °C min⁻¹.

Wide-angle X-ray scattering (WAXS) experiments were performed using a pinhole camera (Older Rigaku SMAX2000 upgraded by SAXSLAB/Xenocs) attached to a microfocused X-ray beam generator (Rigaku MicroMax 003) operating at 50 kV and 0.6 mA (30 W). The camera was equipped with a vacuum version of a Pilatus 300K detector. The experimental setup covered a q range of 0.004–3 Å⁻¹. Scattering vector, q , is defined as:

$$q = 4\pi/\lambda \sin \theta$$

where λ is the wavelength and θ is the scattering angle. Calibration of primary beam position and sample-to-detector distances was performed using the Si powder sample.

The transmission electron micrographs were obtained using a Tecnai G2 Spirit (FEI).

The photoluminescence (PL) spectra of the PEDOT suspension in an aqueous solution were recorded on an FS5 fluorescence spectrophotometer (Edinburgh Instruments Ltd, UK). The wavelength of the pulsed laser was $\lambda_{exc} = 485$ nm. The PEDOT suspension was deposited on quartz glass and the PL spectra of the thin film were recorded by the excitation dependent photoluminescence spectrometer Jasco FP-6200 model. The excitation wavelength was 442 nm.

Optical microscopic and polarized microscopic images of the PEDOT films were taken with Zetopan Pol (Reichert). The PEDOT suspension was deposited by drop casting on the FTO support. The PEDOT film was dried in an oven to a constant weight.

The X-ray photoelectron spectroscopy (XPS) measurements were performed using a K-Alpha+ XPS spectrometer (ThermoFisher Scientific, UK) operating at a base pressure of 1.0×10^{-7} Pa. The

data acquisition and processing were performed using the Thermo Avantage software. All samples were analysed using microfocused, monochromated Al K_α X-ray radiation (400 μm spot size) with a pass energy of 200 eV for the survey and 50 eV for high-energy resolution core level spectra. The X-ray angle of incidence was 30° and the emission angle was along the surface normal. The binding energy scale of the XPS spectrometer was calibrated by the well-known positions of the C 1s C-C and C-H, C-O and C(=O)-O peaks of polyethylene terephthalate and Cu 2p, Ag 3d, and Au 4f peaks of Cu, Ag and Au metals, respectively. The obtained high-resolution spectra were fitted with Voigt profiles to probe the individual contributions of the present chemical species.

Matrix-assisted laser-desorption ionization time-of-flight mass spectra (MALDI-TOF MS) were obtained using a Bruker microflex MALDI-TOF spectrometer using *trans*-2-[3-(4-*tert*-butylphenyl)-2-methyl-2-propenyldene]malononitrile (DCTB) as a matrix in negative ionization mode.

Raman spectra excited with near-infrared diode 785 nm lasers were collected on a Renishaw inVia Reflex Raman spectrometer.

Conclusions

In summary, we demonstrate that hydrated PEDOT chains (that have oligomeric nature) have been synthesized in the presence of ions that are able to perturb the water structure (formate and chloride ions). Perturbed water molecules play a crucial role in the physical, physicochemical and electrochemical properties of the PEDOT chains. In particular, hydrated polymer chains are able to re-arrange during the electrochemical treatment with the formation of an anisotropic structure. The photoluminescence spectrum of the anisotropic PEDOT film contains sharp, well-resolved peaks. We proposed that the benzoid sequences are present and could rotate (because of the amorphous structure); as a consequence, the absorbed energy is partly dissipated due to the rotational mode. The rotation is not possible in the semi-crystalline PEDOT film before cyclic voltammetry measurements. That is why the PL spectra have only one main emission peak at $\lambda_{em} = 715$ nm, which corresponds to 273 nm Stokes shift. Moreover, the PL has been detected in the PEDOT suspension and its lifetime is in the range of nanoseconds, which confirms that the PL originates from the singlet excited state. The tuning of the PL in the semiconducting polymer by applying cyclic voltammetry is a promising way to fundamentally study the processes taking place during the emission and is also important for real device applications.

Conflicts of interest

The authors declare no competing financial interests.

Acknowledgements

The authors acknowledge the OPPK (CZ.2.16/3.1.00/21545) from the European Regional Development Fund and the Czech Science Foundation (17-05095S). The authors thank Dr J. Kredatusová for TGA and DSC measurements.

References

- 1 H. L. Li, J. X. Wang, Q. X. Chu, Z. Wang, F. B. Zhang and S. C. Wang, *J. Power Sources*, 2009, **190**(2), 578.
- 2 G. A. Snook, P. Kao and A. S. Best, *J. Power Sources*, 2011, **196**, 1.
- 3 B. E. Conway, *Electrochemical Supercapacitors: Scientific Fundamentals and Technological Applications*, Kluwer Academic, New York, USA, 1999.
- 4 S. Kirchmeyer and K. Reuter, *J. Mater. Chem.*, 2005, **15**, 2077.
- 5 C. Lei, P. Wilson and C. Lekakou, *J. Power Sources*, 2011, **196**, 7823.
- 6 V. D. Pokhodenko and V. A. Krylov, *Theor. Exp. Chem.*, 1994, **30**, 91.
- 7 B. L. Groenendaal, F. Jonas, D. Freitag, H. Pielartzik and J. R. Reynolds, *Adv. Mater.*, 2000, **12**, 481.
- 8 K. S. Ryu, Y.-G. Lee, Y.-S. Hong, Y. J. Park, X. Wu, K. M. Kim, M. G. Kang, N.-G. Park and S. H. Chang, *Electrochim. Acta*, 2004, **50**, 843.
- 9 A. Laforgue, *J. Power Sources*, 2011, **196**, 559.
- 10 T. Cheng, Y.-Z. Zhang, J.-P. Yi, L. Yang, J.-D. Zhang, W.-Y. Lai and W. Huang, *J. Mater. Chem. A*, 2016, **4**, 13754.
- 11 T. Yu, J. Xu, L. Liu, Z. Ren, W. Yang, S. Yan and Y. Ma, *J. Mater. Chem. C*, 2016, **4**, 9509.
- 12 T. Cheng, Y.-Z. Zhang, J.-D. Zhang, W.-Y. Lai and W. Huang, *J. Mater. Chem. A*, 2016, **4**, 10493.
- 13 L. Zhou, M. Yu, X. Chen, S. Nie, W.-Y. Lai, W. Su, Z. Cui and W. Huang, *Adv. Funct. Mater.*, 2018, **28**, 1705955.
- 14 R. Liu, I. S. Cho and S. B. Lee, *Nanotechnology*, 2008, **19**, 215710.
- 15 Y. Zhang and P. S. Cremer, *Curr. Opin. Chem. Biol.*, 2006, **10**(6), 658.
- 16 E. Tomšik, O. Kohut, I. Ivanko, M. Pekárek, I. Bieloshapka and P. Dallas, *J. Phys. Chem. C*, 2018, **122**, 8022.
- 17 W. E. B. Shepherd, R. Grollman, A. Robertson, K. Paudel, R. Hallani, M. A. Loth, J. E. Anthony and O. Ostroverkhova, *Chem. Phys. Lett.*, 2015, **629**, 29.
- 18 E. E. Jelly, *Nature*, 1937, **139**, 631.
- 19 S. E. Sheppard, *Science*, 1941, **93**, 42.
- 20 C. C. Rich and J. L. McHale, *Phys. Chem. Chem. Phys.*, 2012, **14**(7), 2363.
- 21 V. Villari, P. Mineo, E. Scamporrino and N. Micalia, *RSC Adv.*, 2012, **2**(33), 12989.
- 22 N. Gospodinova, V. Musat, H. Kolev and J. Romanova, *Synth. Met.*, 2011, **161**, 2510–2513.
- 23 N. Gospodinova, E. Tomsik and O. Omelchenko, *J. Phys. Chem. B*, 2014, **118**, 8901.
- 24 E. Tomsik, M. Konefal, O. Kohut, I. Ivanko, J. Hromádková, A. Zhigunov and M. Steinhart, *Macromol. Chem. Phys.*, 2018, **219**, 1700627.
- 25 E. S. Matveeva, R. Diaz Calleja and V. P. Parkhutik, *Synth. Met.*, 1995, **72**, 105; H. Yoshida, T. Hatakeyama and H. Hatakeyama, *Polym. Prepr.*, 1992, **41**, 1287.
- 26 Y. Jin, Q. Chen and P. Lessner, *Electrochemistry*, 2013, **81**, 801.
- 27 S. A. Spanninga, D. C. Martin and Z. Chen, *J. Phys. Chem. C*, 2009, **113**(14), 5585.
- 28 M. Bowker and R. J. Madix, *Surf. Sci.*, 1981, **102**, 542.
- 29 J. Ouyang, Q. Xu, C. Chu, Y. Yang, G. Li and J. Shinar, *Polymer*, 2004, **45**, 8443.
- 30 Q. Zhao, R. Jamal, L. Zhang, M. Wang and T. Abdiryim, *Nanoscale Res. Lett.*, 2014, **9**(1), 577.
- 31 M. Stavitska-Barba and A. Meyers Kelley, *J. Phys. Chem. C*, 2010, **114**, 6822.
- 32 S. Garreau, G. Louarn, J. P. Buisson, G. Froyer and S. Lefrant, *Macromolecules*, 1999, **32**, 6807.
- 33 W. W. Chiu, J. Travas-Sejdic, R. P. Cooney and G. A. Bowmaker, *J. Raman Spectrosc.*, 2006, **37**, 1354.
- 34 H. Sun, B. Lu, X. Duan, J. Xu, L. Dong, X. Zhu, K. Zhang, D. Hu and S. Ming, *Int. J. Electrochem. Sci.*, 2015, **10**, 3236.
- 35 K. P. Prasad, Y. Chen, M. A. Sk, A. Than, Y. Wang, H. Sun, K. H. Lim, X. Dong and P. Chen, *Mater. Horiz.*, 2014, **1**, 529.
- 36 I. Cruz-Cruz, M. Reyes-Reyes, I. A. Rosales-Gallegos, A. Y. Gorbachev, J. M. Flores-Camacho and R. Lopez-Sandoval, *J. Phys. Chem. C*, 2015, **119**, 19305.
- 37 J. Y. Shimano and A. G. MacDiarmid, *Synth. Met.*, 2001, **123**, 251.
- 38 K. E. Aasmundtveit, E. J. Samuelsen, L. A. A. Pettersson, O. Inganas, T. Johansson and R. Feidenhans'l, *Synth. Met.*, 1999, **101**, 561.
- 39 L. Niu, C. Kvarnstrom, K. Froberg and A. Ivaska, *Synth. Met.*, 2001, **122**, 425.
- 40 S. K. M. Jönsson, M. P. de Jong, L. Groenendaal, W. R. Salaneck and M. Fahlman, *J. Phys. Chem. B*, 2003, **107**, 10793.
- 41 T. L. Malkin, B. J. Murray, A. V. Brukhno, J. Anwar and C. G. Salzmänn, *Proc. Natl. Acad. Sci. U. S. A.*, 2012, **109**, 1041.
- 42 P. Garg, Study of Photoluminescence from Amorphous and Crystalline Silicon Nanoparticles Synthesized using a Non-Thermal Plasma, Master thesis, Arizona State University, 2015.
- 43 T. Jansen, J. Gorobez, M. Kirm, M. G. Brik, S. Vielhauer, M. Oja, N. M. Khaidukov, V. N. Makhov and T. Justel, *ECS J. Solid State Sci. Technol.*, 2018, **7**, R3086.
- 44 G. Lang and G. Inzelt, *Electrochim. Acta*, 1991, **36**, 847.

Appendix 2

Ivanko, I.; Svoboda, J.; Lukešová, M.; Šeděnková, I.; Tomšík, E. Hydrogen Bonding as a Tool to Control Chain Structure of PEDOT: Electrochemical Synthesis in the Presence of Different Electrolytes, *Macromolecules*, **53**, 2464-2473 (2020). IF = 5,985.

Hydrogen Bonding as a Tool to Control Chain Structure of PEDOT: Electrochemical Synthesis in the Presence of Different Electrolytes

Iryna Ivanko, Jan Svoboda, Miroslava Lukešová, Ivana Šeděnková, and Elena Tomšík*

Cite This: *Macromolecules* 2020, 53, 2464–2473

Read Online

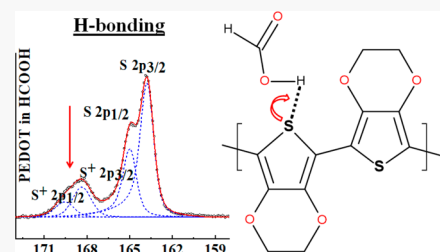
ACCESS |

Metrics & More

Article Recommendations

Supporting Information

ABSTRACT: The current knowledge about the presence of cation radicals in organic semiconductors is connected with oxidized constitutional units and their interaction with counterions. In this work, we have shown that the formation of cation radicals in poly(3,4-ethylenedioxythiophene) is induced by intermolecular electrostatic interactions, particularly by hydrogen-bond formation between formic acid and polymer. Raman, XPS, UV–vis, and EPR spectroscopies were used to prove that by using the simplest carboxylic acid, which can form hydrogen bonding, it is possible to form localized cation radicals. Moreover, it was shown that by replacing formic acid with *o*-phosphoric acid, it is possible to obtain delocalized cation radicals. The gained new understanding how to tune the formation and nature of cation radicals in organic semiconductors can be used in the design of organic electronics.



1. INTRODUCTION

Over the years the synthesis and characterization of conducting polymers have attracted attention due to their unique electronic and optical properties. They can be used in many applications such as electrochromic devices,^{1,2} light-emitting diodes,³ biosensors,^{4,5} and all-solid-state ion sensors.^{6,7} Among electronically conducting polymers, there is a considerable interest in using poly(3,4-ethylenedioxythiophene) (PEDOT) because of its low oxidation potential, high stability in an ambient environment,⁸ mechanical flexibility, and stable oxidized form.⁹ The fundamental understanding of the effects of molecular structure on material characteristics and physicochemical properties in conducting polymers¹⁰ requires the production of materials with well-defined chemical structures. A major effort has been focused on determining the relationship between polymer chemical structure and the corresponding physical and chemical properties. The chemical composition and physicochemical properties of conducting polymers depend on several aspects such as (1) the method of preparation (chemical or electrochemical), (2) temperature, (3) concentration of oxidant, monomer, and/or ionic strength of electrolytes, (4) additives, and (5) post-treatment. Variations of all of the above-described parameters help to provide the tools necessary for tuning the physicochemical properties of polymers.^{11–13} It has been shown that polymers with nitrogen and sulfur atoms offer the possibility of protonation or alkylation of the lone electron pair as a way of modifying their properties. An example of this would be when H-bonding occurs between adjacent polymer chains.¹⁴ Meanwhile, it has been recognized that the deviation from planarity of conjugated segments leads to hypsochromic shifts (shorter wavelength) in optical absorption and often poor conductivity. The planarity of chain structure could be enforced by certain H-bonding interactions.¹⁵

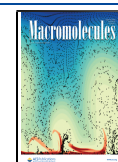
Interaction between –OH groups and the Schiff base (–C=N–), for example, can lead to substantial bathochromic shifts in the absorption of polyazomethine polymers due to the planarization of the polymer.¹⁶ Also, it has been shown that protonation of the pyridyl nitrogen has an important structural effect. The formation of intermolecular hydrogen bonding between the adjacent polymer chain leads to planarization of the polymer backbone, and as a consequence the red-shifts of both the optical absorption and emission spectra are observed.¹⁷ Various approaches involving H-bonding between adjacent chains can also be exploited to planar polymers.^{18,19} The post-treatment effects have an impact on structural modifications and optical properties in addition to effecting the electrical properties of polymers.²⁰ Recently, it has been reported that utilization of protonic acids to treat modified PEDOT chains provides the crucial change of structure and assembling of polymer chains by H-bonding that cause the enhanced electrical conductivity. The improved power factor is caused by the increasing densities of the polaron's state and the stabilized densities of the bipolaron's state.²⁰

In the current work, it is present for the first time the physical and electrochemical properties of PEDOT film synthesized electrochemically in the presence of formic acid. Formic acid is known for its ability to form H-bonds. It is shown the impact of intermolecular electrostatic interactions caused by interactions

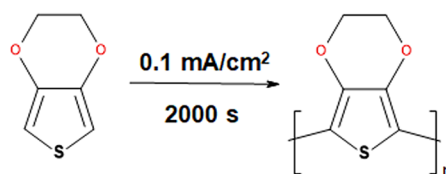
Received: December 11, 2019

Revised: February 19, 2020

Published: March 31, 2020



Electro-chemical polymerization



Electrostatic interaction

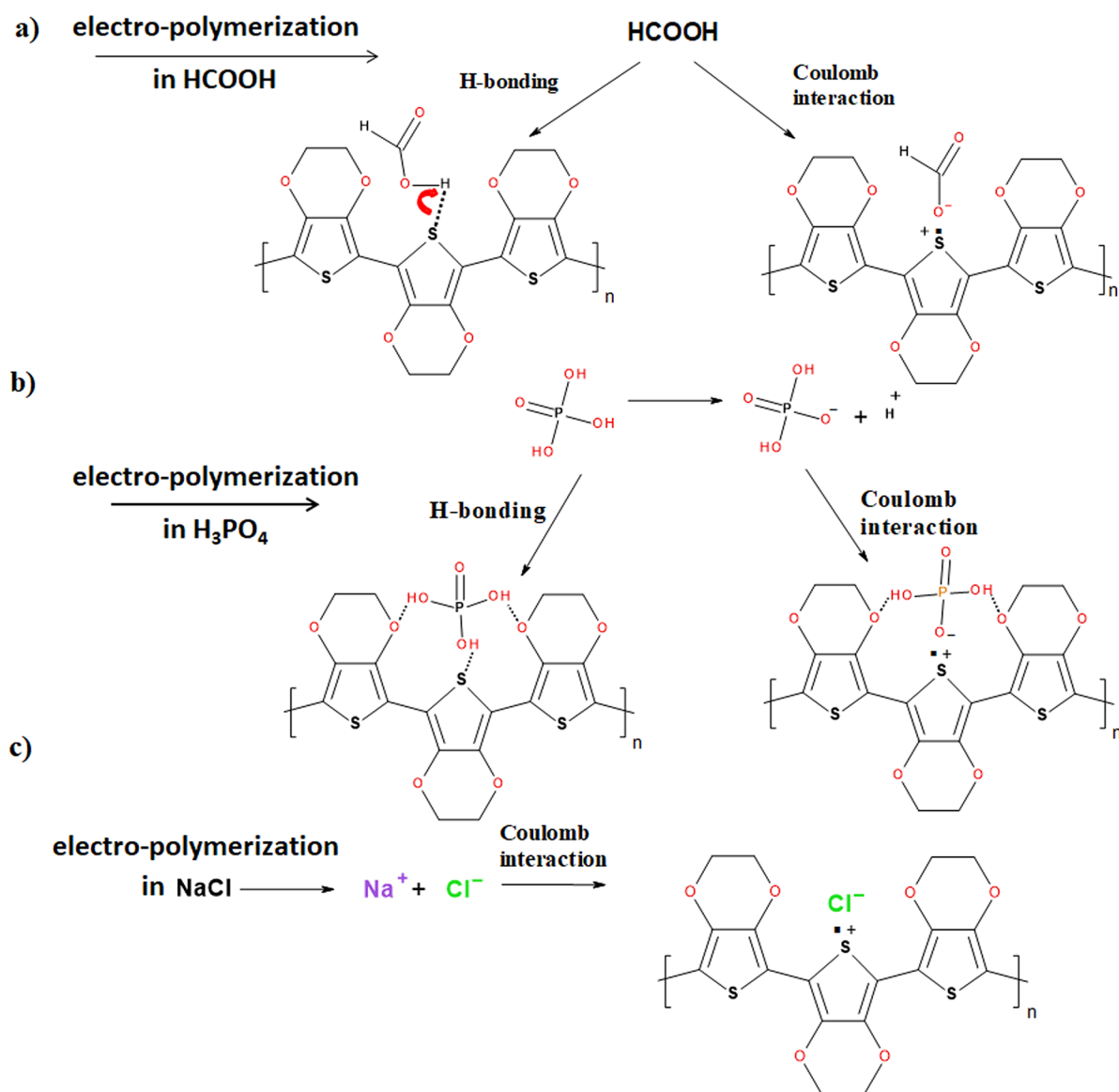


Figure 1. Scheme of PEDOT electrochemical synthesis. Possible formation of Coulomb interaction and H-bonding formation between PEDOT and (a) formic acid, (b) phosphoric acid, and (c) NaCl.

between formic acid and polymer chains and the effects on the structure, electrochemical, and physical properties of PEDOT. The two oxidation peaks were recorded, the origin of which was studied by cyclic voltammetry and explained. Gathered knowledge about chemical structure and physicochemical properties of electrochemically synthesized PEDOT will be

further used by us for the preparation of solid contact transducer in ion-selective electrodes (ISEs).^{21,22}

2. RESULTS AND DISCUSSION

Electrochemical Synthesis in Different Electrolytes.

Electrostatic interaction plays an enormous role in molecular structure and furthermore in the physicochemical properties of

the materials. Among electrostatic interactions, H-bonding and Coulomb interactions are the most important. According to the IUPAC definition, a hydrogen bond is a form of association between an electronegative atom (such as N, O, S, or F) and a hydrogen atom attached to a second, relatively electronegative atom. According to general knowledge, the H-bond interactions possess the following advantages: strong bond interaction and directionality.^{23,24}

It is known that formic acid is a good candidate for the donor of the H-bonds between polymer chains that possess atoms with lone electrons. Formic acid (HCOOH) is the simplest carboxylic acid, and its unusual conformational H-bonding properties have been the topic of numerous studies.²⁵ The detailed description of the geometry of the molecules of formic acid has been studied by a number of authors.^{26,27}

It is proposed that the incorporation of formic acid into PEDOT will play an enormous role. Our idea is based on the fact that formic acid is small in size and can penetrate between different polymer chains and/or between PEDOT repeating units of the same chain. Additionally, through H-bond interaction, it is also possible to have formic acid in the form of formate ions in the polymer structure. Such an interaction is called a Coulomb interaction, and it is an electrostatic interaction between each pair of charged particles: both negative formate ions and positive cation radical monomer units of PEDOT. The scheme of PEDOT electrochemical synthesis is shown in Figure 1a. Briefly, the electrochemical polymerization of EDOT monomer was performed at the FTO electrodes by galvanostatic polymerization in a three-electrode electrochemical cell configuration. The polymerization was performed by applying 0.1 mA/cm² current density; the polymerization solution was purged with nitrogen gas for 10 min before the polymerization. To prove the key role of the formic acid in the physicochemical properties of PEDOT, the electropolymerization also has been done in the presence of 1 M NaCl or 6 M H₃PO₄ as supporting electrolytes.

The two electrostatic interactions between formic acid and PEDOT chains are presented in Figure 1a. These interactions (H-bonding or Coulomb interactions) between formic acid and PEDOT chains will play a crucial role in the optical, electrochemical, and physical properties of the final PEDOT films. However, to distinguish between these two interactions is not an easy task. The electrostatic interaction between *o*-phosphoric acid and PEDOT is presented in Figure 1b, and the Coulomb interaction between dissociated NaCl and PEDOT is shown in Figure 1c.

In practice, the Raman and infrared spectra are reflecting formation of intermolecular interactions (H-bonding or Coulomb) between formic acid and polymer chains. The existence of strong intermolecular forces can lead to the coupling of normal modes and a resonance energy transfer effect and other effects in the spectrum.^{26,27}

To investigate the role of different molecules (HCOOH, NaCl, or H₃PO₄) on the chemical structure, the electrochemical polymerization was done in their presence, as shown in Figure 1a–c. The Raman spectra recorded with excitation wavelength 785 nm are presented in Figure 2. As could be seen from Figure 2, the chemical structure of PEDOT films synthesized in different electrolytes is similar according to the Raman spectroscopy. The only difference is observed by the presence of the peak at 501 cm⁻¹, which could be associated with the oxyethylene ring deformation caused by electrostatic interaction.²⁸ However, further analysis showed that the PEDOT

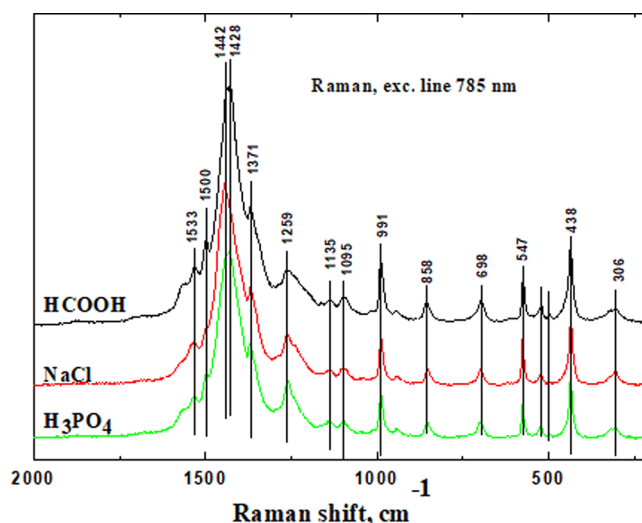


Figure 2. Raman spectra of PEDOT film electrochemically synthesized in the presence of formic acid or NaCl or H₃PO₄, showing that PEDOT chemical structure is similar in all three electrolytes.

film prepared in the presence of formic acid possesses a different elemental composition (sulfur) compared to the PEDOT electrochemically synthesized in the presence of NaCl or H₃PO₄.

To prove that formic acid has different impact compare to NaCl or H₃PO₄ on the chemical structure of thiophene sulfur in PEDOT, the high resolution core-level S 2p and C 1s XPS were recorded for PEDOT films electrochemically synthesized in the presence of different electrolytes (Figure 3). The XPS spectra of PEDOT prepared in NaCl or H₃PO₄ are similar, and the spectra are identical to those reported in the literature so far.²⁹ In high-resolution core-level C 1s spectra (Figure 3) three different peaks located at 284.2, 285.1, and 286.0 eV corresponding to C–S–, C–O–, and –CH₂–CH₂– were observed for the PEDOT film prepared in different electrolytes.³⁰ Additionally, the presence of formic acid in PEDOT in HCOOH was confirmed by XPS analysis; the binding energy peak of –O–C=O is located at 288.4 eV (Figure 3).³¹ On the other hand, the high-resolution core-level S 2p XPS spectrum of PEDOT film in formic acid is completely different (see Figure 3, red rectangle), and a detailed explanation is given below. On the basis of this data, we could make a conclusion that formic acid plays a crucial role in the chemical structure of PEDOT chains compared to H₃PO₄ or NaCl, and furthermore the PEDOT film electropolymerized in the presence of formic acid has different physical properties, shown below.

To elucidate the role of formic acid in the PEDOT structure and properties, the detailed investigation of Raman spectra, XPS, UV–vis, EPR, and electrochemical characterization were performed for PEDOT film electropolymerized in the presence of formic acid.

Detailed Investigation of PEDOT in HCOOH. In an attempt to explain the structure of PEDOT, we chose to measure the Raman spectra of the polymer film as synthesized (PEDOT in HCOOH), after treatment with NaOH, and after the electrochemical measurements: 514, 785, and 1064 nm laser wavelengths were applied. The interaction of radiation with different wavelengths with various oxidation states of PEDOT is complex, and each corresponding Raman spectrum can reflect different features of the polymeric chain. The laser wavelength of 514 nm was used to study the fully reduced PEDOT film by

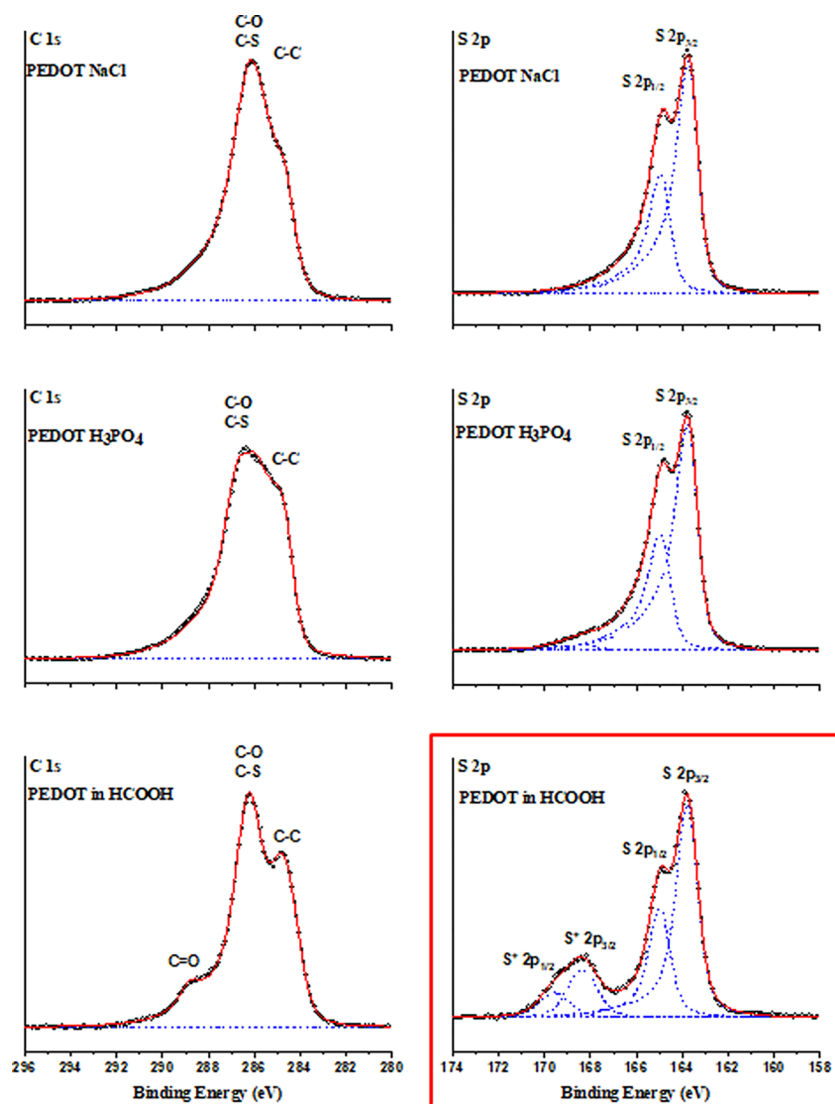


Figure 3. High-resolution core-level of S 2p and C 1s XPS spectra of PEDOT electrochemically synthesized in the presence of NaCl or H_3PO_4 or formic acid. The C 1s XPS spectra of PEDOT electrochemically synthesized in H_3PO_4 or NaCl are similar. The C 1s XPS spectrum of PEDOT in HCOOH has an additional peak corresponding to formic acid. The S 2p XPS spectrum of PEDOT in HCOOH has one more peak at higher binding energy.

Garreau et al.;²⁸ the oxidized part of the PEDOT is reflected in the Raman spectra excited by longer wavelength.²⁸ To investigate electrostatic interactions between the polymer and formic acid, the 785 and 1064 nm wavelength lasers are preferentially used. In Figure 4a, the Raman spectrum of the PEDOT film electrochemically synthesized (PEDOT in HCOOH) is presented; the laser wavelength is 785 nm. The other two spectra (514 and 1064 nm) could be found in the Supporting Information (Figures S1 and S2); moreover, Table S1 with the main peaks and their approximate description for three lasers are presented in the Supporting Information. The main peak at $\sim 1434\text{ cm}^{-1}$ corresponding to the $\text{C}_\alpha=\text{C}_\beta$ stretching vibration for the fully reduced PEDOT³¹ is divided into two peaks for PEDOT in HCOOH, and these are located at 1436 and 1427 cm^{-1} as shown in Figure 4a and Figure S3 (in detail). We suggest that these two peaks correspond to two structures shown in Figure 1a: PEDOT chains and formic acid have Coulomb interactions and H-bonding interactions.

When the PEDOT film was treated with the solution of NaOH, the Raman spectrum had only one peak at 1432 cm^{-1}

(Figure 4a and Figure S3), and this proves that the PEDOT electrochemically polymerized in the presence of HCOOH originally was in a reduced state. This means that during galvanostatic electrochemical deposition the withdrawn electrons led to the formation of reduced PEDOT chains, and more importantly, during electrochemical deposition we did not obtain oxidized PEDOT. Furthermore, the Raman spectrum measured with the 514 nm laser for the PEDOT treated with NaOH shows very narrow and sharp peaks that correspond to reduced constitutional units (Figure S1). This data proves that most of the formic acid was removed from the PEDOT film. And, what is more important, the data also proved that electrostatic interaction occurs between formic acid and PEDOT. However, as mentioned above, the spectral region between 80 and 300 cm^{-1} is assigned to a mode involving hydrogen bonding, and in our Raman spectra (785 and 1064 nm lasers) we observed a peak at 205 cm^{-1} for PEDOT in HCOOH and PEDOT treated with NaOH. We can explain such a vibrational peak by the presence of a small amount of formic acid, which was detected further by other measurements. It must

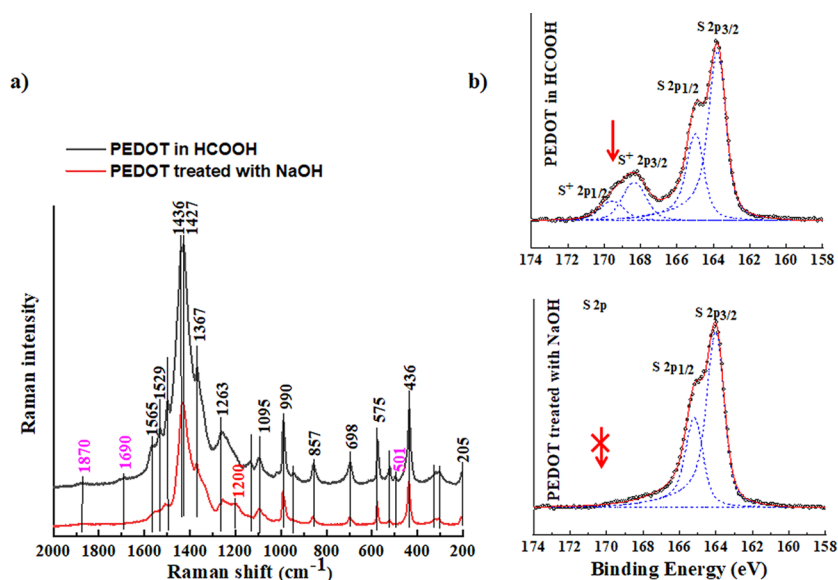


Figure 4. (a) Raman spectra of PEDOT in HCOOH and PEDOT treated with NaOH measured at a 785 nm laser, showing the chemical structure of PEDOT chains with and without formic acid. (b) High-resolution core-level of S 2p XPS spectra of PEDOT in HCOOH and PEDOT treated with NaOH, which show the disappearance of the high binding energy peak only by simply removing formic acid.

be emphasized that the peaks corresponding to formic acid at 1870, 1690, and 501 cm^{-1} disappeared after PEDOT was treated with the NaOH solution. Except for the main peak corresponding to $\text{C}_\alpha=\text{C}_\beta$ stretching vibration, the Raman spectra (785 nm laser) for PEDOT in HCOOH and PEDOT treated with NaOH are similar, which means that the chemical structure of the polymer chains is also similar. The main difference we observed is the formation of the vibration corresponding to the electrostatic interactions between formic acid and PEDOT chains.

The presence of the following peaks located at 698, 857, 1529, and 1565 cm^{-1} for PEDOT, HCOOH, and PEDOT treated with NaOH (small intensity for the last one) also prove in both cases that we have electrostatic interactions between formic acid and polymer.²⁸ In our case, the oxidation state of PEDOT was not changed. Therefore, we conclude that it is not oxidation but intermolecular electrostatic interactions between formic acid and PEDOT, which is reflected by Raman spectroscopy as described above.

Furthermore, to confirm our hypothesis of the role of formic acid in the formation of electrostatic interactions in PEDOT, the high-resolution core-level S 2p X-ray photoelectron spectra (XPS) were recorded and are presented in Figure 4b (top: PEDOT in HCOOH; bottom: PEDOT treated with NaOH). Deconvoluted spectra of electrochemically synthesized PEDOT film have two doublet peaks as shown in Figure 4b (top). In our opinion, these two doublet peaks correspond to reduced thiophene sulfur and thiophene sulfur that underwent a loss of electron density due to Coulomb and/or hydrogen-bonding interactions. In the literature, it was published that the S 2p XPS peak located at ~ 168 eV could correspond to sulfur in counterions such as sulfate or polystyrenesulfonate.²⁹ This was not the case; in our electrochemical synthesis, we used the formic acid as the electrolyte and as doping acid. Also, other authors could observe the S 2p XPS peak located at ~ 168 eV for overoxidized PEDOT³² where the degradation of conjugation in the PEDOT system was observed to have a further loss of conductivity. To prove our idea (hydrogen-bonding or Coulomb interactions between formic acid and PEDOT

chains), the high-resolution core-level S 2p XPS spectrum was measured for PEDOT treated with NaOH (Figure 4b, bottom). The doublet peaks located at higher energy levels are depleted (small tails is present), which confirmed that these peaks matched to thiophene sulfur electrostatically interacted with formic acid as shown in Figure 1a. The PEDOT treated with NaOH has only one doublet in high-resolution core-level S 2p spectra located at 163.8 and 164.9 eV that correspond to S 2p_{2/3} and 2p_{1/2}. It is possible to estimate the amount of thiophene sulfur in PEDOT that electrostatically interacted with formic acid: to do that, we used the ratio of intensity located at ~ 168 eV vs intensity located at ~ 164 eV, and it is 27%. This means that 27% of the thiophene sulfur was in contact with formic acid. On the basis of the XPS measurements, we can conclude that H-bonding interaction is preferable when compared with Coulomb. We discovered that PEDOT electrochemically synthesized in the presence of formic acid (PEDOT in HCOOH) has different physical–chemical properties compared to the PEDOT film prepared in other electrolytes (NaCl or H₃PO₄).

The solid-state UV–vis absorption spectra of PEDOT in HCOOH and after treatment with NaOH are presented in Figure S4. It is obvious from the spectrum that PEDOT treated with NaOH has an absorption maximum shifted to shorter wavelength (higher energy) compared to the spectrum of PEDOT in HCOOH. The last one had a very broad peak starting from 400 to 1000 nm, which could be explained by the presence of localized π -electrons (belonging to different polymer chains, further will be confirmed by XRD measurements) due to the presence of intermolecular electrostatic interactions between formic acid and thiophene sulfur. Such interaction provides conformation alteration of polymer chains and further provides planarization of polymer chains in the polymer matrix. According to UV–vis spectra, it is also possible to estimate the number of chromophores that are in resonance with applied energies. To do that, we deconvolute the obtained spectra, and the results are present in Figure S5. From the deconvolution of UV–vis spectra of PEDOT in HCOOH (Figure S5) two types of chromophores are visible that are

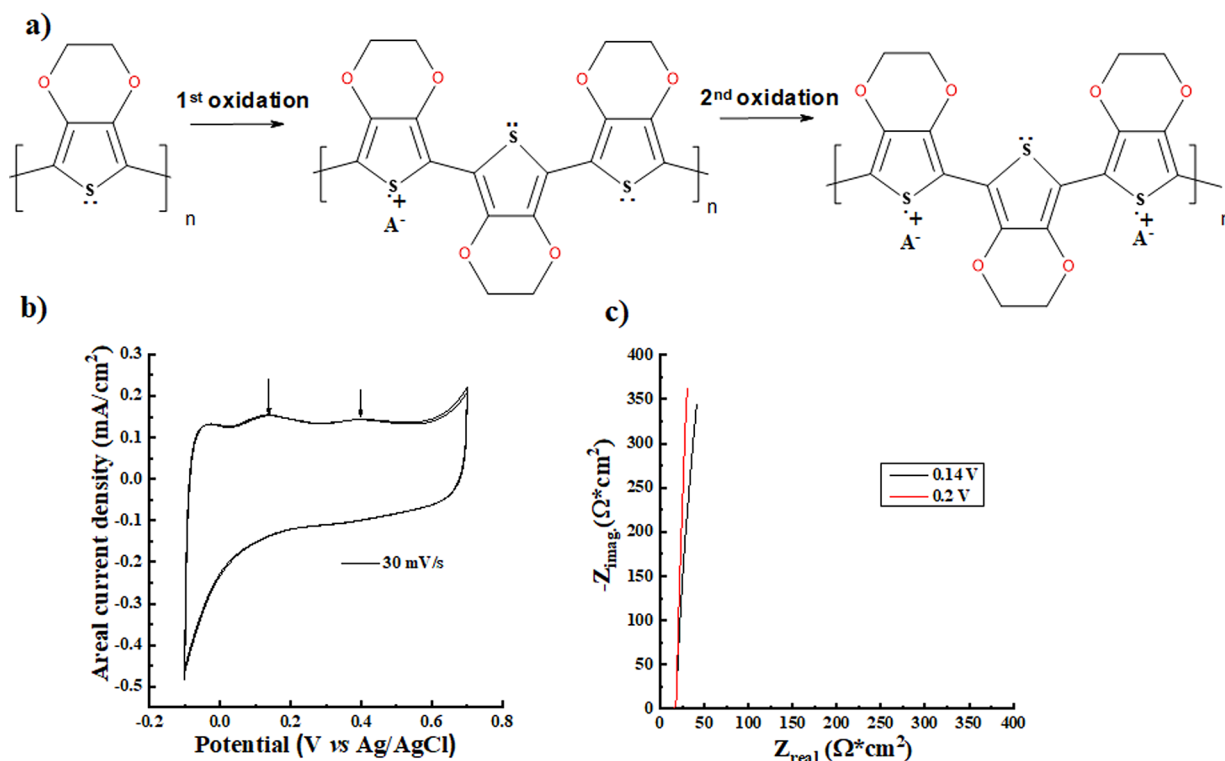


Figure 5. Scheme of PEDOT oxidation, showing the possible explanation of the first and second oxidation peaks (a), cyclic voltammetry of PEDOT scanned at 30 mV/s in 6 M H_3PO_4 (b), and electrochemical impedance spectroscopy curves of PEDOT measured in 6 M H_3PO_4 at various constant applied potentials (c), showing the absence of semicircle at high frequencies.

present in the polymer matrix. There are two peaks located at 535 and 703 nm. It is possible to calculate the optical energy gap according to the equation $E_g = 1240/\lambda_{\text{max}}$ and they are 3.21 and 1.76 eV, respectively. The peak situated at 703 nm has twice the intensity when compared to the peak located at 535 nm. In our opinion, the 703 nm peak corresponds to PEDOT with H-bond interaction and/or Coulomb interaction, and the 535 nm peak corresponds to reduced PEDOT. From the deconvoluted spectra of PEDOT treated with NaOH (Figure S4) we could see that PEDOT consists mainly of reduced polymer with the maximum located at 519 nm ($E_g = 2.39$ eV). The small peak located at 620 nm could be assigned to the PEDOT chains very strongly connected with the formic acid that was not possible to remove by treating it with NaOH. The presence of H-bonding vibrations in the Raman spectrum also confirms this point (Figure 4a).

The primary method to increase polymer conductivity is the solvent annealing, in which a solvent molecule is introduced into the polymer structure. For example, it was shown by Kim and other co-workers that the introduced small molecules (such as dimethyl sulfoxide) change the electrical properties of PEDOT.³³ In our case, the introduction of small organic acid, formic acid, into the PEDOT structure led to the detection of two peaks during cyclic voltammetry measurements (the first at $E_{\text{pa}} = 180$ mV and the second at $E_{\text{pa}} = 400$ mV), but only in acidic medium (Figure 5b). When the cyclic voltammetry measurements were performed in the neutral electrolyte, in 1 M KCl, we did not observe any peak at the voltammetric curve (Figure S6). On the basis of these results, we can conclude that two oxidation peaks are induced by the presence of formic acid and any acid acting as a supporting electrolyte. To illustrate what is happening

with the PEDOT chain, the scheme of oxidation is presented in Figure 5a.

The conductivity improvement of PEDOT film electrochemically prepared in the presence of formic acid could be proved by the electrochemical impedance measurements (EIS), presented in Figure 5c. The impedance was measured at a constant potential 0.14 V (open-circuit potential) and 0.2 V vs Ag/AgCl reference electrode in H_3PO_4 . The result in the form of a complex plane plot is presented in Figure 4c, and it exhibits a straight line without the presence of a semicircle arc at high frequency. This can be explained by the facile processes of charge transfer and charge transport in electrochemically active PEDOT. The equivalent circuit presented in Figure 6 was used to evaluate the measured data.

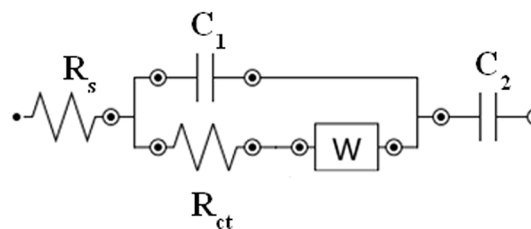


Figure 6. Equivalent circuit that is applied to fit the measured data.

The fitting parameters are summarized in the Table 1, where R_s is the solution resistance, C_1 is a double-layer capacitance, R_{ct} is charge transfer of the PEDOT film, W is Warburg impedance, and C_2 is represented by faradaic capacitance. The corresponding sum of squares of the relative residuals (χ^2 value) for the

Table 1. Fitting Parameters for the Electrochemical Impedance Spectroscopy Measurements

	R_s ($\Omega \text{ cm}^2$)	C_1 (nF/cm 2)	W (mmho)	R_{ct} ($\Omega \text{ cm}^2$)	C_2 (mF/cm 2)	χ^2
0.14 V	1.18 (0.2%)	127 (1.2%)	49.9 (2.1%)	12.8 (0.4%)	6.94 (0.8%)	2×10^{-3}
0.2 V	1.18 (0.2%)	114 (1.9%)	66.8 (3.2%)	12.9 (0.4%)	6.45 (0.7%)	4×10^{-3}

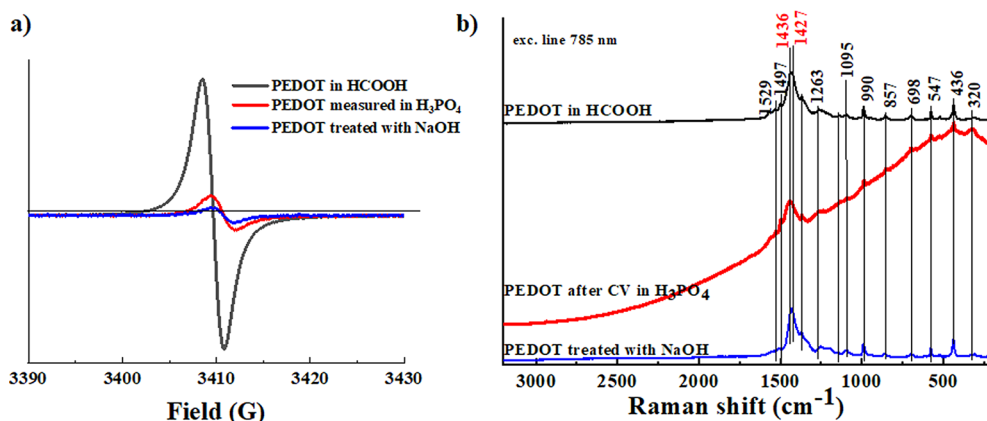


Figure 7. (a) Electron spin resonance spectra of the PEDOT in HCOOH and after being treated by NaOH and after cyclic voltammetry measurements in H_3PO_4 , showing that electrochemically synthesized PEDOT in HCOOH has the highest concentration of cation radicals. (b) Raman spectra of PEDOT in HCOOH and after treated with NaOH and after cyclic voltammetry measurements in H_3PO_4 excited by a 785 nm laser.

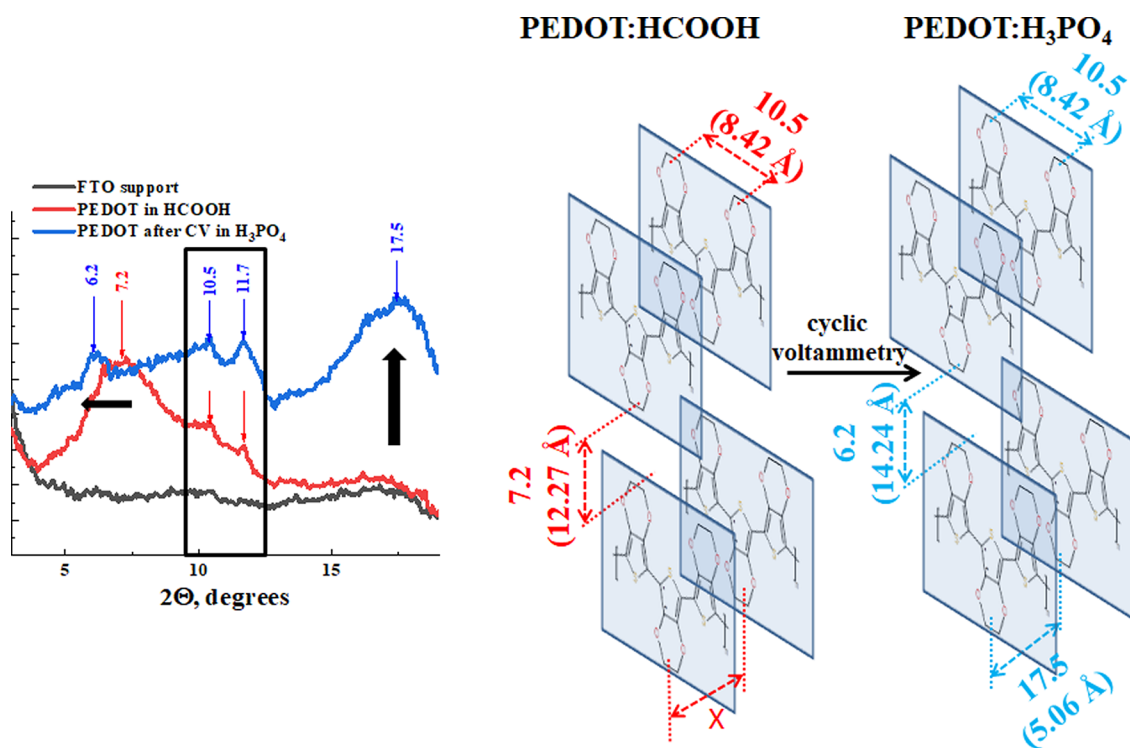


Figure 8. X-ray diffraction of PEDOT in HCOOH and PEDOT film after cyclic voltammetry measurements (left); suggested orientation of polymer chains (right). Formic acid replaced by H_3PO_4 acid during cyclic voltammetry measurements. The intensities of the peaks are increased, indicating the increase of the crystalline order of PEDOT film after electrochemical measurements.

fitting parameters and estimated error (presented in parentheses) could be found in Table 1 as well.

From the fitted data, the most interesting results for us is the R_{ct} , which is in the range of $\sim 13 \Omega \text{ cm}^2$, corresponding to a conductivity of 960 S/cm (for the film thickness of $800 \pm 10 \text{ nm}$).

To confirm our results, the bulk resistivity was measured for dry film for PEDOT in HCOOH and PEDOT film after

electrochemical measurements by four-point probe method (by direct current) and was in the range $0.021 \Omega \text{ cm}$, corresponding to the conductivity 47.6 S/cm for PEDOT in HCOOH, and $1.5 \times 10^{-3} \Omega \text{ cm}$ for PEDOT film after electrochemical measurements (which corresponds to roughly 670 S/cm conductivity). The difference in the measured data could be explained by the role of electrolyte in the conductivity of the PEDOT film. The polymer chains forming the channel are in direct contact with an

electrolyte (in the case of EIS). Because semiconducting polymers are soft and permeable by ions in the electrolyte, the ions can penetrate into the bulk of the PEDOT film and modulate the redox state (i.e., doping level) and as a result change the electrical conductivity.³⁴ Moreover, the crystalline structure of PEDOT films could be tuned by the presence of different ions, which is shown below (Figure 8).

The electron paramagnetic resonance (EPR) was used further to investigate the effect of formic acid on the physical properties of electrochemically synthesized PEDOT film. The cation radical in the PEDOT chain can be stabilized by the counterion—formate ions and/or phosphate ions as presented in Figure 1. On the other hand, we know that H-bonding between formic acid (any acid) and PEDOT chains also takes place: this interaction can induce the charge transfer with the formation of cation radicals. The results of the EPR measurements are presented in Figure 7a, and it is obvious that the PEDOT in HCOOH possesses a sharp and narrow peak located at 3410 G, confirming the presence of cation radicals. After treatment of the PEDOT with the solution of NaOH or cyclic voltammetry measurements in acidic medium, we were still able to detect small amounts of cation radicals in the PEDOT film (Figure 7a). It is surprising that the EPR signal was detected, and to clarify the chemical structure of PEDOT film after the treatment with NaOH or after cyclic voltammetry measurements the Raman spectra for both were measured (Figure 7b) and compared with the Raman spectrum obtained for the PEDOT in HCOOH (785 nm laser). Also, detailed results could be found in Table S1. We could see one very interesting fact, which was the presence of photoluminescence in the Raman spectrum for PEDOT after cyclic voltammetry measurements. Moreover, after looking at the UV–vis data, presented in Figure S4, the absorption maximum is shifted to a higher wavelength: lower energy levels were reported for PEDOT after cyclic voltammetry measurements compared to the PEDOT treated with NaOH or PEDOT in HCOOH. Deconvolution of the peak gave us two peaks that were located at 663 and 835 nm, corresponding to optical energy gaps of 1.87 and 1.48 eV (Figure S5). This red-shift of the absorption in addition to the low EPR signal and the presence of the photoluminescence in the Raman spectrum are connected with the formation of delocalized polaron states in PEDOT film after cyclic voltammetry measurements compare to the localized polaron in PEDOT in HCOOH.

In the next step, our research has focused on the crystalline structure of the PEDOT film, particularly XRD curves were measured for PEDOT in HCOOH and PEDOT after cyclic voltammetry measurements (Figure 8).

The thiophene backbone of the polymer chain is flat,³⁵ as shown in Figure 8 on the right. The evolution of Bragg peak at 2θ (11° – 13°) has been reported to be an indication of the film becomes more metallic due to a decrease in the degree of disorder in direction of polymer chain.^{35,36} The polymer repeat distances are $2\theta = 10.5^\circ$ and 11.7° (corresponding to 8.42 and 7.56 Å) for PEDOT in HCOOH and PEDOT after electrochemical measurements (after at least 100 cycles in 6 M H_3PO_4 electrolyte). These distances do not change after CV measurements as shown in Figure 8 on the left in the black rectangle. Moreover, the intensities of the peaks at $2\theta = 10.5^\circ$ and 11.7° are increased, indicating the increase of the crystalline order of PEDOT film after electrochemical measurements.³⁵ On the other hand, the distance corresponding to the chains stacking on top of each other is changing as the band $2\theta = 7.2^\circ$ is shifted to

6.2° (black arrow), increasing from 12.27 Å for PEDOT in HCOOH to 14.24 Å for PEDOT after CV measurements (Figure 8). We can explain such an increase in the distance by the incorporation of phosphoric acid into the polymer structure. It is obvious that the size of the phosphoric acid is larger compared to formic acid. This contradicted the previously published data, where the size of the counterions did not affect the XRD curves.^{35,36} It is very interesting to observe that PEDOT in HCOOH has a faint peak to be readily visible at $2\theta = 17.5^\circ$, corresponding to interchain distance, and it is marked as *X* in Figure 8 on the right. Therefore, we can conclude that the chains could be randomly oriented in *b*-axes. After cyclic voltammetry measurements, the peak located at $2\theta = 17.5^\circ$ (5.06 Å) is increased in intensity, indicating the orientation of the polymer layers along the surface. We can conclude that during cyclic voltammetry the PEDOT chains not only incorporate in their structure phosphoric acid but also stack on top of each other. Similar rearrangement of polymer layers under high-temperature deposition of PEDOT film was observed by Atanasov et al.³⁶ The authors showed that growth of temperature strongly affects PEDOT crystalline structure and conductivity.³⁷ In our case, we proved that electrostatic interactions (H-bonding or Coulombic interactions) have an enormous influence on the crystallinity and other physical properties of electrochemically synthesized PEDOT in the presence of formic acid.

The diffraction indices of the peaks could be assigned to 100, 200, and 020 at 2θ of 7.2° , 11.7° , and 17.5° for PEDOT in HCOOH and at 2θ of 6.2° , 11.7° , and 17.5° for PEDOT film after electrochemical measurements.^{35,36} Moreover, the shift of the peak (from 7.2° to 6.2°) and the increase in the intensity of the peaks (10.5° , 11.7° , and 17.5°) are the result of the rearrangement of the crystalline domain orientations.^{38–40} This observation also proves our finding from EPR and UV–vis spectroscopies that PEDOT after CV measurements has a decreased EPR signal and a shifted absorption spectrum to lower energy.

3. CONCLUSIONS

In conclusion, it is shown for the first time that electrochemically synthesized PEDOT films in the presence of formic acid possess intermolecular electrostatic interactions. It is recorded that PEDOT electrochemically synthesized in the presence of formic acid has a narrow EPR signal, confirming the presence of cation radicals in its structure. Moreover, Raman spectroscopy showed that PEDOT in HCOOH has electrostatic interactions between formic acid and polymer chains. Furthermore, XPS measurements prove that after PEDOT was treated with base, the peak corresponding to electrostatic interactions of formic acid with thiophene sulfur disappeared from the spectrum. On the basis of the Raman and XPS result, we can conclude that the polymer possesses mostly reduced monomer units in PEDOT treated with NaOH, and 27% of monomer units have intermolecular electrostatic interactions with formic acid in PEDOT in HCOOH. The remaining 73% remains in a reduced state. Also, the electrostatic interaction between formic acid and PEDOT plays a crucial role in the appearance of two oxidation peaks, as was shown by the cyclic voltammetry measurements. Furthermore, we proved that electrostatic interactions (H-bonding or Coulombic interactions) have an enormous influence on the crystallinity of PEDOT film prepared in the presence of formic acid.

■ ASSOCIATED CONTENT

Supporting Information

The Supporting Information is available free of charge at <https://pubs.acs.org/doi/10.1021/acs.macromol.9b02627>.

Experimental part, deconvolution of UV–vis spectra, Raman spectra (excitation lasers 514 and 1064 nm), table with the main vibration mode, cyclic voltammetry of PEDOT measured in 1 M KCl (PDF)

■ AUTHOR INFORMATION

Corresponding Author

Elena Tomsík – Institute of Macromolecular Chemistry, Academy of Sciences of the Czech Republic 162 06 Prague 6, Czech Republic; orcid.org/0000-0002-1749-1091; Email: tomsik@imc.cas.cz

Authors

Iryna Ivanko – Institute of Macromolecular Chemistry, Academy of Sciences of the Czech Republic 162 06 Prague 6, Czech Republic

Jan Svoboda – Institute of Macromolecular Chemistry, Academy of Sciences of the Czech Republic 162 06 Prague 6, Czech Republic; orcid.org/0000-0002-4989-4274

Miroslava Lukešová – Institute of Macromolecular Chemistry, Academy of Sciences of the Czech Republic 162 06 Prague 6, Czech Republic

Ivana Seděnková – Institute of Macromolecular Chemistry, Academy of Sciences of the Czech Republic 162 06 Prague 6, Czech Republic

Complete contact information is available at:

<https://pubs.acs.org/doi/10.1021/acs.macromol.9b02627>

Notes

The authors declare no competing financial interest.

MSc. I. Ivanko is a PhD student at the Faculty of Science, Charles University, Prague 2, 128 00 Czech Republic.

■ ACKNOWLEDGMENTS

The authors acknowledge the Czech Science Foundation (19-04859S). The authors thank Dr. A. Zhigunov for the XRD measurements and Dr. J. Pilař for the discussion of EPR spectra.

■ REFERENCES

- Jelle, B. P.; Hagen, G.; Birketveit, O. Transmission properties for individual electrochromic layers in solid state devices based on polyaniline, Prussian Blue and tungsten oxide. *J. Appl. Electrochem.* **1998**, *28*, 483–489.
- Reddinger, J. L.; Sotzing, G. A.; Reynolds, J. R. Multicoloured electrochromic polymers derived from easily oxidized bis[2-(3,4-ethylenedioxy)thienyl]carbazoles. *Chem. Commun.* **1996**, *15*, 1777–1778.
- Paik, K. L.; Baek, N. S.; Kim, H. K.; Lee, J. H.; Lee, Y. White light-emitting diodes from novel silicon-based copolymers containing both electron-transport oxadiazole and hole-transport carbazole moieties in the main chain. *Macromolecules* **2002**, *35*, 6782–6791.
- Kros, A.; Nolte, R. J. M.; Sommerdijk, N. A. J. M. Conducting polymers with confined dimensions: Track-etch membranes for amperometric biosensor applications. *Adv. Mater.* **2002**, *14*, 1779–1782.
- Chaubey, A.; Gerard, M.; Singhal, R.; Singh, V. S.; Malhotra, B. D. Immobilization of lactate dehydrogenase on electrochemically prepared polypyrrole-polyvinylsulfonate composite film for application to lactate biosensors. *Electrochim. Acta* **2001**, *46*, 723–729.

(6) Lindfors, T.; Ervela, S.; Ivaska, A. Polyaniline as pH-sensitive component in plasticized PVC membranes. *J. Electroanal. Chem.* **2003**, *560*, 69–78.

(7) Gyurcsanyi, R. E.; Nyback, A. S.; Toth, K.; Nagy, G.; Ivaska, A. Novel polypyrrole based all-solid-state potassium-selective microelectrodes. *Analyst* **1998**, *123*, 1339–1344.

(8) Richardson-Burns, S. M.; Hendricks, J. L.; Martin, D. C. Electrochemical polymerization of conducting polymers in living neural tissue. *J. Neural Eng.* **2007**, *4*, L6–L13.

(9) Elschner, A.; Heuer, H. W.; Jonas, F.; Kirchmeyer, S.; Wehrmann, R.; Wussow, K. Gallium complexes in three-layer organic electro-luminescent devices. *Adv. Mater.* **2001**, *13*, 1811–1814.

(10) Baughman, R. H.; Bredas, J. L.; Chance, R. R.; Elsenbaumer, R. L.; Shacklette, L. W. Structural basis for semiconducting and metallic polymer dopant systems. *Chem. Rev.* **1982**, *82*, 209–222.

(11) Alemu, D.; Wei, H. Y.; Ho, K. C.; Chu, C. W. Highly conductive PEDOT:PSS electrode by simple film treatment with methanol for ITO-free polymer solar cells. *Energy Environ. Sci.* **2012**, *5*, 9662–9671.

(12) Tomsik, E.; Kohut, O.; Ivanko, I.; Pekarek, M.; Bieloshapka, I.; Dallas, P. Assembly and Interaction of Polyaniline Chains: Impact on Electro- and Physical-Chemical Behavior. *J. Phys. Chem. C* **2018**, *122*, 8022–8030.

(13) Benor, A.; Takizawa, S. Y.; Chen, P.; Perez-Bolivar, C.; Anzenbacher, P. Dramatic efficiency improvement in phosphorescent organic light-emitting diodes with ultraviolet-ozone treated poly(3,4-ethylenedioxythiophene):poly(styrenesulfonate). *Appl. Phys. Lett.* **2009**, *94*, 193301.

(14) Wang, H.; Helgeson, R.; Ma, B.; Wudl, F. Synthesis and optical properties of cross-conjugated bis(dimethylaminophenyl)-pyridylvinylene derivatives. *J. Org. Chem.* **2000**, *65*, 5862–5867.

(15) Ie, Y.; Okamoto, Y.; Inoue, T.; Tone, S.; Seo, T.; Honda, Y.; Tanaka, S.; Lee, S. K.; Ohto, T.; Yamada, R.; Tada, H.; Aso, Y. Highly planar and completely insulated oligothiophenes: Effects of π -conjugation on hopping charge transport. *J. Phys. Chem. Lett.* **2019**, *10*, 3197–3204.

(16) Yang, C. J.; Jenekhe, S. A. Conjugated aromatic poly-(azomethines) 0.1. Characterization of structure, electronic-spectra, and processing of thin-films from soluble complexes. *Chem. Mater.* **1991**, *3*, 878–887.

(17) Samuelsen, E. J.; Monkman, A.; Pettersson, L. A. A.; Horsburgh, L. E.; Aasmundtveit, K. E.; Ferrer, S. The structure of polypyridine. *Synth. Met.* **2001**, *124*, 393–398.

(18) Monkman, A. P.; Palsson, L. O.; Higgins, R. W. T.; Wang, C. S.; Bryce, M. R.; Batsanov, A. S.; Howard, J. A. K. Protonation and subsequent intramolecular hydrogen bonding as a method to control chain structure and tune luminescence in heteroatomic conjugated polymers. *J. Am. Chem. Soc.* **2002**, *124*, 6049–6055.

(19) Vetrichelvan, M.; Valiyaveetil, S. Intramolecular hydrogen-bond-assisted planarization of asymmetrically functionalized alternating phenylene-pyridinylene copolymers. *Chem. - Eur. J.* **2005**, *11*, 5889–5898.

(20) Yi, C.; Zhang, L.; Hu, R.; Chuang, S. S. C.; Zheng, J.; Gong, X. Highly electrically conductive polyethylenedioxythiophene thin films for thermoelectric applications. *J. Mater. Chem. A* **2016**, *4*, 12730–12738.

(21) Gyurcsanyi, R. E.; Jagerszki, G.; Kiss, G.; Toth, K. Chemical imaging of biological systems with the scanning electrochemical microscope. *Bioelectrochemistry* **2004**, *63*, 207–2015.

(22) Sundfors, F.; Bereczki, R.; Bobacka, J.; Toth, K.; Ivaska, A. Microcavity based solid-contact ion-selective microelectrodes. *Electroanalysis* **2006**, *18*, 1372–1378.

(23) Li, Z.-T.; Wu, L.-Z. *Hydrogen Bonded Supramolecular Structures*; Springer: 2015; Vol.87.

(24) Gospodinova, N.; Tomsik, E. Hydrogen-bonding versus pi-pi stacking in the design of organic semiconductors: From dyes to oligomers. *Prog. Polym. Sci.* **2015**, *43*, 33–47.

(25) Blumenfeld, S. M.; Fast, H. Low frequency Raman spectra of solid and liquid formic acid. *Spectrochim. Acta A-Mol. Spectrosc.* **1968**, *24*, 1449–1459.

(26) Bartholomew, R. J.; Irish, D. E. Raman spectral study of 'neat' formic acid and aqueous and organic solutions of formic acid. *J. Raman Spectrosc.* **1999**, *30*, 325–334.

(27) Jedlovsky, P.; Bako, I.; Palinkas, G.; Dore, J. C. Structural investigation of liquid formic-acid - x-ray and neutron-diffraction, and reverse monte-carlo study. *Mol. Phys.* **1995**, *86*, 87–105.

(28) Garreau, S.; Louarn, G.; Buisson, J. P.; Froyer, G.; Lefrant, S. In situ spectroelectrochemical Raman studies of poly(3,4-ethylenedioxythiophene) (PEDT). *Macromolecules* **1999**, *32*, 6807–6812.

(29) Crispin, X.; Marciniak, S.; Osikowicz, W.; Zotti, G.; van der Gon, A. W. D.; Louwet, F.; Fahlman, M.; Groenendaal, L.; De Schryver, F.; Salaneck, W. R. Conductivity, morphology, interfacial chemistry, and stability of poly(3,4-ethylene dioxathiophene)-poly(styrene sulfonate): A photoelectron spectroscopy study. *J. Polym. Sci., Part B: Polym. Phys.* **2003**, *41*, 2561–2583.

(30) Ivanko, I.; Pánek, J.; Svoboda, J.; Zhigunov, A.; Tomšík, E. Tuning the photoluminescence and anisotropic structure of PEDOT. *J. Mater. Chem. C* **2019**, *7*, 7013–7019.

(31) Bowker, M.; Madix, R. J. M. XPS, UPS and thermal desorption studies of the reactions of formaldehyde and formic acid with the Cu(110) surface. *Surf. Sci.* **1981**, *102*, 542–565.

(32) Amanchukwu, C. V.; Gauthier, M.; Batcho, T. P.; Symister, C.; Shao-Horn, Y.; D'Arcy, J. M.; Hammond, P. T. Evaluation and stability of PEDOT polymer electrodes for Li-O₂ batteries. *J. Phys. Chem. Lett.* **2016**, *7*, 3770–3775.

(33) Park, H.-S.; Ko, S.-J.; Park, J.-S.; Kim, J. Y.; Song, H.-K. Redox-active charge carriers of conducting polymers as a tuner of conductivity and its potential window. *Sci. Rep.* **2013**, *3*, 2454.

(34) Berggren, M.; Crispin, X.; Fabiano, S.; Jonsson, M. P.; Simon, D. T.; Stavrinidou, E.; Tybrandt, K.; Zozoulenko, I. Ion electron-coupled functionality in materials and devices based on conjugated polymers. *Adv. Mater.* **2019**, *31*, 1805813.

(35) Aasmundtveit, K. E.; Samuelsen, E. J.; Pettersson, L. A. A.; Inganäs, O.; Johansson, T.; Feidenhans'l, R. Structure of thin films of poly(3,4-ethylenedioxythiophene). *Synth. Met.* **1999**, *101*, 561–564.

(36) Niu, L.; Kvarnström, C.; Fröberg, K.; Ivaska, A. Electrochemically controlled surface morphology and crystallinity in poly(3,4-ethylenedioxythiophene) films. *Synth. Met.* **2001**, *122*, 425–429.

(37) Atanasov, S. E.; Losego, M. D.; Gong, B.; Sachet, E.; Maria, J.-P.; Williams, P. S.; Parsons, G. N. Highly conductive and conformal poly(3,4-ethylenedioxythiophene) (PEDOT) thin films via oxidative molecular layer deposition. *Chem. Mater.* **2014**, *26*, 3471–3478.

(38) Ouyang, L.; Musumeci, C.; Jafari, M. J.; Ederth, T.; Inganäs, O. Imaging the phase separation between PEDOT and polyelectrolytes during processing of highly conductive PEDOT:PSS films. *ACS Appl. Mater. Interfaces* **2015**, *7*, 19764–19773.

(39) Kim, N.; Lee, B. H.; Choi, D.; Kim, G.; Kim, H.; Kim, J.-R.; Lee, J.; Kahng, Y. H.; Lee, K. Role of interchain coupling in the metallic state of conducting polymers. *Phys. Rev. Lett.* **2012**, *109*, 106405.

(40) Palumbiny, C. M.; Liu, F.; Russell, T. P.; Hexemer, A.; Wang, C.; Muller-Buschbaum, P. The crystallization of PEDOT:PSS polymeric electrodes probed in situ during printing. *Adv. Mater.* **2015**, *27*, 3391–3397.

Appendix 3

Ivanko, I.; Mahun, A.; Kobera, L.; Černochová, Z.; Pavlova, E.; Toman, P.; Pientka, Z.; Štěpánek, P.; Tomšík, E. Synergy between assembly of individual PEDOT chains and their interaction with light, *Macromolecules*, **54**, 10321-10330 (2021). IF = 5,985.

Synergy between the Assembly of Individual PEDOT Chains and Their Interaction with Light

Iryna Ivanko, Andrii Mahun, Libor Kobera, Zulfiya Černochová, Ewa Pavlova, Petr Toman, Zbyněk Pientka, Petr Štěpánek, and Elena Tomsík*

Cite This: *Macromolecules* 2021, 54, 10321–10330

Read Online

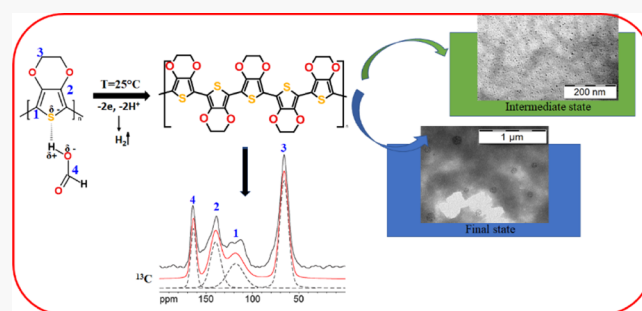
ACCESS |

Metrics & More

Article Recommendations

Supporting Information

ABSTRACT: A new method for poly (3, 4-ethylenedioxythiophene) (PEDOT) synthesis based on acid-assisted polymerization is proposed, and the optical and structural properties of the obtained material are explored. Special attention is given to the effect of the polar Bronsted acid on the formation of oligomer/polymer chains and their ability to assemble into nanoobjects. By using ^1H and ^{13}C NMR spectroscopy (in the liquid and solid state), the formation of PEDOT in a neutral state was proven. Matrix-assisted laser desorption/ionization–time-of-flight, static light scattering, and dynamic light scattering spectroscopies were used to determine the M_w and size of PEDOT nanoobjects. Moreover, we used density functional theory calculations to seek a correlation between the length of the PEDOT oligomer chain and the position of its lowest-energy absorption peak S_1 . All calculations were performed in concentrated formic acid and compared with calculations in the gas phase. In addition, we demonstrate a correlation between the photoluminescence (PL) from individual PEDOT chains and that from PEDOT chains assembled into nanoobjects. While individual PEDOT chains show four PL peaks, the assembled PEDOT nanoobjects show only one PL peak. Tuning the process of self-assembly for individual PEDOT chains is a promising way to control the properties of a polymer material.



1. INTRODUCTION

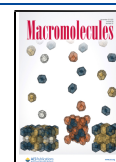
Conjugated polymers and small-molecule organic materials have become omnipresent as active components in a wide range of (opto) electronic applications including organic light-emitting diodes, organic photovoltaic cells, and organic field-effect transistors.^{1–3} Poly(3,4-ethylenedioxythiophene) has received the most attention in this respect because of its tunable electrical conductivity, air stability, and transparency in the p-doped state.⁴ A fundamental understanding of the effects of the molecular structure on material characteristics and physicochemical properties in conducting polymers requires the preparation of materials with very well-defined chemical structures.⁵ There is no doubt that the preparation process is of vital importance for the morphological, electrical, and mechanical properties of the final polymer and, consequently, its application. Generally, the polymerization of poly (3,4-ethylenedioxythiophene) (PEDOT) starts with radical cations generated from the EDOT monomer, proceeds via further radical–radical coupling reactions that grow the polymer chain progressively, and ends with an insoluble PEDOT chain reaching a sufficient length during which negatively charged counter ions of different sizes join to maintain an electrically neutral polymer.⁶ Many methods are available for the synthesis of PEDOT-based materials such as chemical polymerization,^{7,8}

interfacial polymerization,⁹ vapor-phase polymerization (VPP),¹⁰ and electrochemical polymerization.^{11,12} The most widely used synthesis methods are electrochemical deposition under oxidation potentials and chemical polymerization in the presence of powerful oxidants. Chemical polymerization is suitable for the large-scale production of PEDOT nanomaterials. Facile preparation of one-dimensional PEDOT nanomaterials with controlled morphologies ranging from ellipsoidal nanoparticles and nanorods to nanotubes can be realized by carefully adjusting the additive amount of FeCl_3 in the sodium bis(2-ethylhexyl)sulfosuccinate reverse cylindrical micelle phase.¹³ PEDOT can also be electrochemically polymerized in a three-electrode cell containing an electrolyte solution, the monomer (EDOT or EDOT derivatives) through different electrochemical techniques, for example, chronoamperometry,¹⁴ chronopotentiometry,¹⁵ and cyclic voltammetry.¹⁶ PEDOT is formed on the anode's surface, with commonly

Received: September 20, 2021

Revised: October 25, 2021

Published: November 12, 2021



used conducting supports including indium tin oxide, carbon paper, Au, *etc.*^{17,18} Regarding the interest in studying the neutral PEDOT, Yamamoto and Aba carried out polycondensation of 2,5-dichloro-3,4-ethylenedioxythiophene following a reaction with a Ni(0) reagent.¹⁹ The dark purple product was not soluble and, therefore, not amenable for molecular-weight measurements, similar to other doped PEDOT. VPP is another method that consists of exposing a surface covered with a mixture of Fe(tosylate)₃ as the oxidant and pyridine as a base to moderate the strength of the oxidant and EDOT vapors.²⁰ Winther-Jensen and West noticed that EDOT can participate in acid-initiated polymerization, whereby a partially conjugated polymer is formed, which leads to short conjugation lengths.²⁰ The addition of a base is therefore of interest to prevent unwanted acidic side reactions. As a consequence, better results were obtained by adding pyridine to the VPP chamber.^{21–23} Recently, liquid-phase depositional polymerization was reported to overcome some drawbacks inherent to VPP and o-chemical vapor deposition by implementing polymerization directly into the liquid phase.²⁴ Recently, a new method to form conducting polythiophene was invented; in particular, an environmentally friendly and facile method for solid-state polymerization has met with great success in the synthesis of PEDOT and its analogues.^{25,26} Simultaneously, Xia independently found that PEDOT can be formed just by the simple heating of mono-bromo-substituted 3,4-ethylenedioxythiophene (Br-EDOT).²⁷ Meanwhile, Bonillo and Swager successfully synthesized the corresponding polymers based on monochloro-substituted EDOT derivatives in the presence of a Lewis acid.²⁸ All of the above-mentioned methods require prior and time-consuming modification of monomers (derivatives) with further elimination of the byproduct for the reaction. Therefore, it remains a challenge to introduce an additional method for the synthesis of PEDOT with better processing and novel properties for the final material. Recently, our group showed, for the first time, a simple method of polymerization for PEDOT based on acid-assisted polymerization without applying any oxidant and with the formation of a PEDOT solution at room temperature.²⁹ To satisfy the acid-assisted polymerization of PEDOT, the polymerization mixture has to contain an activated reagent that can decrease the oxidation potential of the monomer. It is known that some electrolyte molecules have electrocatalytic properties that activate monomers and decrease their oxidation potentials. For example, the oxidation potential of thiophene in boron trifluoride diethyl etherate was measured to be only 1.2 V (*vs* SCE), which is much lower than that measured in a neutral electrolyte such as acetonitrile (2.1 V *vs* SCE).^{30,31} In particular, an interesting report where authors examined an increase in the rate of polymerization of acrylates due to the formation of hydrogen bonds can be found in ref 32. These authors concluded that hydrogen bonding leads to the “organization” of monomer units, although the nature of the “organization” was not specified. In addition, hydrogen-bonded oligomers display a strong bathochromic shift in the solid-state optical spectrum compared to that for the oligomer solution. Oligothiophenes functionalized by phthalhydrazide, for example, tend to form hydrogen bonds and exhibit redshifted thin-film absorption. In contrast, when the hydrogen bond is “turned off” by methylation, no displacement is observed.³³

In the current work, we elucidated the mechanism for acid-assisted polymerization and the effect of polar Bronsted acid on the formation of oligomers/polymers. By using ¹H and ¹³C

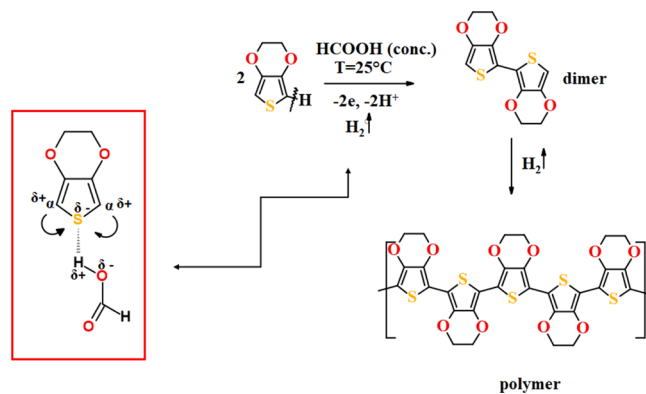
NMR spectroscopy (in the liquid and solid states), the formation of PEDOT in a neutral state was proven. By using matrix-assisted laser desorption/ionization–time-of-flight (MALDI-ToF), static light scattering (SLS), and dynamic light scattering (DLS), we determined the *M_w* and the size of PEDOT nanoobjects in the ultimate solution. In addition, we investigated the nature of the photoluminescence (PL) of chromophores present in individual PEDOT chains in formic acid and the impact of PEDOT chain aggregation (self-assembly) on the light emission properties. Moreover, we used density functional theory (DFT) calculations to seek a correlation between the length of the PEDOT oligomer chain and the position of its lowest-energy absorption peak *S*₁. All calculations were performed in formic acid solution (static dielectric constant 51.1 and optical dielectric constant 1.88) and compared with calculations in the gas phase.

2. RESULTS AND DISCUSSION

2.1. Mechanism for Acid-Assisted Polymerization.

The polymerization of PEDOT was performed in the presence of concentrated formic acid, which possesses a good ability to form intermolecular forces. The impact of the solvent on the course of chemical reactions has been elucidated by Menschutkin. This author postulated a relationship between the rate of the reaction and the structure of the solvent.³⁴ Selection of the solvent, in addition, predominates the rate of the reaction and mechanism. For example, the rate of the reaction in which ionic charges arise increases with increasing polarity of the medium, whereas the reaction is retarded if ionic charges disappear in the nonpolar solvent. In our case (acid-assisted polymerization), the presence of formic acid can result in a new mechanism for the polymerization reaction due to the polarity of the solvent. The polarity of the solvent is specified by its solvation behavior, which in turn depends on the action of intermolecular forces (Coulomb, directional, inductive, dispersion, and charge-transfer forces, as well as hydrogen-bonding forces) between the solvent and solute.³⁵ Formic acid is a good candidate for generating intermolecular interactions (mainly hydrogen-bonding interactions) between its molecules and monomers, resulting in the formation of dimers or even trimers.³⁶ From our point of view, due to the presence of protic acid, formic acid might induce directional intermolecular forces, and, as a result, dramatically decrease the oxidation potential of the monomer by offsetting the electron density from C-*α* in the thiophene ring (see Scheme 1). As

Scheme 1. Scheme for Acid-Assisted Polymerization of the EDOT Monomer in the Presence of Formic Acid



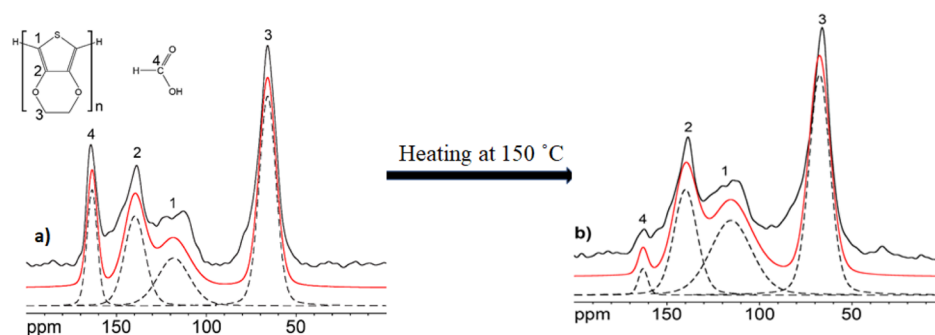


Figure 2. Experimental ^{13}C VF/MAS NMR spectra for the ultimate product (black solid line), simulations of the individual carbon atoms (dashed line), and their sum (red solid line): (a) as-prepared sample and (b) after heating.

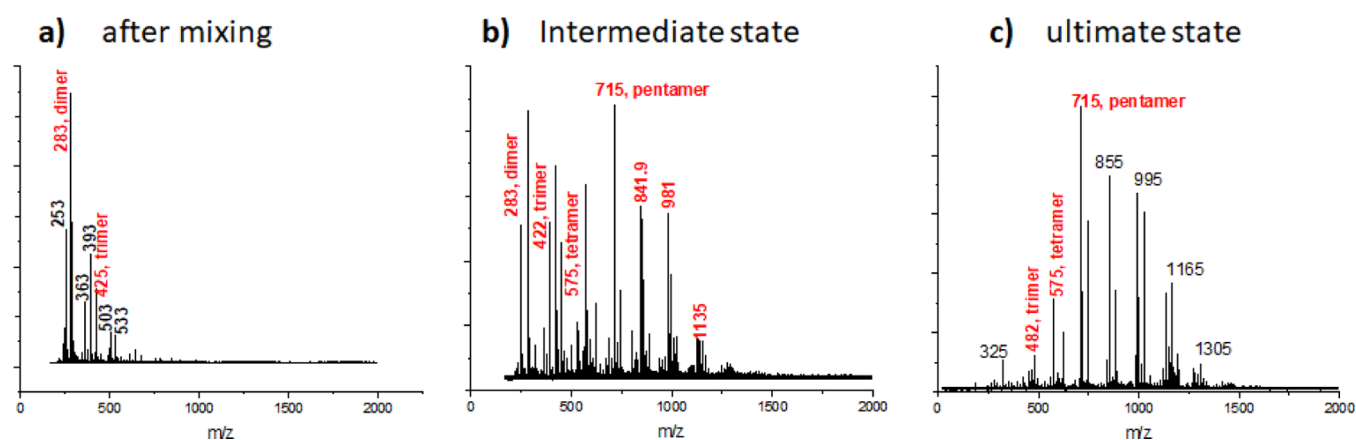


Figure 3. Evolution of M_w for PEDOT measured by MALDI-ToF immediately after mixing (a), intermediate state (b), and ultimate state (c).

EDOT unit (signal “3”) with the integral intensity of the signal from formic acid (signal “4”) shows that there is approximately one molecule of formic acid per three EDOT units in the PEDOT oligomer. However, after heating the PEDOT powder to 150 °C, the peak at 164 ppm (marked as “4”) decreases due to the evaporation of formic acid from the sample. But, the detectable signal corresponding to formic acid residues (signal “4”) that are strongly associated with the PEDOT oligomers is still present.

Furthermore, to investigate in depth the chemical structure and physicochemical properties of PEDOT solution, the M_w must be known. For this purpose, the MALDI-ToF method was used. The MALDI-ToF measurements for acid-assisted polymerization were carried out *in situ* for three different states to determine the evolution of the molecular weight during acid-assisted polymerization: immediately after mixing, Figure 3a, intermediate, 3b, and ultimate states (presented in Figure 3c). As shown in Figure 3a, the M_w for the polymer solution after mixing corresponds to the dimer (283 m/z) and trimer (425 m/z). However, after 48 h, as shown in Figure 3b (intermediate state), the reaction proceeds and the M_w is increasing to pentamers (715 m/z) and tetramers (575 m/z). We proposed that the recorded higher-molecular-weight oligomers ($m/z = 841, 981,$ and 1135) are assembled from shorter chains (e.g., tetramers and/or trimers), which cannot be separated throughout the measurements. However, during the ionization process, neutral clusters of formic acid suffer little defragmentation with the formation of HCO^+ ($m/z = 29$) and H_2CO^+ ($m/z = 30$).^{40,41}

Such defragmentation of formic acid can be observed from the presence of the molecular weights of $m/z = 325, 363, 503,$

or 533. Moreover, under the ionization process, the PEDOT oligomers also yielded fragmented compounds ($m/z = 253, 393,$ and others). Additionally, Liu *et al.* calculated that the dioxethylene ring C–O bonds have high sensitivity and are prone to fragment under laser irradiation.⁴² There is still an open question: are only tetramers and trimers formed? The longer oligomer chains can be a result of the assembly processes for the shorter ones, and the energy of the laser is not sufficient to separate them. For the ultimate state, the most intense peak corresponds to the tetramer (575 m/z) and pentamer ($m/z = 715$); see Figure 3c.

Based on these results, it is concluded that using acid-assisted polymerization, only short oligomer chains are formed. Such short chains are able to assemble into nanoobjects, which is confirmed by cryo-transmission electron microscopy (TEM) and TEM. As shown in Figure 4a, the intermediate state (when the concentration of the short PEDOT chains in the solution is low enough) is composed of nanoobjects with a size of approximately 5 nm. It must be emphasized that the contrast for these black dots (nanoobjects) is very high (compared to the PEDOT reported in the literature),⁹ which suggests compact assembly for the short oligomer chains that possess high electron density. Aggregation of polymer chains in solution plays an important role in phase separation. Therefore, we suggest that the small oligomer chains form nanoobjects first and further form a low-density globular aggregate of PEDOT (so-called nanogels or some cluster-like structures, see DLS and SLS results) with a diameter of ~ 150 nm, as shown in Figure 4b. In addition to TEM, cryo-TEM was used to investigate in detail the presence of nanoobject in the polymer solution (Figure 4c,d). For this purpose, a formic

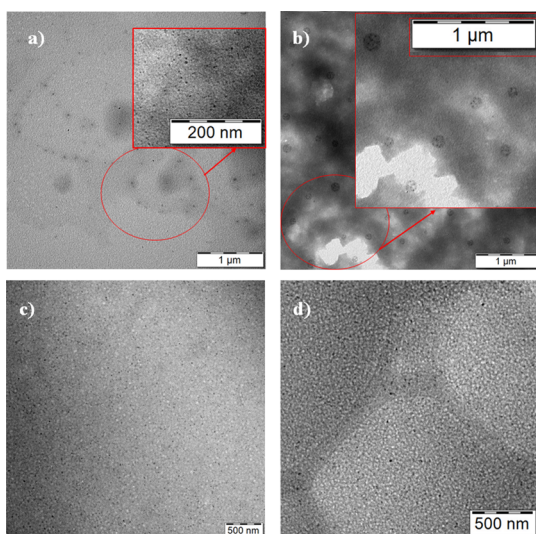


Figure 4. (a) TEM image of PEDOT solution (intermediate state) and (b) PEDOT solution (ultimate state) and (c,d) cryo-TEM for PEDOT ultimate solution with a concentration of 22.4 mg/mL.

acid-based PEDOT solution with a concentration of 22.4 mg/mL was applied to a grid mesh and plunge-frozen in liquid ethane. The obtained images show the presence of small black dots that correspond to PEDOT nanoobjects composed of short oligomeric chains.

Based on information obtained from TEM and cryo-TEM, our next aim was to directly examine the size of the nanoobjects in polymer solution by appropriate methods. For this purpose, SLS and DLS were applied. The DLS measurements at different angles reveal the presence of structures with hydrodynamic radii of approximately 100–200 nm, as shown in the three-dimensional diagram in Figure 5. In this graph, we use equal-area representation [the Z-axis shows $R_h \cdot A(R_h)$, where $A(R_h)$ is the intensity-weighted distribution function for the hydrodynamic radii R_h of particles in the sample] to maintain legibility. The dependence of the decay rate Γ versus the square of the scattering vector q , (see Supporting Information, Figure S4), shows a linear dependence approaching zero, which indicates translational diffusion of these particles. The results obtained from SLS and DLS are represented in Table 1. Structures were observed to be as

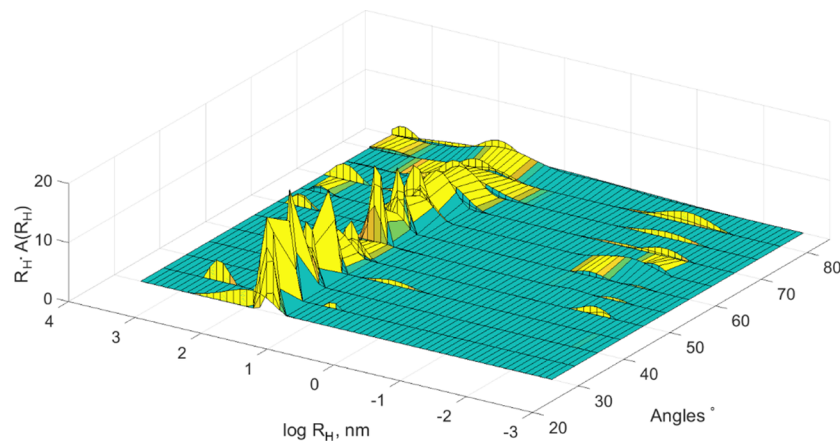


Figure 5. Dependence of hydrodynamic radius and intensity on the scattering angle for ultimate solution with a concentration of 11.55 mg/mL at room temperature.

Table 1. DLS and SLS Data^a

R_{lv} , nm	R_g , nm	$M_w \times 10^6$ of particles, g/mol	$D_{app} \times 10^{15}$, cm^2/s	ρ , g/cm^3
143.5	187.9	1.138	2.752	0.068

^aHere, D_{app} is the diffusion, ρ is the particle density, which is calculated from the particle molecular weight and radius of gyration (R_g), $\rho = M_w/N_A(4/3)\pi R_g^3$ using Avogadro's number N_A .

spherical but with lower molecular weight as a particle have very low particle density ρ . This value can be compared to that for nanogels⁴³ or some cluster-like structures.

2.2. Interaction of PEDOT Chains with Light.

2.2.1. Absorption Spectra. The main goal of this study is to understand the nature of the observed UV–vis and PL transitions.

To explore the obtained oligomers and their assembly in formic acid, the absorption spectra for the intermediate and ultimate states of PEDOT solutions were recorded, and the results are presented in Figure 6. Using DFT methods, the molecular conformations and absorption spectra for EDOT monomers and different oligomers were calculated. To evaluate the solvation effect, these calculations were performed in both formic acid (Table 2) and vacuum (Table S2 in the Supporting Information). As presented in Figure 6, the absorption spectra for the intermediate state (green curve) possess four absorption peaks. We propose that the first two peaks located at 440 and 480 nm correspond to a single vibrationally resolved absorption peak of the tetramer, which is also confirmed by DFT calculations (see Table 2 and Figure 6b). The electronic absorption spectrum of an individual tetramer calculated using the TD PBE0-D3/6-31+G* method in formic acid exhibits a single transition $S_0 \rightarrow S_1$ in the visible region of the spectrum (see Table S3 and shown as the red line in Figure 6a). The vibrational structure of this band, calculated by means of the Franck–Condon approach, is shown in Figure 6b. While the peak at 440 nm in the measured spectrum (Figure 6a) is slightly greater than the second peak at 480 nm, both of these peaks (0–1 at 449 nm and 0–0 at 484 nm) in the calculated spectrum possess almost the same intensity. This discrepancy between the experimental and theoretical spectra arises from the underestimation of the Huang–Rhys factor by approximately 10% due to the neglect of some relaxation processes in the Franck–Condon calculation. On the other

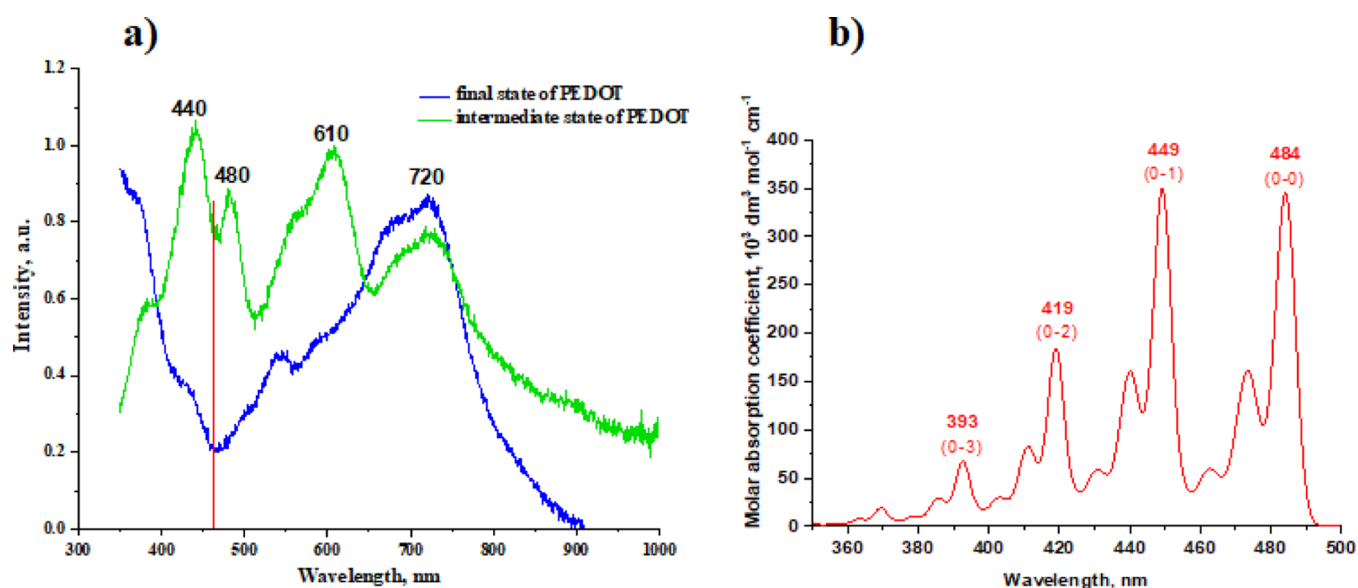


Figure 6. (a) Absorption spectra for the intermediate (green curve) and ultimate states (blue curve) of PEDOT solutions. The DFT-calculated position of the $S_0 \rightarrow S_1$ transition for an EDOT tetramer is shown by the red line. (b) Vibrational structure of the $S_0 \rightarrow S_1$ absorption band for an EDOT tetramer in formic acid calculated by the Franck–Condon approach.

Table 2. Excitation Energies, Wavelengths, and Oscillator Strengths of the First Excited States S_1 of PEDOT Oligomers (up to Decamer) in the Formic Acid Calculated by Means of TD PCM-PBE0-D3/6-31+G* Using the Linear Response Approach with the Nonequilibrium Solvation.

n	Energy(eV)	Wavelength (nm)	Osc.Strength
1	5.24	237	0.23
2	3.82	324	0.60
3	3.09	401	0.99
4	2.68	462	1.48
5	2.42	512	1.93
6	2.25	552	2.39
7	2.12	585	2.82
8	2.03	612	3.24
9	1.96	633	3.65
10	1.90	651	4.06

hand, the peaks located at 610 and 720 nm correspond to the aggregated state of the PEDOT chains and/or longer polymer chains (e.g., octamers). The calculated vibrationally resolved $S_0 \rightarrow S_1$ absorption bands for oligomers of different lengths are shown in Figure S6. Such a behavior has been previously reported in the literature for dyes, where the formation of J-aggregates is detected.⁴⁴

The intensities of the absorption peaks for individual oligomer chains are higher than the absorption intensities of the aggregated chains and nanoobjects, the presence of which is confirmed by TEM.

The role of formic acid in the process of acid-assisted polymerization is described in detail in the Section 2.1. Mechanism for acid-assisted polymerization. Moreover, we assume that the carboxylic group $-\text{COOH}$ of formic acid may be in a position that is close to the coplanarity of the PEDOT

ring, and the resulting interaction induces an intramolecular charge-transfer character to the $\pi \rightarrow \pi^*$ transition with a bathochromic shift of the corresponding absorption band; a similar behavior is observed for dyes.⁴⁴

The recorded absorption peaks for the ultimate solution (blue curve) show one broad peak (located at 720 nm). The intensity of the absorption peaks corresponding to the individual oligomer chains decreased but is still present in the spectrum. This means that most of the oligomer chains are assembled into nanoobjects, which is confirmed by cryo-TEM, TEM, and DLS and SLS measurements. Moreover, the peak at 720 nm is broad, which means that several absorption processes overlap. This indicates that one process is associated with the absorption of individual nanoobjects with a size of 5 nm, and the other process is related to the absorption of larger particles, as observed by TEM (Figure 4b) and confirmed by DLS and SLS measurements (formation of nanogels or some cluster-like structures). The formation of such nanoobjects is likely due to either the planarization of the polymer⁴⁵ or self-assembly of oligomers,⁴⁶ where the formation of intermolecular forces (such as hydrogen bonding) has an important structural effect. Hydrogen-bonded oligomers display a strong bathochromic shift in the solid-state optical spectrum compared to that for the oligomer solution.⁴⁷ Oligothiophenes functionalized by phthalhydrazide, for example, tend to form hydrogen bonds and exhibit redshifted thin-film absorption. In contrast, when the hydrogen bond is “turned off” by methylation, no displacement is observed.⁴⁸ Additionally, our previous experience with polyaniline⁴⁹ (another semiconducting polymer) shows that it is possible to obtain individual polymer chains by diluting concentrated solution, which leads to a tuning of the absorption spectra. Therefore, based on literature data and our own measurements, we conclude that the intermediate state of PEDOT solution consists mainly of individual oligomers, namely, tetra- and/or pentamers, as supported by DFT calculations and MALDI-ToF measurements. The ultimate state of PEDOT consists of assembled oligomer chains associated into nanoobjects, which are further

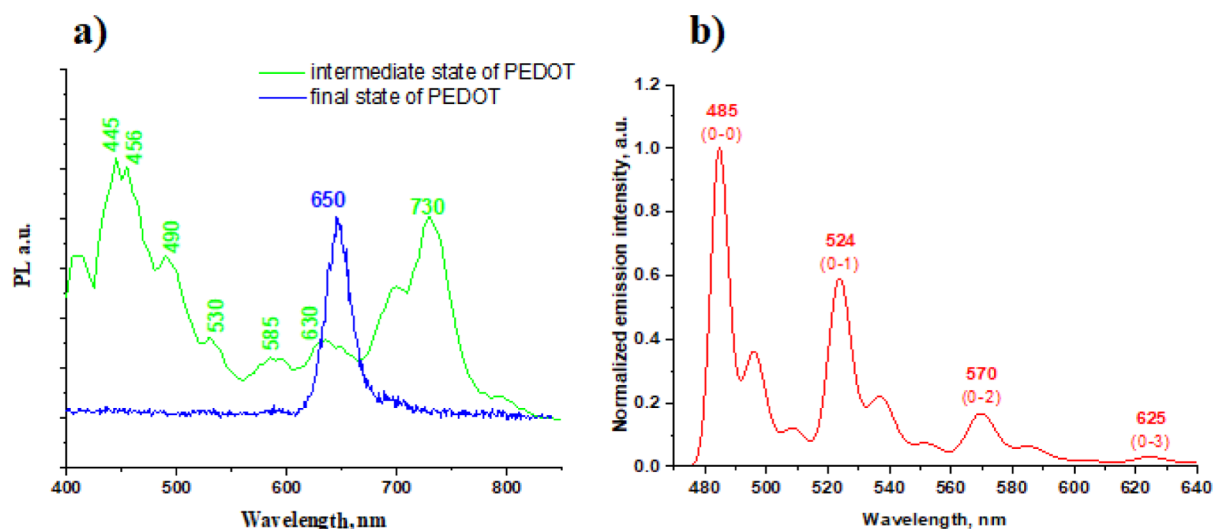


Figure 7. (a) Synchronous PL spectra for intermediate (marked green) and ultimate (marked blue) states of PEDOT solutions and (b) vibrationally resolved emission spectrum of an EDOT tetramer (red) in formic acid calculated by DFT combined with the Franck–Condon approach.

connected to nanogels or some cluster-like structures with a strong bathochromic absorption peak at 720 nm.

2.3. Nature of PL. The PL spectra were recorded to study the influence of light on the aggregated state of PEDOT chains in detail: from individual chains to small nanoobjects and to larger globular aggregates. First, synchronous PL spectrometry was applied because it has been extensively used for multicomponent analysis. The spectra were obtained through simultaneous scanning with the excitation and emission monochromators of a spectrofluorometer, with a fixed difference in wavelength ($\Delta\lambda = 5$ nm) between the two. To prove that we are dealing with the PL process rather than Raman scattering, individual excitation wavelengths were applied as the second method, and the results are presented in Supporting Information, Figure S5. As shown in Figure S5, the PL emission is independent of the excitation wavelengths, and the spectra do not shift as the excitation wavelengths are varied, proving that we are dealing with PL. However, in the final case, broader PL peaks were recorded. On the other hand, when the synchronous PL method was used, narrow peaks were recorded, and, as shown in Figure 7, the PL for the intermediate state (green curve) possesses three peaks at 445/456, 630, and 730 nm compared to that for the ultimate state (blue curve), which has only a peak located at 650 nm.

From the absorption spectroscopy results, we know that in the intermediate-state solution, we have a mixture of individual oligomer chains (tetramer), which is why by using the DFT calculations combined with the Franck–Condon approach, the vibrationally resolved luminescence spectrum of this oligomer in formic acid was calculated (see Figure 7b). Comparing the experimental and calculated spectra, the broad emission band observed between *ca.* 400 and 600 nm (green curve in Figure 7a) was assigned to the luminescence of individual tetramers, while the nature of the other peaks for the intermediate state, in our point of view, refers to the PL of aggregated oligomer chains (nanoobjects, with a size of ~ 5 nm) in solutions at 630 and 730 nm.

As shown in Figure 7, the ultimate state of the PEDOT solution (blue curve) possesses one peak at 650 nm. The intensity of the peak is smaller than the intensity of the intermediate state. This observation agrees with the theory that

associated molecules are able to annihilate the excitation energy. There is no peak located at 730 nm. This means that larger nanogels have quenching properties. On the other hand, small nanoobjects (size ~ 5 nm) show PL, located at 650 nm. Scheibe discovered that the PL from the J-aggregates of PIC can be very easily quenched.⁵⁰ He demonstrated that less quencher is required with an increase in the dye concentration and explained this observation by the rapid propagation of excitons throughout the aggregate composed of thousands of molecules. The solid-state exciton delocalization theory is currently being used to describe the excited state of J-aggregates.⁵¹ According to this theory,⁵² strong interactions between the transition dipole moments of adjacent molecules lead to a splitting of the individual molecular levels and the emergence of new molecules with lower energy (Davydov splitting).

Based on the measured and literature data, we conclude that it is possible to tune the PL properties of PEDOT by simply choosing an appropriate method for its synthesis. Individual short oligomers possess narrow emitting spectra. On the other hand, small nanoobjects (~ 5 nm) show a PL peak located at 730 nm; however, large globular aggregates (formed from these small nanoobjects) did not show a PL. The possibility of tuning the PL from PEDOT is due to the discovery of an acid-assisted polymerization method. Most importantly, the obtained PEDOT is in the reduced state, which also has an impact on the PL.

Such assemblies of PEDOT into nanoobjects can find application, for example, as materials for supercapacitors, as recently shown by us.⁵³

We must emphasize that the effect of hydrogen bonding on the conductivity of well-known composite PEDOT:PSS is studied in the literature.^{54–56} However, the treatment of the final product—PEDOT:PSS—with formic acid and/or other molecules containing groups that can form hydrogen bonding is different from the observation in the current study. In this work, it is demonstrated the ability to use concentrated formic acid in obtaining solution of PEDOT in a neutral state, and we explained the synergy between the assembly of individual PEDOT chains and their interaction with light.

3. CONCLUSIONS

In the current work, we used liquid ^1H hr-NMR and liquid and solid ^{13}C NMR methods to investigate the mechanism for the EDOT polymerization reaction. ^1H hr-NMR spectroscopy was applied to investigate the reaction kinetics for acid-assisted polymerization. Moreover, liquid- and solid-state ^{13}C NMR spectroscopies were used to confirm the formation of PEDOT oligomers. The narrowness of the peaks in the ^1H and ^{13}C NMR spectra indicated the absence of cation radical formation (which leads to the formation of a vortex field that makes it impossible to carry out measurements) during acid-assisted polymerization.

Based on the results obtained from MALDI-ToF measurements, it is concluded that by using acid-assisted polymerization, only short oligomer chains are formed. Such short chains are able to assemble into nanoobjects with a size of 5 nm, which is confirmed by cryo-TEM and TEM. These small nanoobjects are further capable of aggregation to form globular aggregates with a size of 150 nm. Moreover, DLS measurements at different angles reveal the presence of structures with hydrodynamic radii of approximately 100–200 nm. SLS and DLS results can be used to describe the structures as spherical, but they have lower molecular weight as a particle and very low particle density ρ . This value can be compared to that for nanogels or some cluster-like structures.

Quantum-chemical calculations were applied to calculate the absorption and emission spectra of individual PEDOT chains. The absorption spectra for the intermediate state possess four absorption peaks. We propose that the first two peaks located at 440 and 480 nm correspond to a single vibrationally resolved absorption peak for the tetramer, which is also confirmed by DFT calculations combined with the Franck–Condon approach. The absorption peaks recorded for the ultimate solution show only one broad peak (located at 720 nm). The intensities of the absorption peaks corresponding to the individual oligomer chains decrease, but this signal is still present in the spectrum. This means that most of the oligomer chains are assembled into nanoobjects, which is confirmed by cryo-TEM, TEM, and DLS and SLS measurements. It is also shown that only individual oligomer chains or small nanoobjects (~ 5 nm) show PL peaks; on the other hand, large globular structures did not show PL peaks.

The present study suggests a new method for the synthesis of EDOT monomers and their acid-assisted polymerization. The obtained short oligomers dissolved in concentrated formic acid were characterized by spectroscopic methods. Furthermore, it was shown that these oligomers are prepared in the neutral form and are capable of self-aggregation. Additionally, this study shows the possibility to determine the properties of not only the aggregated state of a polymer but also individual chains. Such a discovery gives us a method for controlling the assembly process, and on the other hand, enables one to obtain reproducible conducting polymer films for real applications.

■ ASSOCIATED CONTENT

Supporting Information

The Supporting Information is available free of charge at <https://pubs.acs.org/doi/10.1021/acs.macromol.1c01975>.

Synthesis of PEDOT by acid-assisted polymerization; method of polymerization characterization; molecular mass determination; morphology; DFT calculations; kinetic of acid-assisted polymerization; Raman spectra;

XPS spectra; Electron paramagnetic resonance spectra; mass spectrum of H, ethanol, and formic acid; dependence of the decay rate Γ on squared scattering vector q for the PEDOT sample; emission spectra of PEDOT; excitation energies, wavelengths, and oscillator strengths of the first excited states S_1 of PEDOT oligomers (up to decamer) in the gas phase (vacuum) calculated by means of the TD PBE0-D3/6-31+G* method; and vibrational structure of the lowest-energy absorption band $S_0 \rightarrow S_1$ of EDOT oligomers in formic acid solution calculated by means of the Franck–Condon approach (PDF)

Coordinates (ZIP)

■ AUTHOR INFORMATION

Corresponding Author

Elena Tomšik – Institute of Macromolecular Chemistry of the Czech Academy of Sciences, 162 06 Prague, Czech Republic; orcid.org/0000-0002-1749-1091; Email: tomsik@imc.cas.cz

Authors

Iryna Ivanko – Institute of Macromolecular Chemistry of the Czech Academy of Sciences, 162 06 Prague, Czech Republic; Faculty of Science, Charles University, 128 00 Prague, Czech Republic

Andrii Mahun – Institute of Macromolecular Chemistry of the Czech Academy of Sciences, 162 06 Prague, Czech Republic; Faculty of Science, Charles University, 128 00 Prague, Czech Republic; orcid.org/0000-0003-1057-2910

Libor Kobera – Institute of Macromolecular Chemistry of the Czech Academy of Sciences, 162 06 Prague, Czech Republic; orcid.org/0000-0002-8826-948X

Zulfiya Černochová – Institute of Macromolecular Chemistry of the Czech Academy of Sciences, 162 06 Prague, Czech Republic

Ewa Pavlova – Institute of Macromolecular Chemistry of the Czech Academy of Sciences, 162 06 Prague, Czech Republic

Petr Toman – Institute of Macromolecular Chemistry of the Czech Academy of Sciences, 162 06 Prague, Czech Republic; orcid.org/0000-0002-1607-0332

Zbyněk Pientka – Institute of Macromolecular Chemistry of the Czech Academy of Sciences, 162 06 Prague, Czech Republic

Petr Štěpánek – Institute of Macromolecular Chemistry of the Czech Academy of Sciences, 162 06 Prague, Czech Republic; orcid.org/0000-0003-1433-678X

Complete contact information is available at:

<https://pubs.acs.org/10.1021/acs.macromol.1c01975>

Notes

The authors declare no competing financial interest.

■ ACKNOWLEDGMENTS

The authors acknowledge the Visegrad Scholarship program, ref. no.: 52010795, and Czech Science Foundation (21-01090S and 19-04859S). The authors also thank Z. Walterová for the MALDI-ToF measurements and Dr. O. Trhliková for the fruitful discussion. Computational resources for DFT calculations were supplied by the project “e-Infrastruktura CZ” (e-INFRA CZ LM2018140) supported by the Ministry of Education, Youth and Sports of the Czech Republic. The

authors also thank to Dr. I. Šeděnková for the Raman measurement and Dr. J. Svoboda for the XPS measurement.

REFERENCES

- (1) Karg, S.; Scott, J. C.; Salem, J. R.; Angdopoulos, M. Increased brightness and lifetime of polymer light-emitting diodes with polyaniline anodes. *Synth. Met.* **1996**, *80*, 111–117.
- (2) Cao, Y.; Yu, G.; Zhang, C.; Menon, R.; Heeger, A. J. Polymer light-emitting diodes with polyethylene dioxythiophene–polystyrene sulfonate as the transparent anode. *Synth. Met.* **1997**, *87*, 171–174.
- (3) Carter, S. A.; Angelopoulos, M.; Karg, S.; Brock, P. J.; Scott, J. C. Polymeric anodes for improved polymer light-emitting diode performance. *Appl. Phys. Lett.* **1997**, *70*, 2067–2069.
- (4) Groenendaal, L.; Jonas, F.; Freitag, D.; Pielartzik, H.; Reynolds, J. R. Poly (3, 4-ethylenedioxythiophene) and its derivatives: past, present, and future. *Adv. Mater.* **2000**, *12*, 481–494.
- (5) Baughman, R. H.; Bredas, J. L.; Chance, R. R.; Elsenbaumer, R. L.; Shacklette, L. W. Structural basis for semiconducting and metallic polymer dopant systems. *Chem. Rev.* **1982**, *82*, 209–222.
- (6) Zanardi, C.; Terzi, F.; Seeber, R. Polythiophenes and polythiophene-based composites in amperometric sensing. *Anal. Bioanal. Chem.* **2013**, *405*, 509–531.
- (7) Yoon, H.; Chang, M.; Jang, J. Formation of 1D poly (3, 4-ethylenedioxythiophene) nanomaterials in reverse microemulsions and their application to chemical sensors. *Adv. Funct. Mater.* **2007**, *17*, 431–436.
- (8) Jiang, F.; Yue, R.; Du, Y.; Xu, J.; Yang, P. A one-pot ‘green’ synthesis of Pd-decorated PEDOT nanospheres for non-enzymatic hydrogen peroxide sensing. *Biosens. Bioelectron.* **2013**, *44*, 127–131.
- (9) Zuo, Y.; Xu, J.; Zhu, X.; Duan, X.; Lu, L.; Gao, Y.; Xing, H.; Yang, T.; Ye, G.; Yu, Y. Poly (3, 4-ethylenedioxythiophene) nanorods/graphene oxide nanocomposite as a new electrode material for the selective electrochemical detection of mercury (II). *Synth. Met.* **2016**, *220*, 14–19.
- (10) Spain, E.; Keyes, T. E.; Forster, R. J. DNA sensor based on vapour polymerised pedot films functionalised with gold nanoparticles. *Biosens. Bioelectron.* **2013**, *41*, 65–70.
- (11) Özcan, A.; İlkbay, S. Preparation of poly (3, 4-ethylenedioxythiophene) nanofibers modified pencil graphite electrode and investigation of over-oxidation conditions for the selective and sensitive determination of uric acid in body fluids. *Anal. Chim. Acta* **2015**, *891*, 312–320.
- (12) Kaur, N.; Thakur, H.; Kumar, R.; Prabhakar, N. An electrochemical sensor modified with poly (3, 4-ethylenedioxythiophene)-wrapped multi-walled carbon nanotubes for enzyme inhibition-based determination of organophosphates. *Microchim. Acta* **2016**, *183*, 2307–2315.
- (13) Yoon, H.; Chang, M.; Jang, J. Formation of 1D poly (3, 4-ethylenedioxythiophene) nanomaterials in reverse microemulsions and their application to chemical sensors. *Adv. Funct. Mater.* **2007**, *17*, 431–436.
- (14) Zhang, O.; Wen, Y.; Xu, J.; Lu, L.; Duan, X.; Yu, H. One-step synthesis of poly (3, 4-ethylenedioxythiophene)–Au composites and their application for the detection of nitrite. *Synth. Met.* **2013**, *164*, 47–51.
- (15) Bobacka, J. Potential stability of all-solid-state ion-selective electrodes using conducting polymers as ion-to-electron transducers. *Anal. Chem.* **1999**, *71*, 4932–4937.
- (16) Özcan, A.; İlkbay, S. Preparation of poly (3, 4-ethylenedioxythiophene) nanofibers modified pencil graphite electrode and investigation of over-oxidation conditions for the selective and sensitive determination of uric acid in body fluids. *Anal. Chim. Acta* **2015**, *891*, 312–320.
- (17) Pei, Q.; Zuccarello, G.; Ahlskog, M.; Inganäs, O. Electrochromic and highly stable poly (3, 4-ethylenedioxythiophene) switches between opaque blue-black and transparent sky blue. *Polymer* **1994**, *35*, 1347–1351.
- (18) Aleshin, A.; Kiebooms, R.; Menon, R.; Heeger, A. J. Electronic transport in doped poly (3, 4-ethylenedioxythiophene) near the metal-insulator transition. *Synth. Met.* **1997**, *90*, 61–68.
- (19) Yamamoto, T.; Aba, M. Synthesis of non-doped poly (3, 4-ethylenedioxythiophene) and its spectroscopic data. *Synth. Met.* **1999**, *100*, 237–239.
- (20) Winther-Jensen, B.; West, K. Vapor-phase polymerization of 3, 4-ethylenedioxythiophene: a route to highly conducting polymer surface layers. *Macromolecules* **2004**, *37*, 4538–4543.
- (21) Brooke, R.; Cottis, P.; Talemi, P.; Fabretto, M.; Murphy, P.; Evans, D. Recent advances in the synthesis of conducting polymers from the vapour phase. *Prog. Mater. Sci.* **2017**, *86*, 127–146.
- (22) Lock, J. P.; Im, S. G.; Gleason, K. K. Oxidative chemical vapor deposition of electrically conducting poly (3, 4-ethylenedioxythiophene) films. *Macromolecules* **2006**, *39*, 5326–5329.
- (23) Kim, J.-Y.; Kwon, M.-H.; Min, Y.-K.; Kwon, S.; Ihm, D.-W. Self-Assembly and Crystalline Growth of Poly (3, 4-ethylenedioxythiophene) Nanofilms. *Adv. Mater.* **2007**, *19*, 3501–3506.
- (24) Li, J.; Ma, Y. In-situ synthesis of transparent conductive PEDOT coating on PET foil by liquid phase depositional polymerization of EDOT. *Synth. Met.* **2016**, *217*, 185–188.
- (25) Meng, H.; Perepichka, D. F.; Wudl, F. Facile solid-state synthesis of highly conducting poly(ethylenedioxythiophene). *Angew. Chem., Int. Ed.* **2003**, *42*, 658–661.
- (26) Yin, X.; Wu, F.; Fu, N.; Han, J.; Chen, D.; Xu, P.; He, M.; Lin, Y. Facile synthesis of poly (3, 4-ethylenedioxythiophene) film via solid-state polymerization as high-performance Pt-free counter electrodes for plastic dye-sensitized solar cells. *ACS Appl. Mater. Interfaces* **2013**, *5*, 8423–8429.
- (27) Yin, Y.; Li, Z.; Jin, J.; Tusy, C.; Xia, J. Facile synthesis of poly (3, 4-ethylenedioxythiophene) by acid-assisted polycondensation of 5-bromo-2, 3-dihydro-thieno [3, 4-b][1, 4] dioxine. *Synth. Met.* **2013**, *175*, 97–102.
- (28) Bonillo, B.; Swager, T. M. Chain-growth polymerization of 2-chlorothiophenes promoted by lewis acids. *J. Am. Chem. Soc.* **2012**, *134*, 18916–18919.
- (29) Tomšík, E.; Ivanko, I.; Svoboda, J.; Šeděnková, I.; Zhigunov, A.; Hromádková, J.; Janisová, L. Method of Preparation of Soluble PEDOT: Self-Polymerization of EDOT without Oxidant at Room Temperature. *Macromol. Chem. Phys.* **2020**, *221*, 2000219.
- (30) Audebert, P.; Bidan, G. Electrochemical behaviour and some characteristics of conducting polymers issued from the autoxidation of some bromopyrroles. *Synth. Met.* **1986**, *15*, 9–22.
- (31) Li, C.; Bai, H.; Shi, G. Conducting polymer nanomaterials: electrosynthesis and applications. *Chem. Soc. Rev.* **2009**, *38*, 2397–2409.
- (32) Lee, T. Y.; Roper, T. M.; Jönsson, E. S.; Guymon, C. A.; Hoyle, C. E. Influence of hydrogen bonding on photopolymerization rate of hydroxyalkyl acrylates. *Macromolecules* **2004**, *37*, 3659–3665.
- (33) Schulze, B. M.; Shewmon, N. T.; Zhang, J.; Watkins, D. L.; Mudrick, J. P.; Cao, W.; Zerdan, R. B.; Quartararo, A. J.; Ghiviriga, I.; Xue, J.; Castellano, R. K. Consequences of hydrogen bonding on molecular organization and charge transport in molecular organic photovoltaic materials. *J. Mater. Chem. A* **2014**, *2*, 1541–1549.
- (34) Menschutkin, N. Beiträge zur Kenntnis der Affinitätskoeffizienten der Alkylhaloide und der organischen Amine. *Z. Phys. Chem.* **1890**, *5U*, 589–600.
- (35) Reichardt, C. Empirical parameters of the polarity of solvents. *Angew. Chem., Int. Ed.* **1965**, *4*, 29–40.
- (36) Bartholomew, R. J.; Irish, D. E. Raman spectral study of ‘neat’ formic acid and aqueous and organic solutions of formic acid. *J. Raman Spectrosc.* **1999**, *30*, 325–334.
- (37) Han, D.; Li, J.; Zhang, Q.; He, Z.; Wu, Z.; Chu, J.; Lu, Y. Synthesis of π -conjugated polymers containing benzotriazole units via palladium-catalyzed direct C-H cross-coupling polycondensation for OLEDs applications. *Polymers* **2021**, *13*, 254.
- (38) Chaloner-Gill, B.; Euler, W. B.; Mumbauer, P. D.; Roberts, J. E. Direct evidence of a bipolaron charge carrier in conducting polyazines from ^{13}C and ^{15}N solid-state NMR spectroscopy: detection of a

nitrenium cation by natural abundance ^{15}N solid-state NMR spectroscopy. *J. Am. Chem. Soc.* **1991**, *113*, 6831–6834.

(39) Meng, H.; Perepichka, D. F.; Bendikov, M.; Wudl, F.; Pan, G. Z.; Yu, W.; Dong, W.; Brown, S. Solid-state synthesis of a conducting polythiophene via an unprecedented heterocyclic coupling reaction. *J. Am. Chem. Soc.* **2003**, *125*, 15151–15162.

(40) Heinbuch, S.; Dong, F.; Rocca, J. J.; Bernstein, E. R. Single photon ionization of hydrogen bonded clusters with a soft x-ray laser: $(\text{HCOOH})_x$ and $(\text{HCOOH})_y (\text{H}_2\text{O})_z$. *J. Chem. Phys.* **2007**, *126*, 244301.

(41) Abessolo Ondo, D.; Loyer, F.; Chemin, J.-B.; Bulou, S.; Choquet, P.; Boscher, N. D. Atmospheric plasma oxidative polymerization of ethylene dioxythiophene (EDOT) for the large-scale preparation of highly transparent conducting thin films. *Plasma Processes Polym.* **2018**, *15*, 1700172.

(42) Liu, C.; Goeckner, M. J.; Walker, A. V. Plasma polymerization of poly(3,4-ethylenedioxyethene) films: The influence of plasma gas phase chemistry. *J. Vac. Sci. Technol. A* **2017**, *35*, 021302.

(43) Kolouchova, K.; Groborz, O.; Cernochova, Z.; Skarkova, A.; Brabek, J.; Rosel, D.; Svec, P.; Starcuk, Z.; Slouf, M.; Hruby, M. Thermo- and ROS-Responsive Self-Assembled Polymer Nanoparticle Tracers for ^{19}F MRI Theranostics. *Biomacromolecules* **2021**, *22*, 2325–2337.

(44) Förster, T. Energy migration and fluorescence. *J. Biomed. Opt.* **2012**, *17*, 011002.

(45) Ie, Y.; Okamoto, Y.; Inoue, T.; Tone, S.; Seo, T.; Honda, Y.; Tanaka, S.; Lee, S. K.; Ohto, T.; Yamada, R.; Tada, H.; Aso, Y. Highly Planar and Completely Insulated Oligothiophenes: Effects of π -Conjugation on Hopping Charge Transport. *J. Phys. Chem. Lett.* **2019**, *10*, 3197–3204.

(46) Monkman, A. P.; Pålsson, L.-O.; Higgins, R. W. T.; Wang, C.; Bryce, M. R.; Batsanov, A. S.; Howard, J. A. K. Protonation and subsequent intramolecular hydrogen bonding as a method to control chain structure and tune luminescence in heteroatomic conjugated polymers. *J. Am. Chem. Soc.* **2002**, *124*, 6049–6055.

(47) Suna, Y.; Nishida, J.-i.; Fujisaki, Y.; Yamashita, Y. Ambipolar behavior of hydrogen-bonded diketopyrrolopyrrole thiophene co-oligomers formed from their soluble precursors. *Org. Lett.* **2012**, *14*, 3356–3359.

(48) Schulze, B. M.; Shewmon, N. T.; Zhang, J.; Watkins, D. L.; Mudrick, J. P.; Cao, W.; Zerdan, R. B.; Quartararo, A. J.; Ghiviriga, I.; Xue, J.; Castellano, R. K. Consequences of hydrogen bonding on molecular organization and charge transport in molecular organic photovoltaic materials. *J. Mater. Chem. A* **2014**, *2*, 1541–1549.

(49) Tomšík, E.; Kohut, O.; Ivanko, I.; Pekárek, M.; Bieloshapka, I.; Dallas, P. Assembly and interaction of polyaniline chains: Impact on electro- and physical–chemical behavior. *J. Phys. Chem. C* **2018**, *122*, 8022–8030.

(50) Scheibe, G.; Schontag, A.; Katheder, F. Fluorescence and energy transmission in reversible polymerized pigments. *Sci. Nat.* **1939**, *27*, 499–501.

(51) Würthner, F.; Kaiser, T. E.; Saha-Möller, C. R. J-aggregates: from serendipitous discovery to supramolecular engineering of functional dye materials. *Angew. Chem., Int. Ed.* **2011**, *50*, 3376–3410.

(52) Davydov, A. *Theory of Molecular Excitons*; Springer, 2013.

(53) Ivanko, I.; Tomšík, E. Effect of hydrogen bonding on a value of an open circuit potential of poly-(3,4-ethylenedioxythiophene) as a beneficial mode for energy storage devices. *Adv. Funct. Mater.* **2021**, *31*, 2103001.

(54) Yemata, T. A.; Zheng, Y.; Kyaw, A. K. K.; Wang, X.; Song, J.; Chin, W. S.; Xu, J. Modulation of the doping level of PEDOT:PSS film by treatment with hydrazine to improve the Seebeck coefficient. *RSC Adv.* **2020**, *10*, 1786–1792.

(55) Ouyang, J.; Chu, C. W.; Chen, F. C.; Xu, Q.; Yang, Y. Polymer Optoelectronic Devices with high-conductivity poly(3,4-ethylenedioxythiophene) anodes. *J. Macromol. Sci., Part A: Pure Appl. Chem.* **2004**, *41*, 1497–1511.

(56) Funda, S.; Ohki, T.; Liu, Q.; Hossain, J.; Ishimaru, Y.; Ueno, K.; Shirai, H. Correlation between the fine structure of spin-coated

PEDOT:PSS and the photovoltaic performance of organic/crystalline-silicon heterojunction solar cells. *J. Appl. Phys.* **2016**, *120*, 033103.

Appendix 4

Tomšík, E.; Ivanko, I.; Svoboda, J.; Zhigunov, A.; Hromádková, J.; Pánek, J.; Lukešová, M.; Velychkivska, N.; Janisová, L. Method of Preparation of Soluble PEDOT: Self-Polymerization of EDOT without Oxidant at Room Temperature, *Macromol. Chem. Phys.* **221**, 2000219 (2020). IF = 2,527.



Method of Preparation of Soluble PEDOT: Self-Polymerization of EDOT without Oxidant at Room Temperature

Elena Tomšík,* Iryna Ivanko, Jan Svoboda, Ivana Šeděnková, Alexander Zhigunov, Jiřina Hromádková, Jiří Pánek, Miroslava Lukešová, Nadiia Velychkivska, and Larysa Janisová

The preparation of soluble conducting polymers proceeds by the chemical oxidation method in the presence of water-soluble polyelectrolytes. Among conducting polymers, polyethylene-(3,4-dioxythiophene) (PEDOT) is the most investigated due to its intrinsic properties. In this work, for the first time a simple method of ethylene-(3,4-dioxythiophene) self-polymerization without applying any oxidant and with the formation of PEDOT solution at room temperature with a yield of 100% is presented. This PEDOT solution could be deposited on many desirable surfaces (by simple evaporation of the solvent) for various applications from photovoltaic cell to pseudocapacitors. Moreover, it is discovered that the self-polymerization method does not produce byproducts, which makes the method environmentally friendly. The effect of light and different acids is explored. Fourier transform infrared spectroscopy, X-ray photoelectron spectroscopy (XPS), and Raman spectroscopy confirm the formation of PEDOT by the self-polymerization method. Moreover, this method provides a way to obtain and study individual PEDOT chains. The self-polymerization method may be applied for the preparation of other conducting polymers.

polymerization,^[12] photoinduced polymerization and oxidant-free acid polymerization at high temperature.^[13–15] In chemical oxidation polymerization, different oxidants are used to achieve polymerization of monomers. Such a method suffers from difficulty of separation of the polymer and the oxidants and leads to contamination of water. Recently, oxidative chemical vapor deposition was reported, where sulfuric acid vapor was used as the oxidant and dopant simultaneously.^[16] In electrochemical polymerization, the polymer is deposited only on a conducting substrate, which is a disadvantage if large-area films are required. In Lewis acid-assisted polymerization and photoinduced polymerization, only specific monomers can be polymerized. Therefore, it is desirable to find a simple and green method to prepare SP that can be easily deposited on any chosen surface for different applications.

1. Introduction

There is a demand for a simple and reliable method for the synthesis of conjugated polymers with controllable morphologies and properties that reflect their applications in different devices. The following methods currently exist to prepare semiconducting polymers (SP): chemical oxidation polymerization,^[1] electrochemical polymerization,^[2] metal catalyzed coupling,^[3,4] solid-state polymerization,^[5–11] Lewis acid-assisted

It is common knowledge that all SPs are poorly soluble in many solvents. If a water-soluble polyelectrolyte is used (for example, polystyrene sulfonate) during chemical polymerization, a solution of semiconducting polymer/polyelectrolyte is obtained—for example, polyethylene-(3,4-dioxythiophene)/polystyrene sulfonate (PEDOT:PSS).^[17]

Among semiconducting polymers, PEDOT and its derivatives are some of the most widely researched SPs. PEDOT is usually prepared either by chemical oxidative polymerization or by electrochemical oxidation of the monomer 3,4-ethylenedioxythiophene (EDOT). Recently, a new method to form conducting polythiophene was invented, in particular, an environmentally friendly and facile method of solid-state polymerization (SSP) had great success in the synthesis of PEDOT and its analog.^[18] However, this process is slow progress, mainly due to the shortage of suitable monomers.^[19] In addition, SSP requires symmetrical di-halogen-substituted monomers and usually produces moderately to highly conductive polymers because of the generation of an oxidant of bromine or iodine during its polycondensation procedure.^[20] Recently, Officer^[21] and Xia^[22] independently found that PEDOT can be formed just by the simple heating of mono-bromo-substituted EDOT(Br-EDOT).

Dr. E. Tomšík, I. Ivanko, Dr. J. Svoboda, Dr. I. Šeděnková,
Dr. A. Zhigunov, J. Hromádková, Dr. J. Pánek, Dr. M. Lukešová,
N. Velychkivska, Dr. L. Janisová
Institute of Macromolecular Chemistry AS CR
Heyrovsky Sq. 2, Prague 6 16206, Czech Republic
E-mail: tomsik@imc.cas.cz

I. Ivanko
Faculty of Science
Charles University
Prague 2 12800, Czech Republic

The ORCID identification number(s) for the author(s) of this article can be found under <https://doi.org/10.1002/macp.202000219>.

DOI: 10.1002/macp.202000219

Meanwhile, Swager group successfully synthesized corresponding polymers based on mono-chloro-substituted EDOT derivatives in the presence of a Lewis acid.^[12]

In our work, we present for the first time a simple method of EDOT self-polymerization without applying any oxidant and with the formation of PEDOT solution at room temperature with a yield of 100%. This PEDOT solution could be deposited on many desirable surfaces (by simple evaporation of the solvent) for various applications from photovoltaic cells to pseudocapacitors. Moreover, we discovered that the self-polymerization method does not produce any byproducts, which makes the method environmentally friendly. Additionally, we applied the discovered self-polymerization reaction for other monomers: and it worked for some of them, particularly for polypyrrole, *para*-phenylenediamine, and benzothiophene. The effect of light and different acids was explored.

2. Results and Discussion

It is generally accepted that the chemical polymerization or electropolymerizations of SP proceeds with the withdrawal of electrons from aromatic monomer units, and relatively stable cation radicals are consequently formed. The coupling of two cation-radicals or one radical and a monomer and successive removal of two protons results in the formation of a dimer^[23,24] (schematically presented in **Figure 1b**). This reaction involves an electrochemical process of oxidation and a chemical process of coupling and eliminating protons. Further oxidation of the dimer and coupling produces oligomers. Elongation of oligomers through the same procedures results in the final product—a polymer that is not soluble in the electrolyte and thus precipitates (see **Figure 1a**).

The oxidation potentials of aromatic compounds mainly depend on the structure of the compounds and the nature of the electrolytes. Electron-donating groups or large dense aromatic rings can stabilize the corresponding cation radicals, thus reducing the oxidation potentials. For example, the oxidation potential of 3-methylthiophene is much lower than that of thiophene, while those of 3-halidethiophenes are higher than that of thiophene.^[25] Some electrolyte molecules have electrocatalytic properties. They activate the monomers and decrease their oxidation potentials. For example, the oxidation potential of thiophene in boron trifluoride diethyl etherate (BFEE) was measured to be only 1.2 V (vs SCE), which is much lower than that measured in a neutral electrolyte such as acetonitrile (2.1 V, vs SCE).^[26,27] In short, although these various investigations have contributed to elucidating some aspects of the electropolymerization mechanism, several steps of the process are not yet fully understood and are still subject to controversial interpretations.^[4]

2.1. Self-Polymerization of PEDOT

In our case, the self-polymerization of monomer EDOT started spontaneously at room temperature without any oxidant, as shown in **Figure 1a**. The reaction began without applying any oxidant, which is why we use the term self-polymerization.

Formic acid was used as the electrolyte. To elucidate the nature of the processes taking place during monomer self-polymerization, we applied following methods: in situ UV–vis spectroscopy, in situ Fourier transform infrared spectroscopy (FTIR), Raman spectroscopy, electron paramagnetic resonance (EPR) spectroscopy, matrix-assisted laser-desorption/ionization time-of-flight mass spectra (MALDI TOF), X-ray photoelectron spectroscopy (XPS) spectroscopy, X-ray diffraction (XRD), scanning electron microscopy (SEM), transmission electron microscopy (TEM) measurements, and electrochemical investigation of the product by two methods (cyclic voltammetry and electrochemical impedance spectroscopy (EIS)). Moreover, the role of the electrolyte and light was also investigated. It was also shown that other monomers could be polymerized in the same way.

The formation of PEDOT was confirmed by different methods, as presented below. What surprised us the most is the fact that the PEDOT synthesized by our self-polymerization method is completely dispersed in the electrolyte: formic acid (shown in **Figure 2**). The explanation of the phenomenon is also presented below in the text.

Figure 1b,c shows two possible ways in which dimer formation occurs. Detailed discussion and proof of the mechanism of dimer formation are offered in the electron paramagnetic resonance measurement section. However, the ¹H NMR investigation of EDOT monomer self-polymerization (during first 144 h) shown in **Figure 1d** proves that oligomer formation occurred. The integrated intensity of CH decreased over time (6.3239 ppm, **Figure 1d**) with simultaneous increase of the peak corresponding to oligomers.

Our discovery of the self-polymerization method of PEDOT synthesis started with the observation of the color changes during the addition of monomer (EDOT) to formic acid, as shown in **Figure S1** (Supporting Information). After ≈30 min, blue coloration of the solution was visible; after 1 h, the intensity of the blue color increased, and after 48 h, the solution became dark blue (see **Figure S1** in the Supporting Information). We must say that the reaction of self-polymerization proceeds in any acid (acetic acid or *ortho*-phosphoric acid). However, the kinetics of the self-polymerization reaction depend on the nature of the acid: in acetic acid, the self-polymerization proceeds more slowly than it does in formic acid or *ortho*-phosphoric acid. The other interesting fact is the solubility of the PEDOT chains; the obtained PEDOT does not precipitate in any studied acid, as shown in **Figure 2** for formic acid.

In **Figure 2**, we present optical images of the polymerization solution in a quartz cuvette at different stages of self-polymerization and dilution. We must emphasize that the color of the solution at the beginning of the self-polymerization is blue (see **Figure S1** in the Supporting Information), which is the color commonly observed in the literature for PEDOT. However, when the blue solution was diluted by formic acid, the color became green, as shown in **Figure 2**. After 2 d, the color of the solution became more intense, and after 2 weeks, it turned blue again. Based on our previous experience with polyaniline,^[28] we proposed that the green color of the diluted PEDOT solution is the color of individual PEDOT chains, and the blue color of the PEDOT is associated with the assembly of PEDOT chains into nanostructures (confirmed later by TEM,

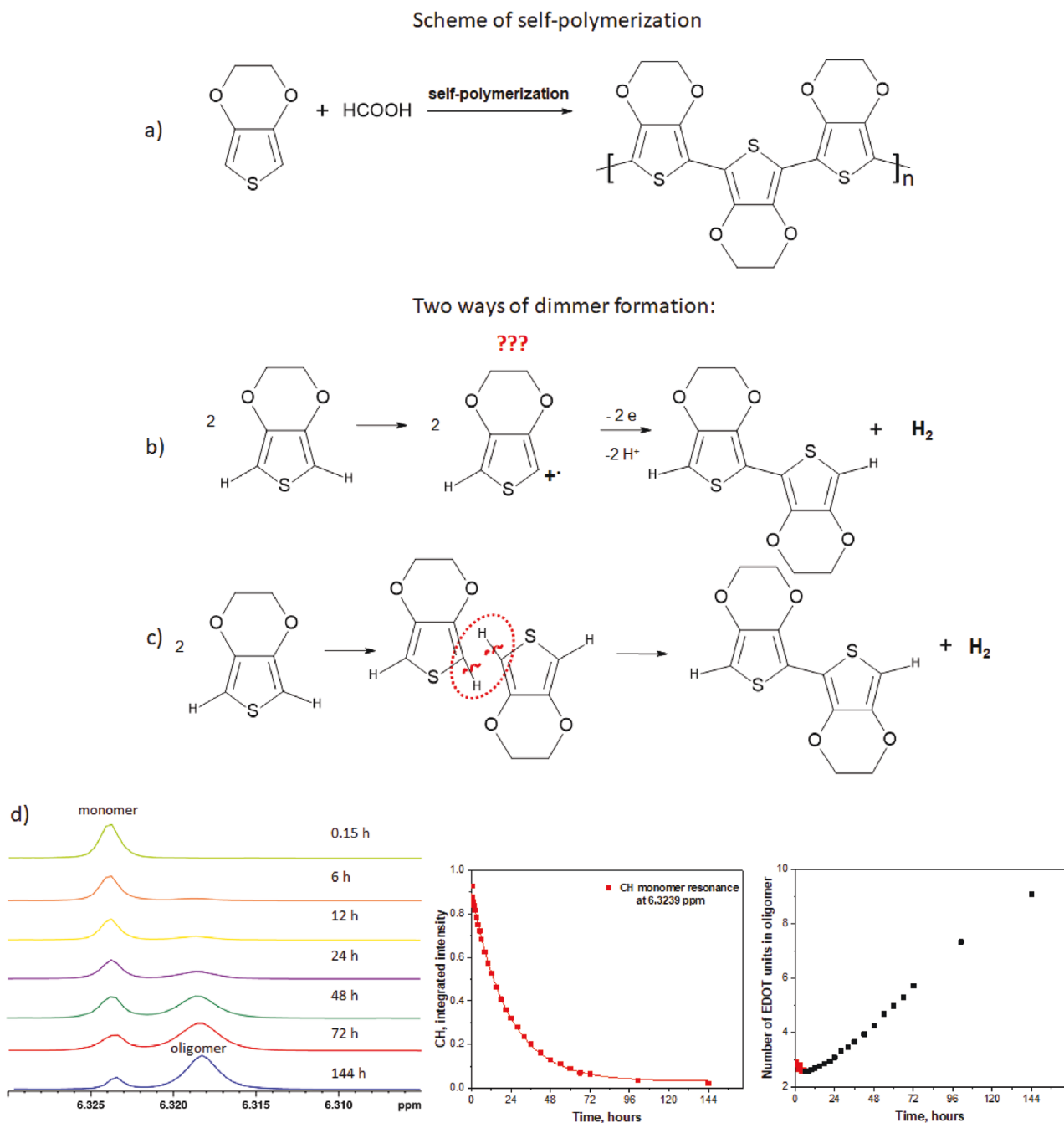


Figure 1. a) Scheme of the self-polymerization of the EDOT monomer in the presence of formic acid, b) possible formation of cation radicals and dimer formation, c) polycondensation reaction with the removal of H_2 gas, d) ^1H NMR spectra of EDOT monomer during first 144 hours; and dependences of CH (6.3239 ppm) intensity versus time and number of EDOT units in oligomer versus time.

Figure 6a). It is also interesting to study the process of dilution of the PEDOT solution: if distilled water (DW) is used for dilution, a blue precipitate is formed immediately (Figure 2); on the other hand, when formic acid is used for the dilution, a green solution is again obtained. We must highlight that the green solution after some time turns blue (the time needed for conversion from green to blue depends on the solution concentration).

2.2. In Situ UV-vis, EPR, and IR Spectroscopies

To study the kinetics of EDOT self-polymerization, we decided to measure in situ UV-vis spectra. The change in the color of the polymerization solution over time indicates a chemical transformation taking place during monomer polymerization.

In situ UV-vis spectra were recorded during the self-polymerization of EDOT for the first 5 h (Figure 3a) and then after

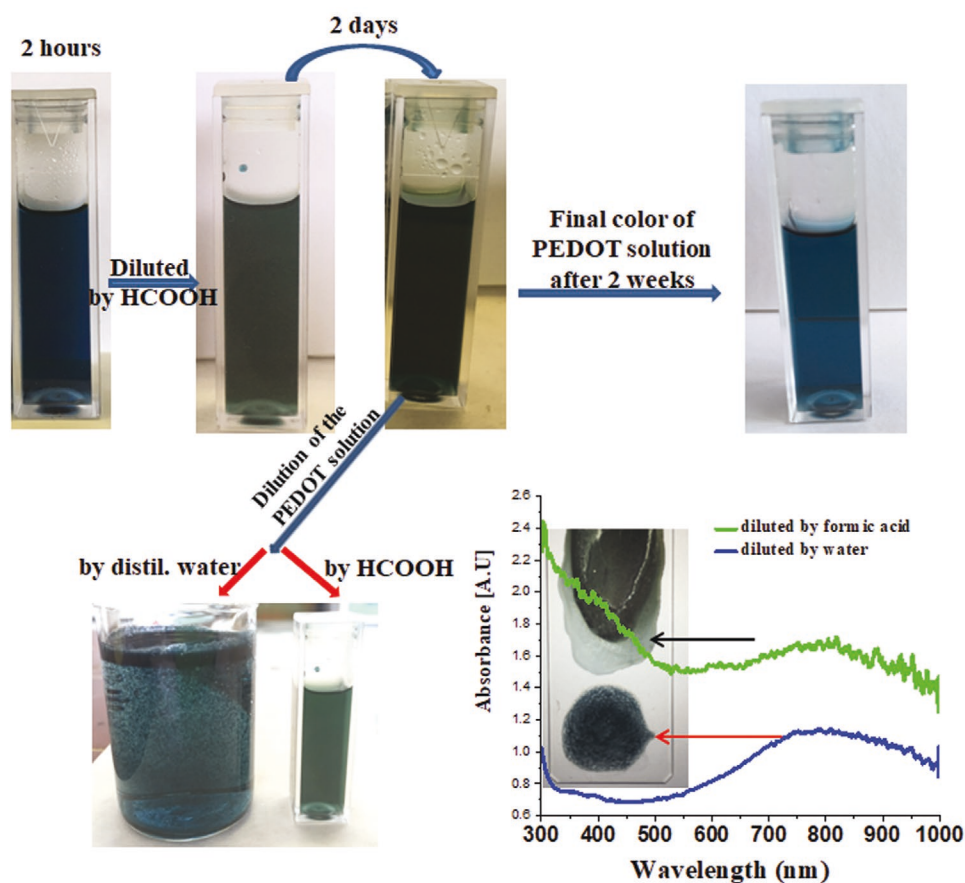


Figure 2. Color changes of the PEDOT solution during time and dilution.

2 weeks (Figure 3b) of polymerization, as shown in Figure 3. The spectral feature of EDOT self-polymerization is absolutely different from that reported in the literature so far. At the beginning of the reaction, we observed an absorption maximum at 480 nm (Figure 3a), marked by the black arrow and asterisk. The presence of this particular peak was calculated using TD-DFT by the Zozoulenko group and was explained as the absorption spectrum of a neutral chain.^[29] When the time increased to 5 h, new absorption peaks appeared (marked by red arrows): $\lambda_{\text{abs}} = 440, 530, 720$ nm. It is obvious from the UV-vis spectra that the intensity of the absorption increased over time. Based on these measurements, we can conclude that the self-polymerization reaction proceeds more slowly than chemical oxidation. After 5 h, it was no longer possible to measure the spectra due to high absorbance, which is why the following measurements were performed for the polymerization solution diluted by formic acid (Figure 3b).

We must emphasize that the polymerization reaction starts immediately if the concentration of monomer is increased by 20 times. However, to be able to record the changes during UV-vis measurements we chose the lower concentration of EDOT.

The absorption spectra of green (diluted) and blue (final) solutions of PEDOT after two weeks are presented in Figure 3b (for the blue PEDOT solution, the spectrum was obtained in a 2 mm cuvette). We proposed that a solution of individual PEDOT chains that do not interact mutually has a green color,

on the other hand, if the PEDOT chains interact with each other and form different nanostructures (supramolecular assembly), the color turns blue, which is commonly observed for PEDOT in the literature. Similar behavior was observed by us for another SP—polyaniline.^[28] It is interesting to observe that the UV-vis spectrum of the green solution (Figure 3b) is different from the UV-vis spectrum of the green film (Figure 2). This fact could be explained by the partial interaction of individual PEDOT chains in the film compared to completely soluble PEDOT chains in formic acid. On the other hand, the UV-vis spectra of the blue solution and the blue precipitated film are similar (Figures 2 and 3b).

To understand the polymerization process, we obtained EPR spectra of the self-polymerization solution at the beginning, after 2 weeks and for the final PEDOT powder, and the results are shown in Figure 3c.

Currently, it is widely accepted that when chemical or electrochemical polymerization takes place, cation radicals are formed, as shown in Figure 1b. Such cation radicals are detected by in situ EPR measurement.^[30] When we observed the coloration of the polymerization solution without applying any potential or adding any oxidant, our question was, what is the mechanism of self-polymerization of EDOT? To answer this question and determine whether the self-polymerization proceeds through the formation of cation radicals or not the EPR spectra were measured. As shown in Figure 3c, no EPR signal was recorded

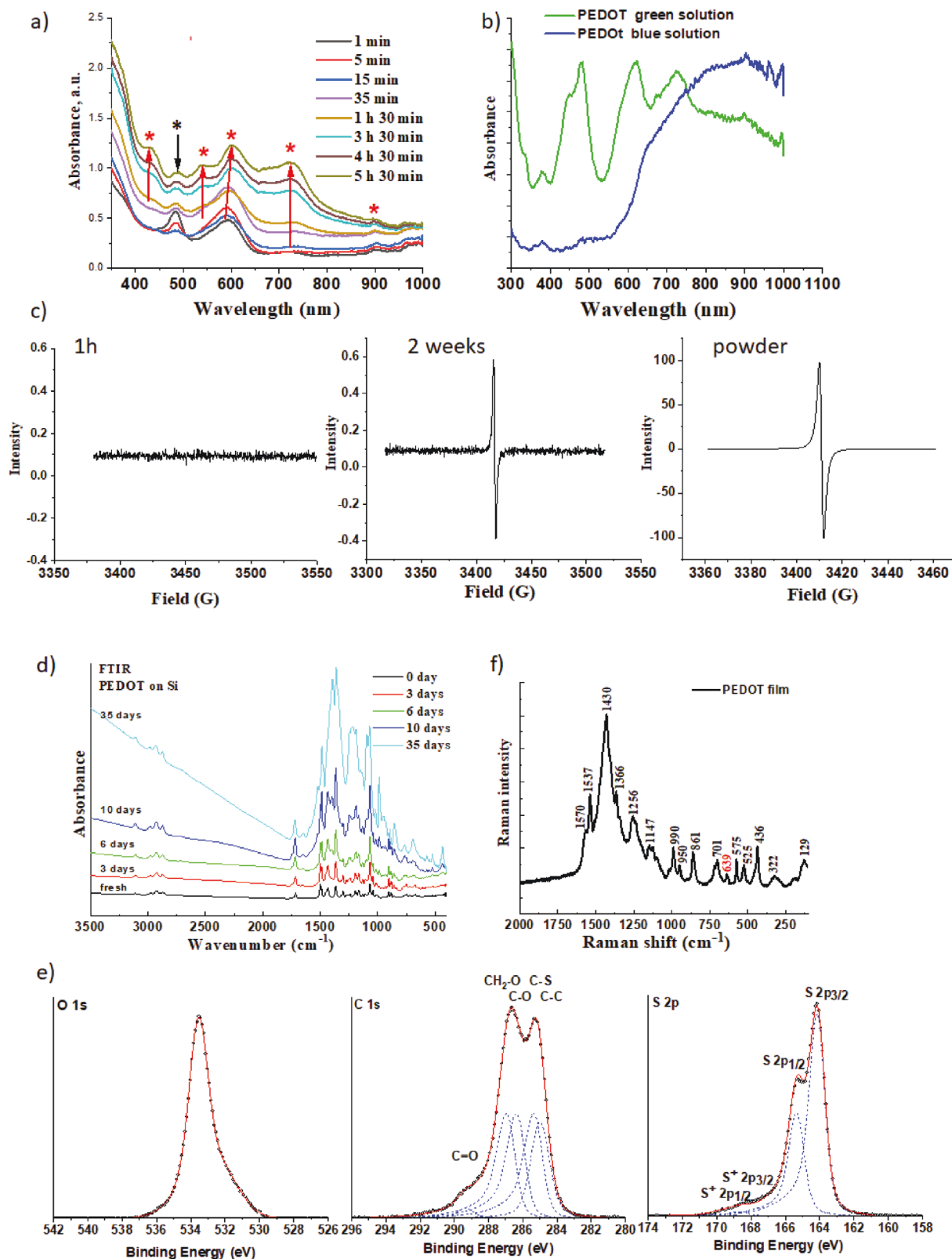


Figure 3. a) UV-vis spectra of EDOT self-polymerization during first 5 h, b) UV-vis spectra of the diluted final PEDOT blue solution and the very diluted green solution, c) EPR signal of the self-polymerization EDOT solution after 1 h, 2 weeks, and of the final powder. d) Kinetic study of PEDOT self-polymerization by FTIR spectroscopy, e) Raman spectra of the final PEDOT film measured upon excitation by a laser 785 nm, f) XPS spectra of the PEDOT film after 2 weeks.

at the beginning of the self-polymerization (at any time). The EPR signal of the empty cuvette is presented in Figure S2 (Supporting Information). Even after 2 weeks, the PEDOT solution has a very weak EPR signal. On the other hand, when EPR measurements were performed on PEDOT powder, the EPR signal was very intense (Figure 3c). Based on these measurements, we could conclude that dimer formation proceeds without the formation of cation radicals. We proposed that the EDOT monomer undergoes a polycondensation reaction with the formation of soluble PEDOT solution and with the elimination of hydrogen gas, as presented in Figure 1c. Our explanation is also based on the literature data, where it was shown that some electrolytes can catalyze polymerization.^[26,27] Further analysis of the EPR signal (Figure S3, Supporting Information) showed that the signal line shape is symmetric and narrow: the line width is 2 G for the PEDOT solution after two weeks and 1.85 G for PEDOT powder. The EPR line width is determined by the relaxation rate of the radical and is a characteristic of the degree of delocalization. Therefore, such a narrow line width indicates the presence of localized cation radicals.^[7] Detection of the cation radicals in the final powder could be explained by the presence of acid (formic acid), which is able to induce electrostatic interactions (hydrogen bonding formation), as recently shown by us.^[31]

It could be debated that oxygen could play a role in monomer oxidation. To prove that the oxygen does not participate in the EDOT polymerization, the first starting solution was purged with nitrogen gas, and the second one was not. Two polymerization solutions were left and compared with each other. It was observed that the reaction of polymerization started in both with similar color changes. Based on this experiment, we concluded that oxygen does not participate and/or affect the polymerization reaction.

To investigate the kinetics of EDOT self-polymerization in more details, FTIR spectra were recorded. A droplet of the solution was placed on the Si support, and after solvent evaporation, a PEDOT layer on the substrate was formed at different times by PEDOT self-polymerization, as shown in Figure 3d. The self-polymerization solution used was the same for all measurements. The final PEDOT film was also measured by Raman spectroscopy with a 785 nm laser (the result is presented in Figure 3f).

The FTIR spectra were measured after 0, 3, 6, 10, and 35 d of EDOT self-polymerization (Figure 3d). The FTIR spectra

changed over time: during the first 6 d, the FTIR spectra corresponded to the low-molecular-weight oligomers, but after 6 d, we observed bands corresponding to PEDOT. Detailed FTIR spectra are presented in Figure S4 (Supporting Information). The vibrations at 1512, 1454, 1394, 1370, and 1168 cm^{-1} originate from the stretching of C–C and C=C in the thiophene ring.^[30] Additional vibrations from the C–S bond in the thiophene ring can be seen at 930, 830, 727, and 697 cm^{-1} .^[32,33] The vibrations at 1183, 1144, 1093, 1076, and 1052 cm^{-1} are assigned to stretching of the alkylene dioxy group.^[34]

The Raman spectra of PEDOT solutions (any) could not be measured due to the presence of photoluminescence; however, the Raman spectrum of the final PEDOT film was measured at an excitation wavelength of laser 785 nm, which is similar to that reported in the literature.^[35] Based on our FTIR and Raman spectroscopy results, we can conclude that the PEDOT obtained by the self-polymerization reaction in the presence of formic acid has a similar chemical structure to the PEDOT reported in the literature.

The role of acid is not yet clear. We know that formic acid can interact with PEDOT by hydrogen bonding.^[31] Such interactions can induce electron-charge transfer from thiophene sulfur to hydrogen in formic acid, accompanied by the formation of cation radicals. This interaction observed in the EPR signal of the final PEDOT powder (Figure 3c). The presence of formic acid was also confirmed by XPS, and the results are shown in Figure 3e (C 1s and S 2p). It is possible to estimate the amount of acid electrostatically interacting with sulfur in PEDOT by the ratio of intensity located at ≈ 168 eV versus intensity located at 164.9 eV, and the amount is 5%.

We think that protons have a catalytic effect on self-polymerization because when the reaction took place in deuterium acetic acid, no self-polymerization occurred.

2.3. Molecular Weight Determination

Our next step was to determine the number of monomer units in PEDOT chains. MALDI-TOF analysis, with *trans*-2-[3-(4-*tert*-butylphenyl)-2-methyl-2-propenylidene] malononitrile in ethyl acetate as the matrix and the voltage used in negative mode, was performed, and the results are presented in Figure 4 for both green and blue PEDOT solutions.

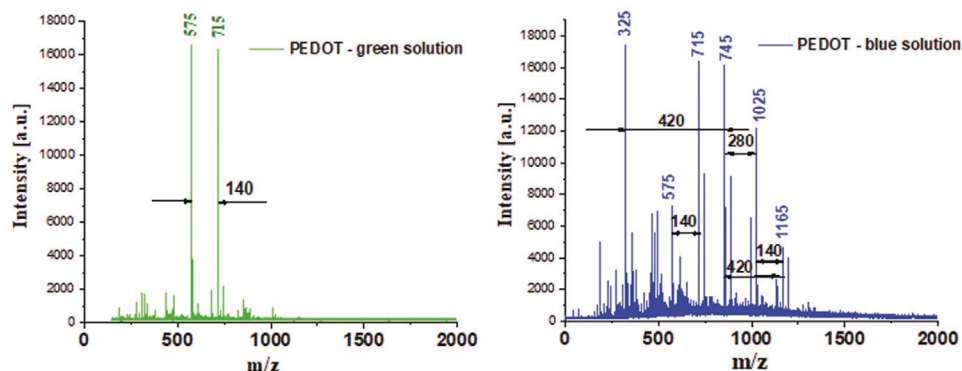


Figure 4. MALDI TOF measurements of PEDOT green solution (left) and blue solution (right).

As shown by optical images (Figure 2), the diluted solution of PEDOT has a green color, and the non-diluted solution is blue, which is why we decided to analyze both solutions. As shown in Figure 4, the green solution has a narrow distribution, and the mass-to-charge ratio values are $m/z = 575$ and 715 , corresponding to four- and five- monomer units (the theoretical values are 562 and 702, respectively). The higher value for individual PEDOT chains is probably due to the attachment of water and/or formic acid molecules to the polymer chain (strong hydrogen interaction). On the other hand, the blue solution contains oligomers with higher molecular weights; the mass-to-charge ratio value is $m/z > 1000$. As we stated above, we think that PEDOT consists of short oligomer sequences that assembled into stable nanostructures (shown by TEM image, Figure 6a). The self-polymerized PEDOT dispersion in formic acid is stable for several months (at least 6 months) without the formation of any precipitate.

2.4. Photoluminescence Measurements

As mentioned above, during Raman measurements, we discovered the presence of photoluminescence (PL) in the PEDOT green and blue solutions. Our next goal was to study this phenomenon. Synchronous PL spectroscopy was performed and the results are presented in Figure 5a,b. The corresponding time-resolved PL measurements are shown in Figure 5c,d, respectively. The PL of formic acid is presented for comparison.

Synchronous PL spectrometry has been extensively used in multicomponent analysis. The spectra were obtained through simultaneous scanning with excitation and the emission monochromators of a spectrofluorometer, with a fixed wavelength difference ($\Delta\lambda$, in our case 10 nm) between them. In the synchronous spectra, the sensitivity associated with PL is maintained while offering several advantages: narrowing of spectral bands, an enhancement in selectivity by spectral simplification and a decrease in measurement time.

The PL spectrum of the PEDOT green solution is different than the PL spectrum of PEDOT blue solution. The appearance of several maximum emission peaks in the spectrum of the PEDOT green solution could be explained by the properties of individual PEDOT chains, and by the presence of only two oligomers (confirmed by MALDI ToF). It is still unclear why the green PEDOT solution gives rise to four distinguished emission peaks (particularly, the nature of such transitions) compared to only one, very narrow, emission peak of PEDOT blue solution. The PL spectra were also measured at different excitation wavelengths (Figure S5, Supporting Information), and as expected, broad emission peaks were observed for both PEDOT solutions compared to synchronous measurements.

In the case of time-resolved PL measurements, the PL decay curve was fitted by a double exponential function for all excitation laser wavelengths, and it gave $\tau_1 = 0.37$ ns and $\tau_2 = 1.44$ ns. The lifetimes of the excited state are in the range of nanoseconds, which confirms that the PL originates from the singlet excited state. Currently, we cannot not offer any explanation of

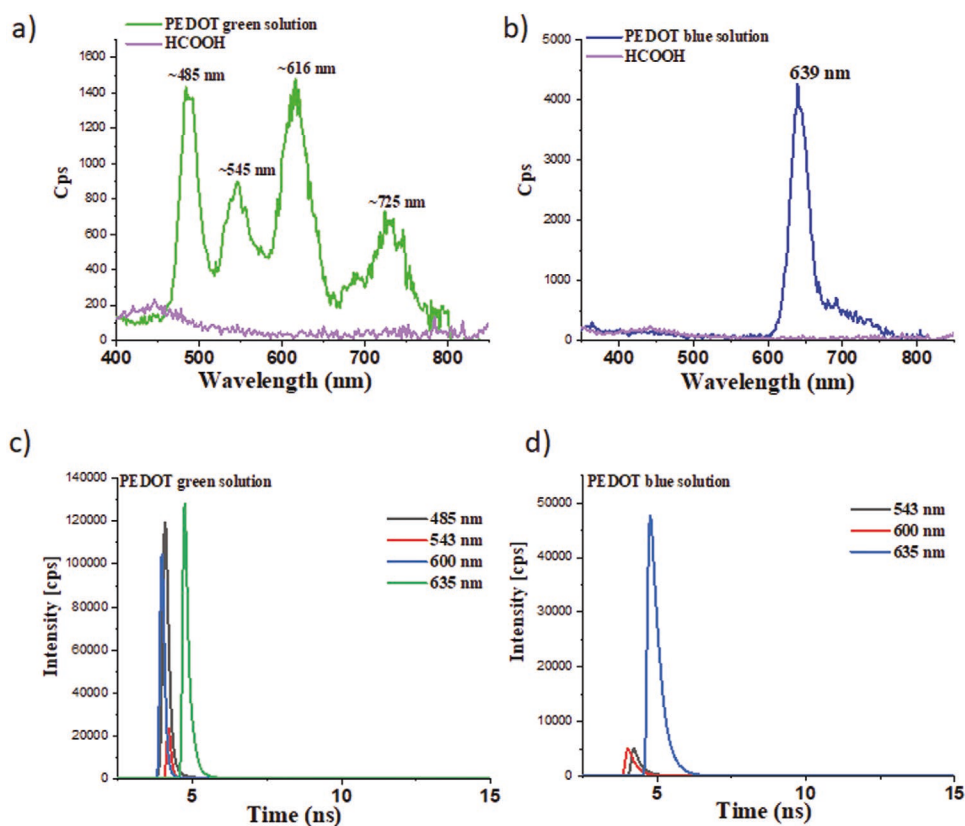


Figure 5. Photoluminescence spectroscopy of a) PEDOT green solution and b) blue solution. Time-resolved PL measurements of c) PEDOT green and d) blue solutions.

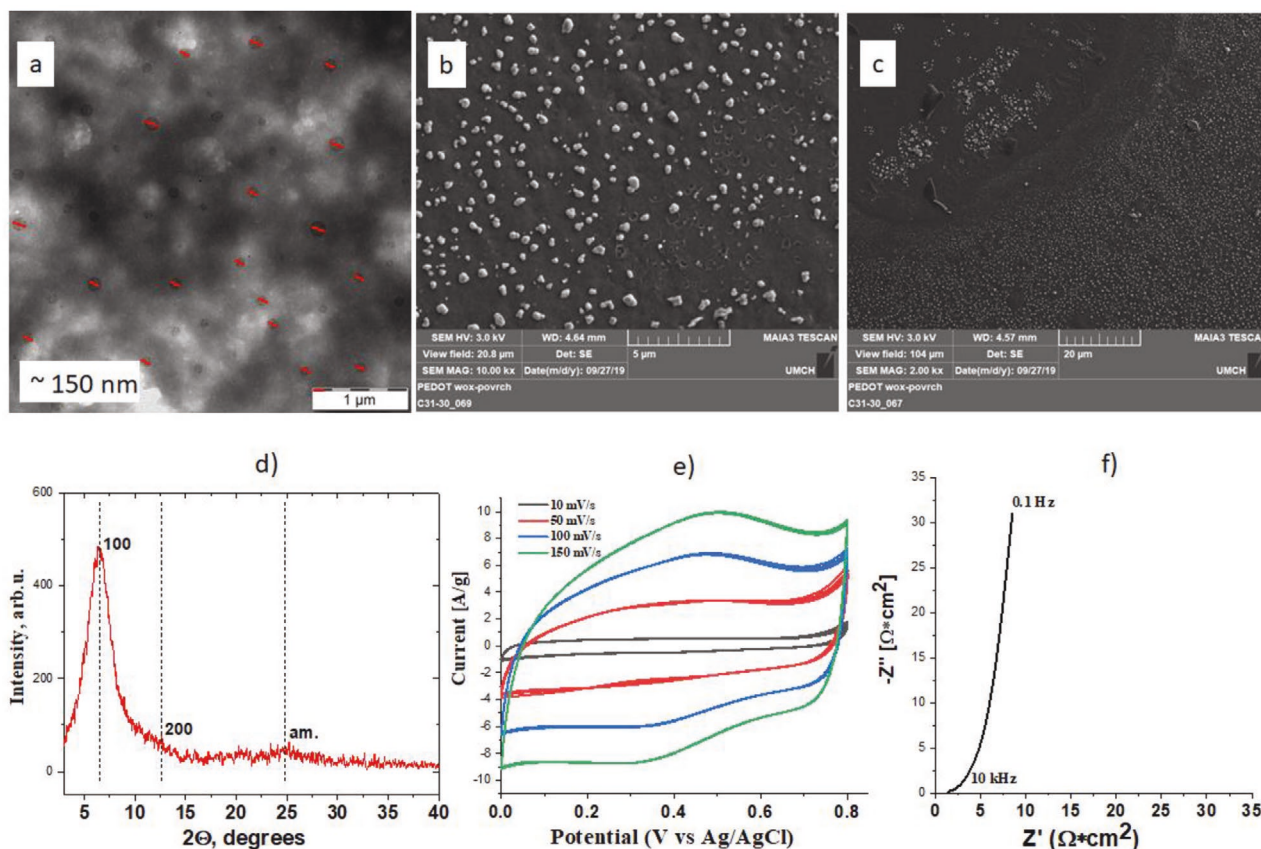


Figure 6. TEM image of a) PEDOT solution after 1 week and b,c) SEM images of PEDOT after 1 week. d) XRD of PEDOT film deposited on the glass substrate. Cyclic voltammetry of e) PEDOT solution deposited on CC and f) electrochemical impedance measurements.

such fast processes taking place during PL. We plan to investigate this phenomenon in detail in the near future, and the results will be published.

It is also interesting to note that the intensity of the time-resolved lifetime of the excited state is higher for the green PEDOT solution than for the blue PEDOT solution (Figure S6, Supporting Information). We think this is because the individual PEDOT chains (green solution) do not have quenching centers, unlike the assembled PEDOT chains (blue solution). The origin of the quenching centers in blue PEDOT could be cation radicals, the presence of which was confirmed by EPR spectra (Figure 3c).

2.5. SEM, TEM, XRD, and Electrochemical Characterization

To visualize the polymer chains in self-polymerized PEDOT solution, TEM and SEM images of blue PEDOT solution and final PEDOT powder are presented in Figure 6a–c. We note that we tried to measure TEM for the green PEDOT solution, but we did not detect any nanostructure (the result is not shown).

However, we observed the formation of nanospheres and nanosheets for the blue PEDOT solution, as shown by the TEM image (Figure 6a), with the diameter of nanospheres ≈ 150 nm. However, when the PEDOT solution was dried, and PEDOT powder was measured by SEM (Figure 6b,c), we could not

see any nanospheres; instead, we detected nanoobjects with a size of ≈ 500 nm. To determine the orientation of the PEDOT chains towards each other, X-ray diffraction measurements were performed for the PEDOT solution and PEDOT powder. Unfortunately, we did not observe any orientation of PEDOT chains (appearing of peak) for PEDOT solution at any time of self-polymerization. However, the PEDOT film possesses peaks, and the XRD results are shown in Figure 6d.

The first peak at $2\theta = 6.5^\circ$ corresponds to the lamellar packing of the PEDOT chains.^[36] The peak could be indexed based on the Aasmundtveit et al. report, suggesting hkl (100).^[37] Using the Bragg equation, we obtained interlamellar distances $d = 13.59$ Å, which is slightly lower than that obtained by Shi et al. ($d = 13.93$),^[36] which means closer packing in our case. The size of the crystalline regions was calculated using the Scherrer equation:

$$L = \frac{K\lambda}{\beta \cdot \cos\Theta} \quad (1)$$

where K is the shape factor, usually equal to 0.9, and β is full width at half maximum of reflection.

We obtained a rather small value of 30 Å only. The film represents a paracrystalline material with the order decaying fast at long distances. There is a wide amorphous halo, located at $2\theta = 24.8^\circ$. That relates to average interchain distances.

To further investigate the self-polymerized PEDOT, the blue solution was deposited on the FTO electrode, and electrochemical measurements were performed in a three-electrode cell configuration in 6 M H₃PO₄ electrolyte. The cyclic voltammetry at different scan rates and electrochemical impedance spectroscopy at open-circuit potential were measured, as shown in Figure 6e,f. The cyclic voltammograms have one oxidation peak and one reduction peak, and with increasing of scan rate, the specific current is increased. Similar behavior was recorded for the PEDOT film deposited by other methods.^[35] Cyclic voltammetry was also recorded in acetonitrile in the range from -1.6 to 1.6 V versus Ag wire, and the results are presented in Figure S7 (Supporting Information). The cyclic voltammetry in organic electrolyte also has one oxidation and one reduction peak.

The electrical conductivity of the self-polymerized PEDOT film could be measured by EIS. The result in the form of a complex plane plot is presented in Figure 6f, and it exhibits a straight line without the presence of a semicircle arc at high frequency. This can be explained by the facile processes of charge transfer and charge transport in the electrochemically active PEDOT film synthesized by self-polymerization. The impedance can be represented in terms of ideal circuit elements, and resistors are dissipative elements that resist the flow of current.^[38] The model and the fitting parameters are presented in Figure S8 (Supporting Information). From the fitted data, the most interesting result for us is R_2 , which is the resistance of the PEDOT film and is in the range of 3.95 Ω , corresponding to a conductivity of 120 S cm⁻¹. The electrical conductivity is lower compare to literature data because we obtained PEDOT in neutral state with 5% of protonation, as proved by XPS data.

We must emphasize that the deposition of the PEDOT film is simple: we used formic acid to prepare the PEDOT solution. Formic acid easily evaporates, and a uniform PEDOT film is obtained.

2.6. Effect of Light and Acids

We know that the EDOT monomer could be self-polymerized in the presence of formic acid without any added oxidant. Our next step was to determine whether the EDOT monomer could be self-polymerized in the presence of other organic or inorganic acids.

Acetic acid was used as the electrolyte; however, the self-polymerization occurred very slowly (first visible change in color started only after 5 d, with the same monomer concentration). However, if *ortho*-phosphoric acid is used, the EDOT self-polymerization proceeds immediately with the formation of a green color. We also observed the effect of light on EDOT self-polymerization. If EDOT self-polymerization took place in the dark, the reaction was slower than self-polymerization under light (laboratory conditions).

We measured the UV-vis spectra of three different PEDOT solutions, and the results are presented in Figure S9 (Supporting Information). It is obvious that all three spectra are different. However, EDOT self-polymerized in the dark or light has similar spectra at the end of polymerization. The PEDOT solution prepared in *ortho*-phosphoric acid is stable and green (we did not observe any precipitation after 1 month, the color stayed the same—green) and similar to the PEDOT solution in

formic acid; however, the viscosity of *ortho*-phosphoric acid is higher compared to formic acid, which is why the work with formic acid is more convenient.

2.7. Different Monomers

We decided to determine whether the self-polymerization method could be used to obtain soluble solutions of other monomers. The chemical structures of different monomers are presented in Figure S8 (Supporting Information). Among the tested monomers, pyrrole, benzothiophene, and para-phenylenediamine could be self-polymerized with the formation of the corresponding polymer solution, as shown in Figure S10 (Supporting Information).

Based on these results, we conclude that our self-polymerization method is suitable for the synthesis of polymer solutions.

3. Conclusions

We have demonstrated a successful self-polymerization method for PEDOT. Such a self-polymerization method proceeds at room temperature without applying potential or adding oxidant and does not produce any byproduct. The self-polymerized PEDOT solution is stable for at least 6 months and could be deposited on a desirable surface simply by drop coating or spin coating. Moreover, the self-polymerized PEDOT solution possesses photoluminescence. It was also demonstrated that it is possible to obtain individual PEDOT chains, in solution, which have a green color. Our study provides a new self-polymerization method for preparing stable and soluble semiconducting polymers. In particular, our study provides the possibility to obtain and study individual polymer chains.

4. Experimental Section

Monomers were bought from Sigma-Aldrich and were used without further purification. Formic acid 98% G.R. and ethyl alcohol 99.8% for UV spectroscopy were bought from Lach-ner, Czech Republic and were used as received.

EDOT Self-Polymerization: 4.7 mL of 98% formic acid was used for self-polymerization reaction. 56 μ L of EDOT monomer was dissolved in 2 mL of ethyl alcohol, and then EDOT solution was added to formic acid to start the self-polymerization reaction. The whole volume of polymerization solution was kept in the closed vessel to prevent the evaporation of formic acid. When the self-polymerization reaction ended the PEDOT solution was kept in the closed vessel. The PEDOT powder was obtained by solvent evaporation from PEDOT solution in Petri dish under room temperature. PEDOT film was deposited on FTO electrode to measure cyclic voltammetry and electrochemical impedance spectroscopy.

Wide-Angle X-Ray Diffraction: Diffraction patterns were obtained using high-resolution diffractometer Explorer (GNR Analytical Instruments, Italy). The instrument is equipped with 1D silicon strip detector Mythen 1K (Dectris, Switzerland). Samples were measured in reflection mode. The radiation Cu K α (wavelength $\lambda = 1.54$ Å) monochromatized with Ni foil (β filter) was used for diffraction. The measurement was done in range $2\theta = 2$ – 40° with step 0.1° . Exposure time at each step was 10 s.

Electrochemical Measurements: Cyclic voltammetry and galvanostatic charge/discharge were performed using an AUTOLAB PGSTAT302N

potentiostat with FRA32M Module and Nova software 2.1. All measurements were performed at ambient temperature in 6 M H₃PO₄. The electrochemical impedance spectra (EIS) have been measured in the range from 10 kHz to 100 mHz with a 10 mV amplitude, at open-circuit potential (OCP) versus Ag/AgCl. The Kronig–Kramers test was applied to verify the obtained EIS data.

Scanning Electron and Transmission Electron Microscopies: The scanning electron micrographs were obtained using a JEOL 6400 microscope. The transmission electron micrographs were obtained using a Tecnai G2 Spirit (FEI).

UV–Vis Characterization: UV–vis spectra for all solutions were recorded on a Perkin-Elmer Lambda 20 UV–vis spectrophotometer.

FTIR, Raman and XPS Spectroscopies: Infrared spectra were recorded on the Nicolet NEXUS Spectrometer with spectral resolution 2 cm⁻¹, 64 sc. The spectrum of the Si support was measured separately and subtracted from the sample spectra. Raman spectra excited with near-infrared diode 785 nm lasers were collected on a Renishaw in Via Reflex Raman spectrometer.

MALDI-TOF MS were obtained on a Bruker microflex MALDI-TOF spectrometer using trans-2-[3-(4-tert-butylphenyl)-2-methyl-2-propenylidene] malononitrile as a matrix in negative ionization mode.

The XPS measurements were performed using a K-Alpha+ XPS spectrometer (ThermoFisher Scientific, UK) operating at a base pressure of 1.0 × 10⁻⁷ Pa. The data acquisition and processing were performed using the Thermo Avantage software. All samples were analyzed using microfocused, monochromated Al K α X-ray radiation (400 μ m spot size) with a pass energy of 200 eV for the survey and 50 eV for high-energy resolution core level spectra. The X-ray angle of incidence was 30° and the emission angle was along the surface normal. The binding energy scale of the XPS spectrometer was calibrated by the well-known positions of the C 1s C–C and C–H, C–O peaks of polyethylene terephthalate and Cu 2p, Ag 3d, and Au 4f peaks of Cu, Ag, and Au metals, respectively. The obtained high-resolution spectra were fitted with Voigt profiles to probe the individual contributions of the present chemical species.

Photoluminescence Measurements: The PL spectra of the PEDOT suspension in an aqueous solution were recorded on an F55 fluorescence spectrophotometer (Edinburgh Instruments Ltd, UK). The wavelength of the pulsed laser was λ_{exc} = 485 nm. The PEDOT suspension was deposited on quartz glass and the PL spectra of the thin film were recorded by the excitation dependent photoluminescence spectrometer Jasco FP-6200 model. The excitation wavelength was 442 nm.

Supporting Information

Supporting Information is available from the Wiley Online Library or from the author.

Acknowledgements

The authors thank Z. Walterová for MALDI ToF measurements. The authors acknowledge the Czech Science Foundation (19-04859S).

Conflict of Interest

The authors declare no conflict of interest.

Author Contributions

E.T. and I.I. developed the self-polymerization reaction. E.T. conducted the most of the experiments and wrote the manuscript. E.T. directed the project. I.Š. measured FTIR and Raman spectra. A.Z. measured XRD.

J.S. measured XPS. J.P. conducted time resolved PL measurements. M.L. measured EPR spectroscopy. J.H. conducted TEM and SEM measurements.

Keywords

PEDOT, photo luminescence, self-polymerization, UV-vis spectra, XPS spectra

Received: July 1, 2020

Published online:

- [1] K. Yoshino, S. Hayashi, R. Sugimoto, *Jpn. J. Appl. Phys.* **1984**, *23*, L899.
- [2] A. F. Diaz, K. K. Kanazawa, G. P. Gardini, *J. Chem. Soc., Chem. Commun.* **1979**, 635.
- [3] J. Kuwabara, W. Tsuchida, S. Guo, Z. Hu, T. Yasuda, T. Kanbara, *Polym. Chem.* **2019**, *10*, 2298.
- [4] R. Roncali, *Chem. Rev.* **1992**, *92*, 711.
- [5] E. N. Konyushenko, J. Stejskal, M. Trchova, *Synth. Met.* **2008**, *158*, 927.
- [6] I. Sedenkova, E. N. Konyushenko, J. Stejskal, *Synth. Met.* **2011**, *161*, 1353.
- [7] H. Meng, D. F. Perepichka, M. Bendikov, F. Wudl, G. Z. Pan, W. Yu, W. Dong, S. Brown, *J. Am. Chem. Soc.* **2003**, *125*, 15151.
- [8] A. Patra, Y. H. Wijsboom, S. S. Zade, M. Li, Y. Sheynin, G. Leitius, M. Bendikov, *J. Am. Chem. Soc.* **2008**, *130*, 6734.
- [9] M. Lepeltier, J. Hiltz, T. Lockwood, F. Bélanger-Gariépy, D. F. Perepichka, *J. Mater. Chem.* **2009**, *19*, 5167.
- [10] A. Patra, Y. H. Wijsboom, G. Leitius, M. Bendikov, *Chem. Mater.* **2011**, *23*, 896.
- [11] C. Tusy, L. Huang, J. Jin, J. Xia, *RSC Adv.* **2014**, *4*, 8011.
- [12] B. Bonillo, T. M. Swager, *J. Am. Chem. Soc.* **2012**, *134*, 18916.
- [13] B. Aydogan, G. E. Gunbas, A. Durmus, L. Toppare, Y. Yagci, *Macromolecules* **2010**, *43*, 101.
- [14] S. Zhang, W. Zhang, G. Zhang, Y. Bai, S. Chen, J. Xu, Z. Yu, K. Sun, *Mater. Lett.* **2018**, *222*, 105.
- [15] M. N. Gueye, A. Garella, J. Faure-Vincent, R. Demadrille, J.-P. Simonato, *Prog. Mater. Sci.* **2020**, *108*, 100616.
- [16] D. Farka, H. Coskun, J. Gasiowski, C. Cobet, K. Hingerl, L. M. Uiberlacker, S. Hild, T. Greunz, D. Stifter, N. S. Sariciftci, R. Menon, W. Schoefberger, C. C. Mardare, A. W. Hassel, C. Schwarzinger, M. C. Scharber, P. Stadler, *Adv. Electron. Mater.* **2017**, *3*, 1700050.
- [17] T. Takano, H. Masunaga, A. Fujiwara, H. Okuzaki, T. Sasaki, *Macromolecules* **2012**, *45*, 3859.
- [18] H. Meng, D. F. Perepichka, F. Wudl, *Angew. Chem., Int. Ed.* **2003**, *42*, 658.
- [19] H. J. Spencer, R. Berridge, D. J. Crouch, S. P. Wright, M. Giles, I. McCulloch, S. J. Coles, M. B. Hursthouse, P. J. Skabara, *J. Mater. Chem.* **2003**, *13*, 2075.
- [20] C. Tusy, K. Jiang, K. Peng, L. Huang, J. Xi, *Polym. Chem.* **2015**, *6*, 1014.
- [21] P. Wagner, K. W. Jolley, D. L. Officer, *Aust. J. Chem.* **2011**, *64*, 335.
- [22] Y. Yin, Z. Li, J. Jin, C. Tusy, J. Xia, *Synth. Met.* **2013**, *175*, 97.
- [23] Schopf, G. Koßmehl, in *Polythiophenes—Electrically Conductive Polymers* (Eds: A. Abe, H. Benoit, H.-J. Cantow, P. Corradini, K. Dušek, S. Edwards, H. Fujita, G. Glockner, H. Hocker, H.-H. Horhold, H.-H. Kausch, J. P. Kennedy, J. L. Koenig, A. Ledwith, J.-E. McGrath, L. Monnerie, S. Okamura, C. G. Overberger, H. Ringsdorf, T. Sacgusa, J. C. Salamone, J. L. Schrag, G. Wegner), Springer, New York **1997**, Ch. 5.
- [24] S. Sadki, P. Schottland, N. Brodie, G. Sabouraud, *Chem. Soc. Rev.* **2000**, *29*, 283.



- [25] J. Cao, J. W. Kampf, M. D. Curtis, *Chem. Mater.* **2003**, *15*, 404.
- [26] P. Audebert, G. Bidan, *Synth. Met.* **1986**, *15*, 9.
- [27] C. Li, H. Bai, G. Shi, *Chem. Soc. Rev.* **2009**, *38*, 2397.
- [28] E. Tomsik, O. Kohut, I. Ivanko, M. Pekárek, I. Bieloshapka, P. Dallas, *J. Phys. Chem. C* **2018**, *122*, 8022.
- [29] I. Zozoulenko, A. Singh, S. K. Singh, V. Gueskine, X. Crispin, M. Berggren, *ACS Appl. Polym. Mater.* **2019**, *1*, 83.
- [30] X. Du, Z. Wang, *Electrochim. Acta* **2003**, *48*, 1713.
- [31] I. Ivanko, J. Svoboda, M. Lukešová, I. Šeděnková, E. Tomšík, *Macromolecules* **2020**, *53*, 2464.
- [32] R. Dams, D. Vangeneugden, D. Vanderzande, *Chem. Vap. Deposition* **2006**, *12*, 719.
- [33] C. Kvarnström, H. Neugebauer, S. Blomquist, H. J. Ahonen, J. Kankare, A. Ivaska, *Electrochim. Acta* **1999**, *44*, 2739.
- [34] N. B. Colthup, L. H. Daly, S. E. Wiberley, *Introduction to Infrared and Raman Spectroscopy*, Academic Press, New York **1964**, p. 276.
- [35] I. Ivanko, J. Pánek, J. Svoboda, A. Zhigunova, E. Tomšík, *J. Mater. Chem. C* **2019**, *7*, 7013.
- [36] W. Shi, Q. Yao, S. Qu, H. Chen, T. Zhang, L. Chen, *NPG Asia Mater.* **2017**, *9*, e405.
- [37] K. E. Aasmundtveit, E. J. Samuelsen, L. A. A. Pettersson, O. Inganäs, T. Johansson, R. Feidenhans, *Synth. Met.* **1999**, *101*, 561.
- [38] E. Hauff, *J. Phys. Chem C* **2019**, *123*, 11329.

Appendix 5

Ivanko, I.; Tomšík, E. Effect of hydrogen bonding on a value of an open circuit potential of poly-(3,4-ethylenedioxythiophene) as a beneficial mode for energy storage devices, *Adv. Funct. Mater.* **31**, 2103001(2021). IF = 18,808.

Effect of Hydrogen Bonding on a Value of an Open Circuit Potential of Poly-(3,4-ethylenedioxythiophene) as a Beneficial Mode for Energy Storage Devices

Iryna Ivanko* and Elena Tomšik*

Poly(3,4-ethylenedioxythiophene) is one of the semiconducting polymers that has attracted attention as electroactive materials for many different applications such as electrochromic devices, light-emitting diodes, biosensors, and supercapacitors. The fundamental understanding of the origin of its energy storage ability will lead to the proper design of such devices. Generally, the charge storage in supercapacitors is due to the formation of an electrical double layer and/or redox reactions. Recently, it is shown that the formation of cation radicals in PEDOT is induced by the hydrogen-bond formation between formic acid and polymer during electrochemical polymerization. The induced cation radicals play a major role in the charge storage ability of PEDOT, as studied in the current work. Furthermore, the presence of hydrogen bonds in PEDOT leads to the stable in time open circuit potential of 900 mV. This new knowledge leads to the designing of a symmetrical supercapacitor based on PEDOT as active material where hydrogen-bonds play a crucial role in the improved performance of the device.

1. Introduction


Electronic devices have increased demand for the development of easy-fabricated, light-weighted solid-state energy storage units on flexible platforms such as plastic or carbon-based substrates.^[1–3] Pseudocapacitors have become promising energy storage units due to their much higher energy density compared to conventional capacitors and more elevated value of power density compared to batteries.^[4,5] The conjugated polymers are a good candidate for pseudocapacitors due to the fast redox conversion on the surface.^[6] Among electrically conducting polymers, there is considerable interest in using poly(3,4-ethylenedioxythiophene) (PEDOT) because of its low oxidation potential, high stability in an ambient environment,

mechanical flexibility, and stable oxidized form.^[7a] Generally, the electricity comes from a force, such as output voltage, that moves electrons. The output voltage may be generated by the presence of difference of electrical potential of two electrodes and can be an electromotive force for electron movement in the conductor. In order to provide a large value of output voltage, the oxidation level of the two electrodes must differ as much as possible (the potential difference of the neutral (undoped) state and oxidized (doped) state). It is shown in the published literature that the reduced state of semiconducting polymers has low electrical conductivity.^[7b] That is why p/n doping might be done to enhance the conductivity of conducting polymer. It is a possibility of introducing positive or negative charge centers on electrically conjugated polymer chains using oxidation

or reduction reactions, the extent of which depends on electrode potential that has given rise to substantial current and make interest in these materials for electronically storage devices.^[8] Recently, the Crispin group constructed a PEDOT-based air battery with excellent electrochemical properties and high value of an electromotive force.^[9] Specifically, poly-ethyleneimine (PEI) was combined with the low oxidized form of PEDOT (undoped) at the anode (PEI/PEDOT), while PEDOT in the oxidized state (doped) was used at the cathode. The difference between the oxidation levels of the electrodes produced an open circuit voltage of 500 mV. The other promising approach toward increasing open circuit voltage is preparation of hybrid inorganic–organic materials that were applied for silicon heterojunction collar cells.^[10] The open circuit voltage exceeding 660 mV was measured for the device where PEDOT:PSS was used as highly conductive polymer. Another strategy is the combination of PEDOT:PSS with other conducting polymers, which can allow obtaining hybrid organic systems with tunable properties.^[11] Particularly, polyaniline was used by A. Vacca et al. to obtain PEDOT:PSS/PANI electrode with 250 mV open circuit potential at low pH (acidic) and –50 mV at higher pH.^[11] According to Aradilla et al. who declare they were able to gain an open circuit potential of 1100 mV for three-layered PEDOT/PNMPy/PEDOT and PEDOT/clay films by prior electrochemical polarization of electrodes (one was oxidized and the other electrode was reduced).^[11] However, the data were measured for battery type device and it does not

I. Ivanko, Dr. E. Tomšik
Institute of Macromolecular Chemistry, Department of Conducting Polymers AS CR
Prague 6, 162 06, Czech Republic
E-mail: ivanko@imc.cas.cz; tomsik@imc.cas.cz

I. Ivanko
Faculty of Science
Charles University
Prague 2, 128 43, Czech Republic

 The ORCID identification number(s) for the author(s) of this article can be found under <https://doi.org/10.1002/adfm.202103001>.

DOI: 10.1002/adfm.202103001

specify how long the device can keep 1100 mV open circuit potential. Another way to enhance the high value of the electrochemical surface potential of the conjugated polymer can be provided, for example, by utilization of protic acids as dopant which in turn possesses the ability to form hydrogen bonding with polymeric chains. Recently, the ability of the protic acid, namely formic acid, to form hydrogen-bonds with lone pair of electrons of sulfur atoms of PEDOT (and thus to induce the formation of localized cation-radicals in the conjugated system of PEDOT) was studied.^[12] Moreover, by replacing of formic acid with another protic acid, such as ortho-phosphoric acid, the delocalization of cation radicals was observed.

In this work, we report a method of preparation of symmetrical supercapacitor based on PEDOT that possesses a stable in time an open circuit potential of 900 mV value gained without prior to electrochemical pre-polarization of electrodes. We demonstrate that hydrogen-bonds between organic acid and polymer chains can play a major role in such high value of the open circuit potential. The results of galvanostatic charge/discharge also prove that the presence of hydrogen-bonding improves the performance of the symmetrical supercapacitor. The results of our work are important on the one hand from the fundamental point of view, and on the other hand, from the practical application.

2. Results and Discussions

2.1. Symmetrical Supercapacitor Assembly and Measurements of V_{oc}

The electrochemical polymerization of EDOT on the carbon cloth substrate (see **Figure 1** top) has been done by applying constant current in the presence of 5 M of formic acid as a supporting electrolyte. The role of the supporting electrolyte during the electropolymerization from one hand is increasing the conductivity of the monomer solution and on the other hand, is to compensate the charge of the growing conducting layer. Moreover, the choice of electrolyte could play a significant role on the physicochemical properties of the final product. For example, due to the ability of the supporting electrolyte to form hydrogen-bonding between polymer chains and electrolyte it is possible to tune optical and the physicochemical properties of a polymer.^[13,14] Among organic/inorganic acids, formic acid is a good candidate to form dipole-dipole and/or hydrogen-bonding interactions. The excellent ability of formic acid to form hydrogen-bonding and therefore to form dimers or even trimers has been examined in plenty of research works.^[15,16]

Therefore, in this work, formic acid was used as a supporting electrolyte during electropolymerization of PEDOT. Due to the

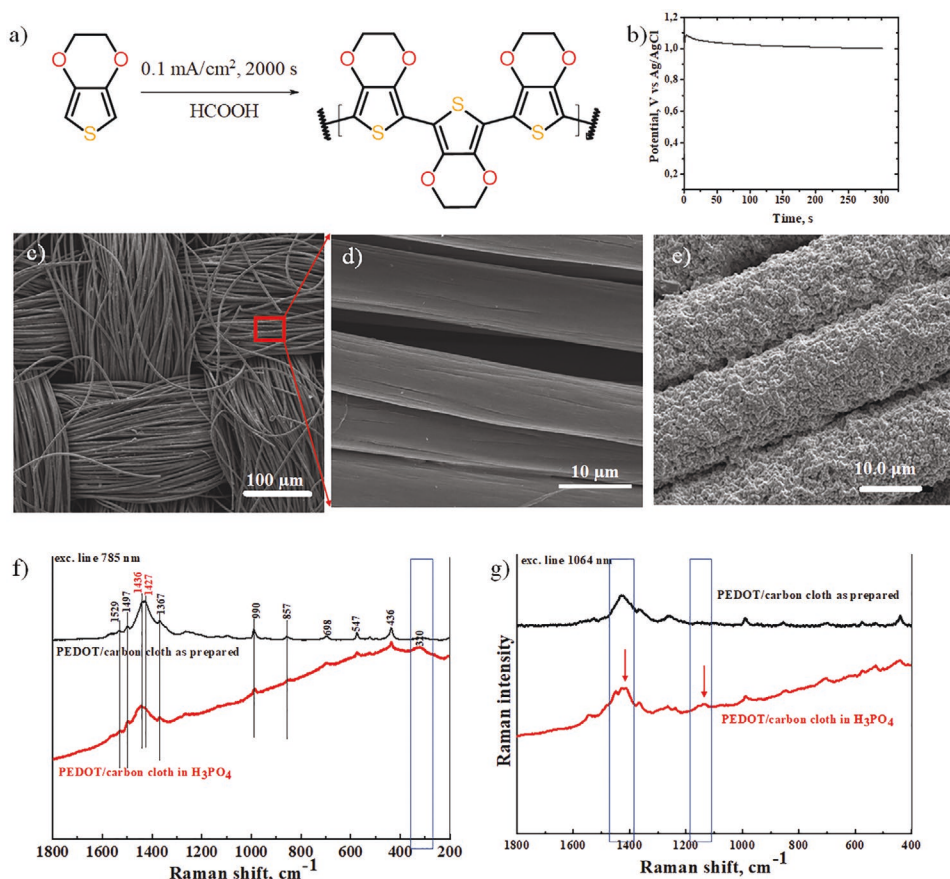


Figure 1. a) Schematic representation of electrochemical polymerization of EDOT; b) kinetic of electropolymerization; c,d) scanning electron microscope images of carbon cloth at different magnifications; and e) PEDOT electrochemically deposited onto carbon cloth substrate; f) Raman spectra of PEDOT/carbon cloth as prepared and after CV at a laser 785 nm; g) Raman spectra of PEDOT/carbon cloth as prepared and after CV at a laser 1064 nm.

small size of formic acid, last can penetrate between polymer chains and interact by the hydrogen-bonding interaction with lone pair electrons located on sulfur of thiophene ring in PEDOT molecules. This interaction led to the formation of cation radicals which are localized on the sulfur atoms of thiophene rings. That fact was confirmed by high-resolution X-ray photoelectron spectroscopy (XPS) by the detailed investigation of the valent electron shell of sulfur in thiophene ring, where two peaks were observed, which correspond to the presence of sulfur in two oxidations states.^[12]

As can be seen in Figure 1a the electropolymerization was carried out by applying constant current, where two electrons and two protons from monomer are released and polymer chains formation occurred. The course of polymer electrodeposition is recorded by measuring potential versus time, as presented in Figure 1b (only the first 300 s is presented). The mass loading of the PEDOT was controlled by the time of the polymerization and using Faraday's law was calculated. In order to increase an area capacitance of the final device, the polymerization of the polymer film was carried out on the top of carbon cloth with the high surface area. As can be seen on the scanning electron microscope (SEM) image (Figure 1c,d) carbon cloth made up of long fibrils that are networking together and provide high surface area. After the electrochemical deposition of PEDOT, as can be seen from the SEM image in Figure 1e, the smooth surface of bare carbon cloth is uniformly covered by PEDOT.

In order to study an effect of hydrogen-bonding on the value of an open circuit potential and electrochemical performances the symmetrical supercapacitor device was assembled, where one electrode was dried PEDOT (as prepared) and the other one was wet PEDOT soaked for 10 min in 6 M H_3PO_4 . To provide runs of electrons through the external circuit during applying an overpotential on the system, the water non-permeable dielectric separator was used. The water non-permeable membrane (separator) was as well preventing the penetration of water and acid molecules from the wet electrode to the dried one (see Figure 2 left).

As shown on the illustration picture of the symmetrical device (Figure 2 left) and the dependence of the open circuit potential (V_{oc}) versus time (Figure 2 right), the potential of the electrodes in an equilibrium state, when no current pass through the system, is 900 mV. This value of V_{oc} could be explained by the difference in an oxidation state of two elec-

trodes in the device. Our hypothesis based on the proposition that one electrode is in a neutral state and the second electrode is in an oxidized state, which is induced by hydrogen-bonding between organic acid and sulfur in polymer chains. Previously it has been proved by us the chemical structure of PEDOT studied by the Raman spectroscopy and XPS and it was shown that PEDOT polymerized in the presence of formic acid is in a reduce state, and there is no oxidized sequence.^[12] On the other hand, it was shown that hydrogen bonds between formic molecules and polymer chains induced the formation of cation radicals and therefore partially oxidized sulfur in thiophene (from XPS spectra it was estimated to be 27%).^[12] Also, it was shown that orthophosphoric acid could interact with PEDOT chains with the formation of delocalized cation radicals. That is why in this work, we decided to investigate the role of delocalized cation radicals on the value of V_{oc} and its effect on charge storage in the assembled device. The orthophosphoric acid is used as a supporting electrolyte.

The value of 900 mV for V_{oc} was measured and it is stable in time; even after 180 h (75 days), see Figure 2. We proposed that a high value of V_{oc} is connected with the formation of delocalized cation radicals for the wet PEDOT electrode interacted with orthophosphoric acid. The formation of delocalized cation radicals is connected with the presence of partially oxidized sequences. This statement was confirmed by measuring Raman spectra of PEDOT/carbon cloth electrodes as prepared and after cyclic voltammetry (CV) measurements in orthophosphoric acid with different excitation lasers 785 and 1064 nm (Figure 1f,g). The main peak at $\approx 1434\text{ cm}^{-1}$ corresponding to $C_{\alpha}=C_{\beta}$ stretching vibration for the fully reduced PEDOT (as prepared) is widened for PEDOT/carbon cloth electrode after CV in orthophosphoric acid. The Raman measurement (1064 nm laser) shows the peak corresponding to orthophosphoric acid (shown by red arrows). Moreover, the presence of orthophosphoric acid was also confirmed by the peak at $\approx 320\text{ cm}^{-1}$ in Figure 1f. On the other hand, the dried PEDOT electrode (as prepared) is in a reduced state. In addition, the stability of delocalized charge carries is stabilized either by counter ions or by the mesomeric effect of unsaturated π -bond in α -position toward vacant p-orbital of cation radical center. It is well known that localized cation radicals are unstable in time due to high reactivity and the stability

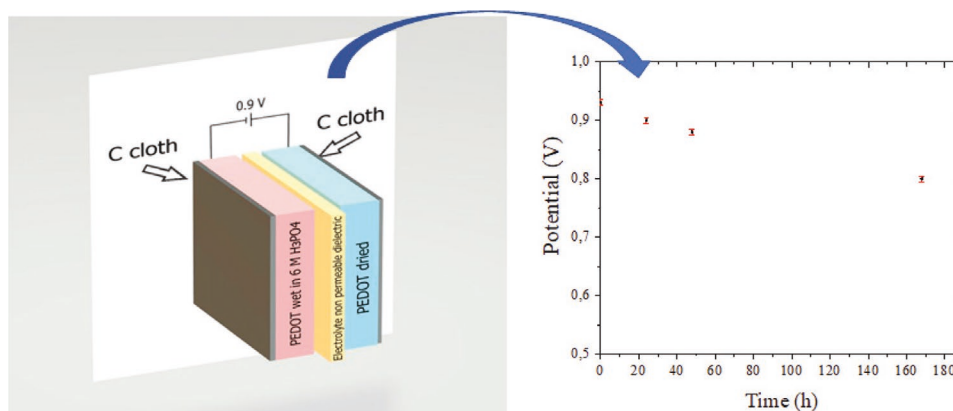


Figure 2. Schematic illustration of the symmetrical supercapacitor device based on PEDOT electrodes (left) and stability of an open circuit potential in time (right).

arise with delocalization of charge.^[17,18] We also suggest that the nature of stable in time V_{oc} connected with the fact that the vacant p-orbital of cation radicals is coplanar to the delocalized π -orbital of α -C and by π -p conjugation the stabilization of cation radicals occurs. A similar effect was observed by Gospodinova et al.^[19] who reported the influence of the polarity of water environment on the value of open circuit potential for mesoporous PANI films. Authors declare that the V_{oc} value of the solar cells increases substantially and becomes stable in time after additions of water containing highly hydrated ions. The authors explain this fact by the more efficient excitons dissociation and enhancement of charge carriers transport after the interaction of PANI and tap water.

Based on the above measurements we conclude that simply by applying the organic acid that is able to form hydrogen bonding it is possible to prepare two electrodes from one semi-conducting polymer, which is different in the oxidation state. The symmetrical supercapacitor device made from these two electrodes (wet and dried PEDOT) has stable in time V_{oc} .

In order to show the influence of the hydrogen bonding on the value of V_{oc} , the electrochemical cell was assembled in different configurations, see Table 1.

As it is presented in Table 1 when the symmetrical supercapacitor was made up of two dried PEDOT electrodes (as it prepared), the value of the open circuit potential was equal to 20 mV and went down to zero in time. However, when both electrodes of the electrochemical supercapacitor after polymerization were soaked in a protic acid (for example, formic acid) for some time the V_{oc} of 100 mV is recorded. We could explain such small difference (the 0 value was expected) by the difference in PEDOT mass loading, even the size of both electrodes was the same. When the neutral electrolyte was used (for example NaCl), we did not observe a high value of V_{oc} (160 mV, see Table 1). We concluded that the high value of V_{oc} for electrodes treated in acid is connected with the ability of protic acids, such as orthophosphoric, to form hydrogen-bonding with polymer chains and form delocalized charge carriers. On the other hand, in the case of a neutral salt, where only Coulomb interactions are present, the symmetrical supercapacitor based on one electrode with neutral salt and the other electrode with the organic acid had a value of V_{oc} at 920 mV (see Table 1). The effect of neutral salt on the value of V_{oc} is marginal, and the assembly of the device requires careful separation where two electrodes are wet. Moreover, it is must be noted that the value of V_{oc} for electrochemical supercapacitor where one electrode was immersed in orthophosphoric acid, and the second electrode was immersed in neutral salt was not stable in time. That is why we decided further to work only with

Table 1. The value of an open circuit potential for different configurations of the electrochemical cell.

Anode	Cathode	OCP [mV]
PEDOT dried	PEDOT dried	20
PEDOT wet in 6 M H ₃ PO ₄	PEDOT dried	900
PEDOT wet in 6 M H ₃ PO ₄	PEDOT wet in 6 M H ₃ PO ₄	100
PEDOT wet in 1 M NaCl	PEDOT dried	160
PEDOT wet in 6 M H ₃ PO ₄	PEDOT wet in 1 M NaCl	920

the symmetrical supercapacitor where one electrode is wet, and the other one is dried. Additionally, it was shown that introduction of small organic acid, into the PEDOT structure led to the detection of two peaks on the cyclic voltammogram in acidic medium, whereas there are no peaks in neutral one.¹²

2.2. Characterization of the Symmetrical Supercapacitor

Further to characterize the pseudocapacitive performance of symmetrical PEDOT/carbon cloth device, the following methods were applied: cyclic voltammetry, galvanostatic charge/discharge measurements, X-ray diffraction (XRD), and electrochemical impedance spectroscopy. The detailed descriptions of the methods are given in Section 4.

In order to investigate the electrochemical process taking place during redox reactions, the CV has been performed at 30 and 100 mV s⁻¹ sweep rates, respectively. The results are presented in Figure 3a. The reversible redox process was observed for both sweep rates. The blue line represents the results of the cell composed only from carbon cloth electrodes. In the case of the device, the stable CV window of 1.3 V was found and for the symmetrical supercapacitor configuration we did not observe the mirror-like voltammograms compare to the 3-electrode cell configuration, reported previously.^[12] The symmetrical supercapacitor was assembled in a way where two electrodes are separated by a non-permeable membrane. That is why we proposed that measured current is connected with the capacitive behavior. Our observation is also in agreement with the recently reported results by I.V. Zozoulenko.^[20]

Generally, charge storage in a supercapacitor is due to electric double-layers formed along with electrode/electrolyte interfaces and/or electrochemical processes.^[21] Galvanostatic charge/discharge (GCD) measurements for PEDOT symmetrical supercapacitor are recorded and the results are presented in Figure 3b. The size of both electrodes is 1.5 cm². The areal metrics for evaluating our supercapacitor is used because these practical parameters are important for the real device application. The areal current density varied from 0.5 to 1.4 mA cm⁻² (Figure 4b). From GCD data, it is seen that charging and discharging curves are consistent with the CV curves. The charging time is longer compared to the discharging one, and with decreasing of the charging current the Coulombic efficiency decreasing too. The iR drop is small for all measured data. Calculated areal capacitance is 58 mF cm⁻² measured at 0.5 mA cm⁻², and 32 mF cm⁻² measured at 1.4 mA cm⁻², as shown in Figure 4b (the potential window is 1 V). It is smaller compare to the CV measurements because the stability of the symmetrical supercapacitor at this potential window was found to be the best one. The areal capacitance recorded by us is higher than those of other symmetric supercapacitors—56.7 mF cm⁻² measured at 0.5 mA cm⁻² (the potential window is 1.6 V).^[22]

In the next step, the XRD of carbon cloth, PEDOT/carbon cloth as prepared and PEDOT/carbon cloth after interaction with orthophosphoric acid were studied and presented in Figure 3c. The data for the carbon cloth (support) were extracted from the data PEDOT/carbon cloth as prepared and PEDOT/carbon cloth after interaction with orthophosphoric acid. The XRD measurements shows the predominance of the peak corresponding to the face-on texture in the PEDOT films (Figure 3c).

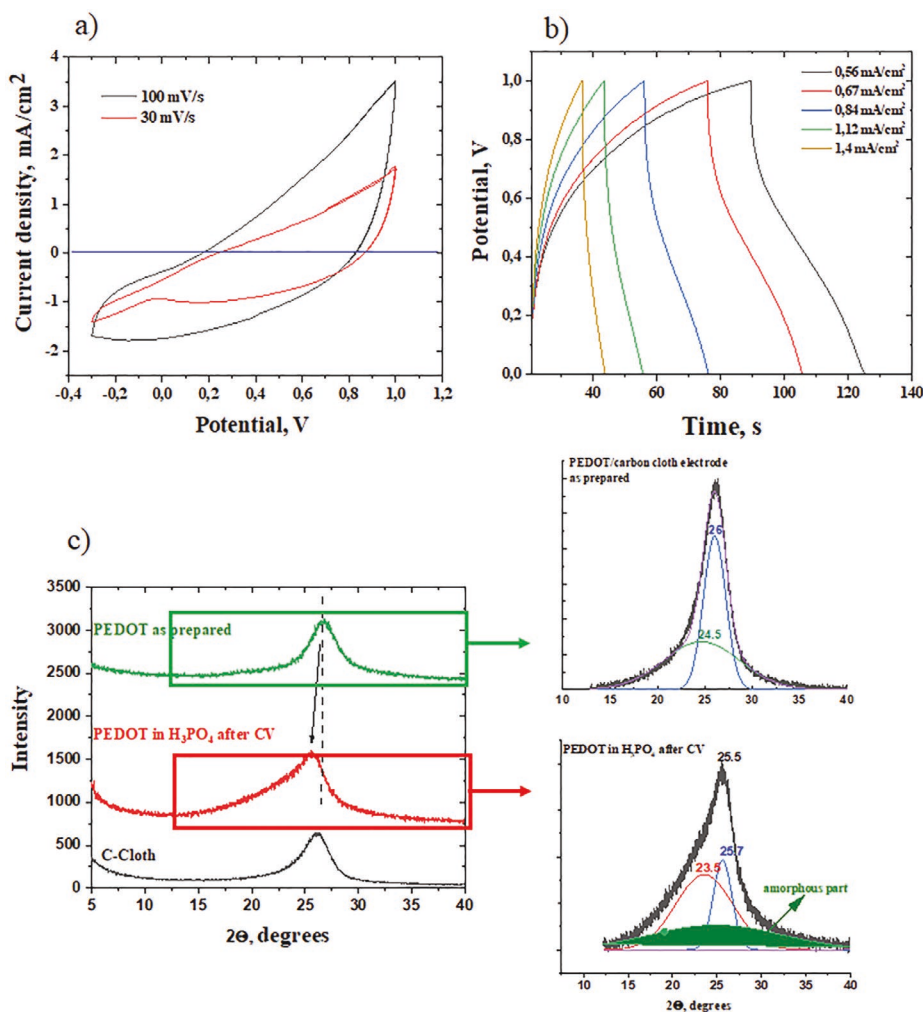


Figure 3. a) Cyclic voltammograms and b) galvanostatic charge–discharge curves of symmetrical supercapacitor based on PEDOT. (c) XRD of carbon cloth, and PEDOT/carbon cloth electrodes at different conditions, and deconvolution of the corresponding main peak.

Such configuration of the polymer chains was proved to be important in order to increase the film conductivity and charge carrier mobility.^[23] Deconvolution of the main peak (for PEDOT/carbon cloth electrode after CV) located at $2\theta = 25.5^\circ$ gives us two peaks with the distance of 3.5 \AA ($2\theta = 25.7^\circ$) and 3.8 \AA ($2\theta = 23.5^\circ$). The increase of the π - π stacking distance in the orthorhombic structure of PEDOT is connected

with the incorporation of orthophosphoric acid into the structure, compare to the PEDOT as prepared, where π - π stacking distance is located at $2\theta = 26^\circ$ and $2\theta = 24.5^\circ$ (Figure 3c).

As was mentioned above, the iR drop is small as was recorded during GCD measurements. This fact is connected with the low resistance between PEDOT and carbon cloth and/or other interfaces in the assembled supercapacitor. To

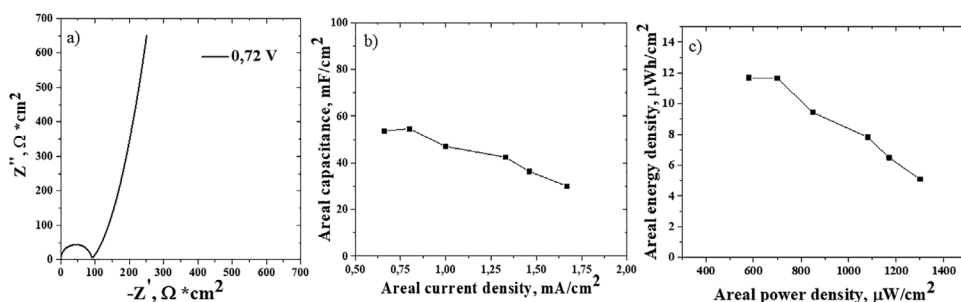


Figure 4. a) Electrochemical impedance spectroscopy, b) the dependence of areal capacitance versus areal current density, and c) dependence of areal energy density versus areal power density.

prove it the electrochemical impedance spectroscopy is measured and the result in the form of a Nyquist plot is presented in Figure 4a. The aggregated internal resistance of the assembled supercapacitor of $\approx 30 \Omega \text{ cm}^{-2}$ is recorded. A small semi-circle is present at high frequency and an almost vertical line is observed at low frequency, indicating capacitive behavior of the assembled supercapacitor.

In tandem with areal capacitance, the areal energy and power are more important parameters for practical applications of the devices. The areal energy and power were calculated from the obtained results by Equations described in the experimental section. In Figure 4c the dependence of areal energy density versus areal power density is presented in the form of a Ragone plot.

The assembled supercapacitor has a high areal energy density of $12 \mu\text{Wh cm}^{-2}$ corresponding to the areal power density of $550 \mu\text{W cm}^{-2}$. The maximum areal power density of $1300 \mu\text{W cm}^{-2}$ is measured, which corresponds to the areal energy density of $750 \mu\text{Wh cm}^{-2}$ (see Figure 4c). The obtained by us areal energy and power densities are much higher compared to the literature data reported for symmetrical supercapacitor based on PEDOT as summarized and presented in Figure 5 ($5 \mu\text{Wh cm}^{-2}$ and $440 \mu\text{W cm}^{-2}$)^[22], PEDOT:PSS fiber ($4.13 \mu\text{Wh cm}^{-2}$ and $250 \mu\text{W cm}^{-2}$)^[24], graphene/PEDOT fiber ($6.8 \mu\text{Wh cm}^{-2}$ and $200 \mu\text{Wh cm}^{-2}$)^[25]. It was also reported the areal energy ($2.57 \mu\text{Wh cm}^{-2}$) and the areal power ($400 \mu\text{W cm}^{-2}$) densities for free standing PEDOT:PSS supercapacitor measured at 1 mA cm^{-2} .^[28]

To conclude this section, we demonstrate that the symmetrical supercapacitor based on one dried PEDOT electrode and one wet PEDOT has capacitive current (shown by CV measurements), small internal resistance (recorded by EIS) and much higher areal energy and power densities compare to the literature data.

3. Conclusion

In conclusion, we demonstrate that hydrogen-bonding plays a major role in the high value of V_{oc} for the symmetrical superca-

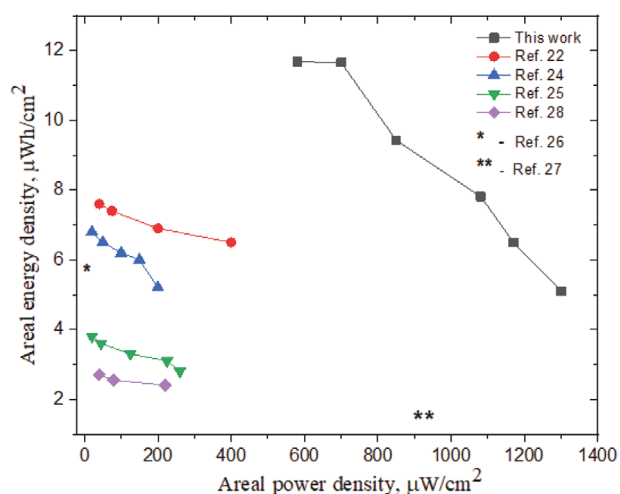


Figure 5. Comparison of Ragone plots of our PEDOT based symmetrical supercapacitors with previously reported results.

pacitor. The device was assembled in a way where one electrode was dried PEDOT separated with non-permeable membrane from the second electrode—wet PEDOT. In order to prove our assumption, the symmetrical supercapacitor was assembled only with two dried electrodes, or with electrode where PEDOT was immersed into neutral salt. Only symmetrical supercapacitor where wet PEDOT was immersed in an organic acid showed V_{oc} of 900 mV value; and moreover, this V_{oc} value was stable in time.

Finally, we showed that symmetrical supercapacitor has much higher areal energy and power densities compared to the literature data. This type of supercapacitor has a capacitive current, proved by CV, GCD, and EIS measurements.

4. Experimental Section

Materials: The monomer 3,4-ethylenedioxythiophene (EDOT), 98 (wt%) of formic acid, 85 (wt%) of orthophosphoric acid, carbon cloth, and ethyl alcohol were purchased from Aldrich.

Synthesis: The electrochemical polymerization of EDOT monomer was performed at the carbon cloth (CC) electrodes by galvanostatic polymerization in a three-electrode electrochemical cell configuration. The polymerization was performed by applying 0.1 mA cm^{-2} current density in the presence of 5 M formic acid as a supporting electrolyte; the polymerization solution was purged with nitrogen gas for 30 min before the polymerization started.

Preparation of the Electrodes: Electrodes for fabricating the device were prepared by electropolymerization of PEDOT onto CC. To oxidize the anode the doping processes of the electrode was done. Oxidized PEDOT (anode) was generated by soaking of the electrode in 6 M H_3PO_4 for a few minutes. The cathode of the device was left in the redox state after the polymerization, without pre-polarization. As a separator, a (10 wt%) of polyphenylene oxide with dielectric constant 2.7 (1 MHz) was used.

Characterization of the PEDOT Symmetrical Cell: Scanning electron micrographs were taken with a JEOL 6400 microscope (Japan).

Electrochemical characterization of the PEDOT symmetrical electrodes was performed in a two-electrode cell configuration using an AUTOLAB PGSTAT302N potentiostat with a FRA32M Module and Nova 2.1 software. The wet electrode (anode) was the working electrode and the dried electrode (cathode) was as counter and a reference electrode, respectively. Cyclic voltammetry was recorded in the potential window from -0.3 to 1 V with a scan rate 30 and 100 mV s^{-1} . Galvanostatic charge–discharge measurements were recorded in the potential window from 0 to 1 V and the applied current density was in the range from 0.5 to 1.5 mA cm^{-2} . Electrochemical impedance spectroscopy was measured in the frequency range from 10 kHz to 100 mHz with a 10 mV amplitude, at a potential of 0.72 V. The Kronig–Kramers test was applied to verify the obtained EIS data.

Wide-angle X-ray diffraction patterns were obtained using high-resolution diffractometer Explorer (GNR Analytical Instruments, Italy). The instrument was equipped with 1D silicon strip detector Mythen 1K (Dectris, Switzerland). Samples were measured in reflection mode. The radiation $\text{CuK}\alpha$ (wavelength $\lambda = 1.54 \text{ \AA}$) monochromatized with Ni foil (β filter) was used for diffraction. The measurement was done in range $2\theta = 2^\circ$ – 40° with step 0.1° . Exposure time at each step was 10 s.

Calculations: All electrochemical measurements were performed in a two-electrode cell configuration, and the calculations correspond to such a set-up. The areal capacitance (for one electrode) was calculated by using Equation (1):

$$C = 2 \times (I \times t) / (\Delta V \times A) \quad (1)$$

where I is the applied discharge current (A), t is the discharge time (s), ΔV is the potential window without iR drop (V), and A is the area of the PEDOT/CC electrode (cm^2);

The areal energy density was calculated by using Equation (2):

$$E = (C \times \Delta V^2) / 3600 \quad (2)$$

where C is the areal capacitance (mF cm^{-2}) and ΔV is the potential window without iR drop (V);

The areal power density was calculated using Equation (3):

$$P = (I \times \Delta V) / A \quad (3)$$

where I is the applied discharge current (A), ΔV is the potential window without iR drop (V) and A is the area of the PEDOT/CC electrode (cm^2).

Deconvolution of the XRD data of the PEDOT films was performed using the Fytik 0.9.8 program. Gaussian profiles were used for the deconvoluted spectra, and the base line was corrected before each deconvolution.^[29]

Acknowledgements

The authors would like to acknowledge Dr. A. Zhigunov for results discussion, J. Hromádková for SEM measurements, and Dr. I. Šeděnková for Raman measurements. The authors acknowledge the Czech Science Foundation (19-04859S).

Conflict of Interest

The authors declare no conflict of interest.

Data Availability Statement

Research data are not shared.

Keywords

hydrogen bonding, open circuit potential, poly(3,4-ethylenedioxythiophene), supercapacitors

Received: March 29, 2021

Published online:

- [1] M. E. Abdelhamid, A. P. O'Mullaneb, G. A. Snook, *RSC Adv.* **2015**, 5, 11611.
 [2] L. Nyholm, G. Nyström, A. Mihranyan, M. Strømme, *Adv. Mater.* **2011**, 23, 3751.
 [3] C. Meng, C. Liu, L. Chen, C. Hu, S. Fan, *Nano Lett.* **2010**, 10, 4025.
 [4] P. Simon, Y. Gogotsi, *Nat. Mater.* **2008**, 7, 845.

- [5] M. Winter, R. J. Brodd, *Chem. Rev.* **2004**, 104, 4245.
 [6] M. Zhi, C. Xiang, J. Li, M. Li, N. Wu, *Nanoscale* **2013**, 5, 72.
 [7] a) S. M. Richardson-Burns, J. L. Hendricks, D. C. Martin, *J. Neural Eng.* **2007**, 4, L6; b) M. C. Morvant, J. R. Reynolds, *Synth. Met.* **1998**, 92, 57.
 [8] B. E. Conway, *Electrochemical Supercapacitors, Scientific, Fundamentals and Technological Applications*, Plenum, New York **1999**.
 [9] Y. Xuan, M. Sandberg, M. Berggren, X. Crispin, *Org. Electron.* **2012**, 13, 632.
 [10] a) S. Jachle, M. Liebhaber, C. Gersmann, M. Mews, K. Jäger, S. Christiansen, K. Lips, *Sci. Rep.* **2017**, 7, 2170; b) D. Zielke, C. Niehaves, W. Lovenich, A. Elschner, M. Horteis, J. Schmidt, *Energy Procedia* **2015**, 77, 331; c) D. Zielke, A. Pazidis, F. Werner, J. Schmidt, *Sol. Energy Mater. Sol. Cells.* **2014**, 131, 110; d) K. A. Nagamatsu, S. Avasthi, G. Sahasrabudhe, G. Man, J. Jhaveri, A. H. Berg, J. Schwartz, A. Kahn, S. Wagner, J. C. Sturm, *Appl. Phys. Lett.* **2015**, 106, 123906 e) Y. Zhang, W. Cui, Y. Zhu, F. Zu, L. Liao, S.-T. Lee, B. Sun, *Energy Environ. Sci.* **2015**, 8, 297.
 [11] D. Aradilla, F. Estrany, F. Casellas, J. Iribarren, C. Alemán, *Org. Electron.* **2014**, 15, 40.
 [12] I. Ivanko, J. Svoboda, M. Lukesova, I. Sedenkova, E. Tomsik, *Macromolecules* **2020**, 53, 2464.
 [13] C. J. Yang, S. A. Jenekhe, *Chem. Mater.* **1991**, 3, 878.
 [14] E. J. Samuelsen, A. Monkman, L. A. Pettersson, L. E. Horsburgh, K. E. Aasmundtveit, S. Ferrer, *Synth. Met.* **2001**, 124, 393.
 [15] S. M. Blumenfeld, H. Fast, *Spectrochim. Acta, Part A* **1968**, 24, 1449.
 [16] R. J. Bartholomew, D. E. Irish, *J. Raman Spectrosc.* **1999**, 30, 325.
 [17] B. P. Sogo, M. Nakazaki, M. Calvin, *J. Chem. Phys.* **1957**, 26, 1343.
 [18] D. H. Reid, *Tetrahedron* **1958**, 3, 339.
 [19] N. Gospodinova, E. Tomsik, J. Romanova, *Chem. Pap.* **2013**, 67, 972.
 [20] A. Volkov, K. Wijeratne, E. Mittra, U. Ail, D. Zhao, K. Tybrandt, J. Andreasen, M. Berggren, X. Crispin, I. Zozoulenko, *Adv. Funct. Mater.* **2017**, 27, 1700329.
 [21] a) G. A. Snook, P. Kao, A. S. Best, *J. Power Sources* **2011**, 196, 1; b) L. L. Zhang, X. S. Zhao, *Chem. Soc. Rev.* **2009**, 38, 2520; c) A. M. Bryan, L. M. Santino, Y. Lu, S. Acharya, J. M. D'Arcy, *Chem. Mater.* **2016**, 28, 5989;
 [22] Z. Wang, J. Cheng, Q. Guan, H. Huang, Y. Li, J. Zhou, W. Ni, B. Wang, S. He, H. Peng, *Nano Energy* **2018**, 45, 210.
 [23] M. H. Gharahcheshmeh, M. T. Robinson, E. F. Gleason, K. K. Gleason, *Adv. Funct. Mater.* **2020**, 2008712.
 [24] D. Yuan, B. Li, J. Cheng, Q. Guan, Z. Wang, W. Ni, C. Li, H. Liu, B. Wang, *J. Mater. Chem.* **2016**, A 4, 11616.
 [25] G. Qu, J. Cheng, X. Li, D. Yuan, P. Chen, X. Chen, B. Wang, H. Peng, *Adv. Mater.* **2016**, 28, 3646.
 [26] L. Kou, T. Huang, B. Zheng, Y. Han, X. Zhao, K. Gopalsamy, H. Sun, C. Gao, *Nat. Commun.* **2014**, 5, 3754.
 [27] Y. Fu, X. Cai, H. Wu, Z. Lv, S. Hou, M. Peng, X. Yu, D. Zou, *Adv. Mater.* **2012**, 24, 5713.
 [28] Y. Jin, Z. Li, L. Qin, X. Liu, L. Mao, Y. Wang, F. Qin, Y. Liu, Y. Zhou, F. Zhang, *Adv. Mater. Interfaces* **2017**, 1700704.
 [29] M. Wojdyr, *J. Appl. Crystallogr.* **2010**, 43, 1126.

Appendix 6

Ivanko, I.; Lindfors, T.; Emanuelsson, R.; Sjodin, M. Conjugated redox polymer with poly(3,4-ethylenedioxythiophene) backbone and hydroquinone pendant groups as the solid contact in potassium-selective electrodes, *Sens. Actuators B Chem.* **329**, 129231(2021). IF = 7,460.



Contents lists available at ScienceDirect

Sensors and Actuators: B. Chemical

journal homepage: www.elsevier.com/locate/snb

Conjugated redox polymer with poly(3,4-ethylenedioxythiophene) backbone and hydroquinone pendant groups as the solid contact in potassium-selective electrodes

Iryna Ivanko^{a,b,1}, Tom Lindfors^{a,*}, Rikard Emanuelsson^c, Martin Sjödin^c^a Åbo Akademi University, Johan Gadolin Process Chemistry Centre (PCC), Laboratory of Molecular Science and Engineering (Analytical Chemistry Group), Biskopsgatan 8, 20500 Åbo, Finland^b Institute of Macromolecular Chemistry AS CR, Heyrovsky Sq. 2, 162 06 Prague 6, Czech Republic^c Nanotechnology and Functional Materials, Department of Materials Science and Engineering, The Ångström Laboratory, Uppsala University, Box 534, SE-751 21 Uppsala, Sweden

ARTICLE INFO

Keywords:

Conjugated redox polymer
 Poly(3,4-ethylenedioxythiophene)
 Hydroquinone
 Covalent attachment
 Standard potential
 Solid-contact ion-selective electrode

ABSTRACT

We have used for the first time a conjugated redox polymer with hydroquinone (HQ) pendant groups covalently attached to the poly(3,4-ethylenedioxythiophene) (PEDOT) backbone as the solid contact (SC) in plasticized poly(vinyl chloride) (PVC) based K⁺-selective electrodes (K-SCISE). Redox couples are one of the simplest ways to precisely adjust the standard potential (E°) of the SCISEs, but usually the initially high E° reproducibility is lost quite quickly due to leaching out of non-covalently bound redox molecules from the SCISE. In PEDOT-HQ, the covalently attached HQ groups prevent the leaching and simultaneously allow additional charge storage in PEDOT-HQ that is ca. 25–30 times higher than for unsubstituted PEDOT. Before the ion-selective membrane (ISM) deposition, we controlled the potential of the SC with high reproducibility (± 0.4 mV, $n = 5$) by pre-polarization in a mixture of acetonitrile containing potassium tetrakis(pentafluorophenyl)borate and perchloric acid as proton source. Pre-polarization of the SC close to the formal potential where the redox buffer capacity is highest gave the best potential reproducibility. However, after the ISM deposition, the K-SCISEs showed in the best case an E° reproducibility of ± 2.8 mV ($n = 5$). Chronopotentiometric measurements reveal that only a minor fraction of the very high redox capacitance of PEDOT-HQ can be utilized for the ion-to-electron transduction beneath the ISM. The influence of this shortcoming on the E° reproducibility of the SCISEs has been underestimated for most SC materials. Modification of the commonly used PVC-ISM formulations to allow faster ion transfer at the SC/ISM interface could be one way of overcoming the disadvantage.

1. Introduction

Potentiometry is a simple and non-destructive technique requiring only inexpensive instrumentation for measuring the electrical potential between the ion-selective electrode (ISE) and a reference electrode. The potential of the ISE is related to the ion activity of the sample solution through Nernst equation predicting a potential change of 59.2 mV/ n upon a tenfold increase/decrease of the ion activity. Today, ISE are available for ca. 100 different analytes that are mostly inorganic ions [1]. Since the introduction of electrically conducting polymer (ECP) based solid-contact ISEs (SCISE) in 1992 [2], the focus of the ISE

research has shifted from the liquid contact ISEs towards SCISEs. This is due to the replacement of the liquid contact with a solid ion-to-electron transducer (solid contact, SC) facilitating miniaturization of the SCISEs [3]. Recently, the possibility of fabricating SCISEs by printing [4] on flexible and stretchable substrates [5,6], and the possibility of incorporating SCISEs in wearable devices for health diagnostics and sports applications, and in disposable single-use test stripes has become the biggest driving force for the SCISE research [7,8].

Despite of many SC materials that have been recently reported [9–29], the ECPs [2,30–32], different type of carbon materials [29, 33–36] and redox couples [37–39] are currently the most popular SC

* Corresponding author.

E-mail addresses: ivanko@imc.cas.cz (I. Ivanko), tom.lindfors@abo.fi (T. Lindfors), rikard.emanuelsson@kemi.uu.se (R. Emanuelsson), martin.sjodin@angstrom.uu.se (M. Sjödin).¹ Iryna Ivanko is a PhD student at Charles University, Faculty of Science, Prague 2, 128 00 Czech Republic.<https://doi.org/10.1016/j.snb.2020.129231>

Received 24 September 2020; Received in revised form 12 November 2020; Accepted 13 November 2020

Available online 22 November 2020

0925-4005/© 2020 Elsevier B.V. All rights reserved.

materials. Ideally, the SC should have high double layer/redox capacitance [40], electrical conductivity and exchange currents at the substrate/SC and SC/ion-selective membrane (ISM) interfaces. In addition, it must be insensitive to light [41], oxygen and carbon dioxide [31,42], and have high hydrophobicity to prevent the aqueous layer formation [30,31,43], which results in potential instability of the SCISEs [44]. While several SC fulfill many of these criteria, the researchers are still looking for the perfect SC.

There is a big demand for remote controlled and autonomous SCISEs that are maintenance-, conditioning- and calibration-free, but their commercialization has been hampered by the insufficient reproducibility of the standard potential (E^0). Even with sophisticated and often time-consuming non-robust fabrication protocols, which are tailor-made for research laboratories, it is challenging to obtain an E^0 reproducibility ≤ 3.0 mV within the same batch of SCISEs [30]. It is even more challenging to achieve high E^0 reproducibility between different electrode batches and especially for SCISEs prepared with identical preparation protocols at different research laboratories [30]. The SC plays an important role in achieving high E^0 reproducibility as it functions as an ion-to-electron transducer between the electrically conducting electrode substrate and the ionically conducting ISM. The phase boundary potential at the electrode substrate/SC and SC/ISM interfaces must be constant and reproducible to obtain SCISEs with high E^0 reproducibility. Poor reproducibility is often caused by sluggish and insufficient ion-/electron transfer processes at these interfaces, diffusion of oxygen and carbon dioxide through the ISM influencing the redox state and pH of the SC [42], and partial dissolution of the SC into the ISM.

Incorporation of redox couples in the SCISEs is one of the simplest ways of improving their potential reproducibility [37,38] as the E^0 of the SCISE can be easily tuned by adjusting the $a_{\text{ox}}/a_{\text{red}}$ ratio of the redox couple [9]. However, the initially very good E^0 reproducibility is often (± 0.7 mV, $n = 5$ [38]) deteriorating rather quickly because non-covalently bound redox compounds easily leach out to the sample solution. In contrast to redox couples, the ECPs have a broad distribution of energy levels due to polymer segments with different conjugation length, making it challenging to fabricate SCISEs with satisfactory E^0 reproducibility. Therefore, the SC must be pre-polarized at a potential located in the conducting regime to improve the potential reproducibility of the ECP based SCISEs [30,31,41,43].

Conjugated redox polymers (CRP) are a relatively new class of ECPs in which redox groups are covalently attached via linkers to the ECP backbone, thus preventing them from leaving the backbone [45,46]. Especially the modification of polypyrrole (PPy) [47–55] and PEDOT [56–64] with redox pendant groups have received much attention. One of the most successful approaches is the covalent modification of PEDOT

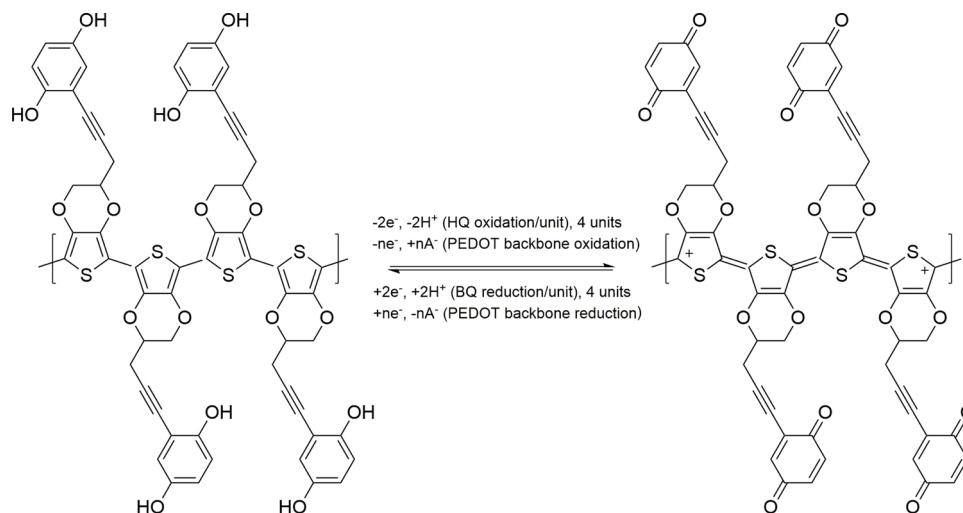
with hydroquinone (HQ) pendant groups (Scheme 1) [61,62]. In contrast to PPy, the stiffer PEDOT backbone prevents it from twisting upon the reversible HQ to benzoquinone (BQ) redox conversion, the twisting has been shown to decrease the number of charge carriers in PPy and therefore decreasing its electrical conductivity [50,51]. PEDOT-HQ has excellent redox matching with the HQ/BQ redox conversion occurring in the potential region where PEDOT is in its electrically conducting form, which is necessary for obtaining a synergistic effect between the polymer backbone providing fast electron transport through the PEDOT matrix and the HQ groups offering a large charge storage capacity [61]. Estimations show that 12 % of the capacitance of PEDOT-HQ originates from its backbone and 88 % from the HQ pendant groups [61]. Most importantly, the HQ pendant groups provide PEDOT-HQ with a well-defined redox reaction that has been explored in this work. At neutral pH, where the SCISEs are usually used, the oxygen transported by water to the SC/ISM interface cannot oxidize HQ to BQ due to the lower standard potential of the oxygen half-cell [39,65], and therefore minimizing the risk for potential instability caused by changes in the $a_{\text{HQ}}/a_{\text{BQ}}$ ratio.

To the best of our knowledge, we are not aware of any similar works where CRPs have been applied as ion-to-electron transducers in SCISEs. We have used PEDOT-HQ as a model compound to study its influence on the initial potential stability and E^0 reproducibility of K^+ -selective SCISEs (K-SCISE). Prior to the ISM deposition, the potential of the PEDOT-HQ solid contact could be controlled very precisely (± 0.4 mV, $n = 5$) by pre-polarization in a mixture of acetonitrile (MeCN) containing 0.01 M potassium tetrakis(pentafluorophenyl)borate (KTFAB) and perchloric acid (HClO_4) acting as a proton source for the HQ groups. However, the E^0 deviation of the K-SCISE increased to ± 2.8 mV ($n = 5$) indicating that the ISM deposition influences the potential reproducibility [31]. The K-SCISEs prepared with PEDOT-HQ pre-polarized in 0.01 M KTFAB-MeCN without HClO_4 had excellent initial potential stability with a potential drift of only ca. 0.1 mV h^{-1} during 24 h. PEDOT-HQ solid contacts and the corresponding K-SCISEs have been characterized with the state-of-the-art techniques.

2. Material and methods

2.1. Chemicals

PEDOT-HQ was custom-synthesized according to the recently published procedure [61]. High-molecular weight PVC (HMW PVC), bis (2-ethylhexyl) sebacate (DOS), potassium ionophore I (valinomycin), and tetrahydrofuran (THF), and anhydrous acetonitrile (MeCN) (99.5 %) were purchased from Sigma-Aldrich, and potassium tetrakis



Scheme 1. Oxidation and reduction of the PEDOT backbone and the HQ/BQ pendant groups of the PEDOT-HQ film. A^- refers to the TFAB^- anions.

(pentafluorophenyl)borate (KTFAB) (97 %) from Alfa Aesar. Buffer solution for the electrochemical characterization of the PEDOT-HQ solid contact were prepared from sodium nitrate, sodium acetate, monobasic sodium phosphate, boric acid (all from Sigma-Aldrich) and the pH was adjusted to 0 and 5.5 with HNO₃. The chloride salts (K⁺, Na⁺, Ca²⁺, Mg²⁺, NH₄⁺, Li⁺, H⁺) used for the potentiometric and impedance measurements had a purity > 99 %. Perchloric acid (70 v/v%) was received from Sigma-Aldrich. The aqueous solutions used in this work were prepared from deionized water (DIW) that had a resistivity of 17 MΩ cm.

2.2. Characterization of the K-SCISE substrates and electropolymerization of EDOT-HQ

The glassy carbon (GC) electrodes incorporated in insulating poly-ether ether ketone (PEEK) bodies had a diameter of 1.6 mm (BioLogic) and were used as electrode substrates for the K-SCISEs. The electrochemical response of the GC electrodes ($n = 5$) were measured in 2 mM K₄Fe(CN)₆ with 1.0 M KNO₃ as the supporting electrolyte prior to the electropolymerization of the solid contact on top of them. Prior to the electropolymerization, the WE was polished with a 0.05 μm alumina suspension, rinsed thoroughly with ethanol and DIW followed by ultrasonication for 5 min in DIW, and finally rinsed again with ethanol and DIW. The electropolymerization of 5 mM EDOT-HQ in a 0.01 M KTFAB-MeCN solution was performed in a three-electrode cell (3 mL) with an Autolab potentiostat by cycling the potential 10 times between -0.3 and 1.4 V with a scan rate of 50 mV s⁻¹. The GC disc electrodes, a Pt wire and Ag wire immersed in 0.01 M AgNO₃ and 0.1 M TBAPF₆ dissolved in MeCN (vs. Ag/Ag⁺) served as working (WE), counter (CE) and reference electrode (RE), respectively. Due to the limited amount of the EDOT-HQ monomer, we performed five electropolymerizations from the same monomer solution and purged the solution with N₂ gas that was saturated with MeCN for 5 min prior to each electropolymerization. The solution was blanketed with N₂ during the electropolymerization to protect it from oxygen (air). After the polymerization, we washed the PEDOT-HQ electrodes with MeCN and stored them under inert argon gas.

2.3. Characterization of the PEDOT-HQ solid contact

The PEDOT-HQ films were characterized with cyclic voltammetry (CV; $\nu = 5, 10, 20, 50$ and 100 mV/s) in 1.0 M NaNO₃ buffered to pH 0 and 5.5 with sodium acetate, monobasic sodium phosphate and boric acid (0.1 M each, pH was adjusted with concentrated HNO₃). All measurements were performed using the three-electrode setup at an ambient temperature with Ag/AgCl/3 M KCl and a Pt wire as the RE and CE, respectively. We studied the surface morphology of the PEDOT-HQ solid contacts with scanning electron microscopy by using the LEO1530 Gemini FEGSEM instrument. The light sensitivity measurements of the PEDOT-HQ film were carried out in 1.0 M KNO₃ by exposing them to room light, darkness and to cold light (Leica CLS 150XE light source, $>1.6 \times 10^5$ lx) for 30 min each in this sequence, and simultaneously recording the potential of the film electrodes [41]. To determine the redox capacitance of PEDOT-HQ, the electrochemical impedance spectra were measured in buffered aqueous solutions at pH 0 and 5.5 (see above) in the frequency range from 0.01 Hz to 10 kHz at the open circuit potential (vs. Ag/AgCl/3 M KCl) with $\Delta E_{ac} = 5$ mV. The water contact angles (WCA) of PEDOT-HQ was measured for films that had been pre-polarized for 2 min at 0.0 V and 0.55 V in 1.0 M KNO₃ (pH 5.5), and dried with N₂ gas after the pre-polarization. We applied a water droplet of 2 μL on the PEDOT-HQ surface and recorded images of the droplet with the Dyno-Lite USB digital microscope. The WCAs were estimated from the images with the Inkscape 0.92.3 software. The potentiometric ionic response of the PEDOT-HQ film was determined in 10⁻¹-10⁻⁴ M KCl and 10⁻²-10⁻⁵ M KTFAB (dissolved in MeCN).

2.4. Pre-polarization of the PEDOT-HQ solid contact and the ISM deposition

Prior to the ISM deposition by drop casting, we pre-polarized simultaneously five identically prepared PEDOT-HQ solid contacts for 5 min at 0.25 V either in a 9:1 (v/v%) mixture of 0.01 M KTFAB-MeCN and 0.2 M HClO₄ (acting as a proton source for the HQ groups) or in 0.01 M KTFAB-MeCN without HClO₄. This was done to improve the E^o reproducibility of the K-SCISEs [30,31,41,43]. After the pre-polarization, the PEDOT-HQ solid contacts were dried under N₂ atmosphere for 30 min before drop casting the ISMs on top of the SCs. The ISM had the following composition (wt%): 32.9 % HMW PVC, 65.7 % DOS, 1.06 % valinomycin and 0.34 % KTFAB. All components were dissolved in 1 mL THF to produce a solution with a dry weight of 20 %. The solution was first vortexed for 3 min and was then left on gentle stirring on a shaking table for 24 h to dissolve the ISM components in THF. Finally, 40 μL of the K⁺-selective ISM cocktail was drop cast on the PEDOT-HQ in two consecutive steps (2 × 20 μL). After drying overnight under THF atmosphere, the PVC-ISM had a thickness of ca. 220–240 μm.

2.5. Characterization of the K-SCISEs

We used a 16-channel high input impedance voltmeter with the input impedance of 10¹⁵ Ω, (Lawson Laboratories, Malvern, PA, USA) in all potentiometric measurements. The initial potential stabilities of the K-SCISEs were determined in 0.01 M KCl for 24 h. The K-SCISEs were calibrated from 10⁻¹ to 10⁻⁹ M KCl, and the potential readings at each concentration were taken after 5 min in quiescent solutions (stirring during the first 3 min). The potentiometric aqueous layer test was done with fully conditioned SCISEs by changing the solution from 0.1 M KCl (3 h) to 0.1 M NaCl (24 h) and then back to 0.1 M KCl (24 h). The gas sensitivity of the K-SCISE was determined by measuring the electrode potential while purging a 0.1 M KCl solution with pure gases in the following sequence: N₂ (30 min), O₂ (30 min), N₂ (ca. 35 min), CO₂ (50 min), N₂ (45 min). We determined the potentiometric selectivity coefficients of the K-SCISEs with the separate solution method in 0.1, 0.01 and 0.001 M chloride salts of K⁺, and the interfering ions Li⁺, Na⁺, H⁺, NH₄⁺, Ca²⁺ and Mg²⁺. We used Ag/AgCl/3 M KCl//1 M LiOAc as the RE in all these measurements described above. The chronopotentiograms were recorded with an Autolab potentiostat in 0.1 M KCl by applying first a current of 10⁻⁹ A for 60 s and -10⁻⁹ A for the next 60 s. The impedance spectra of the K-SCISEs were measured in the frequency range of 0.01 Hz - 25 kHz at the open circuit potential with $\Delta E_{ac} = 0.1$ V. Ag/AgCl/3 M KCl was used as the RE in the two last measurements.

3. Results and discussion

3.1. PEDOT-HQ solid contact

Surface functional groups (carbonyl, carboxyl, and hydroxyl) can affect the electron transfer property of the GC electrode substrates used for the K-SCISEs [66]. Therefore, we measured the CVs of the GC electrodes in 2 mM K₄Fe(CN)₆ with 1.0 M KNO₃ as the supporting electrolyte to study their reversibility. The CVs of four identical electrodes in Figure S1 reveal that the electron transfer is reversible with a peak separation of 69.4 ± 2.6 mV, which is close to the theoretically predicted value of 59.2 mV (25 °C) for a one electron redox process (Table S1). Figure S1 shows also that the anodic and cathodic peak potentials ($E_{pa} = 300.4 \pm 0.1$ mV and $E_{pc} = 231.0 \pm 2.5$ mV) had high reproducibility contributing to a high E^o reproducibility of the K-SCISEs.

The electropolymerization of 5 mM EDOT-HQ was carried out by cyclic voltammetry in a MeCN solution containing 0.01 M KTFAB with high fluorine content to enhance the hydrophobicity of the PEDOT-HQ solid contact (Figure S2). Figure S3 shows the CVs recorded during the electropolymerization of three identical PEDOT-HQ films from the same

monomer solution. Almost the same currents that were observed for all CVs reveal that the electropolymerization is reproducible. The monomer oxidation peak at 1322 ± 12 mV ($n = 3$; 10th cycle) indicates that the PEDOT-HQ film grows in the potential interval of ca. 1.1–1.4 V (vs. Ag/Ag⁺), while the oxidation/reduction of the PEDOT backbone and the HQ pendant groups (Scheme 1) occur in the interval of -0.3–1.1 V. As the PEDOT backbone is in its electrically conducting form already at low potentials, it provides a good redox match for the HQ/BQ redox conversion that has the oxidation and reduction peak potentials at 1032 ± 16 mV and 188 ± 23 mV, respectively. The SEM image in Figure S4 reveals that the surface of the PEDOT-HQ solid contact prepared in the presence of the TFAB⁻ anions is rather smooth and compact with some larger sections sticking out from the surface. We expected that a compact surface is beneficial for SCs because it prevents the pores of the SC from being filled with water diffusing through the ISM. It has been shown that the diffusion of water through the ISM promotes the water layer or pool formation at the SC/PVC-ISM interface [67], which causes response instability of the SCISEs [44].

Scheme 1 shows the reversible oxidation and reduction of the PEDOT backbone and the HQ pendant groups. The oxidation of the PEDOT backbone that occurs first at lower potentials results in the formation of charge carriers that make the polymer backbone electrically conducting. To fulfill the electroneutrality condition of PEDOT, the oxidation of the backbone is accompanied by the insertion of charge compensating TFAB⁻ anions, which are also present in the ISM to stabilize the phase boundary potential at the SC/ISM interface. The high charge storage capacity of PEDOT-HQ is due to the HQ groups that can store two electrons in every repeating EDOT unit of the polymer (Scheme 1), in comparison to only ca. 0.4–0.6 electrons for every EDOT unit in the polymer backbone [68] depending on its oxidation degree and nature of the charge compensating counterion.

In buffered aqueous solutions, the HQ/BQ redox reaction is a $2e^-2H^+$ reaction with two coupled electron-proton transfer reactions close to each other in formal potentials (E^0), which usually gives one overlapping oxidation/reduction peak in the CV of HQ/BQ [69]. Fig. 1a shows therefore only one broader oxidation/reduction peak in the CV of PEDOT-HQ measured at pH 0. In PEDOT-HQ, the two step oxidation process of HQ to BQ has been proposed [62] to proceed first via electron transfer from HQ (denoted as H₂Q in [62]) to the PEDOT backbone forming semiquinone radicals (H₂SQ^{•+}), which are then deprotonated to neutral HSQ. In the second step, HSQ is further oxidized either via the HQ^{•+} or SQ⁻ intermediates to the fully oxidized benzoquinone. Due to the very high currents of the HQ/BQ redox conversion, the much smaller oxidation/reduction currents of the PEDOT backbone cannot clearly be distinguished in Fig. 1a. However, the difference in the redox currents of PEDOT-HQ and unsubstituted PEDOT at pH 0 is shown in Fig. 2 illustrating the huge influence of the HQ pendant groups on the redox currents of PEDOT-HQ.

Fig. 1a reveals that the redox peak separation (ΔE_p) of the PEDOT-HQ film measured with the scan rates of 5 mV s^{-1} was 31.0 mV, which is slightly higher than expected for a surface confined reaction (0 mV). The HQ/BQ peak separation increased slightly at higher scan rates ($\Delta E_p = 98.9$ mV at 100 mV s^{-1}) indicating that the electron transfer becomes kinetically somewhat more sluggish. However, the formal potential (E^0) of the HQ/BQ redox reaction varies only between 505.5–514.2 mV and is practically independent of the scan rate, which further confirms the high reversibility of the HQ/BQ conversion in PEDOT-HQ electropolymerized in the presence of KTFAB. Since the SCISEs are usually used in neutral or slightly acidic solutions, we have also studied the reversibility of the HQ/BQ redox conversion at pH 5.5. We assume that the pH at the SC/ISM interface in the K-SCISEs is ca. 5.5 because water that is saturated with CO₂ can easily diffuse through the PVC-ISM to the SC [70]. In Fig. 1b, the CVs of PEDOT-HQ measured at pH 5.5 show lower redox currents and higher peak separation ($\nu = 5\text{--}20 \text{ mV s}^{-1}$) than at pH 0. Since two protons are involved in the HQ/BQ redox reaction, an increase in pH should shift the oxidation/reduction

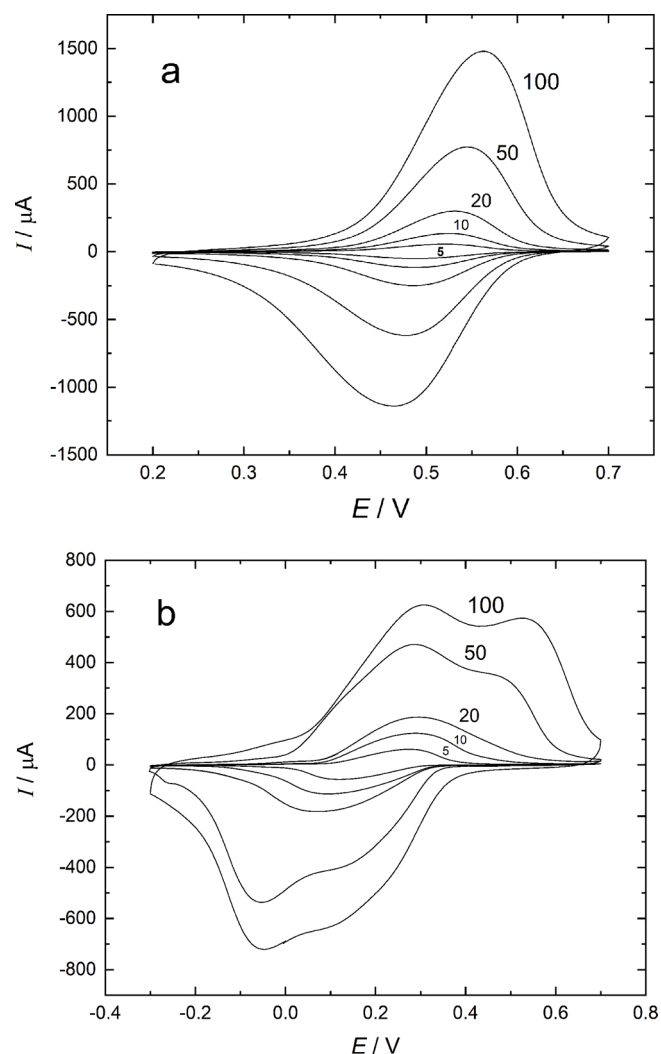


Fig. 1. Cyclic voltammograms of the PEDOT-HQ film recorded in aqueous buffer solutions with (a) pH 0 and (b) pH 5.5 at the scan rates of 5, 10, 20, 50 and 100 mV s^{-1} . RE: Ag/AgCl/3 M KCl.

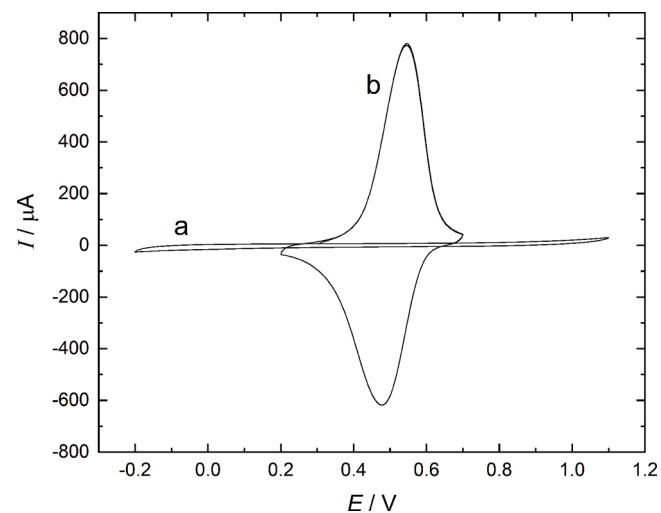


Fig. 2. Cyclic voltammograms of (a) the unsubstituted PEDOT film without HQ pendant groups and (b) the PEDOT-HQ film measured in aqueous buffer solution at pH 0 with $\nu = 50 \text{ mV/s}$. RE: Ag/AgCl/3 M KCl.

peaks to lower potentials with 59.2 mV/one pH unit (at 25 °C). Indeed, the E° shifts to a lower potential with 325.5 mV ($\nu = 20 \text{ mV s}^{-1}$) when pH increased from 0 to 5.5, which is in perfect accordance with the theoretical prediction of 325.6 mV. The higher peak separation at pH 5.5 indicates that the electron transfer kinetics becomes more sluggish. This is in agreement with the theory for proton coupled redox reactions where the apparent standard rate constant (k_s) is expected to reach a minimum at a pH midway between the pK_a of the oxidized and reduced species [71]. At the higher scan rates (50 and 100 mV s^{-1}), the HQ/BQ redox peak splits into two peaks indicating that the second redox reaction is kinetically slower than the first due to the radical disproportionation despite of its higher driving force. This result in a higher difference of the E° values associated with the two processes involved in the $2e^- 2\text{H}^+$ oxidation/reduction. Despite of the kinetically slower redox conversion at pH 5.5, the ratio of the integrated oxidation peak areas at pH 5.5 to pH 0 is ca. 1.3 and ca. 24.9 between PEDOT-HQ at pH 5.5 and unsubstituted PEDOT (Fig. 2a), showing that PEDOT-HQ is most suitable as an ion-to-electron transduction in SCISEs.

To determine the redox capacitance that should be high for the SC, we measured the electrochemical impedance spectra of the PEDOT-HQ films at pH 0 ($E_{\text{dc}} = 0.30, 0.55$ and 0.70 V) and pH 5.5 ($E_{\text{dc}} = 0.00, 0.30$ and 0.55 V). The measurements were performed at the potentials given in the parenthesis corresponding to DC potentials before the HQ/BQ oxidation peak, at the peak and after the peak (cp. Fig. 1a and b; $\nu = 20 \text{ mV s}^{-1}$). The redox capacitance of the films was estimated from the low frequency part of the impedance spectra shown in Figure S5a and S5b by assuming that they have an almost capacitor-like behavior. The capacitances were determined from the $|-Z''|$ vs. f^{-1} relationship by line fitting ($y = ax$) and calculating the capacitance from the slope (a) of the straight line ($C = (2\pi a)^{-1}$) [72]. The estimated redox capacitances of PEDOT-HQ were 43 (0.30 V), 489 (0.55 V) and 18 mF cm^{-2} (0.70 V) at pH 0, and 66 (0.00 V), 123 (0.30 V) and 15 mF cm^{-2} (0.55 V) at pH 5.5. For both pH 0 and 5.5, we obtained the highest redox capacitances when we measured the impedance spectra at a DC potential corresponding to the current maximum of the HQ/BQ oxidation peak. At these potentials, the applied AC potential (ΔE_{ac}) is able to induce an oxidation/reduction of the pendant HQ groups that is reflected as a higher redox capacitance of PEDOT-HQ. This is not possible at the lowest potentials where the amplitude of the AC potential (5 mV) is not enough to oxidize HQ to BQ to any greater extent. At the highest DC potential (0.55 V), the impedance spectrum measured at pH 5.5 shows almost a vertical capacitor-like behavior indicating that the HQ oxidation is completed and the applied AC potential is too low to reduce BQ back to HQ. Hence, we can assume that at 0.55 V only the PEDOT backbone contributes to the estimated redox capacitance of 15 mF cm^{-2} .

Ideally, the conducting polymer SCs should not respond to changes in the illumination conditions. Therefore, we measured the potential response of the PEDOT-HQ solid contact when it was exposed to room light, darkness and intense cold light (Fig. 3). No light sensitivity was observed to room light and darkness, but a very minor response ($< 2 \text{ mV}$) to intense cold light ($1.6 \times 10^5 \text{ lux}$). However, the SCISEs are never exposed to such extreme conditions and we can conclude that PEDOT-HQ is in practice insensitive to light.

3.2. K^+ -selective SCISEs

The pre-polarization of the SC prior to the ISM deposition on top of it has become a common practice to improve the potential reproducibility of the ECP based SCISEs [29–31,41,43]. This is usually done in organic electrolyte solutions to avoid exposing the SC to water that can cause potential drift of the SCISE. Therefore, we did the pre-polarization first in 0.01 M KTFAB-MeCN solution (Figure S6). The CV of PEDOT-HQ shows only one broad HQ oxidation peak at $E > 0.5 \text{ V}$ during the first potential cycle, but no reduction peak. During the HQ oxidation, the protons are lost by diffusion to the bulk of the MeCN solution and due to the absence of protons in the aprotic MeCN, BQ cannot be reduced back

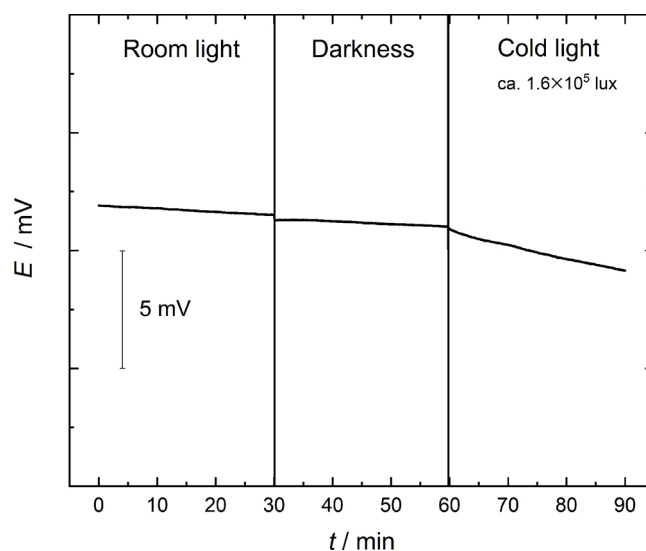


Fig. 3. Light sensitivity of the PEDOT-HQ film measured in 1.0 M KNO_3 at pH 5.5 by exposing it to room light (30 min), darkness (30 min) and intense cold light (30 min; ca. $1.6 \times 10^5 \text{ lux}$). Before starting the measurement, the electrode was polarized to its fully oxidized state at 0.55 V in the same electrolyte solution. RE: Ag/AgCl/3 M KCl.

to HQ via the $2e^- 2\text{H}^+$ reduction process. In aprotic solvents such as MeCN, the reduction of benzoquinone is known to proceed instead via a reversible two-electron process through the Q^- intermediate to the fully reduced Q^{2-} (Scheme S1) [69]. However, in the absence of protons that stabilize the reduced form of PEDOT-HQ, the formal potential is considerably lower than in acidic solutions [73] and thus the redox reaction occurs usually at potentials where the PEDOT backbone is electrically non-conducting. Therefore, the redox peaks cannot be observed in the CV. We found that it was possible to restore the oxidation and reduction peaks of HQ/BQ in the CV by adding 0.2 M HClO_4 as a proton source ($\text{pK}_a = 2.1$ in MeCN [74]) to the 0.01 M KTFAB-MeCN solution (Figure S6). In a 10:1 (v/v%) mixture of 0.01 M KTFAB-MeCN and 0.2 M HClO_4 , the CVs showed high redox currents with a E° of ca. 228 mV for the HQ/BQ redox conversion of PEDOT-HQ. We have used therefore a 9:1 mixture of 0.01 M KTFAB-MeCN and 0.2 M HClO_4 (10 v/v%) for the pre-polarization of the PEDOT-HQ solid contact to 0.25 V prior to the ISM deposition by drop casting. In addition, we have pre-polarized the SC to the same potential in only 0.01 M KTFAB-MeCN (without HClO_4) to study how the absence of HClO_4 influences the initial potential stability and E° reproducibility of the K-SCISEs.

We pre-polarized simultaneously five identical PEDOT-HQ solid contacts for 5 min at 0.10, 0.15, 0.20, 0.25 and 0.30 V (vs. Ag/Ag $^+$). After the pre-polarization, we measured their open circuit potentials for 5 min in the pre-polarization solutions to evaluate the robustness of the pre-polarization. Fig. 4 shows that the PEDOT-HQ films pre-polarized in the 9:1 solution mixture at 0.20 V and 0.25 V had open circuit potentials with the lowest standard deviation (SD) of only 0.6 mV and 0.4 mV, respectively. This confirms that we can precisely control the potential of the PEDOT-HQ solid contact in a robust way with pre-polarization. The pre-polarization potentials are very close to the formal potential of the HQ/BQ pendant groups in the 9:1 mixture (0.228 V) where $a_{\text{HQ}}/a_{\text{BQ}} = 1$, which should give the best redox buffering capacity counteracting processes influencing the electrode potential. The PEDOT-HQ films pre-polarized only in 0.01 M KTFAB-MeCN (without HClO_4) had also the lowest SD of the measured potentials at 0.20 V and 0.25 V (2.6 mV and 2.3 mV), but in general, the potential reproducibility was worse (2.3–8.0 mV) compared to pre-polarization in the 9:1 mixture. We believe that the lower reproducibility is due to the difficulty in adjusting the redox state of the HQ pendant groups in the absence of protons in an aprotic solvent.

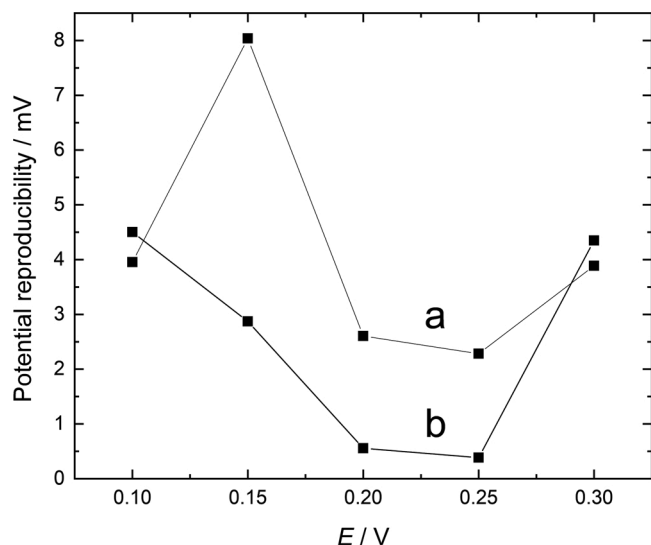


Fig. 4. Potential reproducibility (given as SD) of the PEDOT-HQ solid contacts ($n = 5$) measured at the open circuit potential in (a) 0.01 M KTFAB-MeCN and (b) a 9:1 mixture (v/v %) of 0.01 M KTFAB-MeCN and 0.2 M HClO_4 , after pre-polarization for 5 min at 0.10, 0.15, 0.20, 0.25 and 0.30 V (vs. Ag/Ag^+) in the same solutions.

The initial stability of the K-SCISEs measured for 24 h in 0.01 M KCl is shown in Fig. 5. The K-SCISEs prepared with the PEDOT-HQ solid contact pre-polarized at 0.25 V in the 9:1 mixture of 0.01 M KTFAB-MeCN and 0.2 M HClO_4 (K-SCISE_{mix}; curve b) had a relatively high initial potential drift for ca. 40 min when the electrodes were for the first time contacted with 0.01 M KCl. After that, the potentials drifted slowly towards lower potentials with a speed of -2.8 mV h^{-1} . The initially rather high potential irreproducibility of $\pm 16.0 \text{ mV}$ ($n = 5$) decreased to $\pm 9.3 \text{ mV}$ in the end of the initial potential stability test. For the K-SCISEs that had a PEDOT-HQ solid contact pre-polarized at 0.25 V in only 0.01 M KTFAB-MeCN (K-SCISE_{org}; curve a), we observed a potential drift of ca. 4–5 mV during the first 30 min, but after that a very low drift of 0.1 mV h^{-1} during the rest of the test period of 24 h, similar to the liquid contact ISEs. However, the electrodes showed a low initial potential reproducibility of $\pm 21.2 \text{ mV}$ ($n = 5$) that was practically unchanged after 24 h in 0.01 M KCl ($\pm 19.0 \text{ mV}$). The relatively high potential irreproducibility of both K-SCISE types indicate that the ISM deposition

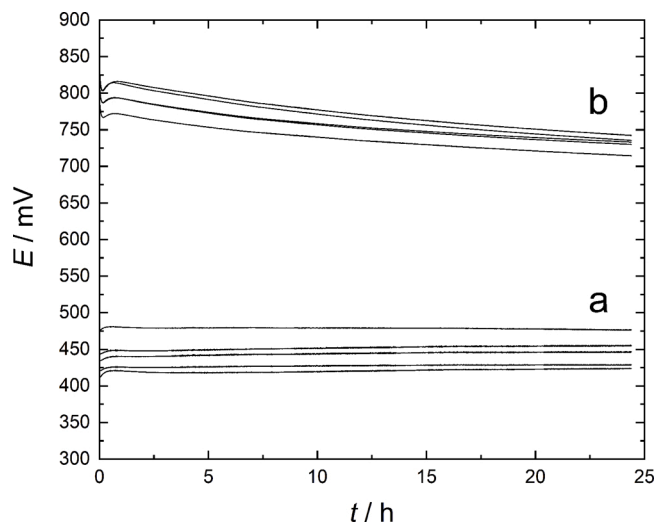


Fig. 5. Initial potential stability and reproducibility of the (a) K-SCISE_{org} and (b) K-SCISE_{mix} ($n = 5$) measured in 0.01 M KCl for 24 h. RE: $\text{Ag}/\text{AgCl}/3 \text{ M KCl}/1.0 \text{ M LiOAc}$.

process affects negatively the initially very good potential reproducibility of the PEDOT-HQ solid contacts ($\pm 0.4 \text{ mV}$ and $\pm 2.3 \text{ mV}$). We have recently observed the same for K-SCISEs that have a SC consisting of highly hydrophobic fluorinated PEDOT (PEDOT-F) [31]. In all cases when we did the pre-polarization of the SC in the aqueous-organic solvent mixture, the initial potential drift of the K-SCISE_{mix} was higher than for the K-SCISE_{org}. It may indicate that there is a correlation between the presence of water in the pre-polarization solution and the higher initial potential drift of the SCISEs. In addition, it is likely that the perchlorate anions will function as secondary doping ions for the PEDOT backbone during the pre-polarization in the 9:1 mixture. We speculate that this may contribute to time-dependent changes (instability) in the phase boundary potential at the SC/ISM interface, which is reflected as the slow drift (-2.8 mV h^{-1}) during the initial potential stability test in Fig. 5 (curve b). Potentiometric measurements in $10^{-5} - 10^{-2} \text{ M}$ KTFAB dissolved in MeCN showed that the PEDOT-HQ solid contact had an anionic response of ca. -50 mV/decade indicating that it primarily exchanges anions. Therefore, the anion exchange of the SC must be accompanied by a release/uptake TFAB⁻ anions at the SC/ISM interface to compensate for any oxidation and reduction changes occurring in the backbone of the PEDOT-HQ solid contact during the potentiometric measurements.

The water contact angles (WCA) of the PEDOT-HQ films pre-polarized at 0.0 V and 0.55 V at pH 5.5 were ca. 70° and 60° , respectively, showing that the polymer backbone interacts with water. Compared to PEDOT-F with a WCA of 133° [31], the WCA reveals that PEDOT-HQ is more hydrophilic, which is most likely due to the hydrophilicity of the HQ pendant groups. On the other hand, the very high initial potential stability of the K-SCISE_{org} (with absence of water in the pre-polarization solution) indicate that the lower hydrophobicity of the PEDOT-HQ solid contact, incorporating the hydrophobic TFAB⁻ anions, does not have a negative impact on the potential stability of the K-SCISEs. However, despite of the intensive research activity for almost three decades [1], more research is still needed to reach a general understanding and consensus about factors governing the potential stability and reproducibility of the SCISEs.

In Fig. 6, the calibration curves of the K-SCISEs measured in $10^{-9} - 10^{-1} \text{ M}$ KCl after the initial potential stability test show that both types of K-SCISEs had a highly reproducible Nernstian slope (60.8 ± 0.1 and $60.9 \pm 0.1 \text{ mV pK}^{-1}$, $n = 5$) and a detection limit of ca. $2 \times 10^{-7} \text{ M}$, which is typical for PVC based SCISEs. The E° of the electrodes were determined from the calibration curves by extrapolation of the linear potential response to $a_{\text{K}^+} = 1$ (i.e. $\log a_{\text{K}^+} = 0$). Fig. 6 reveals that the K-SCISE_{org} had a high E° irreproducibility of $\pm 18.6 \text{ mV}$ ($n = 5$), which did not decrease

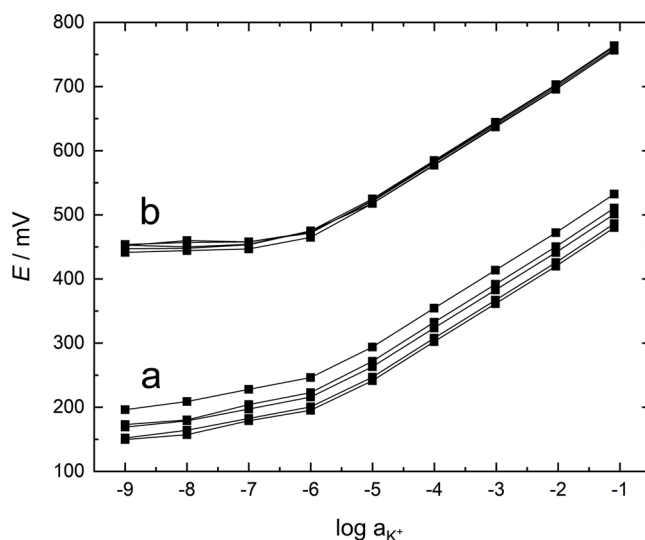


Fig. 6. Potentiometric responses of the (a) K-SCISE_{org} and (b) K-SCISE_{mix} measured in $10^{-9} - 10^{-1} \text{ M}$ KCl ($n = 5$). RE: $\text{Ag}/\text{AgCl}/3 \text{ M KCl}/1.0 \text{ M LiOAc}$.

from the initial potential stability test in Fig. 5 (curve a), whereas the K-SCISE_{mix} showed a high E° reproducibility of ± 2.8 mV ($n = 5$) that is much lower than in Fig. 5 (curve b).

Although the reason for the converging potentials of K-SCISE_{mix} is still unknown, it is probably due to the presence of HClO₄ and/or water in the pre-polarization solution of the PEDOT-HQ solid contact. Because all K-SCISEs had the same ISM thickness of ca. 220–240 μm , it is reasonable to assume that the same amount of water will be present at the SC/ISM interface in both K-SCISE types after being in contact with 0.01 M KCl for 24 h (because of diffusion of water through the ISM) [67]. Indeed, the aqueous layer test shown in Fig. 7 confirms the presence of water at the inner interfaces of both K-SCISE types (only K-SCISE_{mix} shown). Dissolved O₂ and CO₂ are transported to the SC with water, but the gas sensitivity test in Fig. 8 demonstrates that the K-SCISEs were practically insensitive to these gases and we can therefore exclude that they are causing the potential drift observed for the K-SCISE_{mix} in Fig. 5 (curve b). We want to stress that we did not study the long-term potential (E°) stability and reproducibility in this work. However, the convergence of the potential of the K-SCISE_{mix} during the first 2 days they were in contact with KCl solution (Figs. 5 and 6) indicates that the electrodes short-term potential reproducibility improves by time, but also that the HQ pendant groups stay covalently attached to the PEDOT backbone. As this paper focuses largely on fundamental aspects of the PEDOT-HQ as a new SC material for K-SCISEs, a separate study should be devoted to the optimization of the long-term potential stability and reproducibility of the K-SCISEs.

The logarithmic selectivity coefficients of the K-SCISEs for the most relevant interfering ions shown in Table S2 were between -4.2 to -6.7 (except NH₄⁺, -1.7), which is in rather good accordance with K-SCISEs having the same ISM composition [30,31] confirming the high selectivity of the ISM. Further characterization of the ISM with impedance spectroscopy revealed that its bulk resistance (R_b) varied between ca. 4–7 M Ω (determined from the diameter of the semicircle). However, the low frequency (capacitive) tail in the impedance spectrum in Figure S7 indicates some sluggishness in the electron transfer at the SC/electrode substrate interface, which probably contributes to the peak splitting and higher peak separation of the HQ/BQ redox peaks observed in the CVs measured at pH 5.5 (Fig. 1b). We estimated the redox capacitance of the PEDOT-HQ solid contact buried beneath the PVC-ISM from the chronopotentiograms shown in Figure S8. The results reveal that the K-SCISE_{mix} and K-SCISE_{org} had a redox capacitance of 1.1 and 1.5 mF cm⁻², respectively, showing that only a minor fraction of the initially very high redox capacitance of the PEDOT-HQ film can be utilized

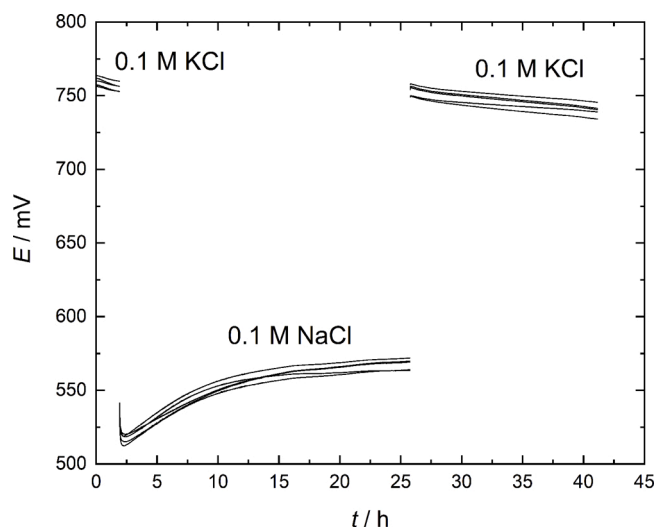


Fig. 7. Potentiometric aqueous layer test performed with the K-SCISE_{mix} ($n = 5$). RE: Ag/AgCl/3 M KCl/1.0 M LiOAc.

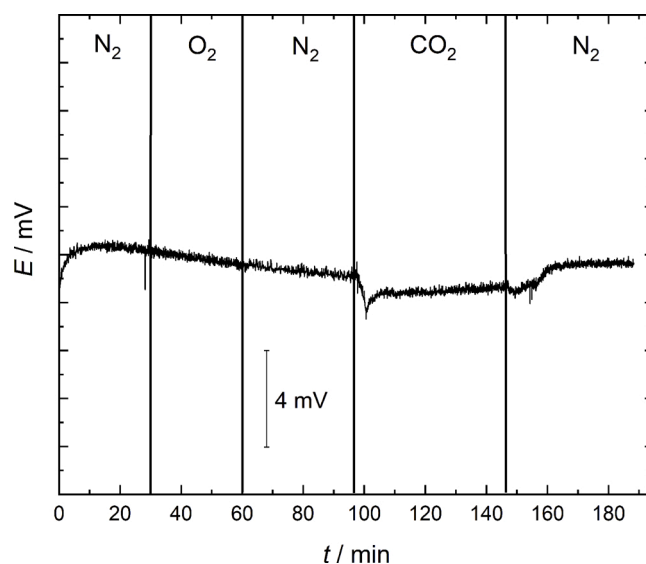


Fig. 8. Typical potentiometric CO₂ and O₂ sensitivity of the K-SCISEs in a stirred 0.1 M KCl solution. The solution was purged with pure gases in the sequence shown in the figure. RE: Ag/AgCl/3 M KCl/1.0 LiOAc.

beneath the ISM. Although Bobacka has previously showed that the redox capacitance of PEDOT is lower beneath the ISM [40], the results presented here demonstrate the drastic decrease of the available redox capacitance more clearly than before. In case of PEDOT-HQ, it is most likely due to the insufficient ion transfer at the SC/ISM interface preventing an efficient oxidation/reduction of the PEDOT backbone, but also because of deficiency of protons hindering the redox conversion of the pendant HQ groups. We note that the redox capacitances of 1.1 and 1.5 mF cm⁻² are still high enough to prevent any considerable changes in the a_{HQ}/a_{BQ} ratio that could be reflected as a potential drift of the K-SCISEs under normal operational conditions. This is because the currents in high input impedance voltmeters are in pA range or below, whereas the K-SCISEs in Figure S8 have been polarized with much higher currents ($\pm 10^{-9}$ A). We can conclude that the composition of the commonly used PVC-ISM might not be the most suitable for the SCISEs. They would benefit from ISMs with higher ion mobilities that facilitate a faster ion transfer at the SC/ISM interface and in addition, match the charge compensating ion transfer process associated with the redox reaction of the conducting polymer SC. In most cases, the PVC-ISM formulations developed for the liquid contact ISEs have been adopted for the SCISEs as such. Hence, we believe that more efforts should be directed in further optimization of their composition or in finding substitutes for the PVC-ISM.

4. Conclusions

We have used for the first time the redox conjugated polymer (PEDOT-HQ) with covalently attached HQ pendant groups as the ion-to-electron transducer (solid contact) in K⁺-selective SCISEs. Due to the HQ pendant groups, the redox capacitance of PEDOT-HQ (ca. 490 mF cm⁻² at pH 0) is superior to unsubstituted PEDOT. With covalent attachment of the redox groups to the polymer backbone, we overcome the usually encountered problem of leaching out of the non-covalently bound redox groups from the SC or ISM, which gives rise to potential drift and potential irreproducibility of the SCISEs. In the best case, we obtained the E° reproducibility of only ± 2.8 mV ($n = 5$) for the K-SCISEs that had been conditioned in 0.01 M KCl for 24 h. We show also that pre-polarization of the SC in a water-free 0.01 M KTFAB-MeCN (prior to the drop casting of the ISM) gave K-SCISEs with a very low initial potential drift of only 0.1 mV h⁻¹, but higher E° irreproducibility. Our results indicate that the presence of HClO₄ and/or water in the pre-

polarization solution causes a much higher initial potential drift of the K-SCISEs (-2.8 mV h^{-1}). However, as a precise tuning of the $a_{\text{HQ}}/a_{\text{BQ}}$ ratio of the PEDOT-HQ solid contact requires access to protons, the K-SCISEs presented here need still further optimization. Chronopotentiometric measurements reveal more clearly than reported previously for ECPs that only a minor fraction of the very high redox capacitance of the PEDOT-HQ solid contact can be utilized when it is buried beneath the PVC-ISM. This leads us to the conclusion that the PVC-ISMs adapted from the liquid contact ISEs may not necessarily be suitable for SCISEs. We believe that ISMs having higher ion mobilities are more advantageous for obtaining faster ion transfer at the SC/ISM interface. This facilitates the redox conversions of the PEDOT backbone and the HQ pendant groups of the buried SC, which increases its available redox capacitance. The K-SCISEs presented here were insensitive to light, O_2 and CO_2 , but the aqueous layer test reveals the presence of water at the inner electrode interfaces probably because of the hydrophilicity of the HQ pendant groups.

CRedit authorship contribution statement

Iryna Ivanko: Investigation, Methodology, Validation, Formal analysis, Visualization, Writing - original draft, Writing - review & editing, Funding acquisition. **Tom Lindfors:** Conceptualization, Supervision, Methodology, Formal analysis, Visualization, Writing - original draft, Writing - review & editing, Project administration, Funding acquisition. **Rikard Emanuelsson:** Resources. **Martin Sjödin:** Resources, Writing - review & editing.

Declaration of Competing Interest

The authors declare that they have no known competing financial interests or personal relationships that could have appeared to influence the work reported in this paper.

Acknowledgements

Iryna Ivanko is most grateful for the EDUFI fellowship (TM-19-11049) from the Finnish National Agency of Education that made it possible for her to carry out the research at Åbo Akademi University.

Appendix A. Supplementary data

Supplementary material related to this article can be found, in the online version, at doi:<https://doi.org/10.1016/j.snb.2020.129231>.

References

- Y. Shao, Y. Ying, J. Ping, Recent advances in solid-contact ion-selective electrodes: functional materials, transduction mechanisms, and development trends, *Chem. Soc. Rev.* 49 (2020) 4405–4465.
- A. Cadogan, Z. Gao, A. Lewenstam, A. Ivaska, D. Diamond, All-solid-state sodium-selective electrode based on a calixarene ionophore in a poly(vinyl chloride) membrane with a polypyrrole solid contact, *Anal. Chem.* 64 (1992) 2496–2501.
- R.E. Gyurcsányi, A.S. Nybäck, K. Tóth, G. Nagy, A. Ivaska, Novel polypyrrole based all-solid-state potassium-selective microelectrodes, *Analyst* 123 (1998) 1339–1344.
- N. Ruecha, O. Chailapakul, K. Suzuki, D. Citterio, Fully inkjet-printed paper-based potentiometric ion-sensing devices, *Anal. Chem.* 89 (2017) 10608–10616.
- M.P.S. Mousavi, A. Ainal, E.K.W. Tan, M.K. Abd El-Rahman, Y. Yoshida, L. Yuan, et al., Ion sensing with thread-based potentiometric electrodes, *Lab Chip* 18 (2018) 2279–2290.
- M. Parrilla, R. Canovas, I. Jeerapan, F.J. Andrade, J. Wang, A Textile-based stretchable multi-ion potentiometric sensor, *Adv. Healthc. Mater.* 5 (2016) 996–1001.
- M. Parrilla, M. Cuartero, G.A. Crespo, Wearable potentiometric ion sensors, *TrAC, Trends Anal. Chem.* 110 (2019) 303–320.
- M. Cuartero, M. Parrilla, G.A. Crespo, Wearable potentiometric sensors for medical applications, *Sensors* 19 (2019) 363.
- X.V. Zhen, C.R. Rousseau, P. Bühlmann, Redox buffer capacity of ion-selective electrode solid contacts doped with organometallic complexes, *Anal. Chem.* 90 (2018) 11000–11007.
- M. Piek, R. Piech, B. Paczosa-Bator, Improved nitrate sensing using solid contact ion selective electrodes based on TTF and its radical salt, *J. Electrochem. Soc.* 162 (2015) B257–B263.
- B. Paczosa-Bator, M. Piek, R. Piech, Application of nanostructured TCNQ to potentiometric ion-selective K^+ and Na^+ electrodes, *Anal. Chem.* 87 (2015) 1718–1725.
- Y. Ishige, S. Klink, W. Schuhmann, Intercalation compounds as inner reference electrodes for reproducible and robust solid-contact ion-selective electrodes, *Angew Chem Int Ed* 55 (2016) 4831–4835.
- S. Klink, Y. Ishige, W. Schuhmann, Prussian blue analogues: a versatile framework for solid-contact ion-selective electrodes with tunable potentials, *ChemElectroChem* 4 (2017) 490–494.
- B. Bartoszewicz, S. Dabrowska, A. Lewenstam, J. Migdalski, Calibration free solid contact electrodes with two PVC based membranes, *Sens. Actuators B Chem.* 274 (2018) 268–273.
- J.H. Li, T.J. Yin, W. Qin, An all-solid-state polymeric membrane Pb^{2+} -selective electrode with bimodal pore C-60 as solid contact, *Anal. Chim. Acta* 876 (2015) 49–54.
- J.J. Ye, F.H. Li, S.Y. Gan, Y.Y. Jiang, Q.B. An, Q.X. Zhang, et al., Using sp(2)-C dominant porous carbon sub-micrometer spheres as solid transducers in ion-selective electrodes, *Electrochem. Commun.* 50 (2015) 60–63.
- G. Matzeu, C. Zuliani, D. Diamond, Solid-contact ion-selective electrodes (ISEs) based on ligand functionalised gold nanoparticles, *Electrochim. Acta* 159 (2015) 158–165.
- T.J. Yin, D.W. Pan, W. Qin, All-solid-state polymeric membrane ion-selective miniaturized electrodes based on a nanoporous gold film as solid contact, *Anal. Chem.* 86 (2014) 11038–11044.
- X.Z. Zeng, S.Y. Yu, Q. Yuan, W. Qin, Solid-contact K^+ -selective electrode based on three-dimensional molybdenum sulfide nanoflowers as ion-to-electron transducer, *Sens. Actuators B Chem.* 234 (2016) 80–83.
- L. Mendecki, K.A. Mirica, Conductive metal-organic frameworks as ion-to-electron transducers in potentiometric sensors, *ACS Appl. Mater. Interfaces* 10 (2018) 19248–19257.
- M. Piek, R. Piech, B. Paczosa-Bator, The complex crystal of NaTCNQ-TCNQ supported on different carbon materials as ion-to-electron transducer in all-solid-state sodium-selective electrode, *J. Electrochem. Soc.* 163 (2016) B573–B579.
- M. Piek, R. Piech, B. Paczosa-Bator, All-solid-state nitrate selective electrode with graphene/tetrathiafulvalene nanocomposite as high redox and double layer capacitance solid contact, *Electrochim. Acta* 210 (2016) 407–414.
- Z.A. Boeva, T. Lindfors, Few-layer graphene and polyaniline composite as ion-to-electron transducer in silicone rubber solid-contact ion-selective electrodes, *Sens. Actuators B Chem.* 224 (2016) 624–631.
- B. Paczosa-Bator, Ion-selective electrodes with superhydrophobic polymer/carbon nanocomposites as solid contact, *Carbon* 95 (2015) 879–887.
- Q. Sun, W. Li, B. Su, Highly hydrophobic solid contact based on graphene-hybrid nanocomposites for all solid state potentiometric sensors with well-formulated phase boundary potentials, *J. Electroanal Chem* 740 (2015) 21–27.
- E. Jaworska, M.L. Naitana, E. Stelmach, G. Pomarico, M. Wojciechowski, E. Bulska, et al., Introducing cobalt(II) porphyrin/cobalt(III) corrole containing transducers for improved potential reproducibility and performance of all-solid-state ion-selective electrodes, *Anal. Chem.* 89 (2017) 7107–7114.
- J.H. Li, T.J. Yin, W. Qin, An effective solid contact for an all-solid-state polymeric membrane Cd^{2+} -selective electrode: three-dimensional porous graphene-mesoporous platinum nanoparticle composite, *Sens. Actuators B Chem.* 239 (2017) 438–446.
- R. Liang, T. Yin, W. Qin, A simple approach for fabricating solid-contact ion-selective electrodes using nanomaterials as transducers, *Anal. Chim. Acta* 853 (2015) 291–296.
- S. Papp, J. Kozma, T. Lindfors, R.E. Gyurcsányi, Lipophilic multi-walled carbon nanotube-based solid contact potassium ion-selective electrodes with reproducible standard potentials, A comparative study *Electroanalysis* 32 (2020) 867–873.
- N. He, S. Papp, T. Lindfors, L. Höfler, R.M. Latonen, R.E. Gyurcsányi, Pre-polarized hydrophobic conducting polymer solid-contact ion selective electrodes with improved potential reproducibility, *Anal. Chem.* 89 (2017) 2598–2605.
- S. Papp, M. Bojtar, R.E. Gyurcsányi, T. Lindfors, Potential reproducibility of potassium-selective electrodes having perfluorinated alkanoate side chain functionalized poly(3,4-ethylenedioxythiophene) as a hydrophobic solid contact, *Anal. Chem.* 91 (2019) 9111–9118.
- M. Guzinski, J.M. Jarvis, P. D'Orazio, A. Izadyar, B.D. Pendley, E. Lindner, Solid-contact pH sensor without CO_2 interference with a superhydrophobic PEDOT-C-14 as solid contact: the ultimate “water layer” test, *Anal. Chem.* 89 (2017) 8468–8475.
- C.Z. Lai, M.A. Fierke, A. Stein, P. Bühlmann, Ion-selective electrodes with three-dimensionally ordered macroporous carbon as the solid contact, *Anal. Chem.* 79 (2007) 4621–4626.
- G.A. Crespo, S. Macho, F.X. Rius, Ion-selective electrodes using carbon nanotubes as ion-to-electron transducers, *Anal. Chem.* 80 (2008) 1316–1322.
- M.A. Fierke, C.Z. Lai, P. Bühlmann, A. Stein, Effects of architecture and surface chemistry of three-dimensionally ordered macroporous carbon solid contacts on performance of ion-selective electrodes, *Anal. Chem.* 82 (2010) 680–688.
- J. Hu, X.U. Zou, A. Stein, P. Bühlmann, Ion-selective electrodes with colloid-imprinted mesoporous carbon as solid contact, *Anal. Chem.* 86 (2014) 7111–7118.
- X.U. Zou, J.H. Cheong, B.J. Tait, P. Bühlmann, Solid contact ion-selective electrodes with a well-controlled Co(II)/Co(III) redox buffer layer, *Anal. Chem.* 85 (2013) 9350–9355.

- [38] X.U. Zou, X.V. Zhen, J.H. Cheong, P. Bühlmann, Calibration-free ionophore-based ion-selective electrodes with a Co(II)/Co(III) redox couple-based solid contact, *Anal. Chem.* 86 (2014) 8687–8692.
- [39] F. Scholz, H. Kahlert, U. Hasse, A. Albrecht, A.C.T. Kuate, K. Jurkschat, A solid-state redox buffer as interface of solid-contact ISEs, *Electrochem. commun.* 12 (2010) 955–957.
- [40] J. Bobacka, Potential stability of all-solid-state ion-selective electrodes using conducting polymers as ion-to-electron transducers, *Anal. Chem.* 71 (1999) 4932–4937.
- [41] T. Lindfors, Light sensitivity and potential stability of electrically conducting polymers commonly used in solid contact ion-selective electrodes, *J. Solid State Electrochem.* 13 (2009) 77–89.
- [42] M. Fibbioli, K. Bandyopadhyay, S.G. Liu, L. Echegoyen, O. Enger, F. Diederich, et al., Redox-active self-assembled monolayers as novel solid contacts for ion-selective electrodes, *Chem. Commun. (Camb.)* (2000) 339–340.
- [43] N. He, R.E. Gyurcsányi, T. Lindfors, Electropolymerized hydrophobic polyazulene as solid-contacts in potassium-selective electrodes, *Analyst* 141 (2016) 2990–2997.
- [44] M. Fibbioli, W.E. Morf, M. Badertscher, N.F. de Rooij, E. Pretsch, Potential drifts of solid-contacted ion-selective electrodes due to zero-current ion fluxes through the sensor membrane, *Electroanalysis* 12 (2000) 1286–1292.
- [45] Z.H. Chen, Y. Zheng, H. Yan, A. Facchetti, Naphthalenedicarboximide- vs perylenedicarboximide-based copolymers. Synthesis and semiconducting properties in bottom-gate N-channel organic transistors, *J. Am. Chem. Soc.* 131 (2009) 8–9.
- [46] Y.L. Liang, Z.H. Chen, Y. Jing, Y.G. Rong, A. Facchetti, Y. Yao, Heavily n-dopable pi-conjugated redox polymers with ultrafast energy storage capability, *J. Am. Chem. Soc.* 137 (2015) 4956–4959.
- [47] C. Karlsson, H. Huang, M. Stromme, A. Gogoll, M. Sjödin, Polymer pendant interactions in poly(pyrrol-3-ylhydroquinone): a solution for the use of conducting polymers at stable conditions, *J. Phys. Chem. C* 117 (2013) 23558–23567.
- [48] C. Karlsson, H. Huang, M. Stromme, A. Gogoll, M. Sjödin, Probing polymer-pendant interactions in the conducting redox polymer poly(pyrrol-3-ylhydroquinone), *J Phys Chem C* 118 (2014) 23499–23508.
- [49] C. Karlsson, H. Huang, M. Stromme, A. Gogoll, M. Sjödin, Quinone pendant group kinetics in poly(pyrrol-3-ylhydroquinone), *J Electroanal Chem* 735 (2014) 95–98.
- [50] C. Karlsson, H. Huang, M. Stromme, A. Gogoll, M. Sjödin, Impact of linker in polypyrrole/quinone conducting redox polymers, *RSC Adv.* 5 (2015) 11309–11316.
- [51] C. Karlsson, H. Huang, M. Stromme, A. Gogoll, M. Sjödin, Ion- and electron transport in pyrrole/quinone conducting redox polymers investigated by in situ conductivity methods, *Electrochim. Acta* 179 (2015) 336–342.
- [52] R. Emanuelsson, H. Huang, A. Gogoll, M. Stromme, M. Sjödin, Enthalpic versus entropic contribution to the quinone formal potential in a polypyrrole-based conducting redox polymer, *J Phys Chem C* 120 (2016) 21178–21183.
- [53] R. Emanuelsson, C. Karlsson, H. Huang, C. Kosgei, M. Stromme, M. Sjödin, Quinone based conducting redox polymers for electrical energy storage, *Russ J Electrochem* 53 (2017) 8–15.
- [54] H. Huang, C. Karlsson, M. Stromme, A. Gogoll, M. Sjödin, Synthesis and characterization of poly-3-((2,5-hydroquinone)vinyl)-1H-pyrrole: investigation on backbone/pendant interactions in a conducting redox polymer, *PCCP* 19 (2017) 10427–10435.
- [55] H. Huang, C. Karlsson, F. Mamedov, M. Stromme, A. Gogoll, M. Sjödin, Polaron disproportionation charge transport in a conducting redox polymer, *J Physical Chem C* 121 (2017) 13078–13083.
- [56] L. Yang, X. Huang, A. Gogoll, M. Stromme, M. Sjödin, Matching diethyl terephthalate with n-doped conducting polymers, *J Phys Chem C* 119 (2015) 18956–18963.
- [57] X. Huang, L. Yang, J. Bergquist, M. Stromme, A. Gogoll, M. Sjödin, Synthesis and redox properties of thiophene terephthalate building blocks for low-potential conducting redox polymers, *J Phys Chem C* 119 (2015) 27247–27254.
- [58] L. Yang, X. Huang, A. Gogoll, M. Stromme, M. Sjödin, Effect of the linker in terephthalate-functionalized conducting redox polymers, *Electrochim. Acta* 222 (2016) 149–155.
- [59] X. Huang, L. Yang, R. Emanuelsson, J. Bergquist, M. Stromme, M. Sjödin, et al., A versatile route to polythiophenes with functional pendant groups using alkyne chemistry, *Beilstein J. Org. Chem.* 12 (2016) 2682–2688.
- [60] L. Yang, X. Huang, F. Mamedov, P. Zhang, A. Gogoll, M. Stromme, et al., Conducting redox polymers with non-activated charge transport properties, *PCCP* 19 (2017) 25052–25058.
- [61] M. Sterby, R. Emanuelsson, X. Huang, A. Gogoll, M. Stromme, M. Sjödin, Characterization of PEDOT-quinone conducting redox polymers for water based secondary batteries, *Electrochim. Acta* 235 (2017) 356–364.
- [62] M. Sterby, R. Emanuelsson, F. Mamedov, M. Stromme, M. Sjödin, Investigating electron transport in a PEDOT/Quinone conducting redox polymer with in situ methods, *Electrochim. Acta* 308 (2019) 277–284.
- [63] N. Casado, G. Hernandez, A. Veloso, S. Devaraj, D. Mecerreyes, M. Armand, PEDOT radical polymer with synergetic redox and electrical properties, *ACS Macro Lett.* 5 (2016) 64–69.
- [64] D. Mantione, N. Casado, A. Sanchez-Sanchez, H. Sardon, D. Mecerreyes, Easy-to-make carboxylic acid dioxithiophene monomer (ProDOT-COOH) and functional conductive polymers, *J. Polym. Sci., Part A: Polym. Chem.* 55 (2017) 2721–2724.
- [65] R.W. Cattrall, D.M. Drew, I.C. Hamilton, Some alkylphosphoric acid-esters for use in coated-wire calcium-selective electrodes. 1. Response characteristics, *Anal. Chim. Acta* 76 (1975) 269–277.
- [66] P.H. Chen, R.L. McCreery, Control of electron transfer kinetics at glassy carbon electrodes by specific surface modification, *Anal. Chem.* 68 (1996) 3958–3965.
- [67] T. Lindfors, F. Sundfors, L. Höfler, R.E. Gyurcsányi, FTIR-ATR study of water uptake and diffusion through ion-selective membranes based on plasticized poly(vinyl chloride), *Electroanalysis* 21 (2009) 1914–1922.
- [68] L. Groenendaal, G. Zotti, P.H. Aubert, S.M. Waybright, J.R. Reynolds, Electrochemistry of poly(3,4-alkylenedioxythiophene) derivatives, *Adv Mater* 15 (2003) 855–879.
- [69] M. Quan, D. Sanchez, M.F. Wasyliw, D.K. Smith, Voltammetry of quinones in unbuffered aqueous solution: reassessing the roles of proton transfer and hydrogen bonding in the aqueous Electrochemistry of Quinones, *J. Am. Chem. Soc.* 129 (2007) 12847–12856.
- [70] N.M.N. Huynh, Z.A. Boeva, J.H. Smatt, M. Pesonen, T. Lindfors, Reduced graphene oxide as a water, carbon dioxide and oxygen barrier in plasticized poly(vinyl chloride) films, *RSC Adv.* 8 (2018) 17645–17655.
- [71] R.M. Haddox, H.O. Finklea, Proton-coupled electron transfer of an osmium aquo complex on a self-assembled monolayer on gold, *J. Phys. Chem. B* 108 (2004) 1694–1700.
- [72] A. Österholm, T. Lindfors, J. Kauppila, P. Damlin, C. Kvarnström, Electrochemical incorporation of graphene oxide into conducting polymer films, *Electrochim. Acta* 83 (2012) 463–470.
- [73] H. Wang, R. Emanuelsson, A. Banerjee, R. Ahuja, M. Stromme, M. Sjödin, Effect of cycling ion and solvent on the redox chemistry of substituted quinones and solvent-induced breakdown of the correlation between redox potential and electron-withdrawing power of substituents, *J Phys Chem C* 124 (2020) 13609–13617.
- [74] K. Izutsu, *Electrochemistry in Nonaqueous Solutions*, Wiley-VCH Verlag GmbH&Co, 2002.

Iryna Ivanko received the MSc degree in Chemistry Sciences from Lviv Ivan Franko University. She is a fourth year PhD student at the Department of Physical and Macromolecular Chemistry at Charles University. Her research focuses on investigation of high-rate pseudosupercapacitors based on semiconducting polymers, poly(3,4-ethylenedioxythiophene) (PEDOT) and polyaniline. In addition, she is interested in fundamental studies of the photoluminescent properties of individual chains and/or aggregates of PEDOT.

Tom Lindfors is working as Associate Professor in Analytical Chemistry at the Laboratory of Molecular Science and Engineering at Åbo Akademi University (ÅAU). He was in 2004 appointed as Docent in Analytical Applications of Conducting Polymers at ÅAU. His research interests cover solid-state ion-selective electrodes, graphene based composite materials, electrically conducting polymers, water uptake of polymeric ion-selective membrane materials and barrier properties of carbon materials.

Rikard Emanuelsson is currently a researcher at the Department of Materials Science and Engineering (Nanotechnology and Functional Materials) at Uppsala University. He has a PhD in organic chemistry and his research interests cover development (synthesis) and characterization (electrochemistry) of organic battery materials with a special focus on proton batteries based on conducting redox polymers for sustainable electrical energy storage applications.

Martin Sjödin is a professor in nanotechnology and functional materials at Uppsala University. He received his Ph. D. degree in Physical Chemistry from Uppsala University in 2004. Between 2004 and 2007 he was a Postdoctoral Fellow, first at Dublin City University (2004–2005) and later at Commissariat à l'Énergie Atomique (Paris) (2005–2007). In 2013, he was appointed Docent in Nanotechnology and Functional Materials and in 2015 he was appointed Full Professor within the same discipline. Currently his research interests are in the area of organic materials for energy conversion and storage.